Fabrication of 316-L Stainless Steel and Composite Micro Machine Components Using Softlithography and Powder Metallurgy Process

by

Mohamed Fawzy Soliman Imbaby

A thesis submitted to
the University of Birmingham
for the degree of

DOCTOR OF PHILOSOPHY

School of Mechanical Engineering
The University of Birmingham
Edgbaston, B15 2TT, UK.

July 2010

ABSTRACT

This thesis presents a new approach to fabricate high precision micro machine components from stainless steel and stainless steel ceramic composite materials, using Softlithography and powder metallurgy processes. Three different 316-L stainless steel powders, including 5, 10 and 16 µm in size, and two different ceramics powders, including 400 nm alumina and 320 nm titania, were tested. The PhD research process can be divided into three main stages. In the first stage, high quality SU-8 master moulds and their negative replicas soft moulds are produced using Softlithography technique. The second stage includes preparing the stainless steel slurries, filling the soft micro moulds, obtaining the green micro components, de-binding and sintering. In the third stage, the fabrication process has been developed further to produce stainless steel-ceramic composite micro components. Fabrication process in each stage was investigated in detail and the optimum properties were produced. Dispersant acrylic-based binder is adopted in this research successfully in producing damage-free green micro components. A cold isostatic pressing technique is also adopted to improve the densities and linear shrinkages of the stainless steel green and sintered micro components. A new mixing method is used to improve the homogeneity of the ceramic inclusions in the stainless steel matrix of the composite micro components. Characterization of the sintered stainless steel and composite micro components in terms of shape retention, density, linear shrinkage, internal structure, hardness and surface roughness were investigated in detail. The resultant stainless steel and composite micro components retain the same high geometric quality as the SU-8 master moulds.

DEDICATION

To my mother, my wife, and my lovely children: Fayrouz, Salma and Yousef. Also dedicated to anyone interested in the subject.

ACKNOWLEDGMENTS

It is the greatest honour to work under supervision of Dr Kyle Jiang. I am thankful and gratified for all of his help, assistance, inspiration and guidance on the all aspects. I would like to thank Dr Isaac Chang, School of Metallurgy and Materials, for his support and supervision. Thanks to all of my colleagues in the Microengineering and Nanotechnology research group in the University of Birmingham, particularly Mr Hossein Ostadi for helping in measuring the surface roughness. Thanks to technicians in our group, particularly Mr Alan for his sincere help throughout my experimental work. Thanks to Dr Mike Keeble in the Bheuler Lab for his assistance of using all facilities in Buhler Laboratory. Thanks to Dr Hany El Shinawi, School of Chemistry; and Miss Aviral Roger, School of Metallurgy and Materials, for helping in using sintering furnaces. I would like to thanks Dr Ahamed Al-dawoody for proofreading chapter 5. I would like to thank the Egyptian Ministry of Higher Education for supporting me financially by tuition fees and living expenses, which enable me to finish my research. Above all, I would like to express my deepest gratitude to my wife for her love and support in every possible way during my PhD study.

TABLE OF CONTENTS

DEDICATION ..... **II**

ACKNOWLEDGMENTS ..... **III**

TABLE OF CONTENTS ..... **IV**

LIST OF TABLES ..... **VIII**

LIST OF FIGURES ..... **IX**

ABBREVIATIONS ..... **XVII**

CHAPTER 1. INTRODUCTION **1**

1.1. Introduction 1

1.2. Aims and objectives 1

1.3. Thesis outline 3

CHAPTER 2. LITERATURE REVIEW **4**

2.1. Introduction 4

2.2. Photolithography 5

2.3. Silicon micro machining 7

2.4. LIGA technique 9

2.5. Laser micro machining 12

2.6. Electrical discharge machining 13

2.7. Hot embossing 16

2.8. Micro machining and micro milling 17

2.9. Micro Metal injection moulding (μMIM) 18

2.10. Softlithography technique 20

2.11. Summary 21

CHAPTER 3. FABRICATION OF SU-8 MASTER MOULDS AND THEIR NEGATIVE REPLICAS SOFT MOULDS **23**

3.1. Production of SU-8 master moulds 23

3.1.1. Procedures for production 1 mm thick SU-8 master moulds 27

3.1.1.1. Mask design 27

3.1.1.2. Casting SU-8 over silicon wafer 27

3.1.1.3. Soft baking 29
3.1.1.4. Exposure 30
3.1.1.5. Post exposure bake (PEB) 31
3.1.1.6. Development 32
3.1.1.7. Hard bake 32
3.1.2. Results 32
3.1.3. Discussion 37
3.2. Production of negative replicas soft moulds 40
3.2.1. Soft moulds 40
3.2.2. Preparation of soft mould slurry 40
3.2.3. Curing and peeling off 41
3.2.4. Results and discussions 42
3.3. Conclusions 43

CHAPTER 4. SELECTION OF STAINLESS STEEL POWDER AND BINDER 45
4.1. Powder selection 45
4.2. Binder selection 48
4.3. Preparation of green micro parts 49
4.3.1. Preparing stainless steel slurries 49
4.3.1.1. Gel casting based slurry 49
4.3.1.2. Cyanoacrylate based slurry 51
4.3.1.3. Dispersant acrylic based slurry 52
4.3.2. Filling the soft micro moulds 54
4.3.3. Drying and de-moulding 55
4.4. Results and discussion 56
4.5. Conclusions 59

CHAPTER 5. PRODUCTION OF THE STAINLESS STEEL GREEN MICRO COMPONENTS 61
5.1. Pressure less filling method 61
5.1.1. Obtaining the optimum amount of dispersant 61
5.1.2. Obtaining the optimum amount of binder 64
5.2. Cold Isostatic pressing (CIP) method 65
5.2.1. Preparation of stainless steel semi solid pastes for CIP method 68
5.2.2. Filling the soft micro moulds by applying pressing 68

5.2.3. Obtaining the green micro components based on CIP method 70
5.3. Results and discussions 71
5.3.1. Effect of dispersant on the densities of green components based on pressure less filling method 71
5.3.2. Effect of dispersant on the fracture green micro components based on pressure less filling method 73
5.3.3. Effect of binder on the retention of green micro components based on pressure less filling method 74
5.3.4. Effect of pressing method on the density of the green components 79
5.3.5. Effect of pressing methods on the fractured green micro components 81
5.3.6. Effect of cold isostatic pressing on the retention of green micro components . 82
5.3.7. Linear shrinkage 84
5.4. Conclusions 85

CHAPTER 6. DE-BINDING AND SINTERING OF THE STAINLESS STEEL MICRO COMPONENTS 87
6.1. Introduction 87
6.2. De-binding and sintering 89
6.2.1. Thermal gravimetric analysis (TGA) 89
6.2.2. Sintering in nitrogen atmosphere 91
6.2.3. Sintering in nitrogen/hydrogen mixture atmosphere 92
6.2.4. Sintering in vacuum 93
6.3. Results and discussion 94
6.3.1. Effect of nitrogen on the sintered micro components 94
6.3.2. Effect of nitrogen/hydrogen mixture and vacuum atmospheres on the sintered micro components 96
6.3.3. Micro engine assembly and other components 101
6.3.4. Other stainless steel components 104
6.4. Conclusions 106

CHAPTER 7. CHARACTERIZATION OF THE SINTERED STAINLESS STEEL MICRO COMPONENTS 107
7.1. Characterization methodology 107
7.1.1. Measuring the density of sintered micro components 107
7.1.2. Measuring linear shrinkage 108
7.1.3. Measuring micro hardness 109
7.1.4. Measuring surface roughness 113

7.2. Results and discussions 116
7.2.1. Density 116
7.2.2. Linear shrinkage 117
7.2.3. Micro hardness 120
7.2.4. Surface morphology, internal structure and porosity 126
7.2.5. Surface roughness 131
7.3. Conclusions 135

CHAPTER 8. FABRICATION OF THE STAINLESS STEEL CERAMIC COMPOSITE MICRO COMPONENTS 137
8.1. Introduction 137
8.2. Production of composite green micro components 139
8.2.1. Powders and binder 139
8.2.2. Preparation of the stainless steel-ceramic slurries 141
8.2.2.1. Optimize the amount of dispersant of ceramic powders 141
8.2.2.2. Mixing the composite powders and forming composite slurry 142
8.2.3. Obtaining composite green micro components 144
8.3. De-binding and sintering 145
8.4. Results and discussions 145
8.4.1. Green composite components and green density 145
8.4.2. Shape retention of composite micro components 150
8.4.3. Composite sintered density 152
8.4.4. Composite linear shrinkage 155
8.4.5. Composite microstructure 157
8.4.6. Micro hardness analysis of the micro composites 161
8.4.7. Various composite components 164
8.5. Conclusions 165

CHAPTER 9. CONCLUSIONS AND FUTURE WORK 167
9.1. Conclusions 167
9.2. Future work 169

LISTS OF PUBLICATIONS 170

REFERENCES 172

LIST OF TABLES

Table 3.1. The properties of SU-8 2075 as delivered by Microchem, USA [108]. 24

Table 3.2. The properties of Polydimethylsiloxane (PDMS) [111]. 41

Table 4.1. The chemical compositions of the 316-L stainless steel powders (Sandvik Osprey, UK.)..... 46

Table 4.2. The Particle size distributions and the tap densities of 316-L stainless steel powders (Sandvik Osprey, UK.)..... 47

Table 4.3. The chemicals of gel casting and their properties (Sigma Aldrich, UK.). 51

Table 4.4. The compositions of two different stainless steel slurries prepared from 5-µm powder and based on gel casting binder..... 51

Table 4.5. The properties of Cyanoacrylate [133]..... 52

Table 4.6. The properties of dispersant D-3005 and binders: B-1000 and B-1007 (Rohm and Hass, Ltd., UK.)..... 54

Table 5.1. Linear shrinkage of the stainless steel green micro components based on different powders and fabricated by pressure less filling method and cold isostatic one. .. 85

Table 7.1. Surface roughness parameters of the stainless steel micro components based on different powders and sintered in nitrogen/hydrogen mixture atmospheres at 1350^{o}C. ... 135

Table 8.1. The properties of alumina powders as supplied by Alfa Aesar UK. 140

Table 8.2. The properties of titania powder as supplied by Huntsman England, UK. 140

LIST OF FIGURES

Figure 2.1. A schematic diagram showing the complete photolithography procedures. 7

Figure 2.2. A schematic diagram showing the silicon micro machining process. 9

Figure 2.3. A schematic diagram showing the LIGA fabrication processes: (i) synchrotron irradiation of photoresist, (ii) development of exposed photoresist, (iii) electroforming of metallic microstructures, (iv) making of mould insert, (v) mould filling and (vi) de-moulding [38]. 11

Figure 2.4. SEM images showing the micro components fabricated by using UV-LIGA process: (a) SU-8 micro master mould over silicon wafer and (b) Nickel negative replica after removing SU-8 moulds [43]. 12

Figure 2.5. A schematic diagram showing: (a) laser micro machining process and (b) SEM image of micro gear with internal teeth machined using lased micro machining [54]. 13

Figure 2.6. A schematic diagram showing the three types of the micro-EDM: (a) hole boring, (b) shaped working electrode, (c) wire EDM [11]. 14

Figure 2.7. SEM images showing the WC-Co micro structure: (a) 1 mm gear pattern and initial shape of the patterned negative type electrode: (b) before use and (c) after use [65]. 15

Figure 2.8. A schematic diagram showing hot embossing equipment [67]. 16

Figure 2.9. SEM image showing a milled membrane by using FIB for TEM study [73]. . 18

Figure 2.10. A schematic diagram showing the processing procedures of PIM technique: (i) mixing, (ii) injection moulding, (iii) de-binding, (iv) sintering and (v) microstructure [87]. 19

Figure 2.11. A schematic diagram showing the soft moulding processes: (i) preparing master mould, (ii) replicating by soft mould, (iii) obtaining the soft mould, (iv) filling the soft mould by slurries, (v) de-moulding and obtaining green components and (vi) sintering. 21

Figure 3.1. A schematic diagram showing the micro engine assembly with dimensions and the micro engine parts fabricated in this research, designed by Peng Jin [109]. 25

Figure 3.2. A schematic diagram showing the completed fabrication process of SU-8 master moulds: (i) casting SU-8 slurry over silicon wafer, (ii) soft baking, (iii) exposing to UV-light, (iv) post exposure baking (PEB) and (v) developing. 26

Figure 3.3. A photograph showing the SU-8 resist on a silicon wafer is put on top of a hot plate for soft baking..... 30

Figure 3.4. A photograph showing a Cannon PLA-501 mask aligner machine used for exposing the SU-8 by UV-light. 31

Figure 3.5. SEM images showing the SU-8 micro components and their side walls exposed by using 4500 mJ/cm^2 without filter: (a) side walls of the micro piston and (b) micro gear, micro linkage rod and gear teeth side wall. 34

Figure 3.6. SEM image showing the SU-8 micro gear and its teeth side walls exposed by using 7000 mJ/cm^2 without filter. 34

Figure 3.7. SEM images showing the SU-8 micro components and their side walls exposed by using 9000 mJ/cm^2 without filter: (a) side walls of the micro linkage rod and (b) micro gear and its gear teeth side wall. 35

Figure 3.8. SEM images showing the SU-8 micro gears and their side walls exposed by using PL-360 filter and the exposure energy are: (a) 4500 mJ/cm^2, (b) 7000 mJ/cm^2 and (c) 9000 mJ/cm^2. 36

Figure 3.9. SEM images showing the SU-8 micro engine components exposed by using PL-360 filter and the exposure energy is 9000 mJ/cm^2: (a) micro engine cylinder parts, (b) micro linkage rods and (c) micro pistons. 37

Figure 3.10. A graph showing the optical transmittance of SU-8 with UV-light wavelength [108]. 39

Figure 3.11. A graph showing spectral distribution of Hg mercury lamp used for photolithography process [110]. 39

Figure 3.12. A photograph showing the degassing chamber used in this research. 41

Figure 3.13. A schematic diagram showing the complete replication process of the soft mould insert: (i) mixing, (ii) degassing, (iii) pouring, (iv) curing and (v) peeling off. 42

Figure 3.14. SEM images showing defected PDMS negative micro moulds due to: (a) no degassing is applied and (b) insufficient degassing. 43

Figure 3.15. SEM images showing defect free PDMS negative micro mould inserts: (a) micro gear, (b) micro piston, (c) micro linkage rod and (d) micro engine cylinder. 43

Figure 4.1. SEM images showing the 316-L stainless steel powders: (a) 5-µm, (b) 10-µm and (c) 16-µm sizes. 47

Figure 4.2. Optical images showing the soft moulds of micro gears filled by using: (a) gravity method and (b) degassing chamber. 55

Figure 4.3. SEM images showing the stainless steel green micro gears based on 5-µm powder and fabricated by using gel casting binder, which contains: (a) 20% monomer, (b) 25% monomer and (c) 25% monomers. 58

Figure 4.4. SEM images showing the stainless steel green micro gears based on 5-µm powder and fabricated by using Cyanoacrylate binder. 58

Figure 4.5 SEM images showing the stainless steel green micro gear based on 5-µm powder and fabricated by using dispersant acrylic-based binder. 59

Figure 5.1. A schematic diagram showing the effect of the dispersant on the aggregated particles..... 63

Figure 5.2. Optical images showing the: (a) cylindrical soft mould inserts with 5 mm in both diameter and height and (b) their corresponding green components. 64

Figure 5.3. A schematic diagram and a photograph showing the: (a) hydraulic cylinder design with dimensions and (b) photograph of hydraulic cylinder parts and the pressing assembly. 67

Figure 5.4. Optical images showing the soft micro moulds filled by stainless steel pastes: (a) by applying hand pressing method and (b) by applying cold isostatic pressing method. 69

Figure 5.5. A schematic diagram showing the complete process for obtaining green micro components using cold isostatic pressing method. 70

Figure 5.6. A graph showing the effect of dispersant ratio on the density of stainless the green components fabricated from 5, 10 and 16-µm powders. 72

Figure 5.7. SEM images showing the fracture green micro components fabricated from 5-µm stainless steel powder using pressure less filling method and fabricated with: (a) no dispersant and (b) optimum dispersant..... 73

Figure 5.8. SEM images showing the fracture green micro components fabricated from 10-µm stainless steel powder using pressure less filling method and fabricated with: (a) no dispersant and (b) optimum dispersant..... 74

Figure 5.9. SEM images showing the fracture green micro components fabricated from 16-µm stainless steel powder using pressure less filling method and fabricated with: (a) no dispersant and (b) optimum dispersant..... 74

Figure 5.10. SEM images showing the stainless steel green micro components fabricated by using pressure less filling method and defected due to insufficient strength: (a) micro linkage rod and (b) micro gear with crack..... 76

Figure 5.11. SEM images showing the stainless steel green micro components fabricated by using pressure less filling method and defected during de-moulding: (a) micro piston and (b) micro piston edges..... 76

Figure 5.12. SEM images showing the stainless steel green micro piston fabricated by using pressure less filling method and defected due to insufficient degassing. 77

Figure 5.13. SEM images showing the stainless steel defect free green micro components fabricated by using pressure less filling method: (a) micro gear (b) micro linkage rod and (c) micro piston. 77

Figure 5.14. SEM images showing the stainless steel defect free green micro engine cylinder components fabricated by using pressure less filling method. 78

Figure 5.15. SEM images showing the stainless steel defect free green micro gear tooth tips fabricated by using pressure less filling method and based on: (a) 5-µm, (b) 10-µm and (c) 16-µm powders. 79

Figure 5.16. A graph showing the effect of the applied pressure on the green density of the stainless steel components fabricated from 5, 10 and 16-µm powders by using cold isostatic pressing technique. 80

Figure 5.17. SEM images showing the fracture stainless steel green micro components fabricated from 5-µm powder by using: (a) hand pressing and (b) cold isostatic pressing methods (116 MPa). 81

Figure 5.18. SEM images showing the fracture stainless steel green micro components fabricated from 10-µm powder by using: (a) hand pressing and (b) cold isostatic pressing methods (116 MPa). 82

Figure 5.19. SEM images showing the fracture stainless steel green micro components fabricated from 16-µm powder by using: (a) hand pressing and (b) cold isostatic pressing methods (116 MPa). 82

Figure 5.20. SEM images showing the stainless steel green micro components fabricated by using cold isostatic pressing method (116 MPa): (a) micro gear (b) micro linkage rod and (c) micro piston. 83

Figure 5.21. SEM images showing the top views of: (a) SU-8 micro gear and (b) stainless steel green micro gear 85

Figure 6.1. A photograph showing the NETZSCH Simultaneous Thermal gravimetric Analyser (STA) 449C used for investigating the degredation behaviours of the binder and dispersant. 90

Figure 6.2. A graph showing the thermal degradation behaviours of the binder B-1000 and B-1007, and dispersant D-3005, which was performed in thermal gravimetric analyser at the temperature range of 25–800^{o}C. 91

Figure 6.3. A photograph showing the tube furnace used for de-binding and sintering stainless steel micro components under nitrogen atmosphere. 92

Figure 6.4. A photograph showing a tube furnace used for de-binding and sintering stainless steel micro components under nitrogen/hydrogen mixture atmosphere. 93

Figure 6.5. A photograph showing the vacuum furnace used for sintering stainless steel micro components under vacuum atmosphere. 94

Figure 6.6. SEM images showing the stainless steel micro components fabricated from 5-µm powder using pressure less filling method and sintered in nitrogen atmosphere at 1200 ^{o}C by using: (a) heating cycle A and (b) heating cycle B. 95

Figure 6.7. SEM images showing the stainless steel micro gears fabricated from 5-µm powder by using pressure less filling method and sintered at 1200^{o}C in: (a) nitrogen/hydrogen mixture and (b) vacuum atmospheres. 97

Figure 6.8. SEM images showing the stainless steel micro linkage rods and pistons fabricated from 5-µm powder by using pressure less filling method and sintered at 1200^{o}C in: (a) nitrogen/hydrogen mixture and (b) vacuum atmospheres. 98

Figure 6.9. SEM images showing the stainless steel micro components fabricated from 5-µm powder by using cold isostatic pressing method and sintered at 1200^{o}C in vacuum atmosphere: (a) micro gear, (b) micro piston and (c) micro linkage rod. 99

Figure 6.10. SEM images showing the stainless steel micro components fabricated from 10-µm powder using pressure less filling method and sintered at 1200^{o}C in vacuum atmosphere: (a) micro gear, (b) micro piston and (c) micro linkage rod. 100

Figure 6.11. SEM images showing the stainless steel micro components fabricated from 16-µm powder using pressure less filling method and sintered at 1200^{o}C in vacuum atmosphere: (a) micro gear and (b) micro linkage rod. 101

Figure 6.12. Optical and SEM images showing the stainless steel micro components fabricated from 5-µm powder using pressure less filling method and sintered at 1200^{o}C in nitrogen/hydrogen mixture atmosphere: (a) optical image of micro engine assembly and (b) SEM image of micro engine cylinder assembly. 102

Figure 6.13. SEM images showing the stainless steel micro gears fabricated from 5-µm powder using pressure less filling method and sintered at 1200^{o}C in nitrogen/hydrogen mixture atmosphere: (a) micro gear and its teeth side walls and (b) two gears engaged to each other. 103

Figure 6.14. Optical images showing: (a) spur gears have 12 mm pitch diameter and fabricated from: SU-8 material and stainless steel green and sintered materials fabricated from 5-µm powder using pressure less filling method, and (b) different sintered stainless steel components fabricated from 5-µm powder using pressure less filling method. 105

Figure 7.1. SEM images showing the top view of micro gear components fabricated in: (a) SU-8 and (b) sintered stainless steel materials. 109

Figure 7.2. Images showing: (a) Vector Beta Grinder/Polisher machine and (b) aluminium holder containing the micro gears after polishing. 111

Figure 7.3. Images showing: (a) MicroMet 5100 Series Micro indentation Hardness Testers and schematic diagrams of: (b) diamond indenter with pyramid shape and (c) square impression. 112

Figure 7.4. A schematic diagram showing stereo imaging technique. 115

Figure 7.5. The effects of sintering temperature on the density of the sintered stainless steel micro components fabricated in different powders using two filling methods and sintered in: (a) nitrogen/hydrogen mixture and (b) vacuum. 118

Figure 7.6. The effects of sintering temperature on the linear shrinkage of the sintered stainless steel micro components fabricated in different powders using two filling methods and sintered in: (a) nitrogen/hydrogen mixture and (b) vacuum. 119

Figure 7.7. Optical images of the micro indentation marks of the stainless steel micro components fabricated from different powders and sintered at 1200^{o}C in: (a) nitrogen/hydrogen mixture atmosphere and (b) vacuum. 122

Figure 7.8. Optical images of the micro indentation marks of the stainless steel micro components fabricated from different powders and sintered at 1350^{o}C in: (a) nitrogen/hydrogen mixture atmosphere and (b) vacuum. 123

Figure 7.9. A graph showing the effects of sintering temperatures on Vickers hardness of stainless steel micro components fabricated from different powders and filling methods; and sintered in: (a) nitrogen/hydrogen mixture and (b) vacuum atmospheres. 124

Figure 7.10. A graph showing X-ray diffraction patterns of the stainless steel components fabricated from 5-µm powder and sintered in nitrogen/hydrogen mixture and vacuum atmospheres at 1200 and 1350^{o}C. 125

Figure 7.11. SEM images showing the surface morphologies of the stainless micro components fabricated from different powders and sintered in nitrogen/hydrogen mixture atmosphere at: (a) 1200^{o}C and (b) 1350^{o}C. 127

Figure 7.12. SEM images showing the surface morphologies of the stainless micro components fabricated from different powders and sintered in vacuum at: (a) 1200^{o}C and (b) 1350^{o}C. 128

Figure 7.13. SEM images showing the polished stainless steel micro components fabricated from different powders, and sintered in nitrogen/hydrogen mixture atmosphere at: (a) 1200^{o}C and (b) 1350^{o}C. 129

Figure 7.14. SEM images showing the polished stainless steel micro components fabricated from different powders, and sintered in vacuum at: (a) 1200^{o}C and (b) 1350^{o}C. 130

Figure 7.15. SEM images showing the top surface of the stainless steel micro components fabricated from 5-µm powder, sintered at 1350^{o}C in nitrogen/hydrogen mixture atmosphere and taken at two different tilting angles: (a) 0^{o} & (b) 7^{o}. (c) 3D surface profile constructed from the two SEM images using ALOCINA MEX software. 132

Figure 7.16. SEM images showing the top surface of the stainless steel micro components fabricated from 10-µm powder, sintered at 1350^{o}C in nitrogen/hydrogen mixture atmosphere and taken at two different tilting angles: (a) 0^{o} & (b) 7^{o}. (c) 3D surface profile constructed from the two SEM images using ALOCINA MEX software. 133

Figure 7.17. SEM images showing the top surface of the stainless steel micro components fabricated from 16-µm powder, sintered at 1350^{o}C in nitrogen/hydrogen mixture atmosphere and taken at two different tilting angles: (a) 0^{o} & (b) 7^{o}. (c) 3D surface profile constructed from the two SEM images using ALOCINA MEX software. 134

Figure 8.1. SEM images showing of the ceramic powders: (a) alumina and (a) titania. . 140

Figure 8.2. A graph showing the effect of dispersant on the green densities of ceramics based on alumina and titania powders..... 142

Figure 8.3. A photograph showing a turbula mixer used for pre-mixing stainless steel and alumina powders. 143

Figure 8.4. A schematic diagram showing the two mixing methods used for the preparation of stainless steel ceramic composite slurries: (a) dispersing-together method and (b) dispersing-separately method. 144

Figure 8.5. A graph showing the effect of composite compositions on the green densities of stainless steel alumina composites fabricated by using dispersing-separately and dispersing-together for 3, 6, 12 and 24 hours pre-mixed by turbula mixer..... 146

Figure 8.6. SEM images showing the fracture surface of green micro composites based on 10% alumina and fabricated by using: (a) dispersing-separately method and (b) dispersing-together method for 3 h pre-mixed by turbula mixer..... 147

Figure 8.7. The effect of composite compositions on the green densities of stainless steel titania composites fabricated by using dispersing-separately method. 148

Figure 8.8. SEM image of the fracture green micro composites based on 10% titania and fabricated by using dispersing-separately method..... 148

Figure 8.9. SEM image of the stainless steel ceramic composite green micro components fabricated by using dispersing-separately method and based on: (a) 10% alumina and (b) 10% titania..... 149

Figure 8.10. SEM images showing the stainless steel alumina composite micro components made of 10% of alumina and sintered in nitrogen/hydrogen mixture atmosphere at 1350^{o}C..... 151

Figure 8.11. SEM images showing the stainless steel titania composite micro components made of 10% of titania and sintered in vacuum at 1350^{o}C. 152

Figure 8.12. A graph showing the effect of composite composition on the density of the composite micro components fabricated from stainless steel alumina and titania; and sintered at 1350^{o}C in nitrogen/hydrogen mixture and vacuum atmospheres. 154

Figure 8.13. SEM images of polished composite micro components with: (a) 10% alumina and (b) 10% titania, sintered in nitrogen/hydrogen mixture atmosphere at 1350^{o}C. Black arrows showing some of the ceramic particles are loose in stainless steel matrix. 154

Figure 8.14. SEM images showing top views of micro gears: (a) SU-8 and (b) stainless steel alumina composite based on 10% alumina and sintered in nitrogen/hydrogen mixture at 1350^{o}C. 156

Figure 8.15. A graph showing the effect of composite compositions on the linear shrinkage of the composite micro components fabricated from stainless steel alumina and titania, and sintered in nitrogen/hydrogen mixture and vacuum atmospheres at 1350^{o}C. 156

Figure 8.16. SEM images of the polished stainless steel alumina composite micro components based on 10% of alumina, sintered in nitrogen/hydrogen mixture atmosphere at 1350^{o}C and fabricated by using: (a) dispersing-together and (b) dispersing-separately methods..... 158

Figure 8.17. SEM images showing the polished stainless steel alumina composite micro components fabricated by dispersing-separately method, based on different composite compositions and sintered at 1350^{o}C in: (a) nitrogen/hydrogen mixture and (a) vacuum atmospheres. 159

Figure 8.18. SEM images showing the polished stainless steel titania composite micro components fabricated by dispersing-separately method, based on different composite compositions and sintered at 1350^{o}C in: (a) nitrogen/hydrogen mixture and (a) vacuum atmospheres. 160

Figure 8.19. Optical images showing the micro hardness indentation marks on the surfaces of stainless steel alumina composite micro components sintered at 1350^{o}C in: (a) nitrogen/hydrogen mixture and (b) vacuum atmospheres. 162

Figure 8.20. Optical images showing the micro hardness indentation marks on the surfaces of stainless steel titania composite micro components sintered at 1350^{o}C in: (a) nitrogen/hydrogen mixture and (b) vacuum atmospheres. 163

Figure 8.21. A graph showing the effect of composite composition on the hardness of the composite micro components fabricated from stainless steel alumina and stainless steel titania, and sintered in nitrogen/hydrogen mixture and vacuum at 1350^{o}C. 164

Figure 8.22. Optical image showing the spur gears each of which has 18 teeth and 12 mm pitch diameter fabricated from stainless steel, stainless steel alumina composite and stainless steel titania composite and sintered in nitrogen/hydrogen mixture atmosphere at 1350^{o}C 165

ABBREVIATIONS

MEMS	Micro electromechanical system
MST	Microsystems technology
IC	Integrated circuit
EDM	Electro-discharge machining
MIM	Micro injection moulding
CAD	Computer aided design
RIE	Reactive ion etching
CNC	Computer numerical controlled
FIB	Focus ion beam
TEM	Transmission electron microscope
PIM	Powder injection moulding
PDMS	Polydimethylsiloxane
IPA	Isopropyl alcohol
MAM	Methacrylamide
HMAM	Hydroxymethylacrylamide
TEMED	Tetramethylethylenediamine
AP	Ammonium Persulfate
CIP	Cold Isostatic pressing
TGA	Thermal gravimetric analysis
STA	Simultaneous Thermal Analyser
MMC	Metal matrix composite
ODS	Oxide dispersion strengthening

CHAPTER 1. INTRODUCTION

1.1. Introduction

The research work presented in this thesis is an investigation to the fabrication of micro machine components from stainless steel powders and stainless steel based composite materials by combining both Softlithography and powder metallurgy processes. It is a part of the efforts to develop processes of producing high temperature resistant micro components for micro-engines, a project lead by Dr. K. Jiang at University of Birmingham. The design of a micro engine requires its components to be high precision, both in geometry and in dimension. Some of the early micro-engine research adopted silicon components fabricated using deep reactive ion etching process; a popular MEMS process attempted at MIT and Berkley [1-4]. However, the poor temperature resistant property of silicon makes it unsuitable to work in high temperature conditions. Stainless steel and its composites are some of the promising materials for such applications [5]. In addition, high precision metallic components can find wide applications from luxury watches and precision gauges to biomedical devices and instruments. Therefore, the research is both needed by a specific project and has potential for general applications.

1.2. Aims and objectives

The aims of this research were to develop a high precision fabrication process to break the limit of traditional silicon-based micro fabrication technique and test the approach for stainless steel and composite materials. The proposed process started from making high precision master moulds in non-metallic materials using micro-electro mechanical system (MEMS) technology. Then soft moulds are fabricated from the masters. Final components

are achieved by sintering green patterns formed from stainless steel and composites. Both pressure-less and cold isostatic pressing methods can be applied to achieve high precision and improve properties of micro components.

The main challenges in using Softlithography and powder metallurgy processes are shape retention and high shrinkage accompanied by sintering process, which affects the precision of the micro components. The planned fabrication processes to be investigated includes testing of three different stainless steel powders of different particle sizes to obtain the optimum properties. In order to reduce the shrinkage, a cold isostatic pressing technique will be investigated. Stainless steel-ceramic composites micro components was also fabricated and studied. The target micro engine components to be fabricated in this research are micro gears, micro linkage rods, micro pistons and micro engine cylinders. The minimum feature size is the tip of micro gear teeth, which measures ~ 75 µm.

To reach these aims, the following objectives are identified for implementation.

1. Fabrication of high quality SU-8 master moulds and their negative replicas soft moulds using Softlithography processes.
2. Selection of the powders and binder suitable for the preparation of metallic and composite slurries.
3. Optimization of slurry properties in order to obtain high density packing of the green micro components.
4. Using the cold isostatic pressing technique to improve the density and the linear shrinkage of the micro components.
5. Characterization of the sintered micro components in terms of shape retention, density, linear shrinkage, microstructures and porosity, micro hardness and surface roughness.

6. Fabrication of 316-L stainless steel-ceramic composite micro components.

1.3. Thesis outline

Chapter One is the introduction of the thesis, including the aim, objectives and thesis outlines. Chapter Two presents a literature review of micro fabrication techniques relevant to the contents presented in this thesis and a comparison between the techniques. The detailed fabrication processes of SU-8 master moulds and their negative replicas soft moulds are given in Chapter Three. Chapter Four explains the study of powders and binders selections used in this research. Chapter Five presents the preparation and optimization of the stainless steel slurries and the production of the green micro components using pressure-less and cold isostatic pressing processes. Chapter Six provides the details of the de-binding and sintering processes of the green micro components using different atmospheres. Chapter Seven presents the characterization of the sintered stainless steel micro components, in terms of shape retention, density, linear shrinkage, internal structure, hardness and surface roughness. Chapter Eight presents the detailed fabrication process of micro components in stainless steel ceramics composites. In Chapter Nine, the conclusions of the research are drawn and future work is discussed. Finally, a list of publications produced from this PhD research is presented.

CHAPTER 2. LITERATURE REVIEW

This Chapter is a summary of the literature review on current fabrication techniques of micro components. The applications and limitations of each fabrication technique are discussed. It presents a general literature review of current fabrication techniques of micro components in various materials, while leaving more background details closely related to the specific techniques adopted in this research to the following chapters.

2.1. Introduction

In the fabrication of micro components, many processes are borrowed from the micro electro mechanical system (MEMS) industry, others are developed for specific applications. A micro electromechanical system is a system consisting of sensors, actuators or devices with dimensions starting from just a micro meter. The acronym MEMS was coined in the United States in the late 1980s, while in Europe the name Microsystems Technology (MST) is used. [4].

MEMS has been used in different areas, including pressure and biomedical sensors, ink jet printers, drug delivery systems, wireless electronics, radio frequency (RF) and processing devices, [6-7]. According to the technical market research report, the global market of MEMS devices was worth an estimated $5 billion in 2005 and it is expected to increase to $12.5 billion through 2010 [8]. Conventional integrated circuit (IC) processes that include lithography, deposition and etching techniques dominated the fabrication of MEMS devices and components. Silicon and its relevant materials such as silicon oxides, silicon nitrides and silicon carbides are usually used as base materials in the most IC fabrications due to the availability in cheap values and functionally adopted with the electronics. While,

other metals such as gold, aluminium, titanium, tungsten, and copper in addition to polymers are incorporated with the silicon wafer to fabricate different micro structures for the electronic applications [9-11]. Due to the demands for different applications, different materials have expanded outside the silicon domain, which includes various types of metals, ceramics and polymers in response to the development of micro fabrication techniques. The micro fabrication techniques are listed under two categories: traditional MEMS techniques (lithographic processes), such as photolithography, silicon micromachining, LIGA etc., and non-lithographic methods, such as electro-discharge machining (EDM), hot embossing, micro machining, laser micromachining, micro injection moulding (MIM) and Softlithography . These techniques are reviewed in the next sections [6-12].

2.2. Photolithography

Photolithography is a process of transferring geometric shapes from a certain mask created from the data held by the computer aided design (CAD) package to light sensitive materials called photoresist, casted on a substrate, using a light source. The origin of this technique is dated back to Nicéphore Niépce, a French scientist, 1822 [13]. He successfully transferred an image to a glass plate covered with a mixture of lavender oil and bitumen (asphalt) [14]. The process is performed by placing an oil-painted paper on the top of glass plate and exposed it to the sun. Afterwards, the illuminated areas are hardened and the unexposed areas were dissolved by using turpentine oil solution. This process is later called the photolithography technique. Typically, ultraviolet (UV) is widely used in the lithographic process due to its low cost source. However, electron beam and X-ray are other sources of high costs due to the expensive beam lines, which are not available to

many researchers. The schematic diagram of the photolithography principal is illustrated in Figure 2.1. The aim of this process is to transfer two-dimensional features printed on a mask into a three-dimensional pattern of photoresist material. The main steps include deposition of the photoresist on top of a silicon wafer, soft baking, exposure to UV light, and development process on which the un-exposed or exposed area is dissolved by a chemical developer, depending on the type of photoresist materials. All the steps are done in a clean room. The mask is normally produced from a chromium pattern on a glass or quartz plate. The chromium is opaque to UV light and quartz is transparent. The wafer is cleaned and coated with a photoresist material sensitive to UV light. The photoresist is exposed to UV light through the mask and then developed in order to transfer the pattern from the mask onto the photoresist. There are two basic types of photoresists: positive resists and negative resists. In the positive resists, the chemical bonds within the resist are weakened when exposed to UV light, while they are strengthened in negative resists. As a result, after developing, the exposed area is dissolved in the former type, while the unexposed area is dissolved in the later one. Much detail of the photolithography technique can be found in [10, 14–17]. Although, the process is successful in producing different structures from a few microns to over 1mm thick, it is still limited to polymeric materials (photoresist) such as, SU-8, Shipley, AZ, KMPR and PMGI [18-23]. A few research activities are on-going to incorporate nano particles into the SU-8 photo resist in order to fabricate SU-8 composite based components with improved properties and reduced the stress and cracks [24-25].

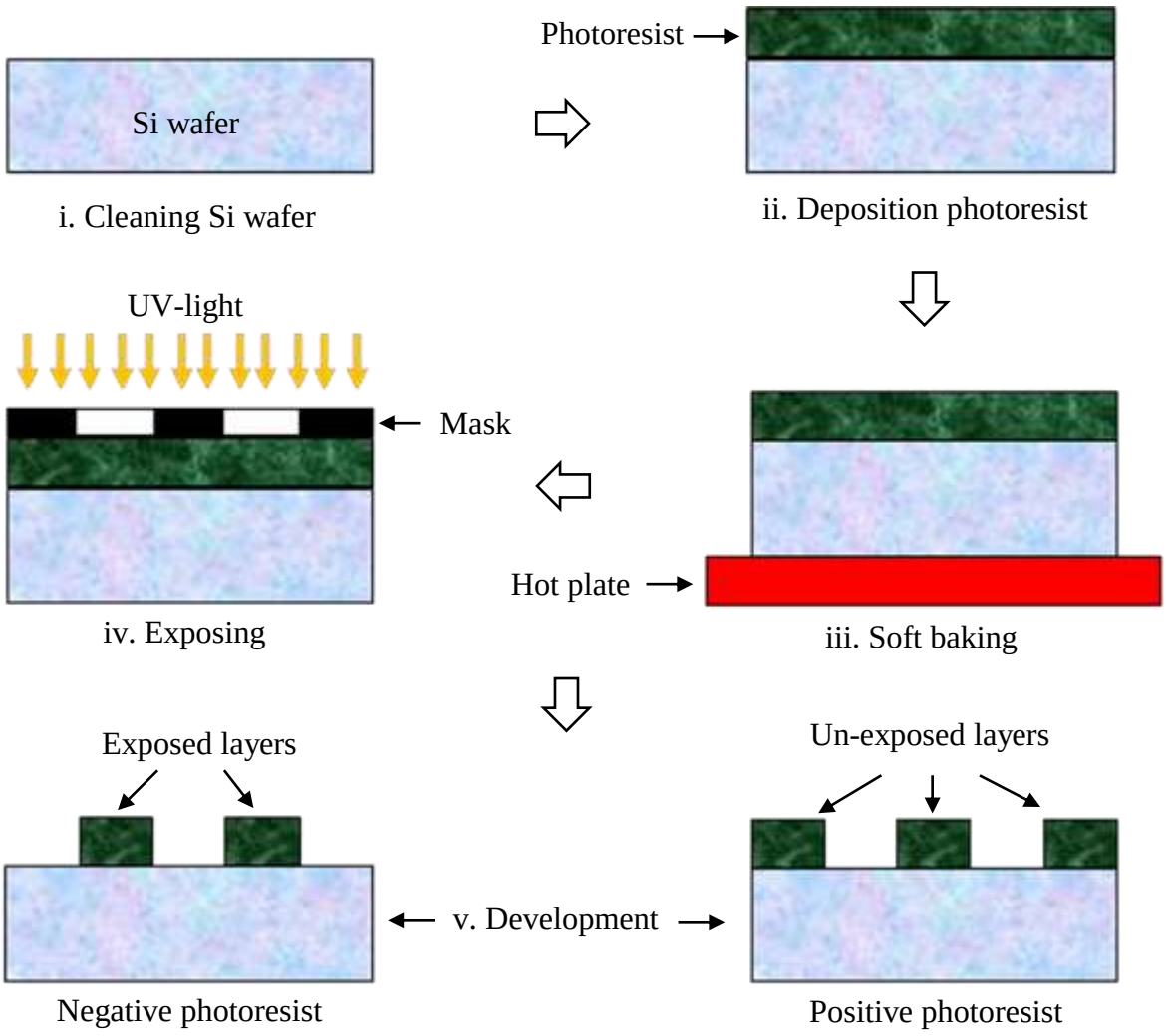

Figure 2.1. A schematic diagram showing the complete photolithography procedures.

2.3. Silicon micro machining

Micromachining of silicon-based devices shows a similarity to conventional machining in forming features in blocks of materials. However, there are distinct differences between them. In the silicon micromachining process, a great number of identical elements can be fabricated simultaneously on the top of the same wafer and dozens of wafers can be processed at the same time. Moreover, the minimum feature size in a range of 1 μm can be fabricated, which is difficult to fabricate using conventional micro machining [4]. The machining process includes material deposition on the top of silicon wafer, patterning and

etching techniques. In order to obtain very thin films of different materials deposited over the silicon wafer, a number of different techniques that facilitate the deposition are used, such as thermal oxidation, sputtering and chemical vapour deposition (CVD) [26-31]. The materials commonly deposited over the silicon wafers or other suitable substrates are silicon dioxide, silicon nitride, polycrystalline silicon, aluminium and some noble metals such as gold. Photolithography process is served as a mask for etching oxide film deposited over the wafers, through which a layer of photoresist is formed over the oxide film. Etching is a process of removing the oxides or metallic layers deposited on the silicon wafer using various etching processes. Etching can be in a form of wet or dry. In wet etching process, the materials are removed by immersing the wafer in a liquid bath of the chemical etchant [32-33]. On the dry etching process, the materials can be removed by using reactive ion etching (RIE) as a chemical processes or ion beam milling as a purely physical process [34-35]. Figure 2.2 shows a schematic diagram of the silicon machining process. Silicon micro-machining involves only silicon-based materials, which are restricted to a very narrow range. Although silicon-based materials are easily machined with microelectronic processing techniques they have obvious disadvantages over metal materials when they are used as the structuring material.

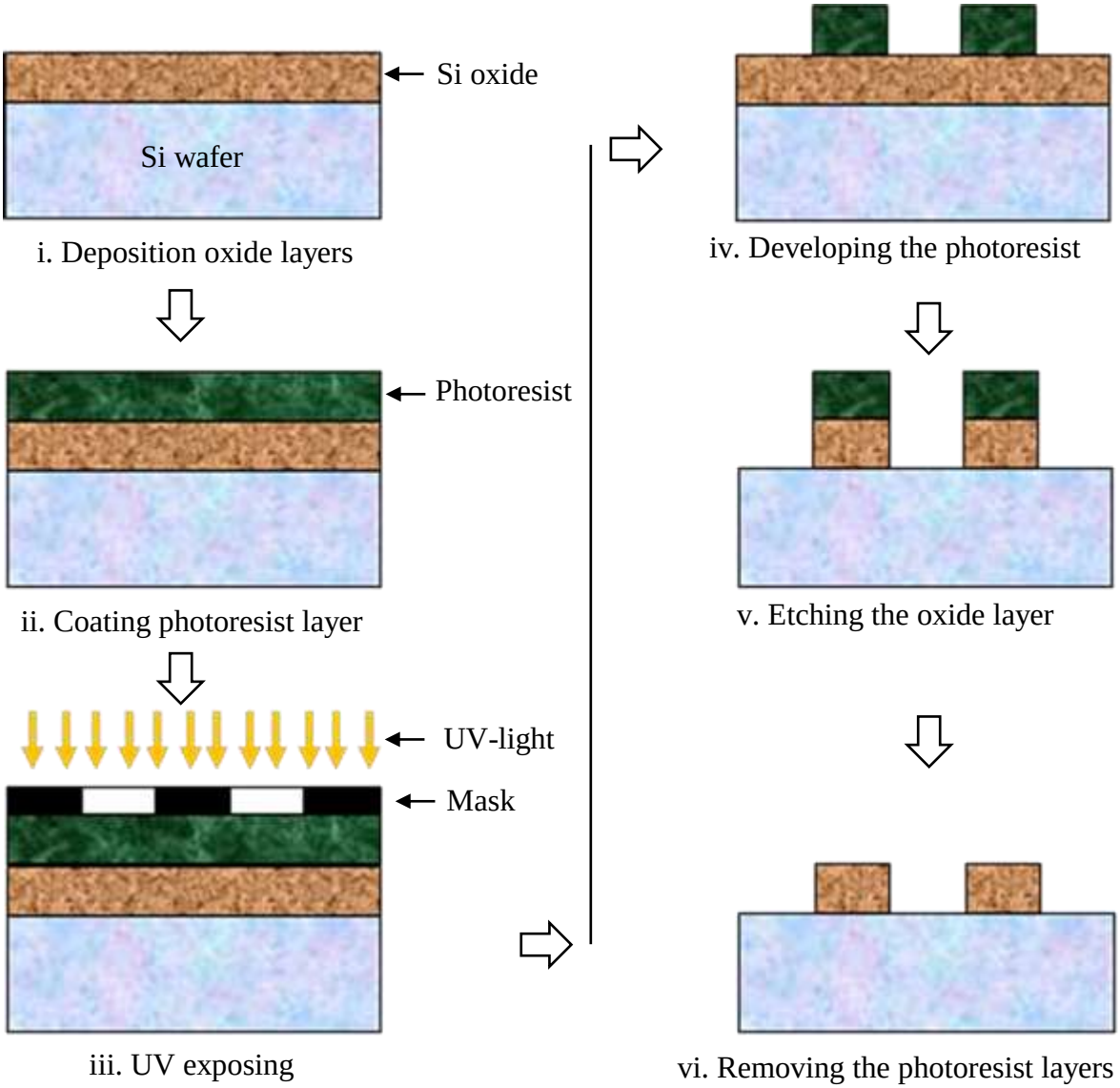

Figure 2.2. A schematic diagram showing the silicon micro machining process.

2.4. LIGA technique

LIGA is an acronym of a German word for lithography, electroforming, and moulding. In this process, high aspect ratios and great structural height are produced based on the combination of synchrotron radiation lithography, galvanoforming and plastic moulding [36]. There are two types of LIGA techniques depending on the radiation and perform used: X-Ray LIGA and UV-LIGA. In the former technique, X-ray is produced by using

synchrotron, while in the later one, UV rays are produced using a mercury lamp. In both cases the photoresist is shone and developed following the photolithography process discussed in section 2.2 and then, the metallic structures are electroplated in the removed resist areas. Figure 2.3 shows a schematic diagram describing the LIGA process [37]. It is noted that the LIGA process combines two techniques: photolithography and electroforming. The photolithography process is used for producing template moulds and electroforming is used for producing metallic structures on the templates. Different metallic structures are electroplated using the LIGA process such as copper [38], gold [39] and nickel, which is commonly used in this technique [40-41]. Figure 2.4 (a) and (b) show examples of using the LIGA process for producing SU-8 and nickel micro structures, respectively [42]. Although the LIGA process is based on the lithography and electroforming processes to build up the micro components over the wafer, a few ranges of materials are used so far. It is also showing a disadvantage of producing metallic structures with thick side-walls due to the very low deposition speed of electroforming. To obtain 1mm thick, five continuous days are need [23]. However, a new process is provided to electroform nickel-alumina micro composite, but so far, the composition of the alumina content is very small when compared with nickel and is difficult to be control [43].

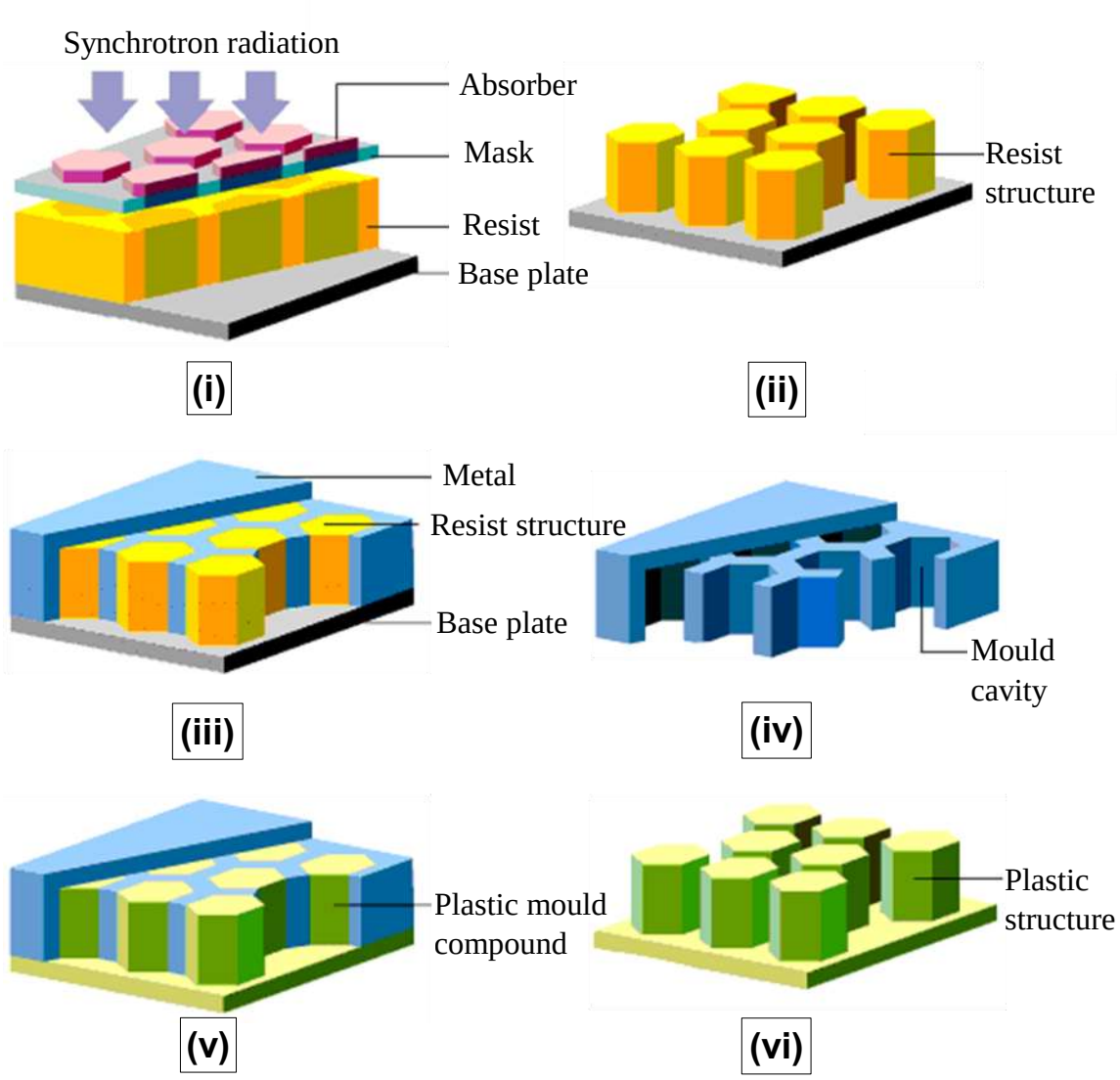

Figure 2.3. A schematic diagram showing the LIGA fabrication processes: (i) synchrotron irradiation of photoresist, (ii) development of exposed photoresist, (iii) electroforming of metallic microstructures, (iv) making of mould insert, (v) mould filling and (vi) de-moulding [38].

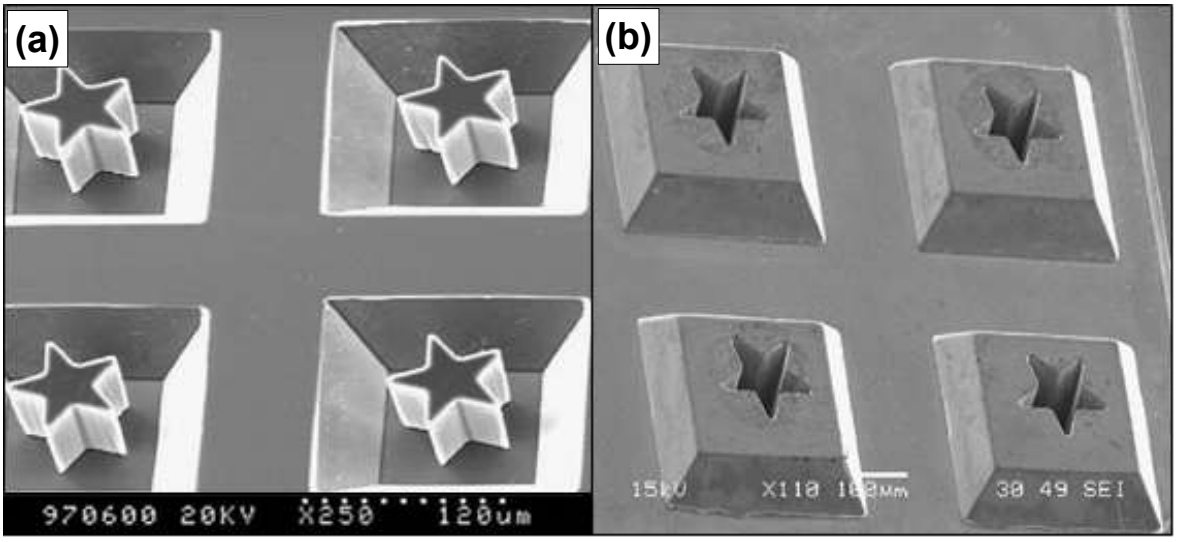

Figure 2.4. SEM images showing the micro components fabricated by using UV-LIGA process: (a) SU-8 micro master mould over silicon wafer and (b) Nickel negative replica after removing SU-8 moulds [43].

2.5. Laser micro machining

Laser micro-machining is a non-lithographic fabrication process. The laser beam is emitted in narrow and low divergence well-defined wavelengths with high power that can remove materials such as fine particles and vapour from a substrate. Laser is operated in the pulsed mode in which the materials are removed with each pulse. The amount of material removed depends on the material itself, the length of the pulse, and the intensity of the laser light. The desired shape is produced and controlled by using chromium on a quartz mask that is placed in contact with the material being machined, and then the laser light is shone through it. Material is removed where the laser light strikes it. Laser machining is used in different applications such as spectroscopy, material processing, medicine, military, industrial, and MEMS applications [44]. In micro fabrication, laser plays a big role in cutting, drilling, etching materials such as plastics, glass, ceramic and thin metals with dimensions from 1 micron to 1 mm [45-50]. Laser micromachining has a capability of

producing micro structure by machining different materials with vertical and tapered sidewalls, but it produces some problems in the micro features such as the induced stress and heat-affected zone [51-52]. Figure 2.5 (a) and (b) show a schematic diagram of laser micromachining process and micro gear structure with internal teeth on a silicon wafer [53].

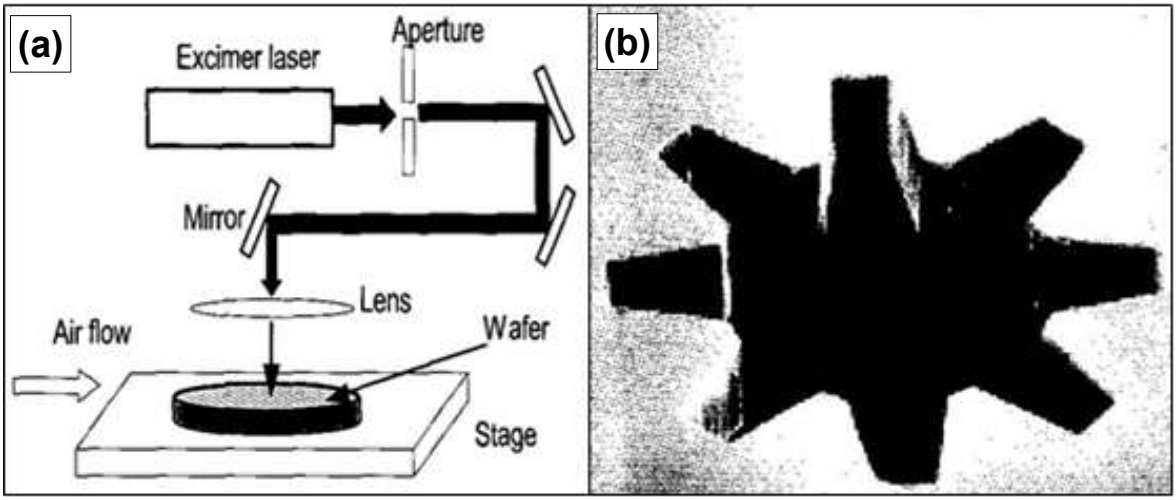

Figure 2.5. A schematic diagram showing: (a) laser micro machining process and (b) SEM image of micro gear with internal teeth machined using lased micro machining [54].

2.6. Electrical discharge machining

Electrical discharge machining is a non-lithographic process in which an electrical discharge is formed between the electrode (machine tool) and the work piece to erode the materials from work piece. Micro-EDM is the machining process developed from EDM for the fabrication of the micro components. Micro-EDM is categorised into three types: hole boring, shaped working electrode and wire EDM [10]. Figure 2.6 show a schematic diagram of the three micro-EDM types [10]. For both hole boring and shaped working electrode, the electrodes are degraded during usage; therefore they are replaced during the process. These types are successfully used for the production of different features with

micro sizes [54-57]. On the other hand, Micro-wire EDM is developed to fabricate high accuracy 3D microstructures. Through this process, the working electrode is a wire which is continually drawn through the work piece [58-60]. Therefore, there is always a new part of the electrode available for the machining. Micro-EDM produces a good micro fabrication process of different miniature components [61-63], when the work piece material is too hard or the desired shape cannot easily be conventionally machined. However, the process is limited to the conductive materials. Electrode wear is another issue affecting the final machined parts. Figure 2.7 shows the SEM images of the high aspect ratio WC-Co (tungsten carbide super hard alloy) fabricated by LIGA and micro-EDM processes in which the electrode is fabricated using LIGA process [64]. The electrode is changed three times during the process due to the occurrence of wear, as seen in Figure 2.7 (b) and (c). Heat affected zone is another problem always accompanied with EDM due to the high temperature charge formed [8000–12000^{o}C]. However, the parameters affecting the EDM process is studied to improve the quality of the micro features [65].

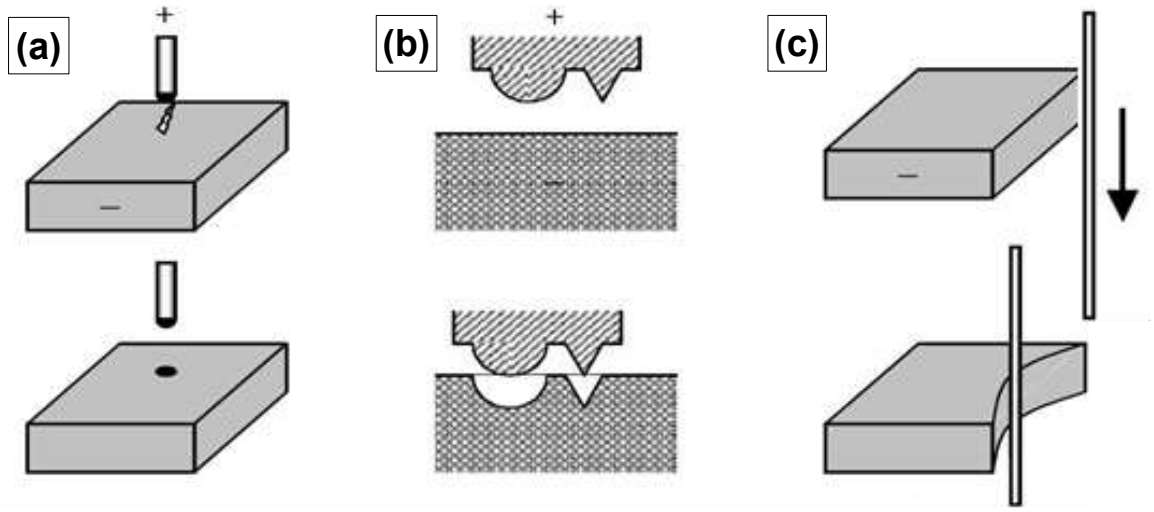

Figure 2.6. A schematic diagram showing the three types of the micro-EDM: (a) hole boring, (b) shaped working electrode, (c) wire EDM [11].

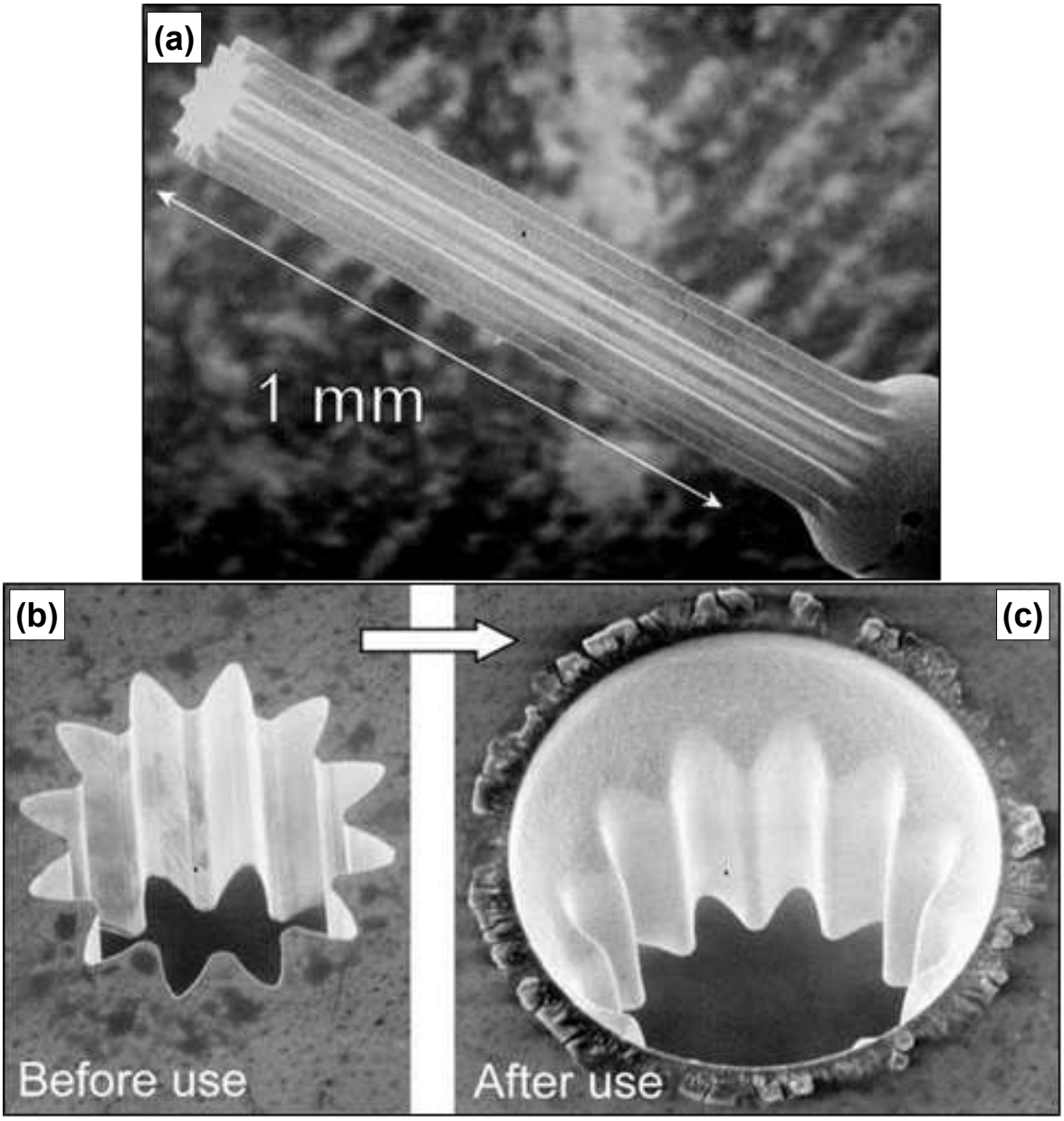

Figure 2.7. SEM images showing the WC-Co micro structure: (a) 1 mm gear pattern and initial shape of the patterned negative type electrode: (b) before use and (c) after use [65].

2.7. Hot embossing

Hot embossing is a simple process for mass production of different sizes of components. The process starts by producing the mould insert using one of the various methods, such as micromachining, computer numerical controlled machine (CNC), LIGA and EDM. Afterwards, both polymeric materials and the mould insert are heated until the target materials are softened, and then the mould inserts are pressed into the surface of the polymer material so that it takes up the impression of the model structure. After cooling, the stamped pattern is obtained by de-embossing. Figure 2.8 shows the hot embossing process [66]. Although the process is successful in producing a wide range of micro components from different polymeric materials [66-69] it is limited in the fabrication of other materials, such as metals and ceramics.

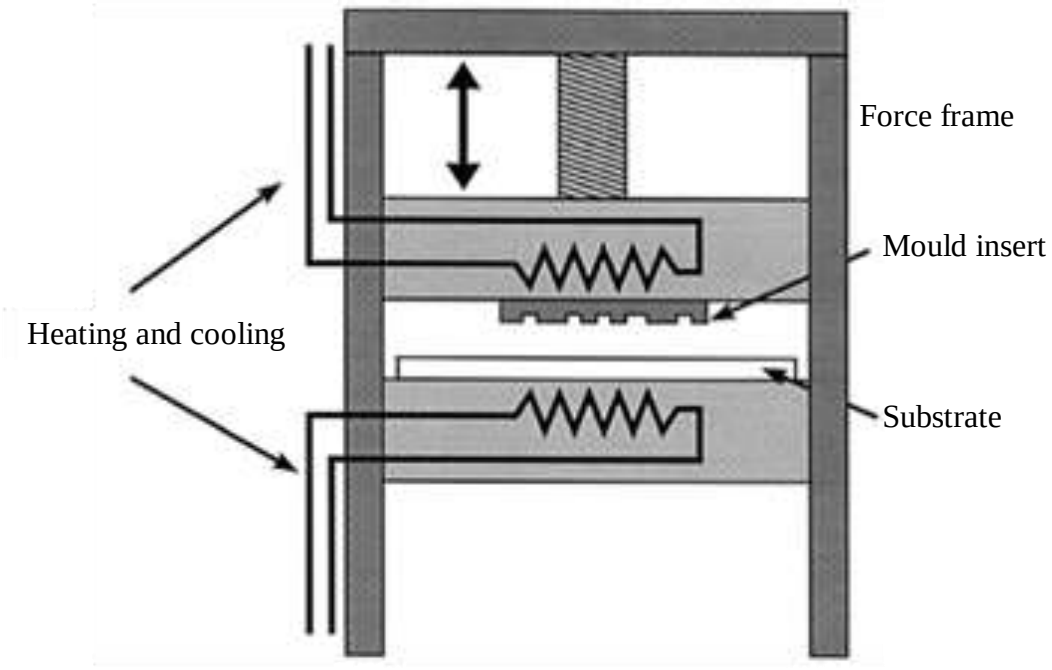

Figure 2.8. A schematic diagram showing hot embossing equipment [67].

2.8. Micro machining and micro milling

Cutting tools such as mills, lathes, and drills have been in use for the production of macroscopic components with different shapes for over a century. Recently, many micro features are machined from metals and silicon to a desired shape with some features smaller than 10 μm using modern computer numerical controlled (CNC) machines with sharply tipped diamond-cutting tools [70-71]. The applications for using CNC machines include optical mirrors and computer hard drive disks. Micro milling is a very versatile technique for producing the 3D micro scale features when complicated feature geometry is needed. A wide range of materials, including metallic materials and metal alloys, can be machined. Focus ion beam (FIB) is a milling technique used for milling various micro structures. As the ion beam hits the surface of the sample it sputters a small amount of material in the form of ions or neutral atoms; therefore micro or even nano feature is shaped. Because of the ability of FIB to remove atoms from the surface of materials, it is used as a micro machining tool for different applications such as transmission electron microscope (TEM) [72], oblique sub-micron cut [73], micro cantilever beam [74] and different silicon micro milling [75]. Figure 2.9 shows the milled membrane for TEM study using FIB [71]. However, the FIB is a promising technique of milling micro and nano structures; the material removal in the form of atoms or ions makes it a very slow milling process.

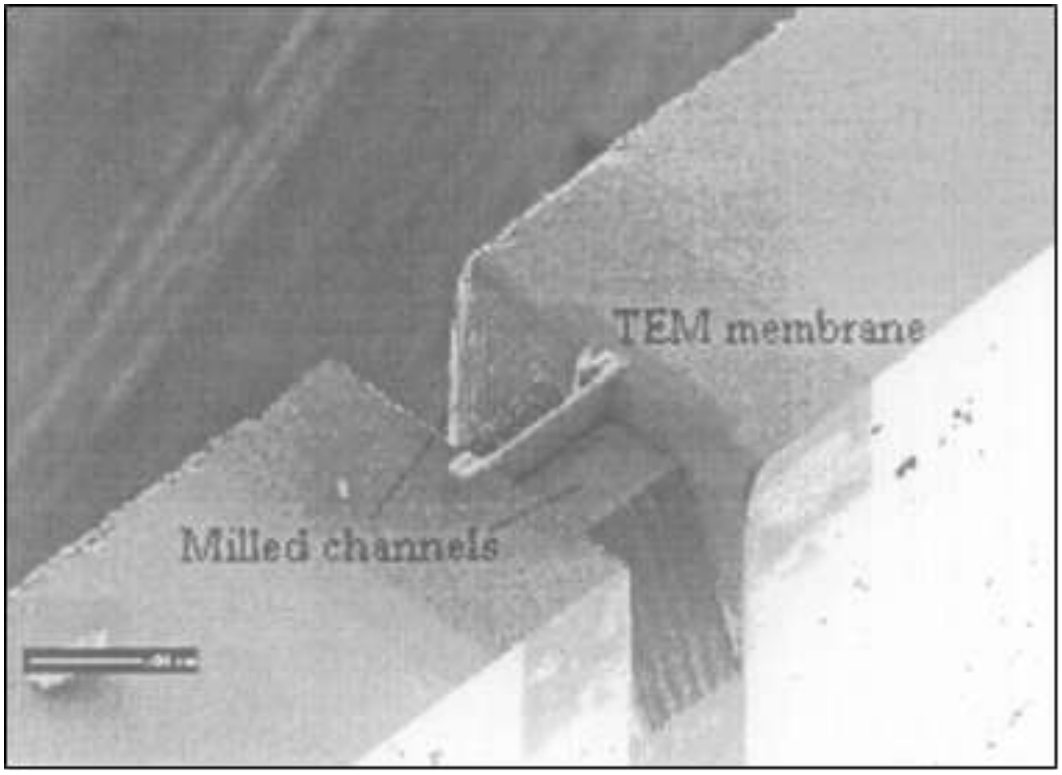

Figure 2.9. SEM image showing a milled membrane by using FIB for TEM study [73].

2.9. Micro Metal injection moulding (µMIM)

Powder injection moulding (PIM) is an economical method of producing components from polymers, metals and ceramics, which is developed from plastic injection moulding. It has the advantages of plastic injection moulding and the powder metallurgy process of producing flexible designs and a wide range of materials. This technique is called metal injection moulding (MIM) or ceramic injection moulding (CIM) when the metal or ceramic powders are used, respectively. The fabrication process includes mixing powder and binder, injection moulding, de-binding and sintering. Figure 2.10 show a schematic diagram of the detailed fabrication process of PIM technique [76]. Micro metal injection moulding (µMIM) is an emerging technique developed from PIM to produce miniature components. The process depends on solid micro mould insert, so it is always dependent on other micro fabrication techniques to fabricate those moulds, such as LIGA, EDM and

CNC. Like PIM, the fabrication process includes the same procedures. The first micro metallic components fabricated by µMIM were reported in [77-78]. However, the technique is developed further to include a wide range of materials, such as stainless steel [79], alumina [80] and tungsten [81]. Although µMIM is an economical micro fabrication process, there are still some technological aspects to be addressed, including better feedstock with smaller particle size, mould insert with longer lifetime and better surface quality of the sintered microstructures, reduction of tolerances in shrinkage due to sintering and improved economic efficiency [82-86].

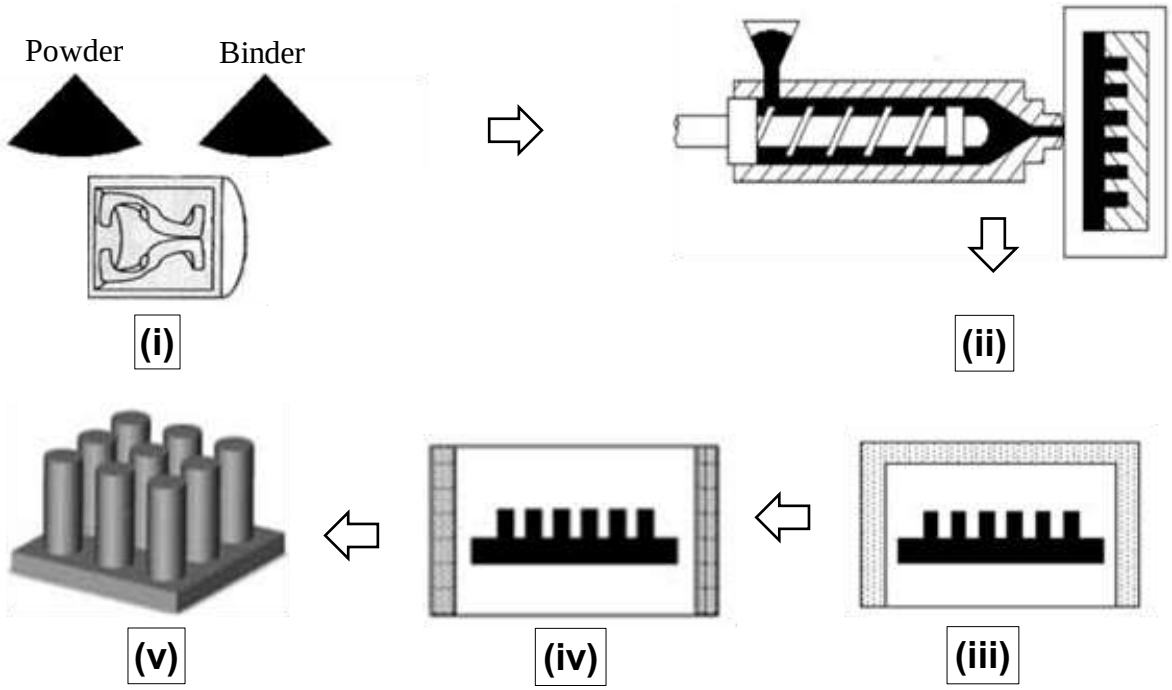

Figure 2.10. A schematic diagram showing the processing procedures of PIM technique: (i) mixing, (ii) injection moulding, (iii) de-binding, (iv) sintering and (v) microstructure [87].

2.10. Softlithography technique

Softlithography is a process of shaping three dimensional micro components by using a soft mould insert. It was developed as a new approach to fabricate micro components for optical system [88], micro fluidic system [89] and microelectronic devices [90]. More recently, soft lithography has used for producing pure epoxy and epoxy-based composite micro components [91-93]. The combination of Softlithography and powder metallurgy processes is used successfully in the production of micro components from different metallic and ceramic materials [94-99]. The process is similar to that presented in the micro metal injection moulding process in using powder metallurgy process for producing material slurry or paste, filling the soft micro mould, obtaining the green micro components, de-binding and sintering. It also shows a similarity to using the other micro fabrication techniques to produce the master moulds. The main different between Softlithography and micro metal injection moulding is the type of mould inserts used. In the former technique the mould inserts are always soft mould, usually Polydimethylsiloxane (PDMS), while in the later one, rigid mould inserts are used. Figure 2.11 shows the schematic diagram of the complete soft moulding process. Due to the ability of the PDMS moulds to produce a high impression replica of the master mould, the quality of the shaped micro components depends on the quality of their corresponding master moulds. Although soft moulding is a simple and low cost micro fabrication process applicable to a wide range of materials and patterns, it is still under development. Because the soft moulding process requires additional processes, such as de-binding and sintering, the process needs more investigation to address different issues such as shrinkage accompanied by sintering processes.

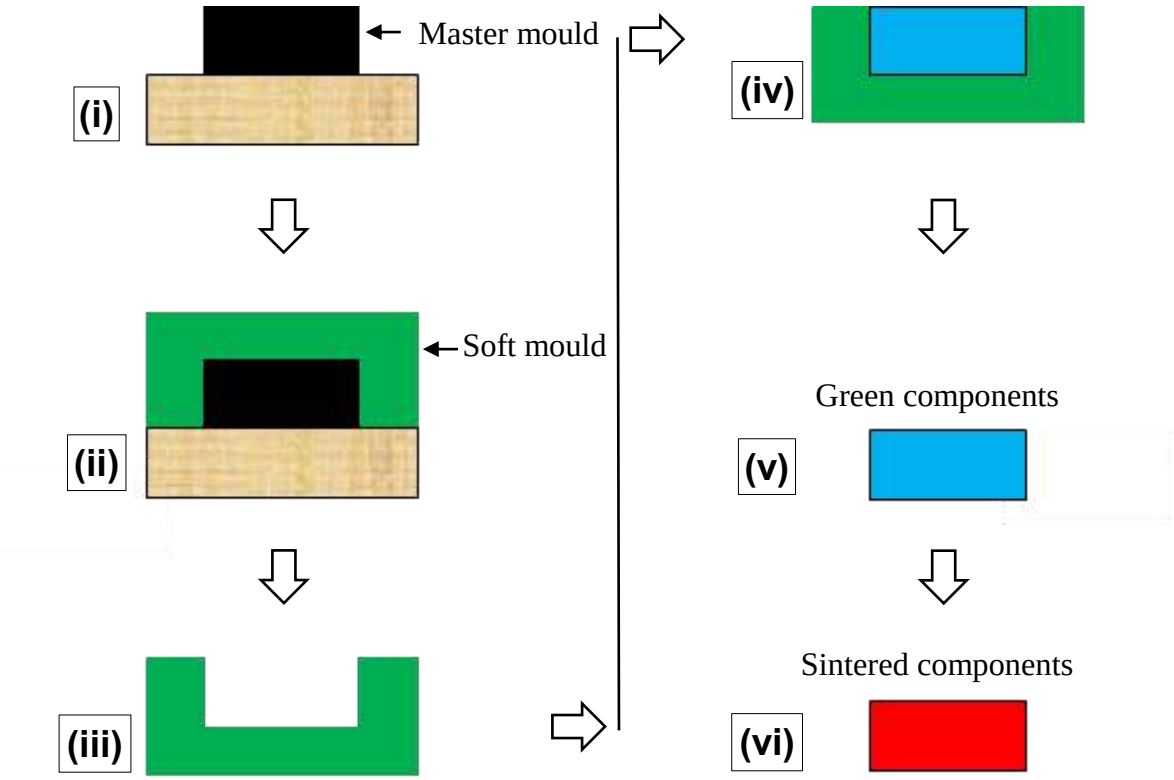

Figure 2.11. A schematic diagram showing the soft moulding processes: (i) preparing master mould, (ii) replicating by soft mould, (iii) obtaining the soft mould, (iv) filling the soft mould by slurries, (v) de-moulding and obtaining green components and (vi) sintering.

2.11. Summary

In this chapter, several micro fabrication techniques for the production of the micro scale components are discussed. Some of them are combined with others to fabricate micro components such as LIGA, μMIM, Softlithography and silicon micro machining, while EDM, laser micro machining, CNC and FIB can fabricate micro structure without combination with other techniques. For both photolithography and LIGA processes, the materials fabricated are polymer and a restricted range of metals so far. While micro components can be fabricated with complex shapes using non lithographic techniques such as EDM, CNC and FIB, the material limitation and time consuming processes are the main

issue. For both µMIM and soft moulding, powder metallurgy based process, the techniques can be used for different types of monolithic and composite materials and they show a mass production process. In Softlithography process, the final linear shrinkage accompanied by sintering process which reach 22% of the master mould needs to be improved [87, 97].

CHAPTER 3. FABRICATION OF SU-8 MASTER MOULDS AND THEIR NEGATIVE REPLICAS SOFT MOULDS

This Chapter presents the first stage of this research, which includes the detailed fabrication process of SU-8 master moulds and their negative replicas soft mould inserts. The optimization of the SU-8 micro moulds and their negative replicas soft moulds in terms of high quality and straight side walls is investigated in detail.

3.1. Production of SU-8 master moulds

SU-8 is a negative tone photoresist which was developed by IBM [100]. It is composed from three different components: EPON epoxy resin, organic solvent and photo-initiator [100-101]. EPON epoxy resin is responsible for high functionality and optical transparency while the organic solvent produces the viscosity of the solvent and determines the final thickness of the coated film. The function of the photo-initiator is to polymerize the EPON epoxy resin. The polymerization takes place when the photoresist mixture is exposed to ultraviolet light. The exposed mixture generates a strong acid which facilitates polymeric cross-linking during post exposure bake. The early fabrication process of SU-8 was performed by mixing the three components together with different ratios in a clean room [100-101]. While later, the SU-8 photoresist is produced as single component. It is used for producing the different structures from few microns to over one millimetre thick [102-105]. The most important SU-8 fabrication techniques are UV [106] and X-ray photolithography [107]. However, the X-ray process incurs much cost when compared with UV lithography due to the need to access to a synchrotron, which is not available to many researchers. SU-8 has good optical properties in the near i-light UV range 360-420

nm [108]. Therefore, homogeneous exposure from the top to the bottom layers can be obtained and ultra-thick micro patterns can be fabricated. These properties, in addition to excellent thermal stability, make it well suited for fabrication of master moulds. SU-8 2075 is the type of photoresist used in this research and its properties are presented in Table 3.1, supplied by Microchem, USA. Figures 3.1 and 3.2 show schematic diagrams of the micro engine components to be fabricated in this research and the complete fabrication process of SU-8-2075, respectively.

Table 3.1. The properties of SU-8 2075 as delivered by Microchem, USA [108].

Thermal properties		Physical and mechanical properties	
Glass transition temperature	210^{o}C	Tensile strength	60 (MPa)
Thermal stability	315^{o}C	Density	1.236 (g/ml)
Thermal conductivity	0.3 (W/mK)	Young's modulus	2 (GPa)
Coefficient of thermal expansion	52 (1/^{o}K)	Viscosity	22000 (cSt)
		Tensile strength	60 (MPa)

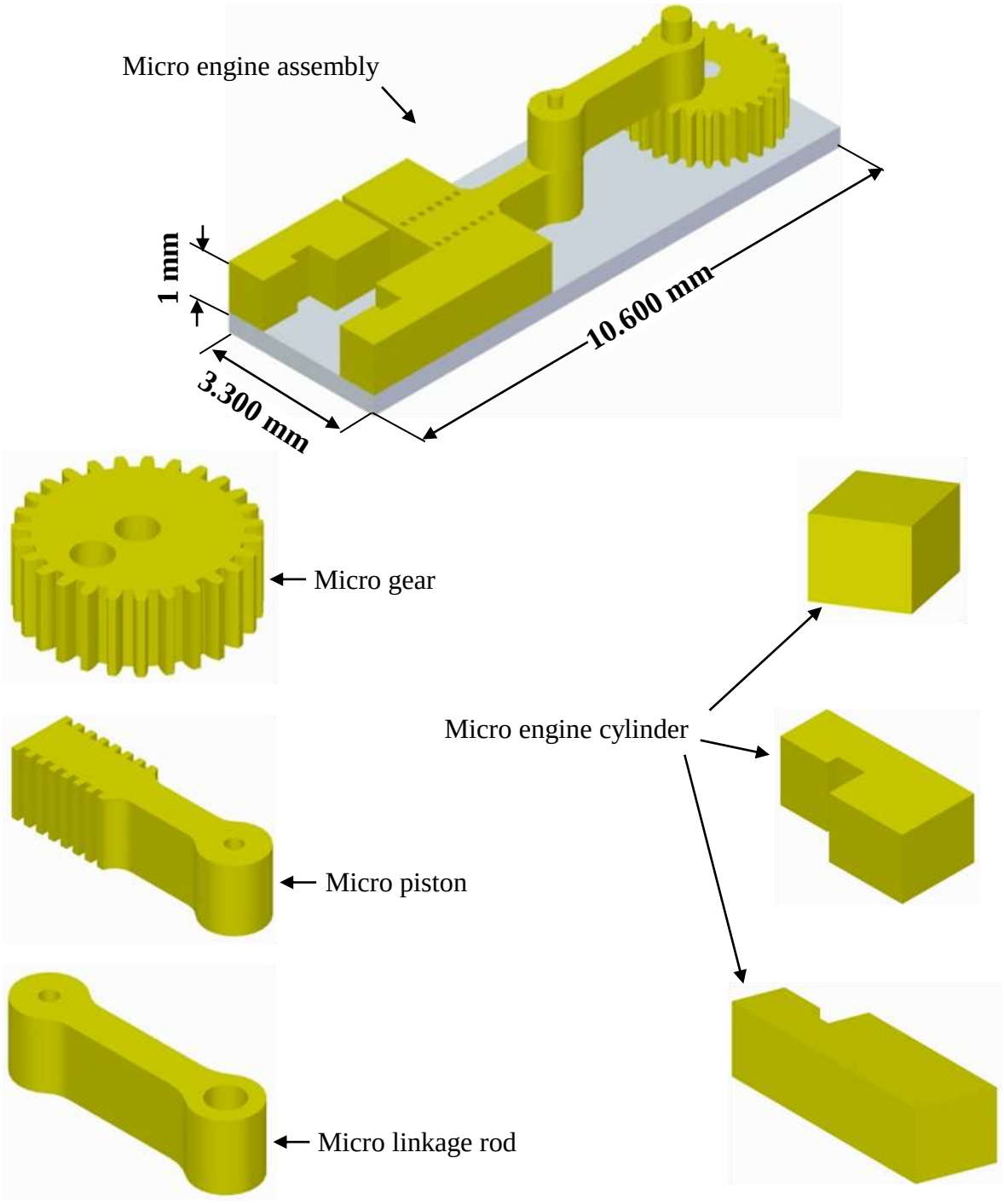

Figure 3.1. A schematic diagram showing the micro engine assembly with dimensions and the micro engine parts fabricated in this research, designed by Peng Jin [109].

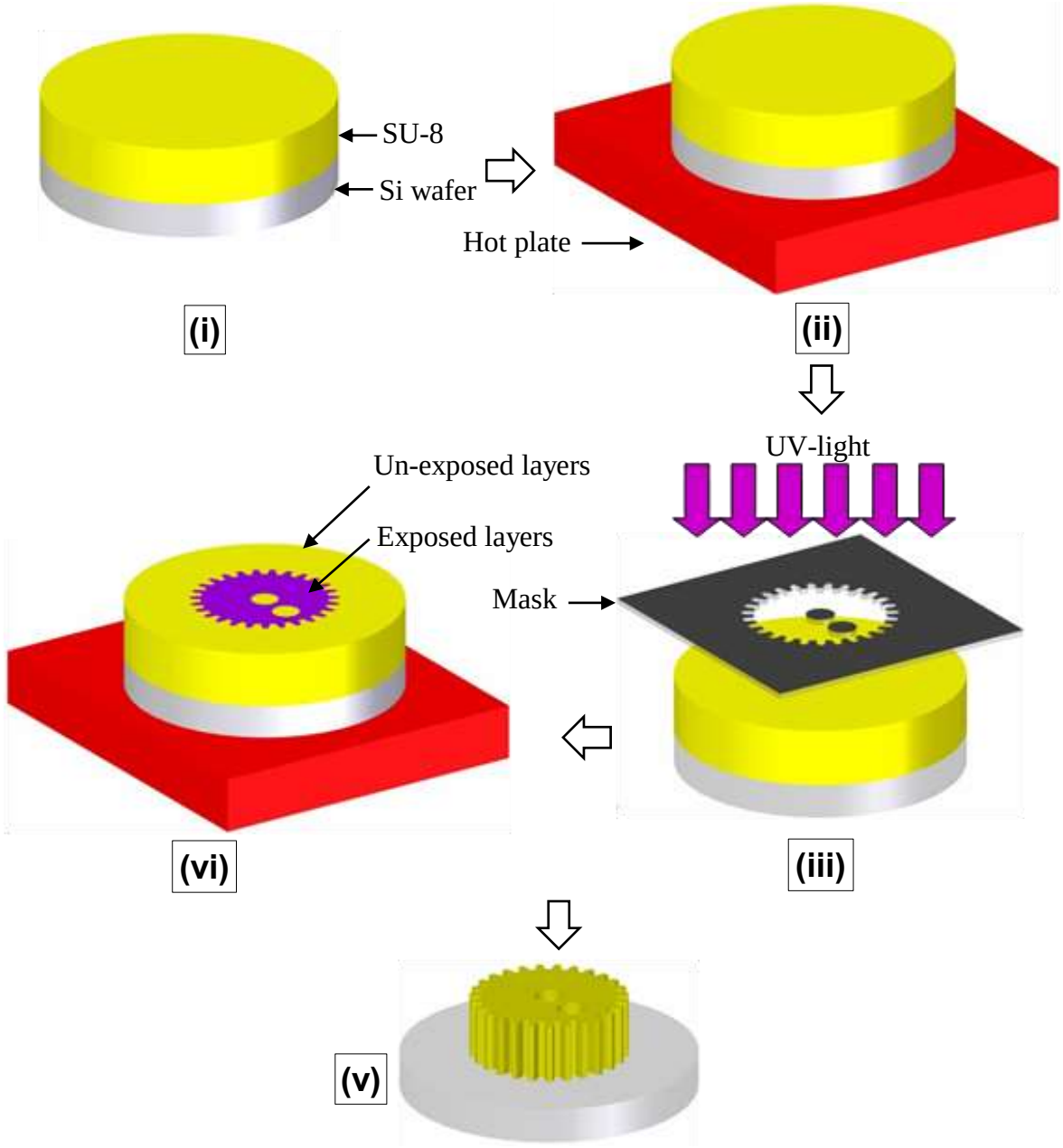

Figure 3.2. A schematic diagram showing the completed fabrication process of SU-8 master moulds: (i) casting SU-8 slurry over silicon wafer, (ii) soft baking, (iii) exposing to UV-light, (iv) post exposure baking (PEB) and (v) developing.

3.1.1. Procedures for production 1 mm thick SU-8 master moulds

The fabrication procedures of SU-8 master moulds were performed in a fume cabinet at the clean room under continuous ventilation to avoid contamination, which affects the properties of SU-8. The procedures needed to fabricate SU-8 master moulds are discussed in different literatures presented in SU-8 home page [105] and [109]. However, changing the SU-8 type and the desired thickness needs to change the procedures. As presented by Jin P. et al [109], the SU-8 micro engine components have been produced using SU-8 50 type with three different filters during exposure and the overall exposure energy is 24.530 J/cm^2. Therefore, the SU-8 fabrication process is modified in this research in order to fabricate high quality SU-8 2075 master moulds; the same quality as those produced by Jin P. et al [109] and to reduce the overall exposure process by using one filter instead of using three filters.

3.1.1.1. Mask design

All the micro components are designed using computer aided design (CAD) and printed to the mask substrate [109]. The mask consists of patterned opaque chromium on a transparent fused-quartz substrate.

3.1.1.2. Casting SU-8 over silicon wafer

The silicon wafer is firstly cleaned using acetone ACS reagent (≥99.5%) and isopropyl alcohol (IPA, 99.9%). Due to higher thickness needed ~1 mm, there is no need to use the spinner coating; hence, the SU-8 slurry is dispensed as one layer. Spinner coating is a machine containing a rotating disc on which the silicon wafer is put and SU-8 is distributed with desired thickness by centrifugal force. A proposed method used in this research to

control the final desired thickness is presented as follows: (i) calculate the theoretical SU-8 volume as a cylinder shape with 4" base diameter (4" silicon wafer) and 1 mm thick, (ii) after soft baking, the solvent is evaporated; therefore, the volume needs to be increased to compensate the evaporated solvent. The calculation is presented as follows:

$$V_{th} = A \times t \tag{3.1}$$

V_{th}: Theoretical volume,

A: Silicon wafer cross section area,

t: Desired thickness.

While the desired thickness $t = 1\text{mm}$, the wafer cross section area $A = 81.7$ cm^2 and then, the theoretical volume $V_{th} = 8.17$ cm^3.

This volume needs to increase because the solvent evaporated during the soft baking needs to be taken into account. According to the SU-8 properties presented in Table 3.1, the solid content in the slurry is 73.45%; therefore the actual volume is calculated as:

$$V_a = V_{th} \div solid\ content\ \% \tag{3.2}$$

The actual volume V_a is 11.04 cm^2.

The actual volume is an approximated value because the solvent may not be completely removed during the soft baking process. In addition, a small amount of solvent must be left in the SU-8 in order to avoid cracking during the exposure [15]. Also, the calculation is based on the ideal cylindrical shape but in fact, the silicon wafer circumference is not covered completely with SU-8.

3.1.1.3. Soft baking

After dispensing the SU-8 over the silicon wafer it was put on a levelled hot plate, as shown in Figure 3.3, for soft baking. SU-8 resist shows a self- levelling mechanism during soft bake, i.e. the top surface tends to be horizontal; therefore, using levelled hot plate removes the edge bead effect and produces good contact between mask and resist top surface during exposure [106]. Soft baking is a critical step of fabricating ultra-thick SU-8 layers, greater than 500 µm thick. If the soft bake time is not sufficient, too much solvent is left in the resist. The excess solvent left in the resist makes it stick with mask during exposure and the image may not be printed properly. On the other hand, over soft bake removes the solvent completely from the resist and the resist become brittle and prone to cracking before exposure. The soft bake time depends on the type of the SU-8 and the desired thickness. After being repeatedly tested, the baking time was verified experimentally in this research and the optimum procedures for soft bake SU-8 2075 are presented as follows:

1. The wafer was put on a levelled hot plate for 15 minutes.
2. The temperature was ramped to 65^{o}C with a heating rate of 5^{o}C/min and maintained at this temperature for two hours.
3. The temperature was ramped again to 95^{o}C with a heating rate of 5^{o}C/min and maintained for 34-36 h.
4. Finally, the wafer was cooled down to room temperature at the ambient atmosphere without forced cooling.

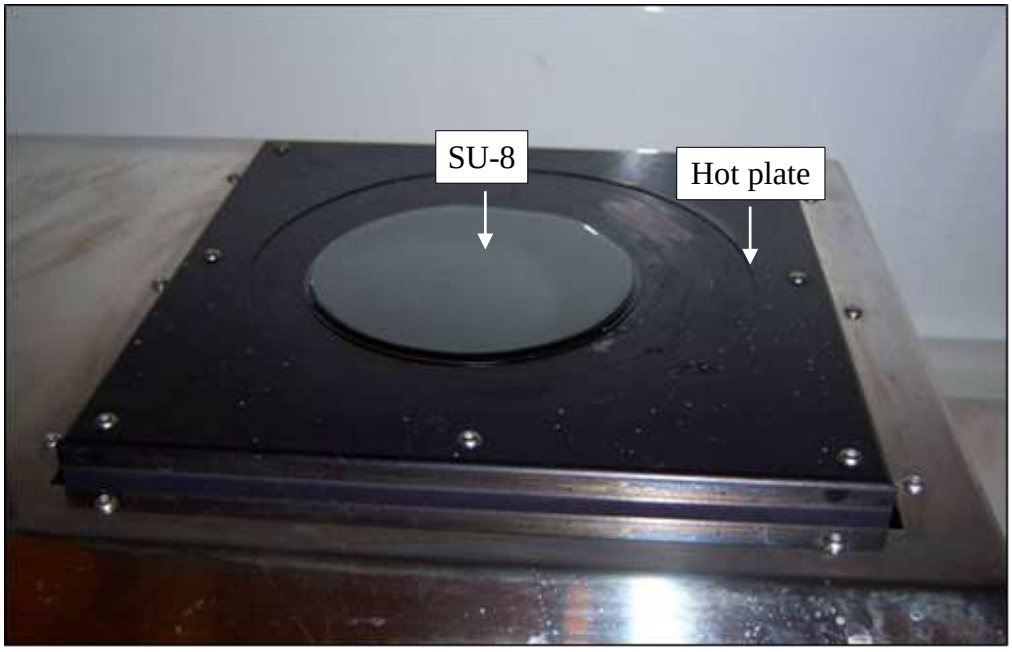

Figure 3.3. A photograph showing the SU-8 resist on a silicon wafer is put on top of a hot plate for soft baking.

3.1.1.4. Exposure

Exposure is the most important step of fabricating ultra-thick SU-8 layers. The exposure is done under a Canon PLA-501 machine with parallel light mask aligner (University of Birmingham, School of Mechanical Engineering), as shown in Figure 3.4. Many factors affect the quality of the exposed SU-8 such as film thickness, type of wafer and type of photoresist [106]. The SU-8 data sheet does not mention how much UV light dose needs to obtain ultra-thick SU-8 layers greater than 500 µm; therefore, the exposure step was repeatedly tested with different exposure doses in order to produce straight side walls.

Figure 3.4. A photograph showing a Cannon PLA-501 mask aligner machine used for exposing the SU-8 by UV-light.

3.1.1.5. Post exposure bake (PEB)

During exposure a strong acid is formed on the exposed SU-8 layer. The post exposure bake is an important step in which thermal epoxy cross-linking of the exposed layer takes place. The post exposure steps were presented as follows:

1. The exposed wafer was put on top of a levelled hot plate.
2. The temperature was ramped to 65^{o}C with 5^{o}C/min and maintained for 15 minutes.
3. The temperature was ramped again to 95^{o}C with 5^{o}C/min and maintained for 25 minutes.
4. The wafer was cooled down to the room temperature without forced cooling.

3.1.1.6. Development

Development is a process of dissolving the unexposed layers using a chemical solvent called EC developer. After post-exposure bake (PEB), the exposed layer is hardened by epoxy thermal cross linking, which resists the chemical solvent attack. On the other hand, the unexposed layer was easily dissolved by EC solvent. In order to completing dissolve the unexposed area, the wafer was put into a quartz dish and the developer (EC) added. Afterwards, the dish was put into the water bath of an ultrasonic machine. After 45-60 minutes, the unexposed features are completely dissolved and the wafer is rinsed several times by Isopropyl alcohol (IPA).

3.1.1.7. Hard bake

Hard bake is the last step of fabricating SU-8 micro structure. This stage may not be required in the SU-8 fabrication process. However, it is desired in this research in order to harden the SU-8 and improve the contact between the SU-8 micro structures and silicon wafer. Consequently, it can be used as a master mould several times. The hard bake procedures are presented as follows: the wafer was put on top of a hot plate; afterwards, the temperature was ramped to 115^{o}C with heating rate 5^{o}C/min and maintained for 10 minutes. Finally, the wafer was cooled down to room temperature without forced cooling.

3.1.2. Results

The fabrication procedures are discussed in detail in the previous sections. It is found that exposure is the most important step to produce vertical sidewalls. The exposure was performed by two different methods. In the first method, the exposure was performed without filtering UV light and the exposure energy varies from 4500 to 9000 mJ/cm^2.

While in the second method, a PL-360 filter, recommended by the SU-8 supplier, was used with the same exposure energy range.

The effect of exposure doses and filtering conditions on the sidewalls of the SU-8 micro components was investigated using SEM micro graphs. Figures 3.5, 3.6 and 3.7 show the SEM micro graphs of SU-8 exposed without filter and the exposure doses are 4500, 7000 and 9000 mJ/cm^2, respectively. At low exposure dose (4500 mJ/cm2), it is clear that the side wall has round edges and differs from the designed mask. Moreover, the top and bottom teeth faces are not completely exposed, which indicates insufficient exposure energy. When the exposure energy increases to 7000 mJ/cm^2, the side wall is improved but it is not sharp. However, the bottom faces of the teeth are still round. Further improvement in the sidewalls is obtained when the exposure energy increases to 9000 mJ/cm^2. Although increasing the exposure energy improves the side wall, T-topping effect has appeared in the micro linkage rod as seen in Figure 3.7(a). T-topping is a phenomenon that occurs in the exposed ultra-thick SU-8 (greater than 500 μm) in which the top layer is bigger than the bottom one.

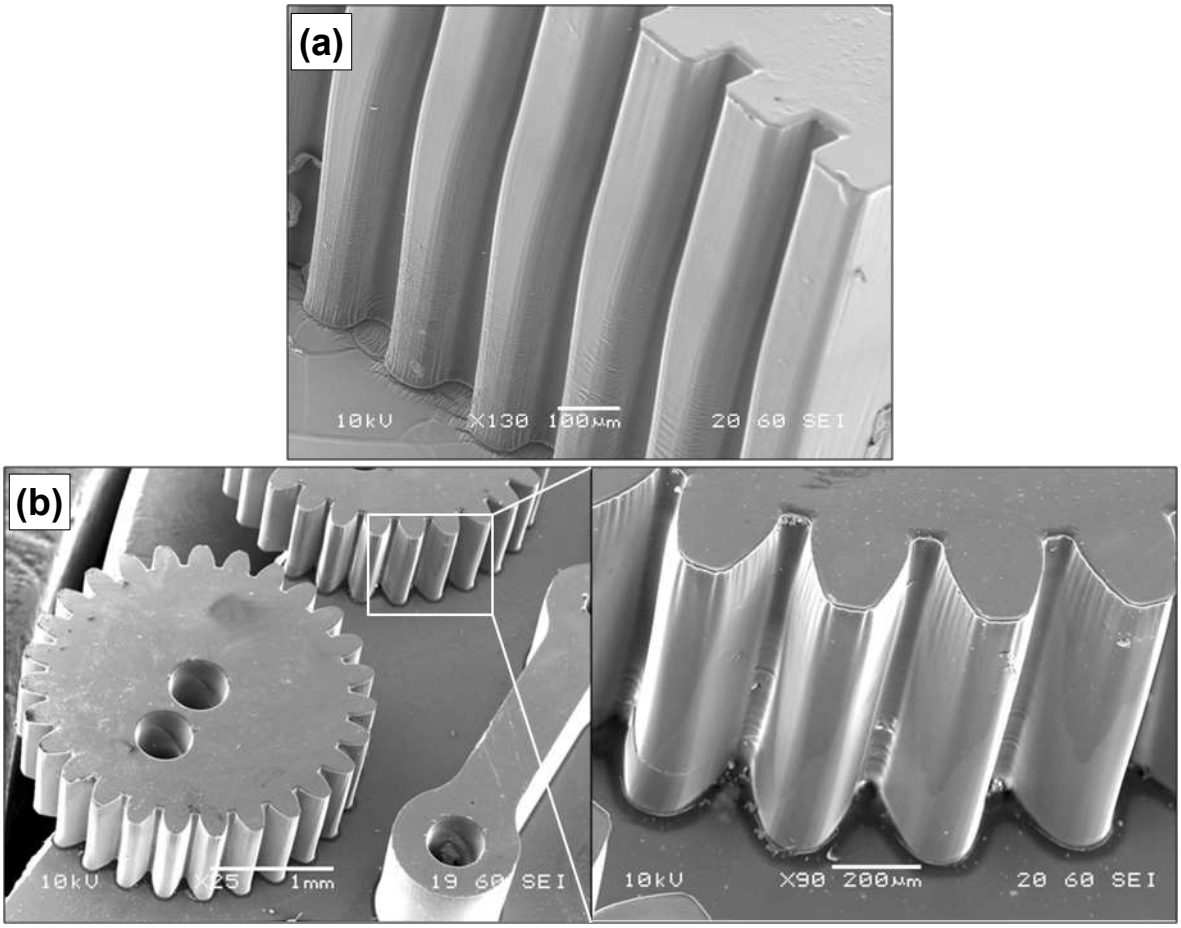

Figure 3.5. SEM images showing the SU-8 micro components and their side walls exposed by using 4500 mJ/cm^2 without filter: (a) side walls of the micro piston and (b) micro gear, micro linkage rod and gear teeth side wall.

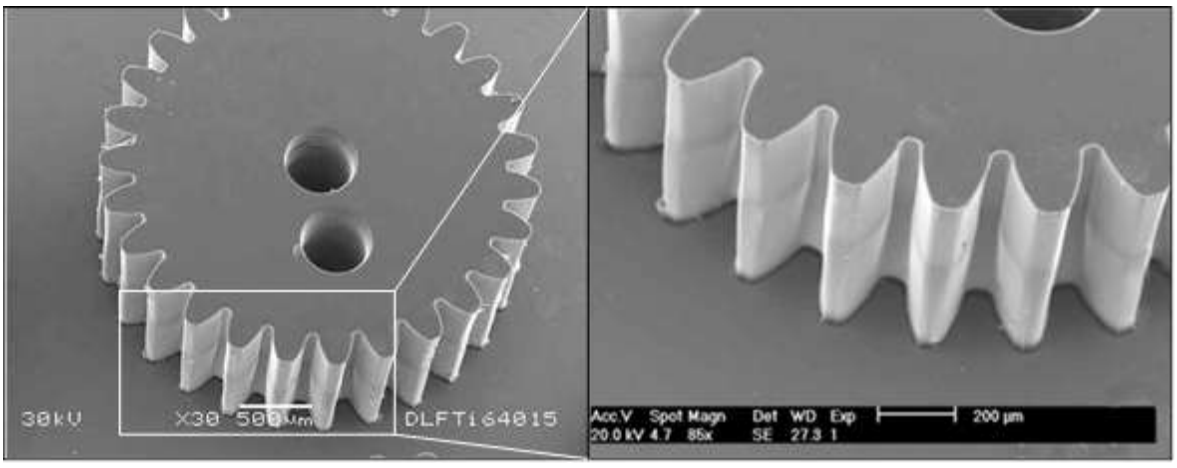

Figure 3.6. SEM image showing the SU-8 micro gear and its teeth side walls exposed by using 7000 mJ/cm^2 without filter.

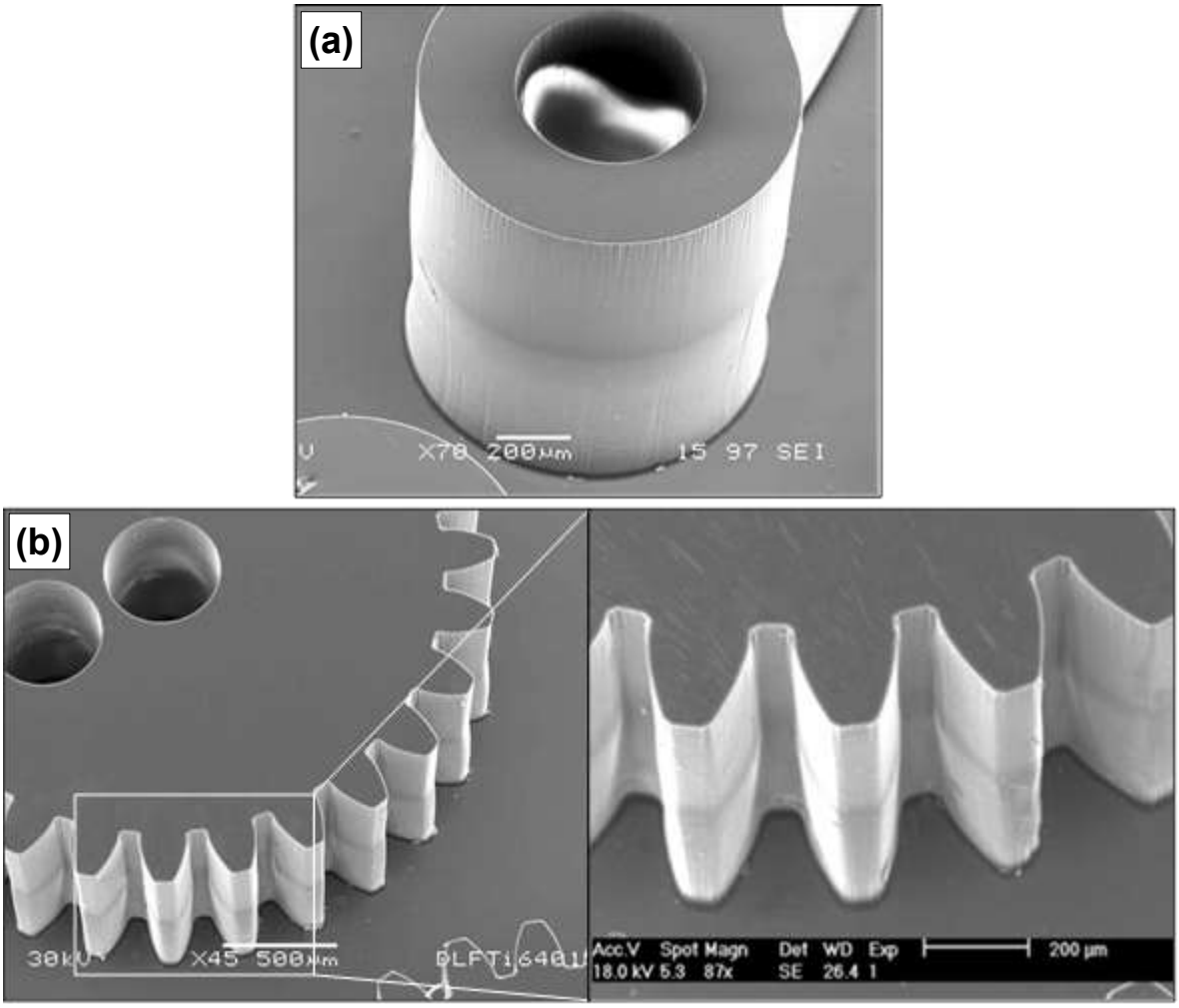

Figure 3.7. SEM images showing the SU-8 micro components and their side walls exposed by using 9000 mJ/cm^2 without filter: (a) side walls of the micro linkage rod and (b) micro gear and its gear teeth side wall.

On the other hand, Figures 3.8 (a), (b) and (c) show the SEM micro graphs of SU-8 micro gears exposed with PL-360 filter and the exposure doses are 4500, 7000 and 9000 mJ/cm^2, respectively. Generally, the side walls are improved significantly when compared with the previous method at the same exposure dose. Increasing the exposure dose increases the sharpness of the side walls. Moreover, line traces are present in the side walls as indicated by black arrows. The optimum SU-8 micro gear, micro engine cylinder, micro linkage rod and micro piston are obtained when the exposure dose is 9000 mJ/cm^2 as shown in Figures 3.8 (c), 3.9 (a), (b) and (c), respectively.

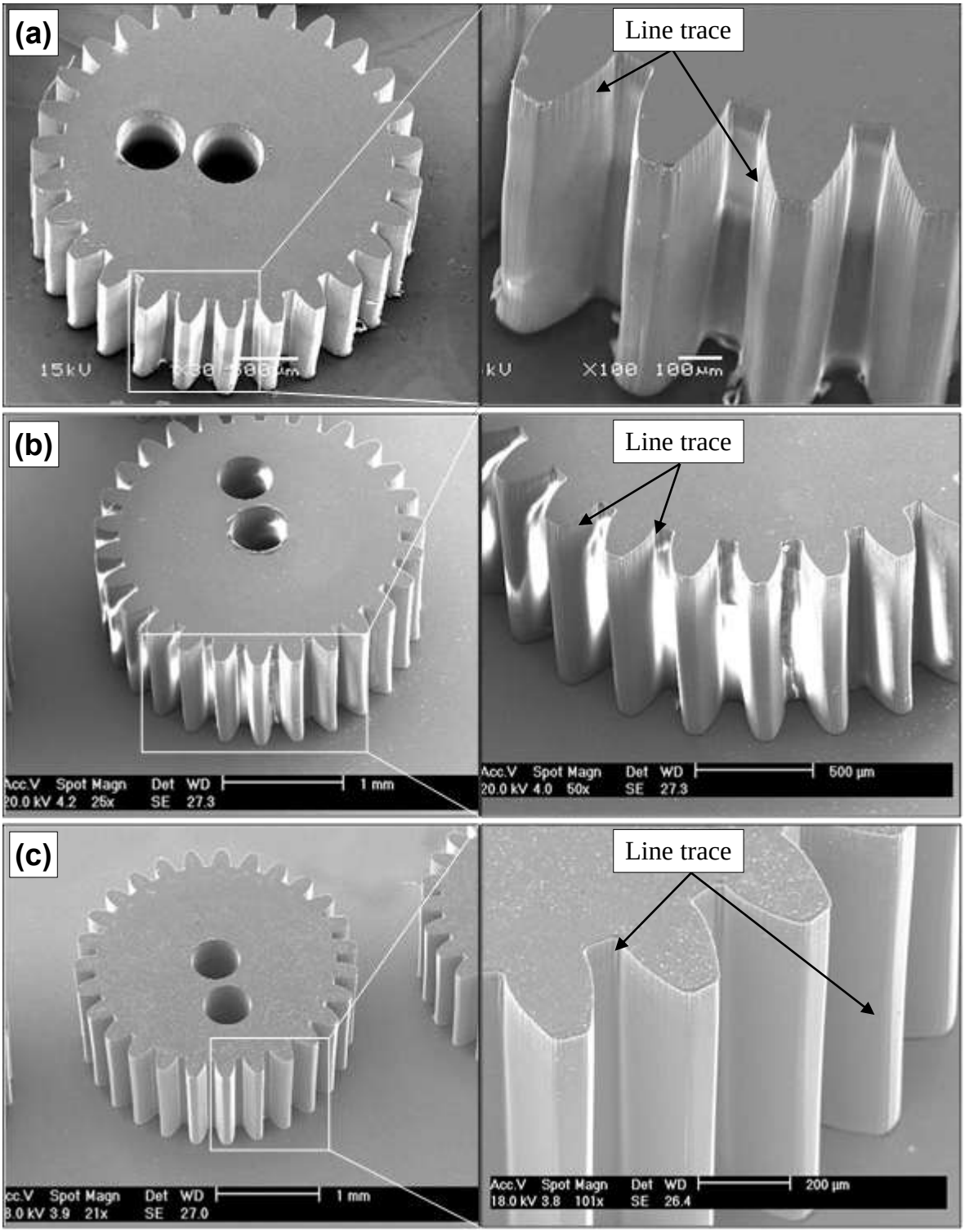

Figure 3.8. SEM images showing the SU-8 micro gears and their side walls exposed by using PL-360 filter and the exposure energy are: (a) 4500 mJ/cm^2, (b) 7000 mJ/cm^2 and (c) 9000 mJ/cm^2.

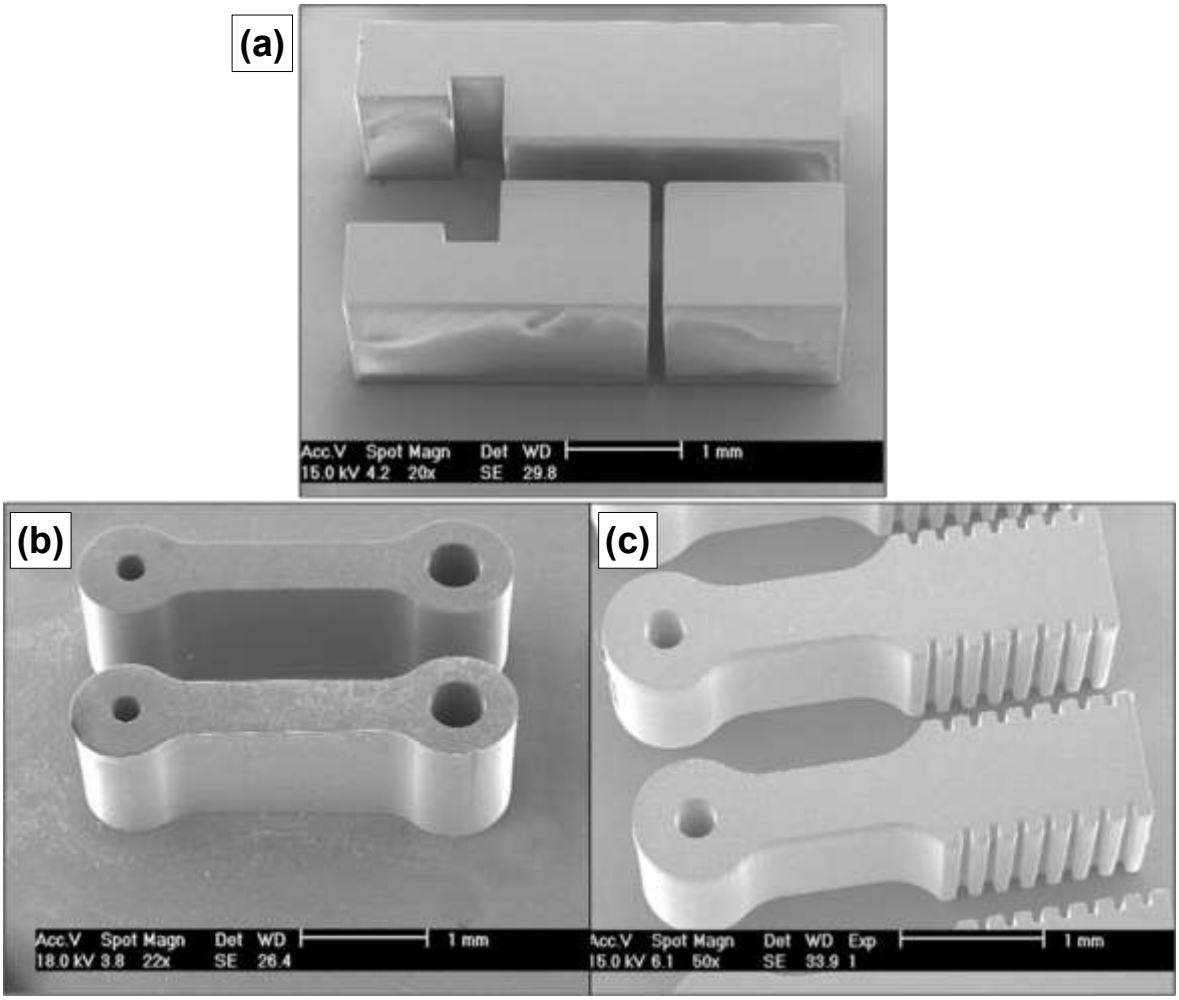

Figure 3.9. SEM images showing the SU-8 micro engine components exposed by using PL-360 filter and the exposure energy is 9000 mJ/cm^2: (a) micro engine cylinder parts, (b) micro linkage rods and (c) micro pistons.

3.1.3. Discussion

To explain the exposure process, the SU-8 optical properties and the UV light spectra are investigated. The optical transmittance of SU-8 in relation to UV exposure wavelength is shown in Figure 3.10 [108]. It is found that increasing the wave length increases the transparency of the SU-8 and decreases its absorbance significantly. Beyond 420 nm, nearly all the SU-8 is completely transparent and all UV light can go through the entire thickness without absorbance. On the other hand, UV light is fully absorbed before 320

nm. UV light is emitted from a mercury lamp (Hg), which contains spectra as shown in Figure 3.11 [110]. The emitted spectra contain i-line, h-line and g-line and their corresponding wave lengths are 365, 405 and 436 nm, respectively. As discussed previously, SU-8 is very sensitive to near i-line spectrum 320-400 nm; therefore, the Hg lamp used in this research is dominated by i-line spectrum.

In the first exposure method, no filter is used, the shorter wavelength is absorbed by SU-8 on the top layers and exposure energy is insufficient to go through to the bottom layers. This explains why the side wall is not straight. Increasing the exposure dose increases the exposure energy going to the bottom layers, which improves the side walls. When the exposure dose increases further, the SU-8 top layers may absorb UV light and gradually hinder the energy to go through the bottom layers. That is why the T-topping effect may have occurred. On the other method, using the PL-360 filter cuts off the UV wavelength below 360 nm and permits the energy above 360 nm to go through. As a result, the UV energy below 360 nm, which absorbed quickly in the top layers, is omitted. Hence, the UV light above 360 nm is gradually absorbed and homogenous exposure doses can go through the entire SU-8 thickness. Thus, sharp side walls are obtained. Consequently, optimum results obtained by using a PL-360 filter and exposure dose 9000 mJ/cm^2 were selected to be master moulds for the next fabrication procedures.

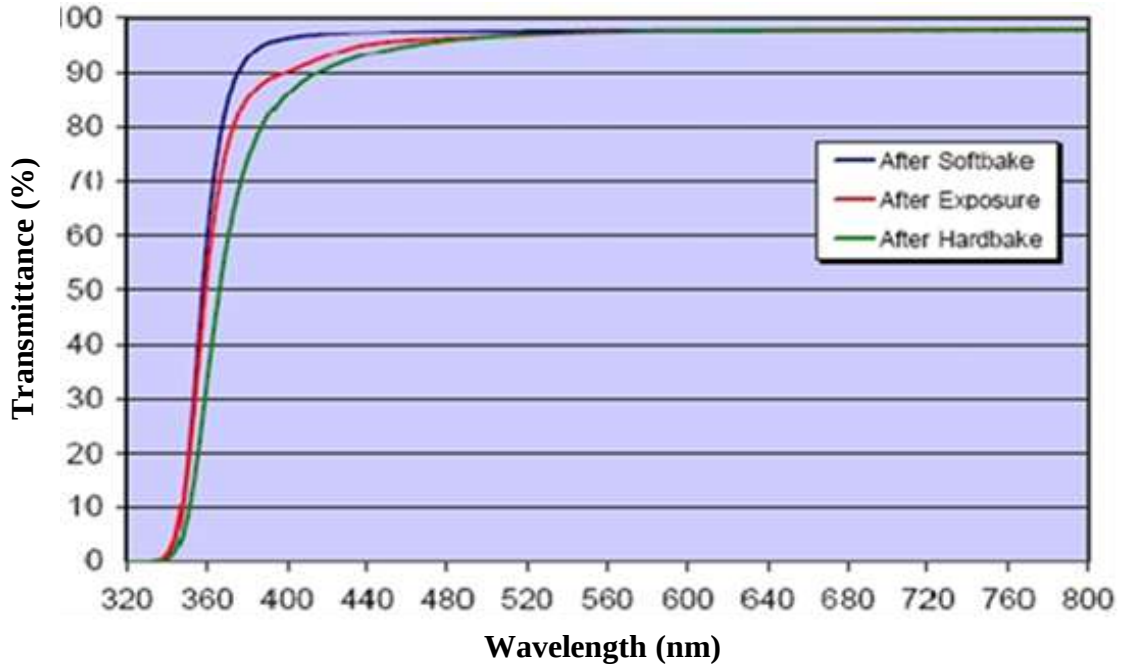

Figure 3.10. A graph showing the optical transmittance of SU-8 with UV-light wavelength [108].

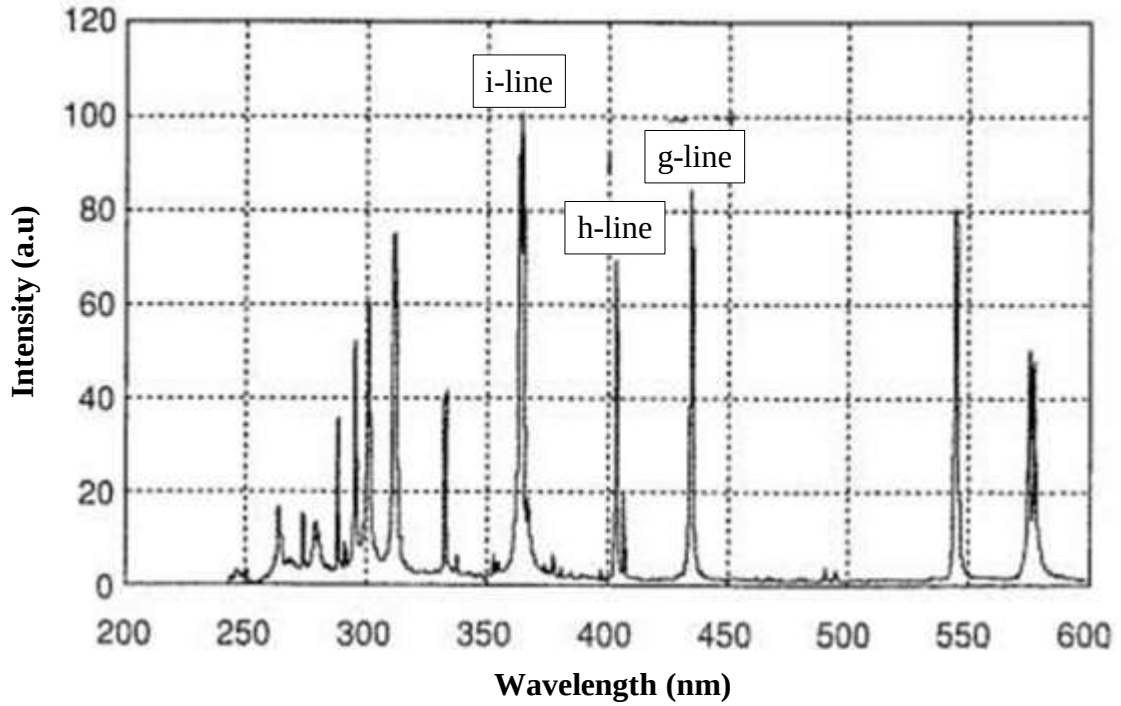

Figure 3.11. A graph showing spectral distribution of Hg mercury lamp used for photolithography process [110].

3.2. Production of negative replicas soft moulds

3.2.1. Soft moulds

Silicon rubber or Polydimethylsiloxane (PDMS) is a silicon-based organic polymer. It is non-flammable, non-toxic and optically clear. Moreover, very accurate impressions of micro structures can be obtained. It is used successfully as a mould insert for production of different micro components [94-99]; therefore, it was selected in this research as a negative mould insert. There are several types of PDMS. Each type produces specific properties and is used for different applications. Dow Syligard 184 Silicone Elastomer (Dow Curing, UK) was selected because it has been utilised before as mould inserts [95, 97 and 99]. The physical properties of the PDMS are presented in Table 3.2 [111].

3.2.2. Preparation of soft mould slurry

The preparation procedures of soft mould inserts are presented as follow as recommended in different articles [97, 99].

1. The elastomer and curing agent were mixed in a ratio 10:1 by weight and stirred by mechanical stirrer for 5 min in order to mix them thoroughly.
2. So many bubbles are formed and the mixture is transferred to milky slurry.
3. Afterward, the mixture was put under vacuum (0.2 bars) for 30 minutes in a degassing chamber in order to remove all the bubbles.
4. After completely removing the bubbles, the PDMS slurry was poured over the SU-8 master moulds.
5. In order to fill the micro features inside SU-8 master moulds and remove the trapped air between master mould and PDMS slurry, the SU-8 master moulds was put again

under vacuum (0.2 bars) for 20 minutes. Figure 3.12 shows the degassing chamber used in this research.

Table 3.2. The properties of Polydimethylsiloxane (PDMS) [111].

Chemical formula	Density	Boiling point	Glass transition temperature)
$(C_2H_6OSi)_n$	0.965 g/ml	$\leq 200^oC$	$\leq$ - 120^oC

Figure 3.12. A photograph showing the degassing chamber used in this research.

3.2.3. Curing and peeling off

After filling the SU-8 master moulds, the PDMS moulds were cured in an oven. The curing procedures recommended by the PDMS data sheet were done at the oven by adjusting the temperature to 100^oC with a holding time of 45 minutes, and then cooling down to the room temperature. After curing, the PDMS transferred to a rubbery mould. The peeling off was done manually by tweezers and cutter help. Figure 3.13 shows a schematic diagram of the soft moulding slurry preparation procedures.

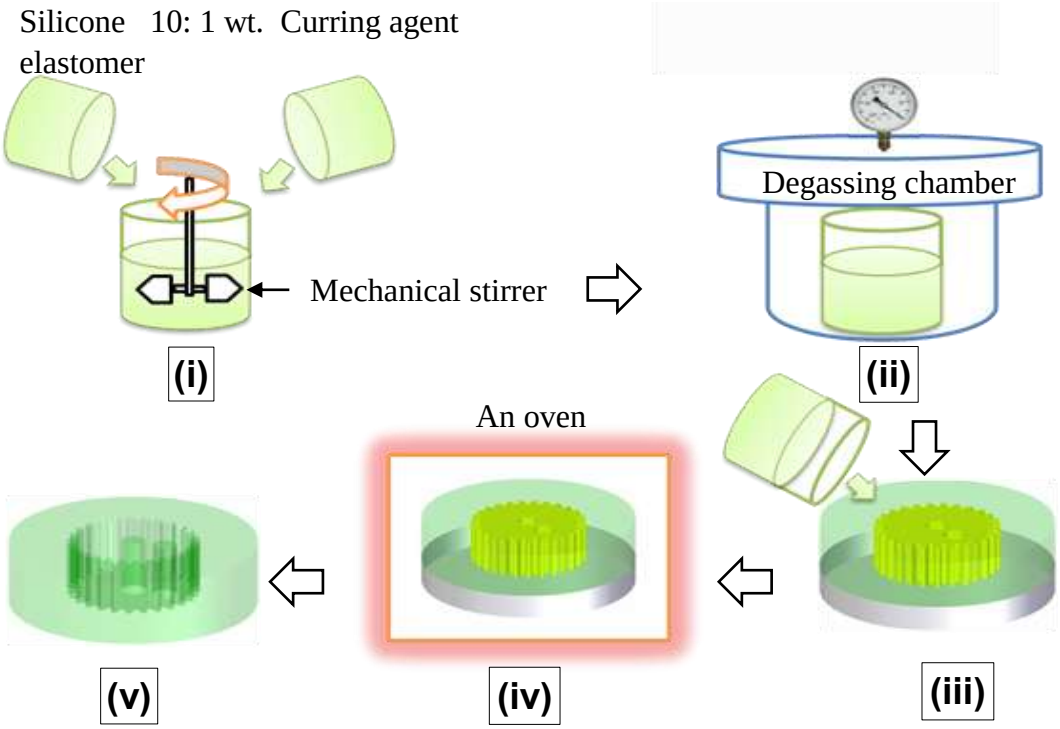

Figure 3.13. A schematic diagram showing the complete replication process of the soft mould insert: (i) mixing, (ii) degassing, (iii) pouring, (iv) curing and (v) peeling off.

3.2.4. Results and discussions

The peeled PDMS micro moulds are coated with gold using a sputtering machine and then inspected under SEM. Figure 3.14 (a) and (b) shows the PDMS negative replicas prepared by no degassing and when insufficient degassing is applied, respectively. It is found that when no degassing is applied, the PDMS negative replicas are damaged in gear teeth and two pins inside. While, insufficient degassing does not produce good negative replicas, the micro holes are not completely filled. On the other hand, using sufficient degassing time produces defect free negative mould inserts; the same quality as SU-8 master moulds of the micro engine as shown in Figure 3.15. These good negative replicas are used as a mould inserts with powder metallurgy process in the following chapters.

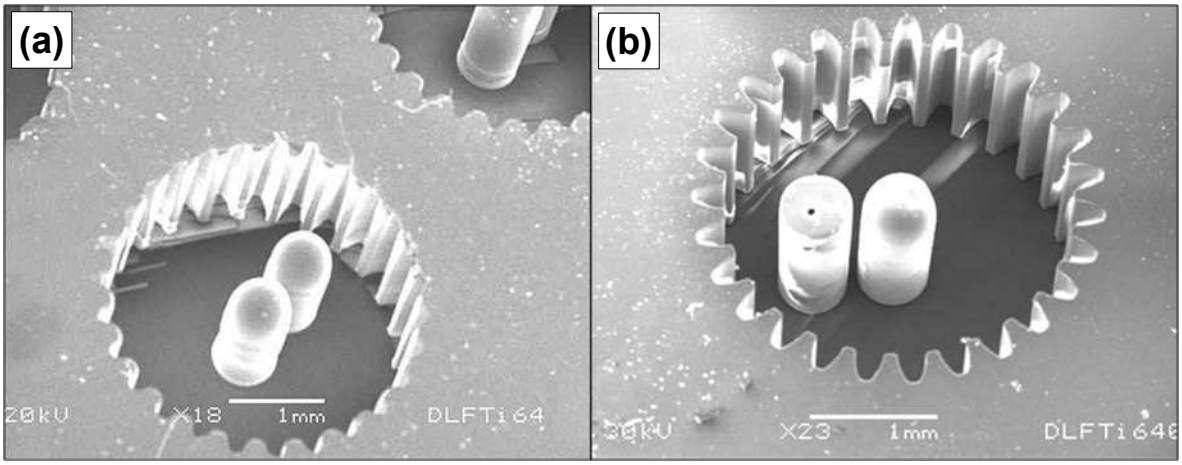

Figure 3.14. SEM images showing defected PDMS negative micro moulds due to: (a) no degassing is applied and (b) insufficient degassing.

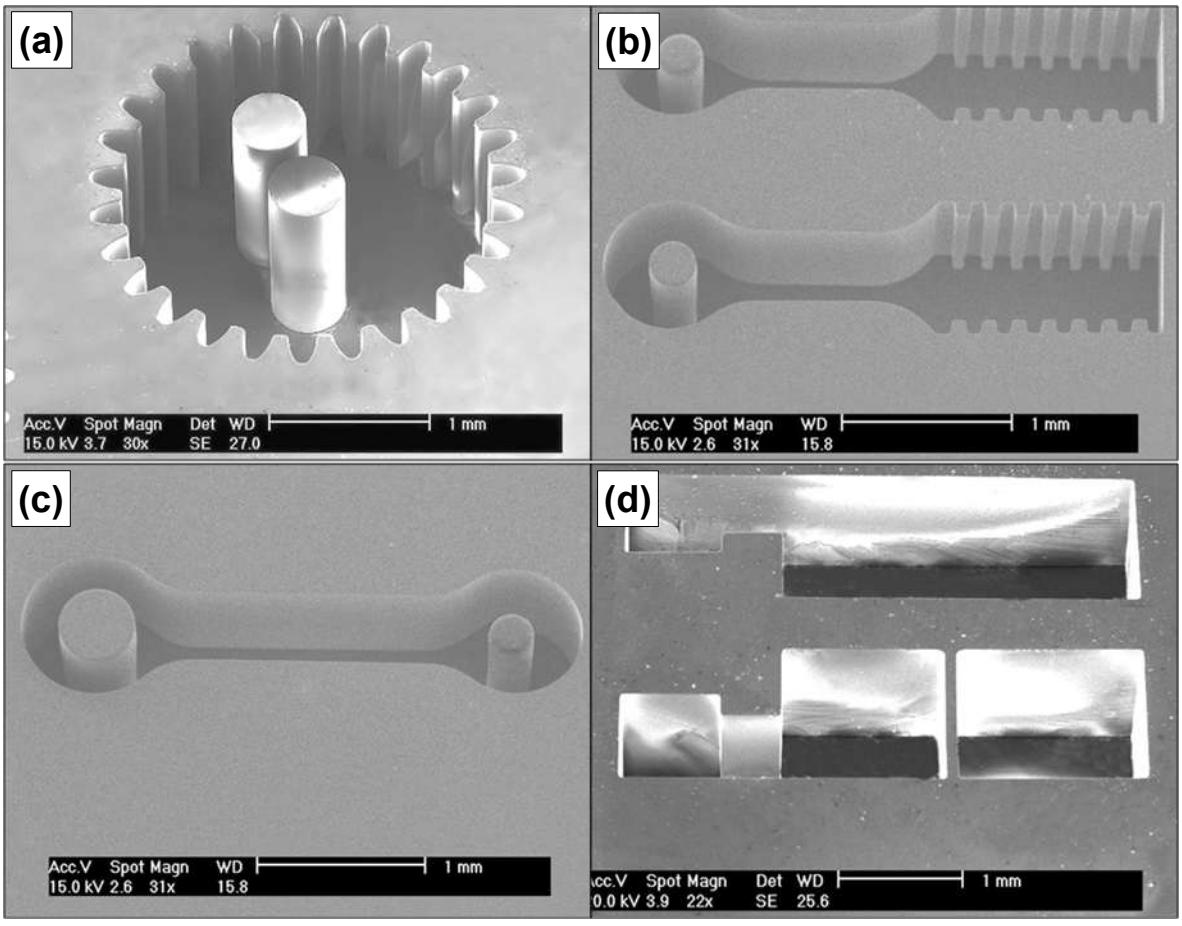

Figure 3.15. SEM images showing defect free PDMS negative micro mould inserts: (a) micro gear, (b) micro piston, (c) micro linkage rod and (d) micro engine cylinder.

3.3. Conclusions

In this Chapter the SU-8 master moulds and their negative replicas soft micro moulds were successfully fabricated with high quality; the same as designed. The following conclusions are obtained:

1. The exposure energy and filtering are the most important parameters affecting the quality of the fabricated SU-8. It is clear that, using one filter during exposure produces high quality SU-8 micro engine components; the same quality as SU-8 fabricated by using three different filters.

2. Degassing is an important step of producing defect-free soft micro moulds.

CHAPTER 4. SELECTION OF STAINLESS STEEL POWDER AND BINDER

This Chapter presents in detail the selection of stainless steel powder and binder to be used in this research. Three different binders are tested in this chapter. The successful one used for producing damage-free green micro gears is selected to be used in the following fabrication processes.

4.1. Powder selection

Selection of powder shape and size is an important parameter which depends on the type and the size of mould inserts. Generally, spherical and irregular powder shapes are widely used in powder metallurgy processes. In micro metal injection moulding (µMIM) where a rigid mould insert is usually used, the irregular powder shape is recommended [112]. The irregularity produces high green strength between the particles and their neighbours by plastic deformation under the applied pressure and it produces good powder integrity in the green part [113]. However, the spherical powder shape is also used in this technique in order to produce a good density packing [114-115]. While soft micro mould inserts are used in this research, the filling technique mainly depends on low applied pressure. Consequently, spherical powder shape is recommended in order to produce good density packing. The minimum feature size of the mould insert is the main factor affecting the selection of the powder size. To obtain isotropic behaviours of the sintered micro components, it is very important that the minimum grain size is smaller than that of the minimum micro feature; therefore, powder size should be at least smaller than the minimum feature to be fabricated [98, 116-117]. As discussed in Chapter One, the

minimum feature to be fabricated is the tip of the micro gear teeth which measure ~ 75 µm. Therefore, gas atomized 316-L stainless steel powders containing three different particle sizes are tested. 316-L Stainless steel has superior properties in wearing, corrosion and oxidation resistance. The presence of chromium-nickel and molybdenum increases resistance to pitting and crevice corrosion in chloride environments. The average particle sizes were 5, 10 and 16-µm, respectively. The chemical compositions, particle size distributions and tap densities delivered by supplier (Sandvik Osprey, UK.) are listed in Tables 4.1 and 4.2, respectively. Samples from each powder were also inspected under SEM and their images are shown in Figure 4.1. Generally, the particles are spherical in shape.

Table 4.1. The chemical compositions of the 316-L stainless steel powders (Sandvik Osprey, UK.).

Sample size	Chemical composition					
	Fe	Cr	Ni	Mo	Mn	Others
81.6% < 5 µm	68.57	16.5	10.5	2.1	1.45	0.88
90.1% < 10 µm	68.41	16.2	11	2.4	1.26	0.73
90.8 < 16 µm	67.93	17.3	10.4	2.3	1.39	0.68

Table 4.2. The Particle size distributions and the tap densities of 316-L stainless steel powders (Sandvik Osprey, UK.).

Sample size	Particles size distribution (µm)			Tap density
	D_{10}	D_{50}	D_{90}	(g/ml)
81.6% < 5 µm	1.9	3.4	5.8	4
90.1% < 10 µm	2.9	5.6	10	4.5
90.8 < 16 µm	3.4	7.7	15.7	4.6

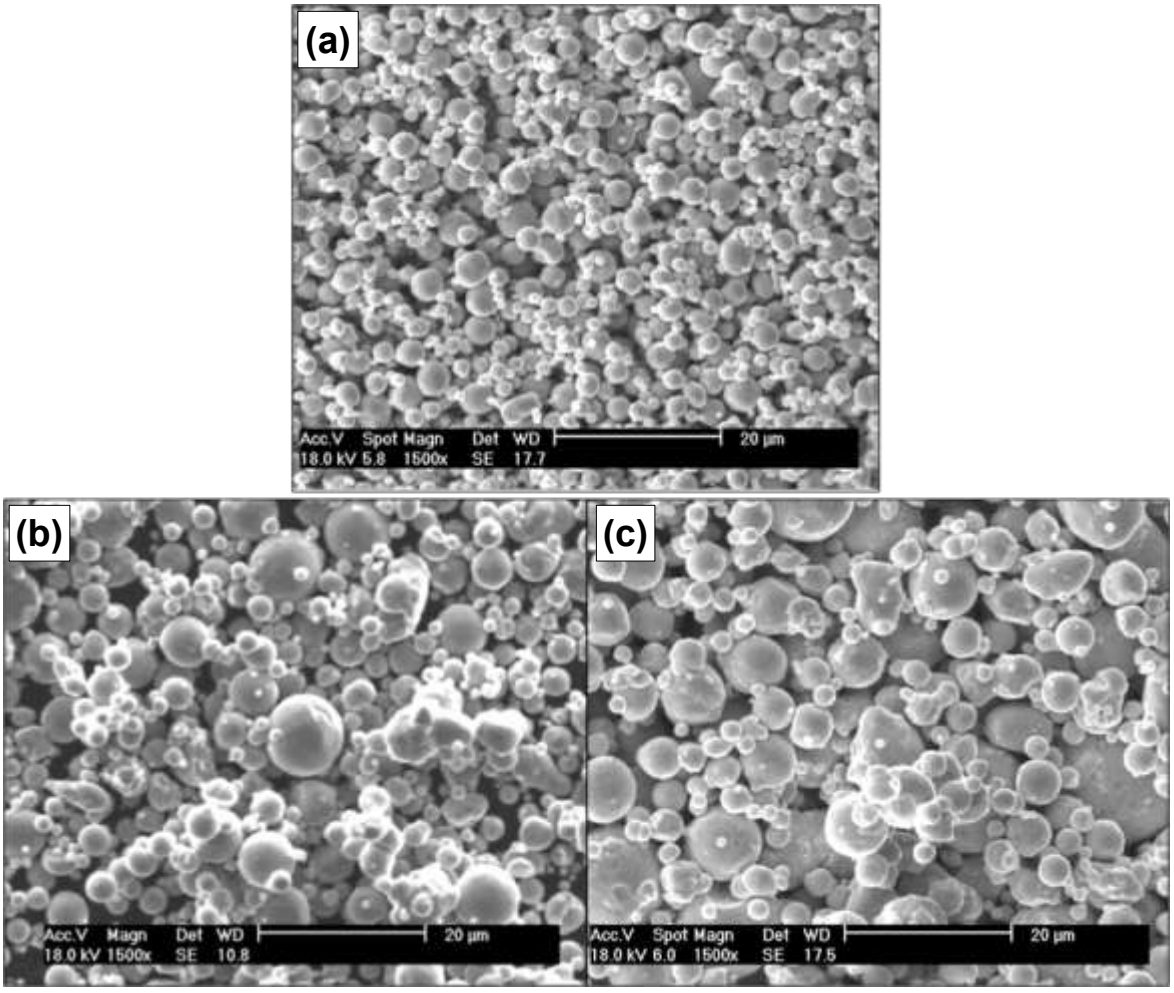

Figure 4.1. SEM images showing the 316-L stainless steel powders: (a) 5-µm, (b) 10-µm and (c) 16-µm sizes.

4.2. Binder selection

The main function of the binder system is to hold the powder into the desired shape and to maintain that shape until the sintering process. In addition, the binder should have good flow characteristics during the moulding process and rapid viscosity during drying. Moreover, the binder should have good interaction with powder and is completely de-bound before the sintering [114, 118-119]. Several types of binders have been used in the powder injection moulding process, which include wax, thermoplastic and thermosetting [112, 114, 116 and 119-120]. The removal behaviour of most types of binder is done thermally below sintering temperature. However, oil is added to the wax-polyethylene (PE) binder in order to be degraded by solvent [121-122]. Gel casting is another approach of binder system used for making complex shapes from ceramic and metallic powders [123-124]. The process includes mixing the powder and organic monomers to form a slurry, which is used to fill a mould insert with the desired shape. The slurry is polymerized chemically by forming cross linked polymer-solvent gel after adding a catalyst and initiator. This type of binder is thermally degraded. Acrylic-based binder is another approach of binder system of forming powder slurry. The process includes dispersion of the fine powder into aqueous or non-aqueous dispersant media. Afterwards, the acrylic binder is added and the mould inserts are filled. This type of binder produces a good interaction with powder after the solvent evaporates and is used in ceramic processing technology [125-126]. Because soft mould inserts are used in this research, the moulding process is done at room temperature; therefore, the binder should have low viscosity at room temperature. Hence, wax, thermosetting and thermoplastic binders are not suitable because they are physically hard at room temperature. On the other hand, gel casting and

acrylic-based binders may be used. Three different binders were tested in this chapter, which includes gel casting, Cyanoacrylate and acrylic-based binders.

4.3. Preparation of green micro parts

The main target of this Chapter is to select an appropriate binder to produce damage-free green micro components. To reach this target, a proposed method is presented as follows: (i) prepare stainless steel slurries from different types of binder, (ii) fill the soft micro mould inserts, (iii) after the slurries have dried, the green micro components are de-moulded. Because the micro gear was the complex shape to be fabricated in this thesis, it is selected in this Chapter to obtain the appropriate binder. The successful binder used to form net shape green micro gear without distortion after de-moulding is selected as the binder for the other process. 316-L stainless steel with 5-µm powder was investigated in this chapter.

4.3.1. Preparing stainless steel slurries

4.3.1.1. Gel casting based slurry

Gel casting is used as a binder for ceramic processing technology, first published in 1991 [127]. However, the process has been developed to include several types of metals and ceramics [128-129]. The slurry is prepared from powder, organic monomer, catalyst, initiator and water or inorganic solvent. After being casted into the desired shape, the slurry polymerises to form high strength green components. The strength of the green part is greater than that of conventional slip casting as presented by Vandeperre et al. [130]. That is why gel casting is selected as a binder in this research where the micro metallic components are liable to damage during de-moulding. The gel casting stainless steel slurry

was prepared following the same procedures presented by Santos et al., [131]. The properties of gel chemicals delivered by the supplier (Sigma Aldrich, UK.) are presented in Table 4.3.

To prepare stainless steel slurry based on gel casting, the following procedures are presented:

1. Premix solution was prepared by adding Methacrylamide (MAM) monomer crystal to distilled water and the mixture was stirred by mechanical stirrer until the solid was completely dissolved. Afterwards, Hydroxymethylacrylamide (HMAM) monomer solution was added and the whole mixture was stirred again for homogenization.
2. Stainless steel powder was added to the premix during the stirring process and the whole mixture was stirred for 30 minutes to form a homogenous metallic slurry.
3. Many bubbles were formed during stirring process. Therefore, the slurry was put under vacuum in the degassing chamber in order to remove the bubble.
4. The catalyst, Tetramethylethylenediamine (TETMED), was added to the metallic slurry in order to stimulate the gelation process.
5. The initiator, 10% aqueous solution of ammonium persulfate (AP), was added.

The main function of the initiator was to initiate the gelation process. It is found that increasing monomer content in the premix increases the strength of the green components [124 and 131]; therefore, two different slurries were prepared in this research containing 20% and 25% monomer solutions. The compositions of two gel casting slurries prepared are listed in Table 4.4.

Table 4.3. The chemicals of gel casting and their properties (Sigma Aldrich, UK.).

	Type	Formula	Molecular weight
Methacrylamide (MAM)	Monomer	C_4H_7NO	85.11 g/mole
Hydroxymethylacrylamide (HMAM)	Monomer	$C_4H_7NO_2$	101.1 g/mole
Tetramethylethylenediamine (TEMED)	Catalyst	$C^6H1_6N_2$	116.2 g/mole
Ammonium Persulfate (AP)	Initiator	$(NH_4)_2S_2O_8$	228.2 g/mole

Table 4.4. The compositions of two different stainless steel slurries prepared from 5-µm powder and based on gel casting binder.

	20% monomer	25% monomer
Stainless steel	12.46 g	12.46 g
Distilled water	1.73 g	1.223 g
MAM	0.237 g	0.355 g
HMAM	0.575 g	0.863 g
TEMED	30 µl	30 µl
AP	50 µl	50 µl

4.3.1.2. Cyanoacrylate based slurry

Cyanoacrylate (superglue) is a type of adhesive material which is composed of liquid acrylic monomers with low viscosity. The polymerization takes place in the presence of adsorbed moisture without catalyst or heat [132]. It can easily polymerize by exposing to

air moisture. Because it dissolves in organic solvents, such as acetone, it is used as a non-aqueous binder for metallic powder [99]. The detailed properties of the Cyanoacrylate are presented in Table 4.4 [133]. While cyanoacrylate is used as a binder in the preparation of aluminium-copper powder slurry as presented by Kim, et al. [99], the same process is used in this Chapter with stainless steel powder.

The stainless steel slurry based on Cyanoacrylate was prepared as follows:

1. Cyanoacrylate was added to acetone in a ratio of 1: 20 by weight and the mixture were stirred for 10 minutes.
2. As the cyanoacrylate was mixing with acetone, it was completely dissolving and the stainless steel powder was added during the stirring process.
3. The whole mixture was put into a degassing chamber to remove the bubbles formed during stirring.

Table 4.5. The properties of Cyanoacrylate [133].

Composition		Formula	Density	Melting point
Ethyl cyanoacrylate	91%	$C_6H_7NO_2$	1.06 (g/ml)	-22^oC
Polymethylmethacrylate	9%	$(C_5H_2N_8)_n$	1.19 (g/ml)	160^oC

4.3.1.3. Dispersant acrylic based slurry

Colloidal processing technique has taken great attention in ceramic processing technology. The tendency of particle aggregation increases as the particle sizes decrease, which produces an inhomogeneous green compact [134]; therefore, using dispersant-based slurry

produces homogenous green components with high density [135-136]. Based on ceramic processing technology [97], dispersant acrylic based binder was adopted in this research in order to prepare stainless steel aqueous slurry. Duramax D-3005 was used as a dispersant. It is an ammonium salt of acrylic homopolymer and is used for dispersing a variety of inorganic pigments [137-138]. A mixture of Duramax B-1000 and B-1007 is used as a binder. Duramax B-1000 and B-1007 are a mixture of an aqueous emulsion of acrylic polymer, used as a binder for ceramic fabrication [95 and 97]. Both dispersant and binder delivered from Rohm and Haas Ltd., UK. Table 4.6 lists the properties of the dispersant D-3005, and the binders B-1000 and B-1007. The stainless steel slurry based on dispersant acrylic based binder was prepared with the following procedures:

1. Dispersant and distilled water were mixed in a specimen tube by using an ultrasonic bath for 5 minutes.
2. Stainless steel powder was added and the mixture was stirred using mechanical stirrer for 20-30 minutes in order to disperse the powder properly. The binder was added and the whole mixture was stirred again for 15 minutes to homogenize the slurry.
3. The bubbles formed during stirring were removed by putting the slurry into the degassing chamber as discussed in the previous sections.
4. Selection of solid loading is based on observations during slurry preparation. Therefore, the solid loading of the stainless steel slurry based on dispersant acrylic based binder was adjusted to be 60% (vol.) which is very reasonable for filling soft mould without additional external pressure. The weight percentages of stainless steel powder, binder and dispersant are 10, 1 and 0.1, respectively. The binder composition is 3: 1 weight% of B-1007 to B-1000.

Table 4.6. The properties of dispersant D-3005 and binders: B-1000 and B-1007 (Rohm and Hass, Ltd., UK.).

	D-3005	B-1000	B-1007
Physical state	Liquid	Liquid	Liquid milky
Density at 23^{o}C (g/ml)	1.1-1.25	1-1.2	1-1.2
PH	6-7	9-10	6-7
Boiling point (^{o}C)	100	100	100
Total solid (%)	34-36	36-42	54-56
Water solubility	completely soluble	dilatable	dilatable

4.3.2. Filling the soft micro moulds

After preparing stainless steel slurries from different binders, the soft micro moulds were filled using the following procedures:

1. The soft micro moulds were put on a petri dish with their openings facing upward.
2. The filling was done by two methods: (i) stainless steel slurries were poured in the micro mould openings and the filling was done under gravity force and (ii) stainless steel slurries were poured in the micro mould openings and the soft moulds were put in the degassing chamber.
3. After filling the soft moulds, the excess slurry on top of soft micro mould openings were removed with the help of a metallic blade in order to keep the patterns flat.

The filled soft micro moulds using gravity and degassing chamber were inspected under an optical microscope and the results are shown in Figures 4.2 (a) and (b), respectively. It is

clear that, filling the soft micro moulds under gravity produces incomplete micro features. The micro gear teeth are difficult to be filled completely. On the other hand, using a degassing chamber not only removes the residual bubbles in the slurry but it also removes the trapped air inside the micro features and help filling the micro features.

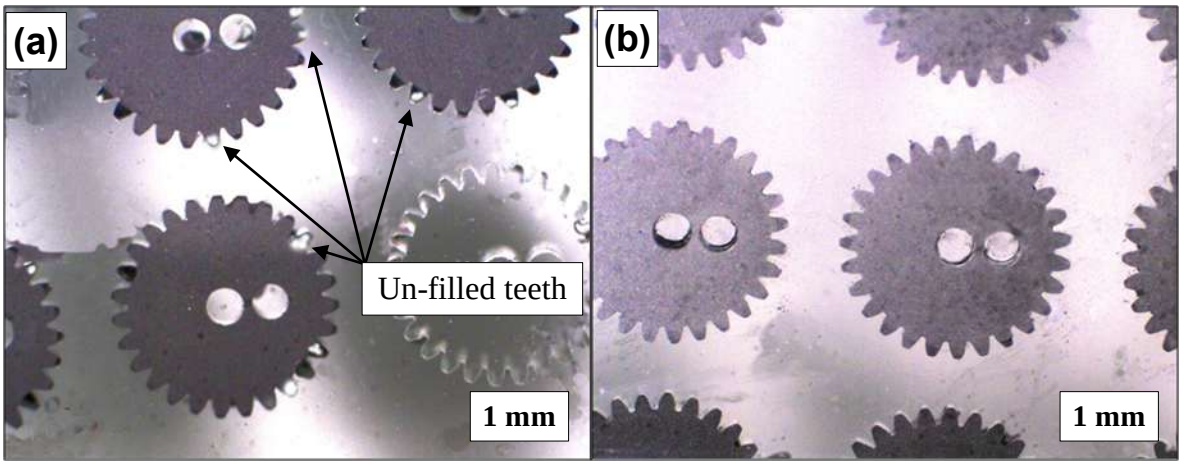

Figure 4.2. Optical images showing the soft moulds of micro gears filled by using: (a) gravity method and (b) degassing chamber.

4.3.3. Drying and de-moulding

The filled micro moulds were left to dry at room temperature without additional process. For gel casting based slurry, the slurry was dried chemically by forming cross linked polymer-solvent gel containing water. The polymerization starts as the initiator is added and the gelation time depends on the amount of initiator and monomers; therefore, the filling was done quickly to prevent gelation before complete filling. For cyanoacrylate based slurry, the acetone evaporates quickly due to its low boiling point (56.4^{o}C). While the acetone evaporates the adhesion bonding of cyanoacrylate is returned again, which bonds the green micro gear. The green micro gear has a sufficient strength because the cyanoacrylate provides immediate and high strength as it polymerizes. On the other hand, the dispersant acrylic based slurry dried by water evaporation. As the water evaporates, the

acrylic binder polymerizes to bond the powder together. Generally, the drying times of slurry based on dispersant acrylic based binder is more than that of slurries based on gel casting and cyanoacrylate. After being completely dried, the green micro gears were de-moulded. The soft micro moulds were bended slightly and then, with the help of metal blade and tweezers, the green micro gears were taken out of the moulds carefully.

4.4. Results and discussion

The de-moulded green micro gears were inspected under SEM. Figures 4.3 (a) and (b) & (c) shows SEM images of the green micro gears fabricated by using gel casting binder with 20%, 25% and 25% monomer solutions, respectively. After several trials, it is found that the teeth of the green micro gears are damaged when 20% monomer is used. When the monomer is 25%, some of the micro gears teeth are retained and the inner holes is damaged as shown in Figure 4.4 (b), while the most of the de-moulded micro gears teeth are completely damaged as shown in Figure 4.4 (c). This happens because the cross linking of the metallic slurry is not completed at this area. However, increasing the monomer increases the strength of the green micro gear, but the outer part of the green micro gear separated from the inner core as seen in Figure 4.4 (c). The separation may happen because the outer part is rapidly dried before the inner part. As a result, the stress is formed between the inner core and outer part, which causes the separation. Furthermore, as discussed by Janney, et. al., [139] that PDMS moulds affect the gelation process of gel casting, which prevents the gelation taking place in the contact layer.

On the other hand, the green micro gears fabricated by using cyanoacrylate binder were inspected under SEM and their images are shows in Figure 4.4. It is found that the most of micro gear teeth were retained. While some tips of the gear teeth are incomplete. This

happens because the rapid polymerization of the slurry, as the acetone evaporates during the filling process, reduces the chance to fill the bottom gear teeth. Finally, the green micro gears fabricated by using dispersant acrylic based binder were also inspected under SEM and their images are shown in Figure 4.5. It is clear that the green micro gears show high quality; the same quality as SU-8 master mould. Moreover, the entire micro features including teeth and the two holes inside gear are retained without distortion. This happens because the drying process is taking place slower than that of gel casting and cyanoacrylate binders, which produces a sufficient time to fill the small features before drying. Moreover, the slurry based on dispersant acrylic based binder is not react with the soft mould insert, and hence the drying is uniform through the entire feature which is retained without damage.

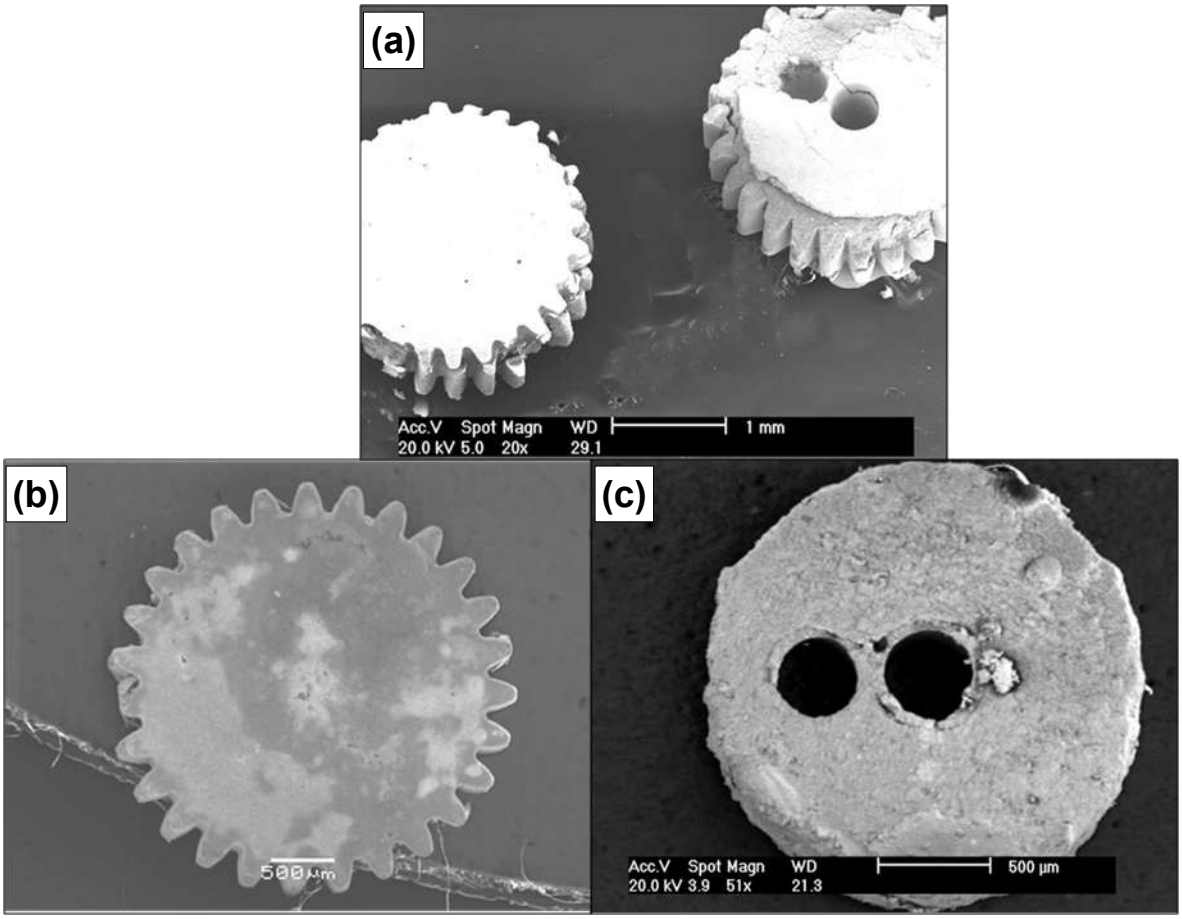

Figure 4.3. SEM images showing the stainless steel green micro gears based on 5-µm powder and fabricated by using gel casting binder, which contains: (a) 20% monomer, (b) 25% monomer and (c) 25% monomers.

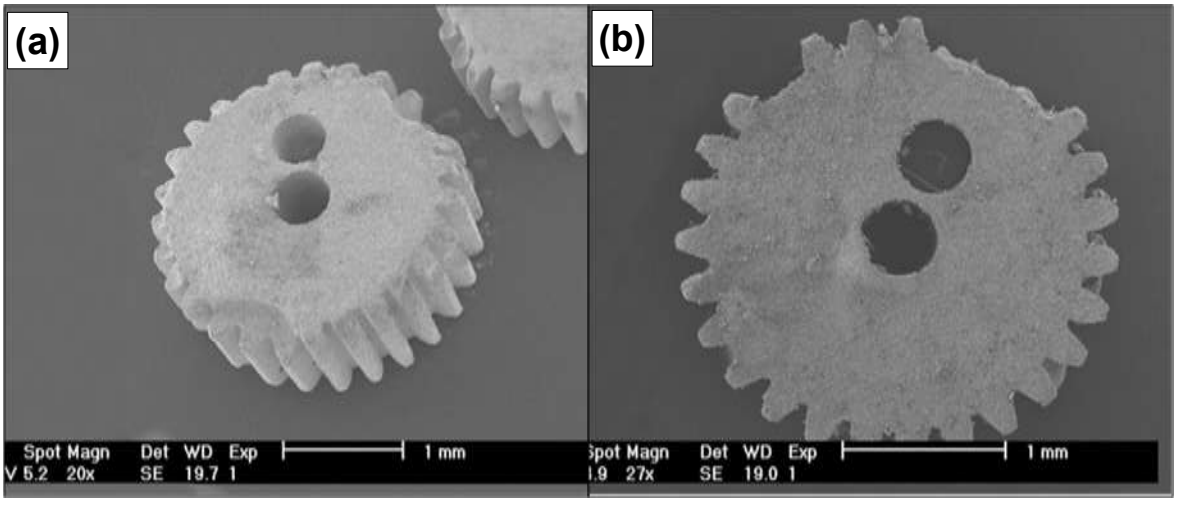

Figure 4.4. SEM images showing the stainless steel green micro gears based on 5-µm powder and fabricated by using Cyanoacrylate binder.

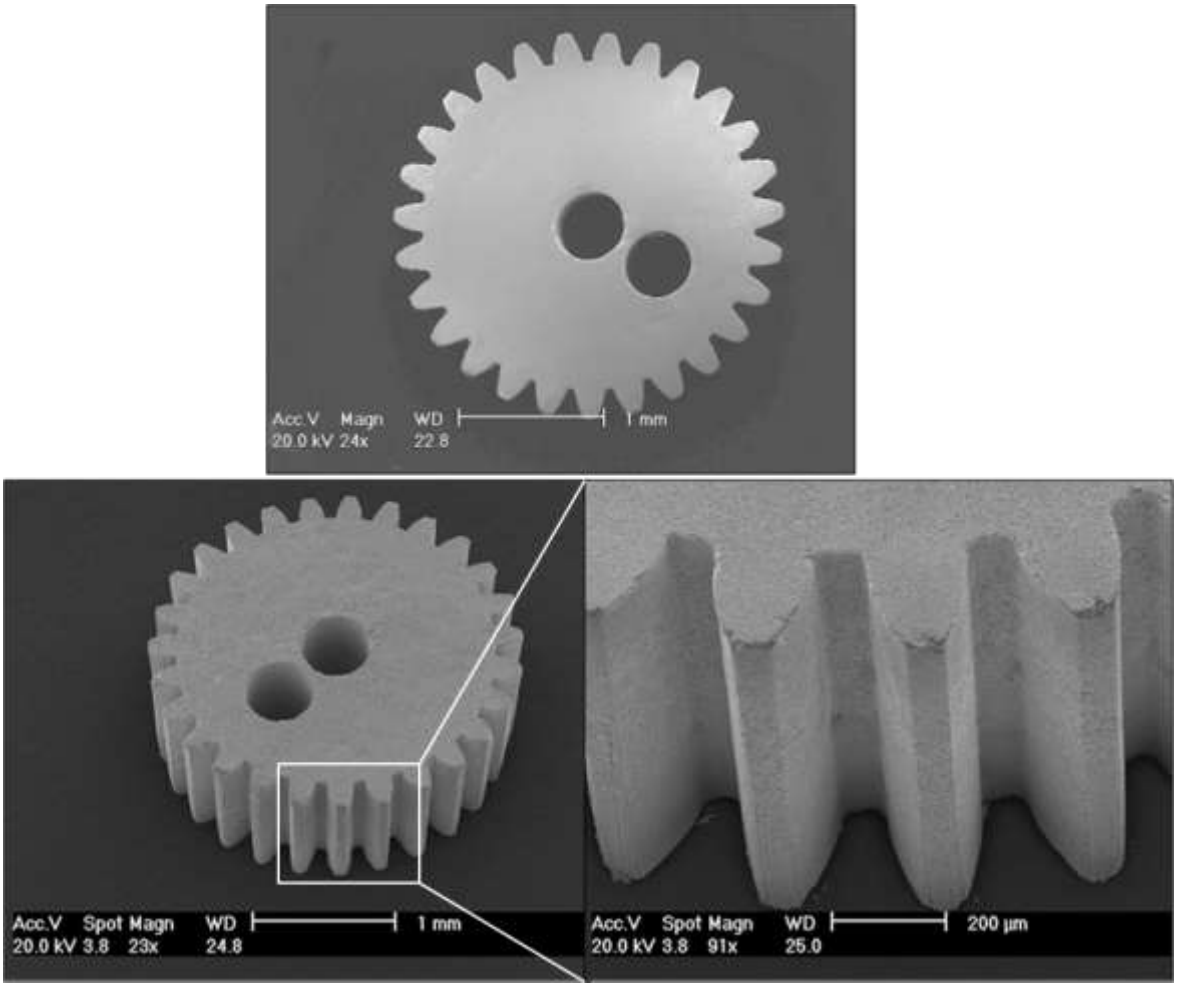

Figure 4.5 SEM images showing the stainless steel green micro gear based on 5-µm powder and fabricated by using dispersant acrylic-based binder.

4.5. Conclusions

Although gel casting process is a promising technique of producing high strength green components, the slurry is not compatible with PDMS mould insert in which un-gelled layers are formed in contact with the PDMS surface. While more steps are needed to improve the compatibility which increases the overall process time and is not optimal from an economical point of view. Thus, gel casting process is not adopted in Softlithography technique in this thesis. On the other hand, cyanoacrylate is not suitable as a binder in this work. It reacts quickly with the atmosphere as the solvent evaporate and it produces

insufficient time to fill the micro features, such as micro gear teeth. Finally, using dispersant acrylic based binder is a very adequate method of filling the soft micro mould properly. It provides sufficient time to fill the micro moulds properly before the slurry dries. Moreover, it provides sufficient binding to the powder after drying which helps produce damage free green micro components after de-moulding. Consequently, the dispersant acrylic based binder was selected in this research as a vehicle to form the green micro components for different types of powders.

CHAPTER 5. PRODUCTION OF THE STAINLESS STEEL GREEN MICRO COMPONENTS

As discussed in Chapter Four, using dispersant acrylic based binder produces high quality green micro gears. This chapter investigates the process further in order to obtain the optimum slurry parameters and produce different green micro components. Three different 316-L stainless steel powders were investigated, including 5, 10 and 16-µm particle sizes. Two filling methods were also adopted in this Chapter including pressure less and cold isostatic pressing methods. The effects of filling method, particle sizes, dispersant and binder on the density, linear shrinkage and shape retention of the green micro components are studied in detail.

5.1. Pressure less filling method

It is clear that, filling the soft micro moulds under degassing chamber produces good green micro components. Because the filling process is done without applying external pressure, it is called pressure less filling method. The stainless steel slurries containing 5, 10 and 16-µm powders are investigated and the optimum slurry properties for each powder are obtained.

5.1.1. Obtaining the optimum amount of dispersant

As the particles aggregate, the slurry tends to be inhomogeneous which affects powder packing in the green components [140-141]. Therefore, the main function of dispersant is to reduce the aggregation of the particles and produce a homogenous slurry [142-144]. Figure 5.1 shows a schematic diagram of the effect of dispersant on the aggregated

particles. When the aggregated particles are mixed with dispersant media, i.e., dispersant and distilled water, they are coated with a very thin layer of dispersion. The coated layers charge the surfaces of the particles by negative charges, which produce a repulsion force between the particles and their neighbourhoods [145-146]. As a result, the aggregated particles are separated from each other. To measure the rheological properties of the dispersed slurries, Zeta potential is an approach widely used for studying the properties of ceramic suspensions [147-149]. However, this approach is also used for studying metallic suspension such as nickel nano powder [138]. Although, Zeta potential is an efficient method of measuring the rheological properties of suspended nano particles, it is not adopted in this thesis because the particles are in micron size and their densities are big enough to be suspended in an aqueous dispersion. Thus a new approach was presented in this Chapter in order to optimize the slurry properties and to improve the green density of the micro components.

To obtain the optimum dispersant for preparing stainless steel aqueous slurries, the proposed method are presented as follows:

1. Prepare stainless steel slurries containing different amount of dispersants for each powders. The binder and solid loading were adjusted to be the same for all slurries in order to study the effect of dispersant only
2. The soft moulds were filled by the stainless steel slurries and the green components were obtained following the same procedures discussed in Chapter Four.
3. The densities of the green components were measured for each amount of dispersant.
4. The maximum green densities were obtained and their corresponding amounts of dispersant were selected to be the optimum dispersant.

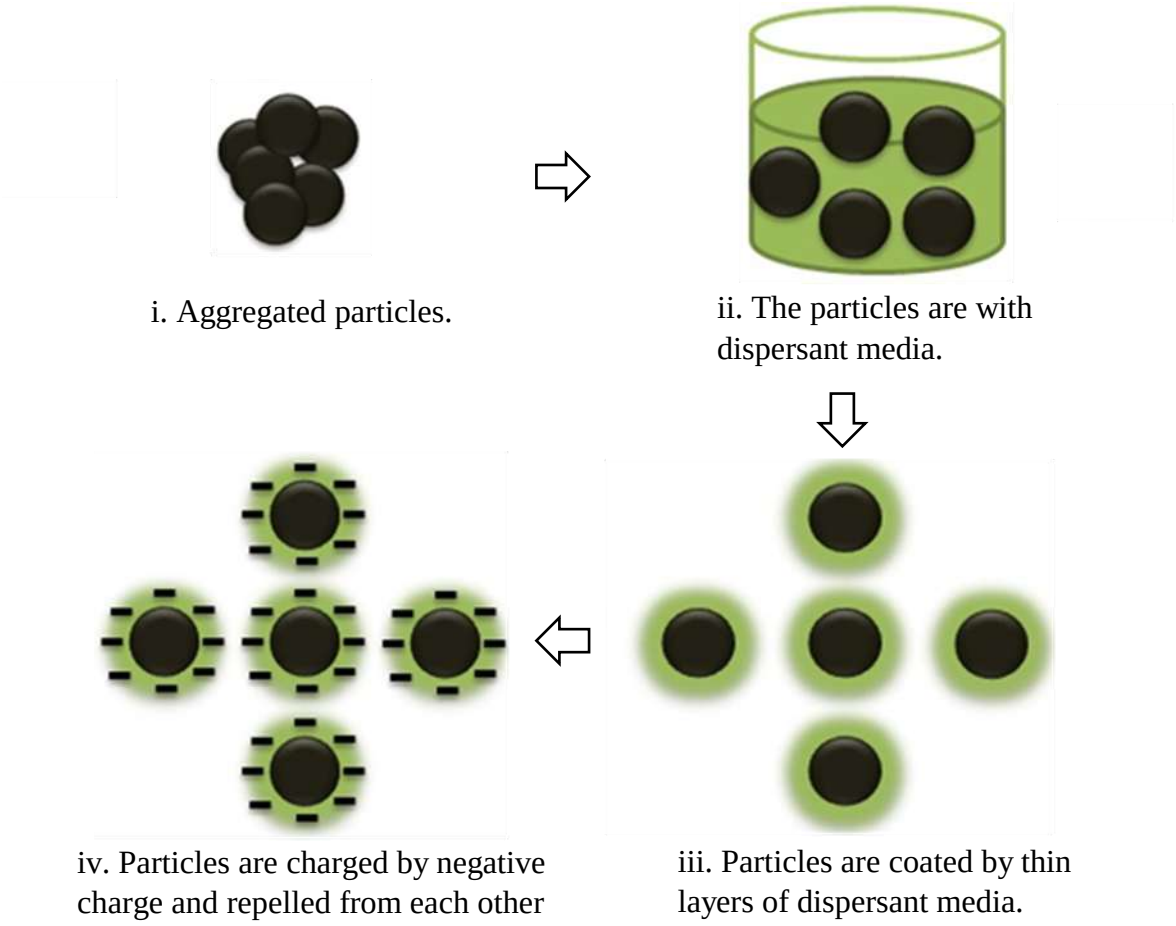

Figure 5.1. A schematic diagram showing the effect of the dispersant on the aggregated particles.

Due to the complex shape of the micro components and the difficulty in measuring their densities accurately, cylindrical soft moulds were prepared. The dimensions of cylindrical soft moulds are 5 mm in both diameter and height as shown in Figure 5.2(a). The stainless steel slurries were prepared from three different powders: 5, 10 and 16-µm. The solid loading was adjusted to be 60% (vol.), as presented in Chapter Four. The binder is a mixture of Duramax B-1000 and B-1007 with ratio 1: 3 wt., respectively. The ratio between the binder and powder was selected to be 0.1: 1 wt. The cylindrical green components were de-moulded after the slurry dried and their images were inspected under optical microscope and shown in Figure 5.2(b). It is clear that the cylindrical green

components were obtained without damage, which helps measuring the density by mass and volume method. The dimensions were measured using calliper with accuracy 0.01 mm, while the mass was measured using a very accurate balance with tolerance ± 0.000001 gram.

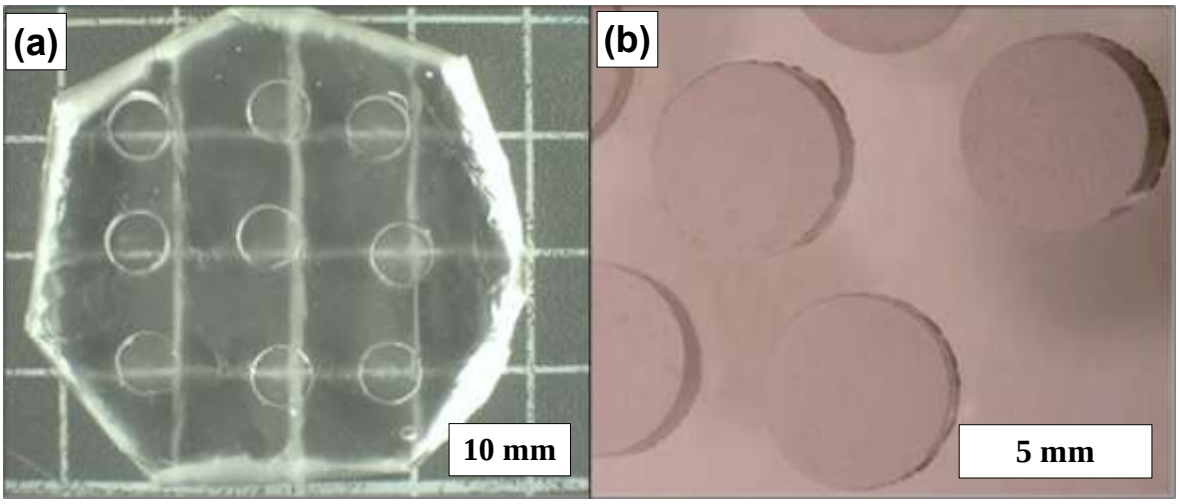

Figure 5.2. Optical images showing the: (a) cylindrical soft mould inserts with 5 mm in both diameter and height and (b) their corresponding green components.

5.1.2. Obtaining the optimum amount of binder

The binder has a great effect on the preparation of stainless steel aqueous slurries and their corresponding green components. It is found that using too much binder can increase the green strength but it also increases the overall de-binding time and shrinkage after sintering. However, using less binder produces green micro components having insufficient strength which is likely to be damaged during the de-moulding process. In fact, there is no rule to select the optimum amount of binder desired for obtaining damage-free green micro components because the de-moulding is done manually. Thus, the components may be damaged due to in-experience de-moulding and/or insufficient strength. Therefore, the method used for the selection of the optimum amount of binder is presented as follow:

1. Prepare stainless steel slurries containing different amount of binders for each powder size. The amount of dispersant was adjusted to be the optimum amount obtained in section 5.1.1. for each powder. The solid loading was also adjusted to be the same for all slurries in order to study the effect of binder only.
2. After the soft micro moulds were filled by metallic slurries and the slurries dried, the green micro components were obtained and inspected under SEM.
3. The minimum amount of binder used for obtaining ~ 50% of the green micro components damage free was selected as the optimum value.

5.2. Cold Isostatic pressing (CIP) method

Powder metallurgy process provides an economical and near net shape forming process. Powder injection moulding (PIM) is a widely used powder shaping process in which the powder is compacted to the desired shape using die and plunger [150]. However, this process produces some defects in the compacted powder due to inhomogeneous density distribution resulted from the friction between the powder and the die wall [151-152]. A cold isostatic pressing is another technique used for powder shaping. Through this process, the powders are compacted to the desired shape with equally applied pressure from all directions to improve the homogeneity and retention of the green components [153-157]. There are two types of cold isostatic pressing process: wet bag and dry bag. In the former type, a rubber bag (mould) is dropped down into the pressure vessel filled by water and it is removed each cycle and refilled. This type is commonly used when large and complex shapes are required. In the later type, dry bag is an integral part of the pressing vessel and is used when small sizes and simple shapes that can be removed easily are required. Many details of the cold isostatic pressing technique can be found in [158-165]. However, cold

isostatic pressing technique is used for production of large scale components; it is limited in the fabrication of micro components [166-167].

As discussed in section 5.1.1, the soft micro moulds were filled by the metallic slurries with 60% vol. solid loading without applying external pressure. Hence, increasing the solid loading decreases the opportunity to fill the micro features without applying pressure. Consequently, a cold isostatic pressing technique was adopted in this thesis in order to apply high solid loading which cannot be used with the pressure less filling method.

The required equipment for isostatic pressing technique is hydraulic press, pressing cylinder and pressing fluid as discussed in reference [168]. The pressing equipment was modified in this research in order to be used for pressing micro components. Figures 5.3 (a) and (b) show a schematic diagram of the pressing cylinder parts including cylinder & piston & lid and a photograph showing the hydraulic press and the pressing assembly, respectively.

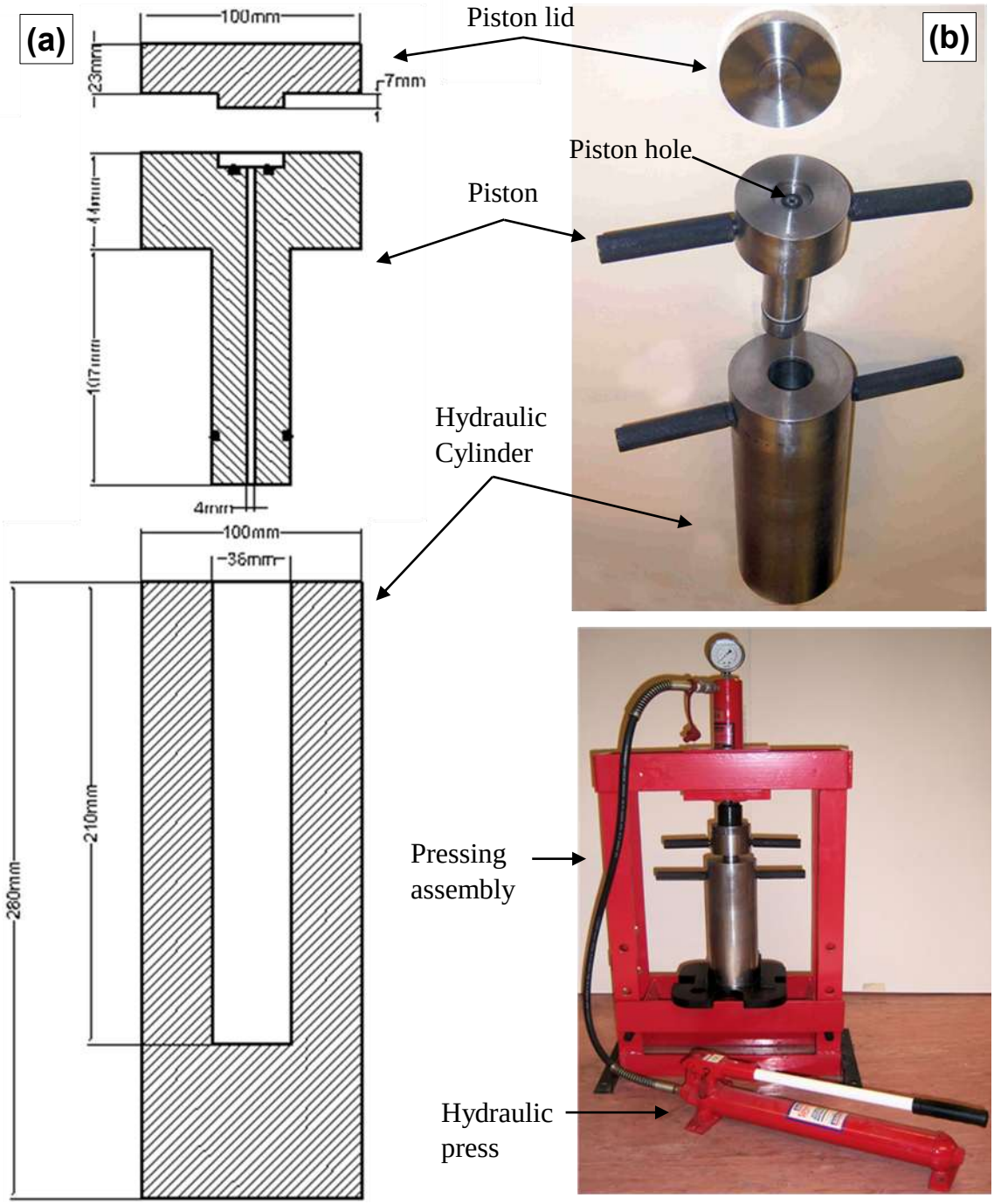

Figure 5.3. A schematic diagram and a photograph showing the: (a) hydraulic cylinder design with dimensions and (b) photograph of hydraulic cylinder parts and the pressing assembly.

5.2.1. Preparation of stainless steel semi solid pastes for CIP method

The stainless steel semi solid pastes are prepared from different powders using the following procedures:

1. Prepare stainless steel slurries with low solid loading 60 % vol. containing the optimum amount of dispersant and binder following the same procedures discussed in pressure less filling method.
2. The slurries were continuously stirred by mechanical stirrer until they transferred to semi solid pastes.

5.2.2. Filling the soft micro moulds by applying pressing

After preparing stainless steel semi solid pastes, the soft micro moulds are filled by two methods: hand pressing and cold isostatic pressing. In the hand pressing method, the semi-solid pastes were put into the soft micro mould opening. Afterwards, the pastes were pressed against an alumina substrate by hand pressing. In the cold isostatic pressing method, the following procedures are presented:

1. The semi-solid pastes were pressed gently to the soft micro moulds using spatula. Afterwards, the filled soft micro moulds were covered by another soft mould as a lid.
2. The soft micro moulds and their lids were sealed well by using rubber glove fingers.
3. The pressing cylinder was filled by water as a pressing fluid and the sealed soft micro moulds containing the stainless steel pastes were dropped down inside the pressing cylinder.

4. The pressing cylinder parts were assembled by moving the piston into the cylinder until the water comes out from the piston hole in order to remove the air trapped inside the cylinder.
5. The piston hole was covered by the piston lid and the cylinder assembly was put under hydraulic press to apply the load.
6. The applied pressure rang was 40-116 MPa. The holding time was selected to be 10 minutes before the pressure releases. This time is sufficient to pack the powder into the soft micro moulds and maintains the integrity of the green micro components.

The effects of filling methods on the filled micro moulds were inspected under optical microscope. Figures 5.4 (a) and (b) show the optical images of the filled micro moulds by applying hand pressing and cold isostatic pressing methods, respectively. It is found that the soft micro moulds are not filled completely when the hand pressing method is used, especially, the micro gear teeth as pointed by black arrows. On the other hand, applying isostatic pressure enables the micro features to be filled without voids and the shapes are retained.

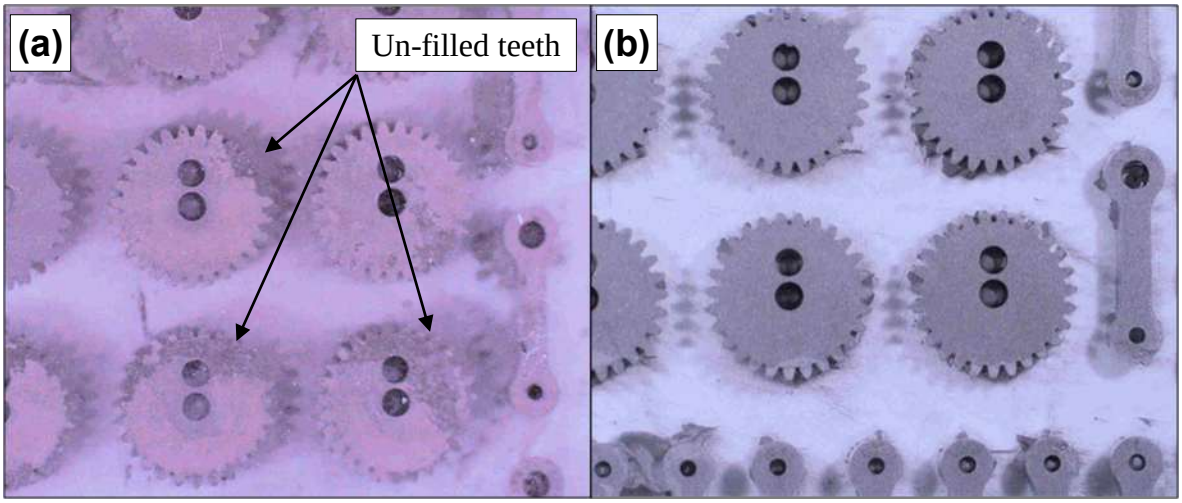

Figure 5.4. Optical images showing the soft micro moulds filled by stainless steel pastes: (a) by applying hand pressing method and (b) by applying cold isostatic pressing method.

5.2.3. Obtaining the green micro components based on CIP method

After the isostatic pressure is released, the rubber seal and soft lid were removed. The residual paste on top of soft mould opening was removed by metal blade. The stainless steel pastes dried quickly and the green micro components were de-moulded following the same procedures discussed in Chapter Four. Figure 5.5 shows a schematic diagram of the complete cold isostatic pressing technique.

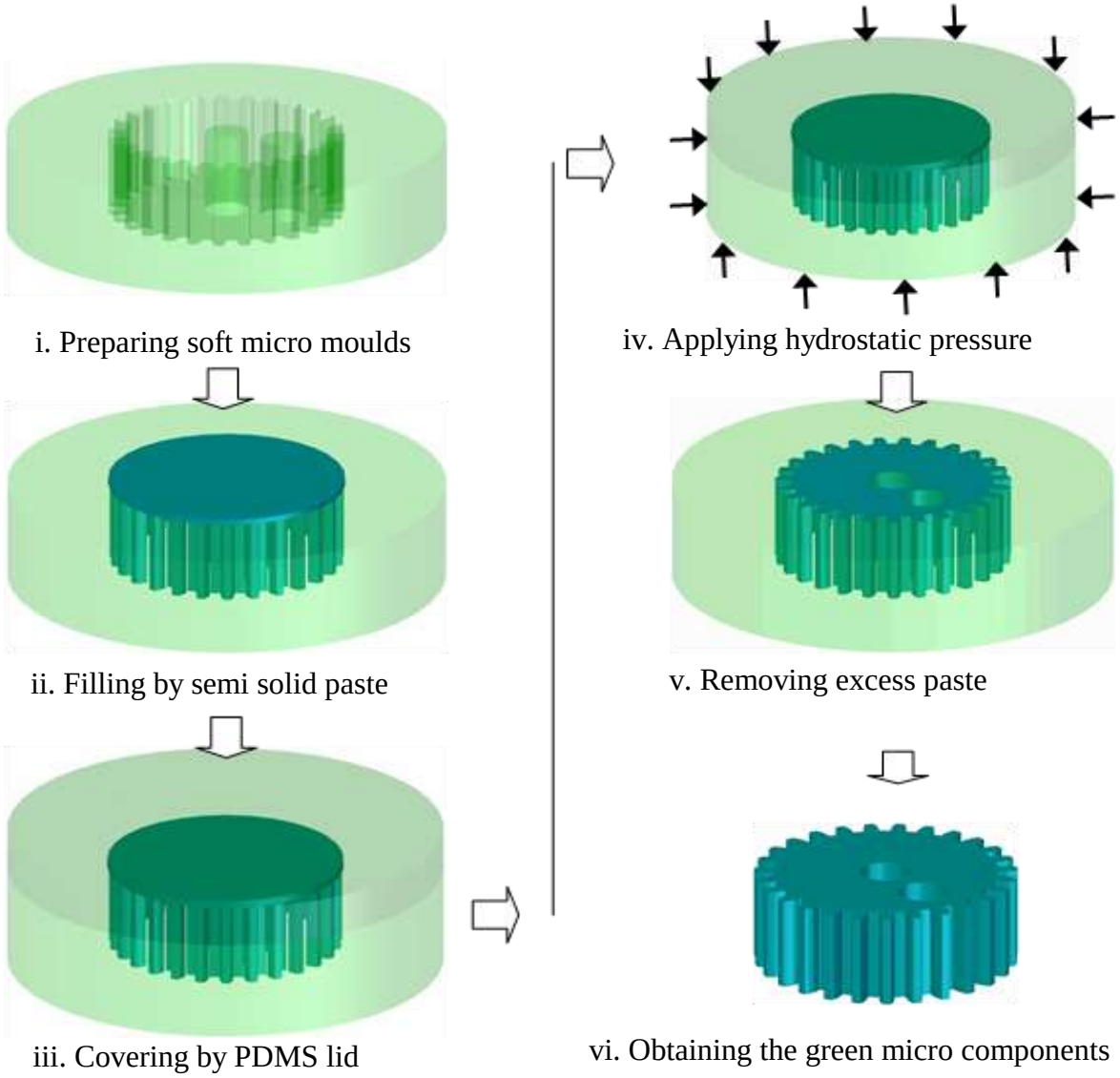

Figure 5.5. A schematic diagram showing the complete process for obtaining green micro components using cold isostatic pressing method.

5.3. Results and discussions

5.3.1. Effect of dispersant on the densities of green components based on pressure less filling method

The densities of the green components were measured as a ratio to the 316-L stainless steel wrought materials which measures 8 g/ml. The amount of dispersant was presented as a weight ratio to the stainless steel powder. The density measurements were presented as a mean value of ten samples measured for each dispersant ratio. The effect of dispersant on the densities of the green components, based on different powders, was investigated and the results were shown in Figure 5.6. It is clear that the dispersant has a significant effect on the densities of the green components. Increasing the dispersant ratios increases the green densities for different powders. For a given dispersant ratio, the bigger the powders are, the greater the green densities and vice versa. It is found that the packing of the particles in the mass powder can be reflected by its tap density [168], which is the weight of unit volume of loose powder. As presented in Table 4.2, the bigger the powder is, the greater the tap density. The small powders have small-size space between each other which cannot fit any other powder to be entered into that space. While, the big powder size provides large space between each other which can fit other small powders and hence increases the powder packing. This explains why the green density of the big powder is greater than that of the small one. Moreover, the maximum green densities of the green components based on 5, 10 and 16-µm powders are found to be 59.12%, 63.82% and 65.61% and their corresponding dispersant/powder ratios are 0.003, 0.0022 and 0.0018, respectively. It is also clear that the bigger the particle sizes are, the smaller the corresponding dispersant ratios. This happens because the amount of dispersant is

dependent on the particles surface areas. Therefore, the greater the surface area is, the greater the dispersant needed and vice versa. As the powder sizes decrease, their surface area increases and hence, it needs large amount of dispersant. Furthermore, there is no significant effect of the dispersant on the green densities after obtaining the maximum. Consequently, these ratios are selected to be the optimum dispersant for preparing the stainless steel aqueous slurries from 5, 10 and 16-µm powders by using pressure less filling method.

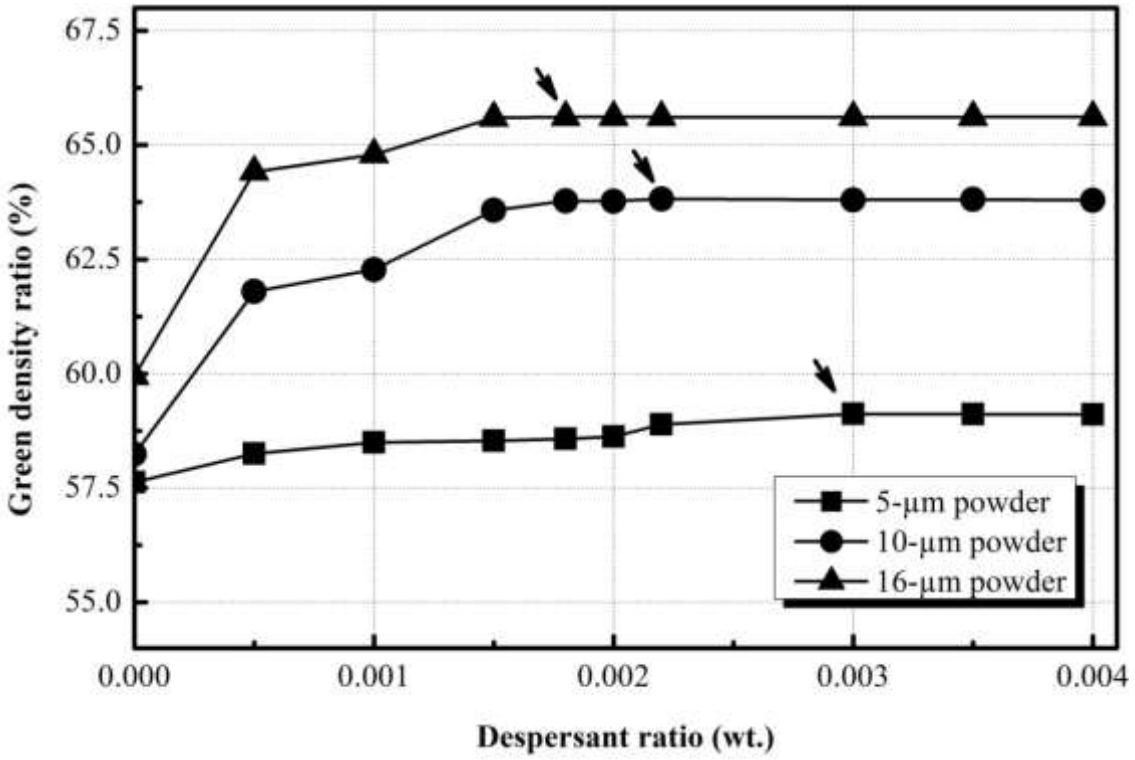

Figure 5.6. A graph showing the effect of dispersant ratio on the density of stainless the green components fabricated from 5, 10 and 16-µm powders.

5.3.2. Effect of dispersant on the fracture green micro components based on pressure less filling method

Figures 5.7 (a) & (b), 5.8 (a) & (b) and 5.9 (a) & (b) show SEM images of the fracture green micro components, fabricated from 5, 10 and 16-µm powders using pressure less filling method with no dispersant and optimum dispersant, respectively. It was found that when no dispersant is used during preparation of the stainless steel slurries, the particles show high tendency of aggregation. The aggregations produce inhomogeneous green micro components and many voids are formed inside the green micro components. On the other hand, using optimum dispersant not only reduces the tendency of particles aggregation but it also reduces the voids inside the green micro components. These results prove that why the green density increases as the dispersant increases.

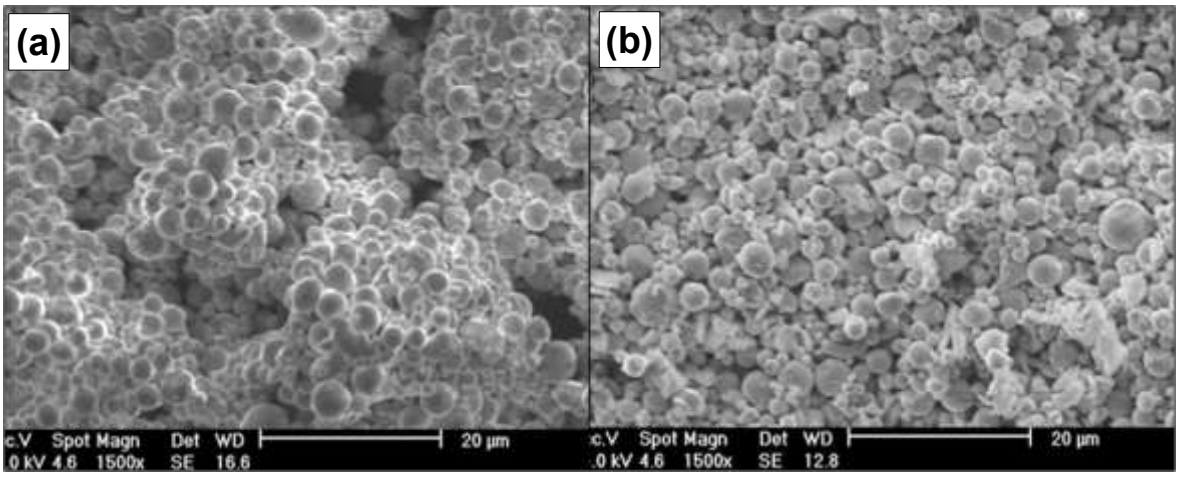

Figure 5.7. SEM images showing the fracture green micro components fabricated from 5-µm stainless steel powder using pressure less filling method and fabricated with: (a) no dispersant and (b) optimum dispersant.

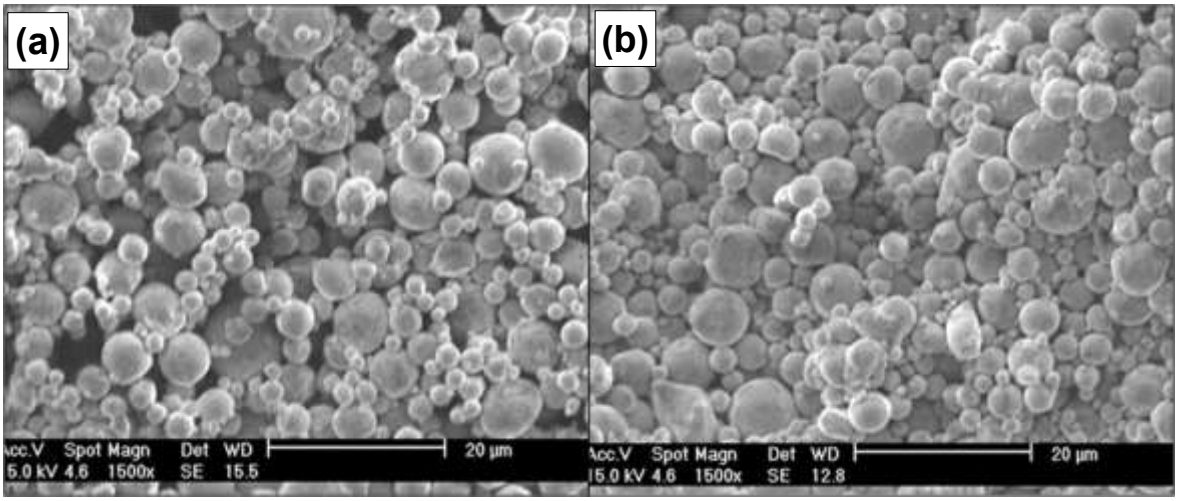

Figure 5.8. SEM images showing the fracture green micro components fabricated from 10-µm stainless steel powder using pressure less filling method and fabricated with: (a) no dispersant and (b) optimum dispersant.

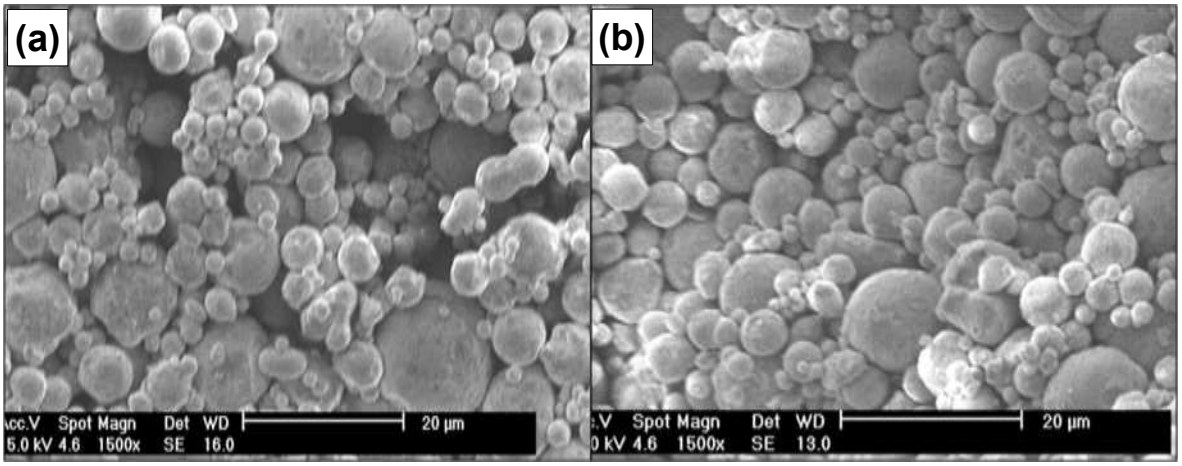

Figure 5.9. SEM images showing the fracture green micro components fabricated from 16-µm stainless steel powder using pressure less filling method and fabricated with: (a) no dispersant and (b) optimum dispersant..

5.3.3. Effect of binder on the retention of green micro components based on pressure less filling method

After several trials, it is found that using binder/powder of 0.04 weight ratio produces nearly half of the de-moulded micro components damage free when careful de-moulding is

taken into account. The green micro components fabricated by using optimum slurry parameters were inspected under SEM. Three different defects were observed. The first defect is resulted from insufficient strength. In this type, a piece of the micro component is damaged and/or a crack is observed, as shown in Figures 5.10 (a) and (b), respectively. The second defect type is commonly occurred in the micro components holes and edges. The holes and/or edges are damaged during extraction from the soft micro moulds, as shown in Figures 5.11 (a) and (b), respectively. This defect type cannot be controlled because the de-moulding is done manually and human error cannot be eliminated. The third defect type is occurred in the corners of micro components. In this type, spherical voids are formed in the corners of micro components as shown in Figures 5.12. This defect type is resulted from insufficient degassing during filling process and it can be controlled by increasing the degassing time. The defect free green micro engine components were also investigated and shown in Figures 5.13 and 5.14. High quality green micro components obtained are the same quality as the SU-8 master mould. The tips of gear teeth fabricated from 5, 10 and 16-µm powders are inspected and shown in Figures 5.15 (a), (b) and (c), respectively. It is clear that net shape micro features are successfully produced from all powders.

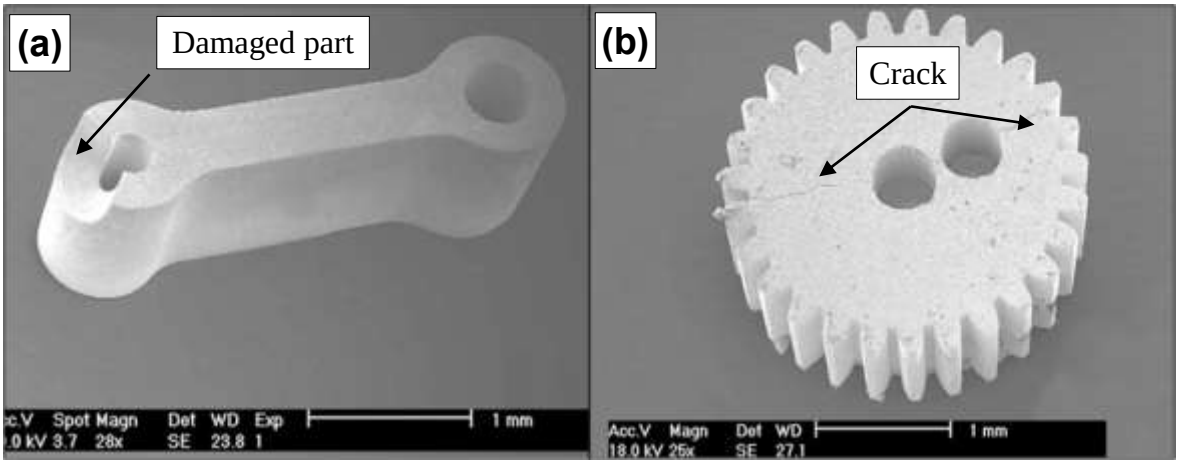

Figure 5.10. SEM images showing the stainless steel green micro components fabricated by using pressure less filling method and defected due to insufficient strength: (a) micro linkage rod and (b) micro gear with crack.

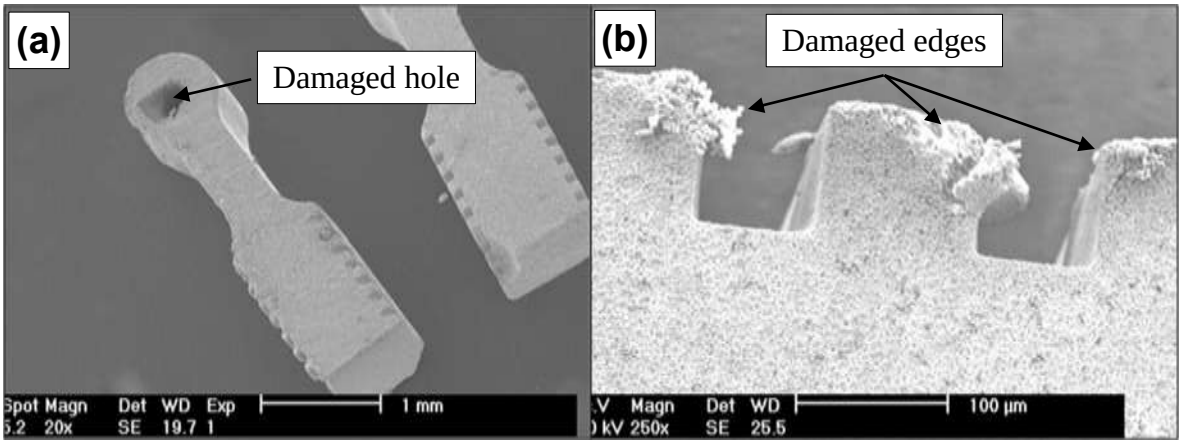

Figure 5.11. SEM images showing the stainless steel green micro components fabricated by using pressure less filling method and defected during de-moulding: (a) micro piston and (b) micro piston edges.

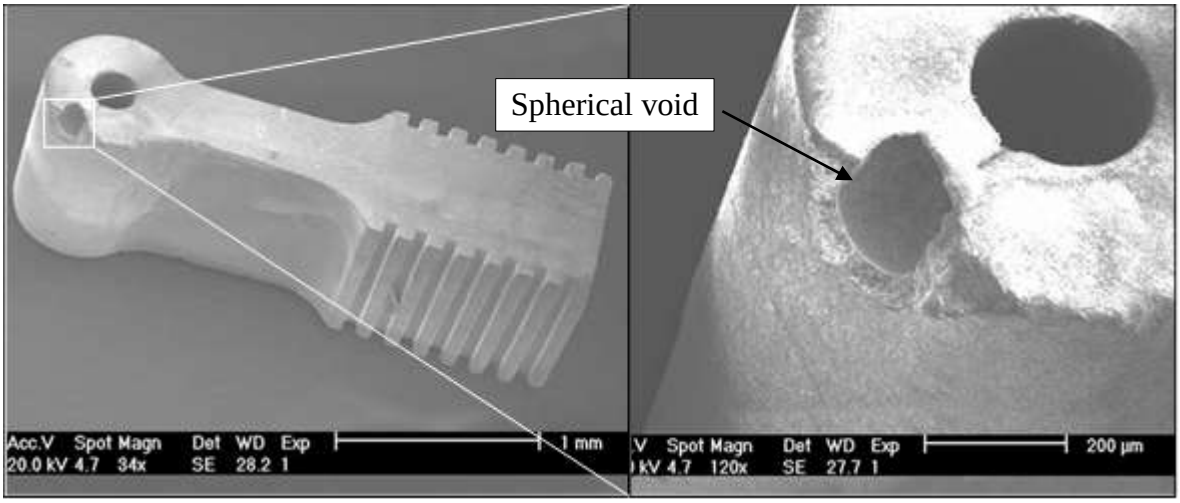

Figure 5.12. SEM images showing the stainless steel green micro piston fabricated by using pressure less filling method and defected due to insufficient degassing.

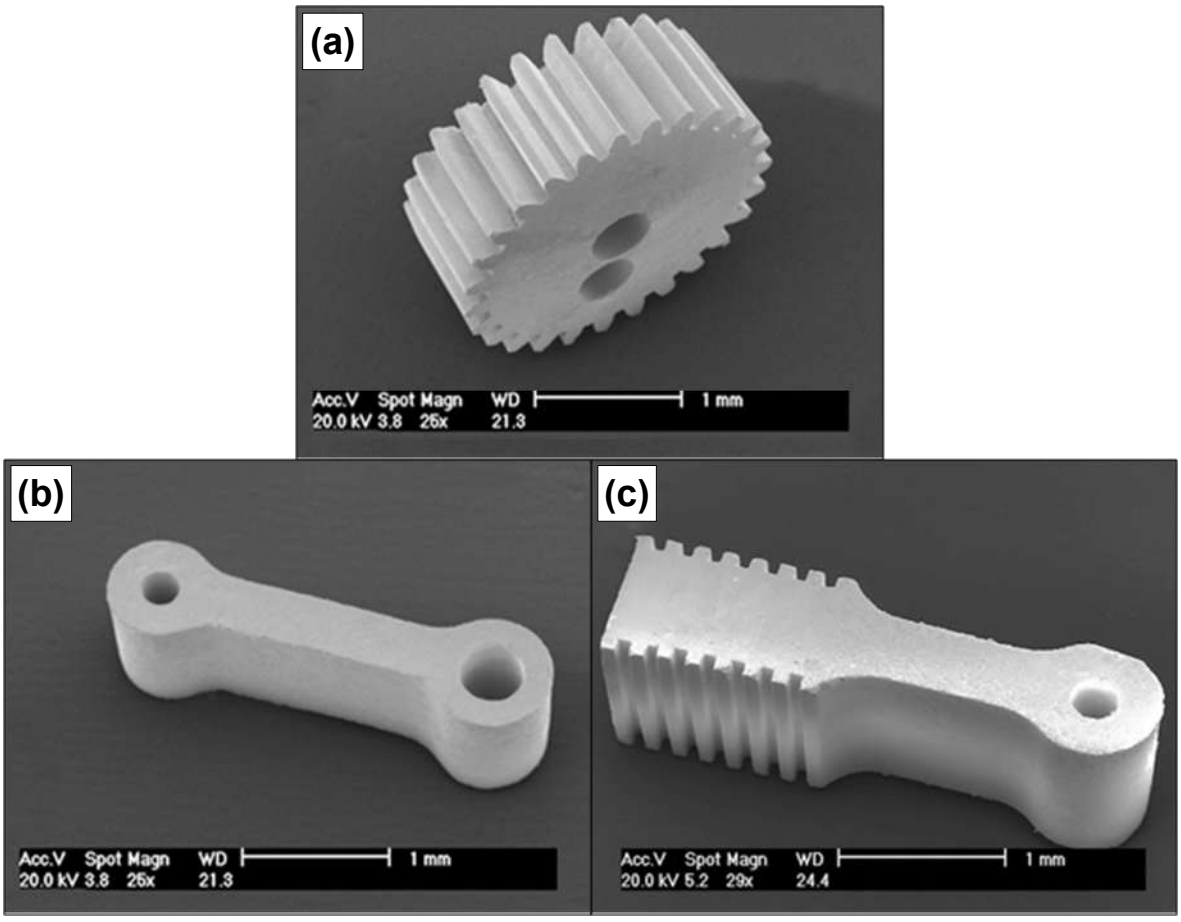

Figure 5.13. SEM images showing the stainless steel defect free green micro components fabricated by using pressure less filling method: (a) micro gear (b) micro linkage rod and (c) micro piston.

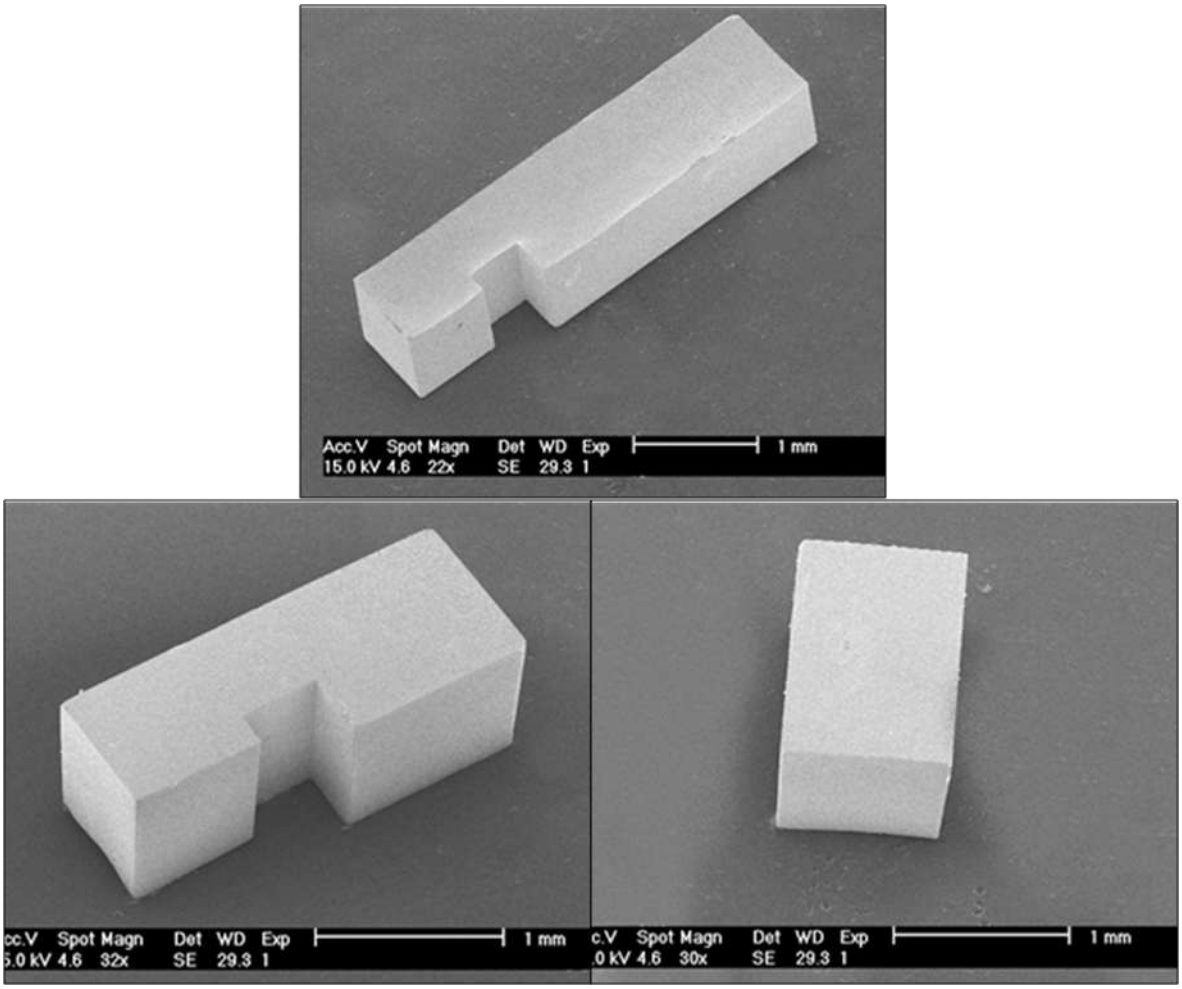

Figure 5.14. SEM images showing the stainless steel defect free green micro engine cylinder components fabricated by using pressure less filling method.

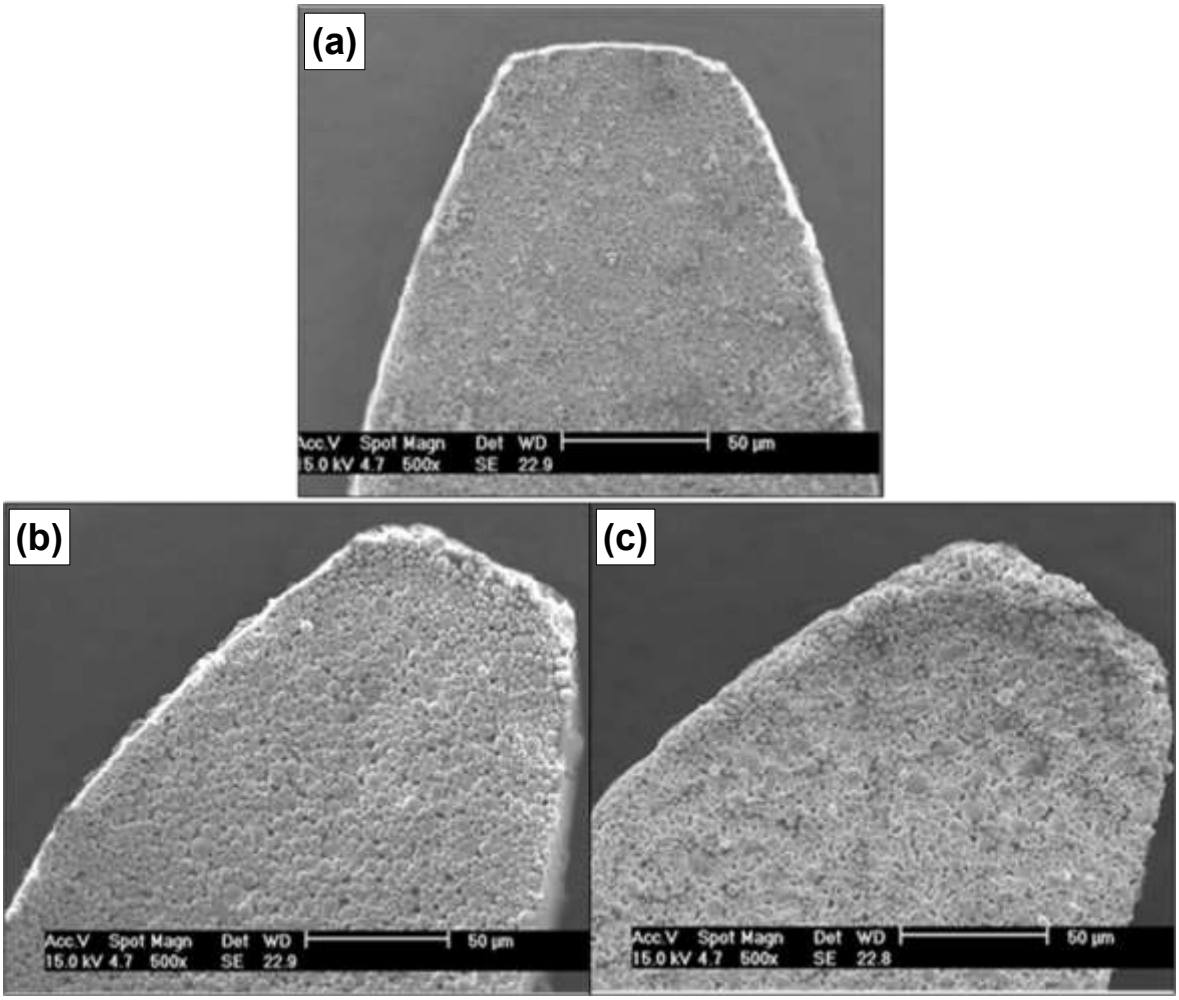

Figure 5.15. SEM images showing the stainless steel defect free green micro gear tooth tips fabricated by using pressure less filling method and based on: (a) 5-µm, (b) 10-µm and (c) 16-µm powders.

5.3.4. Effect of pressing method on the density of the green components

To measure the densities of the green components fabricated by applying external pressure, cylindrical soft moulds, used in section 5.1.1, were also used in this section. The green density measurements are performed using the same procedures discussed in section 5.3.1. The effects of pressing method on the densities of the green components were investigated. It is found that, the densities of the green components based on 5, 10 and 16-µm powders and fabricated by applying hand pressing method are 57.3, 58.7 and 60.1%, respectively.

On the other hand, the effect of isostatic pressure on the densities of the green components based on different powders was also investigated and results were shown in Figure 5.16. It is clear that the isostatic pressure has a great effect on the green density. As the pressure increases the green density increases for all powders. This happens because the pressure increases the packing of particles into the soft mould and hence, increases the green density. For a given applied pressure, the green density based on small powders is smaller than that based on larger one which is explained in section 3.3.1. The maximum densities of the green components, based on 5, 10 and 16-µm powders, are found to be 65.3, 66.1 and 67.5%, when the applied isostatic pressure is 116 MPa, respectively.

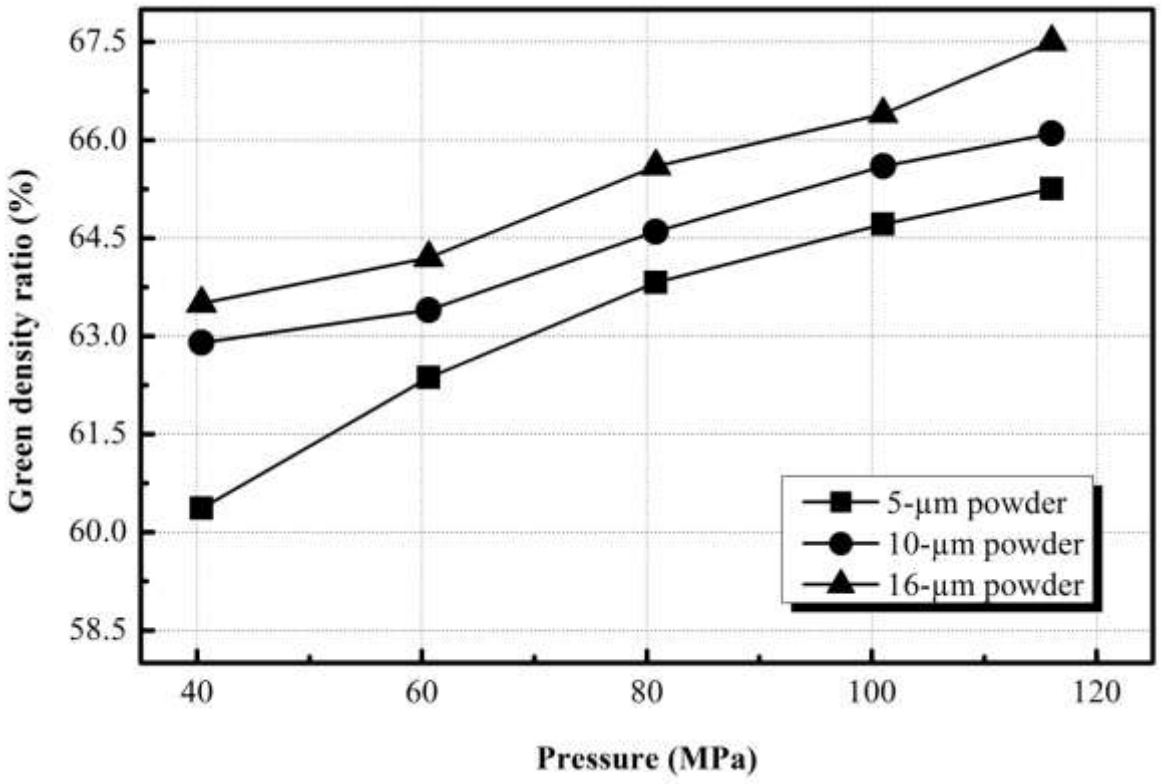

Figure 5.16. A graph showing the effect of the applied pressure on the green density of the stainless steel components fabricated from 5, 10 and 16-µm powders by using cold isostatic pressing technique.

5.3.5. Effect of pressing methods on the fractured green micro components

Figures 5.17 (a) & (b), 5.18 (a) & (b) and 5.19 (a) & (b) show the SEM of the fracture green micro components fabricated from 5, 10 and 16-µm powders by applying hand pressure and cold isostatic pressing, respectively. It is found that applying hand pressure is not sufficient to pack the particles into the soft micro mould and many cavities are existed. On the other hand, using isotactic pressure not only increases the particles packing but it also reduces the tendency of forming cavities inside the green parts. These results explain why the green densities obtained by using hand pressing method are smaller than that obtained by using cold isostatic pressing.

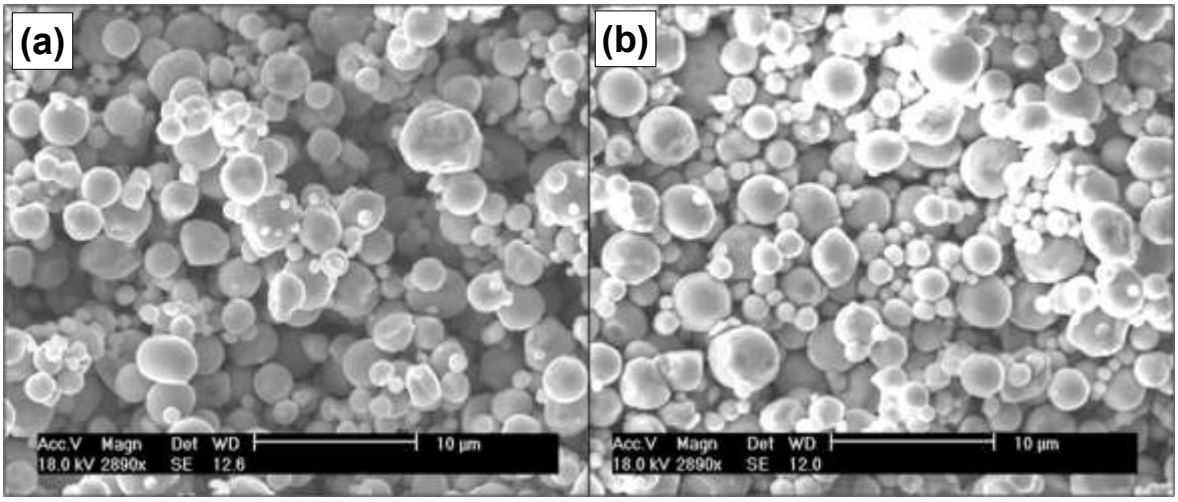

Figure 5.17. SEM images showing the fracture stainless steel green micro components fabricated from 5-µm powder by using: (a) hand pressing and (b) cold isostatic pressing methods (116 MPa).

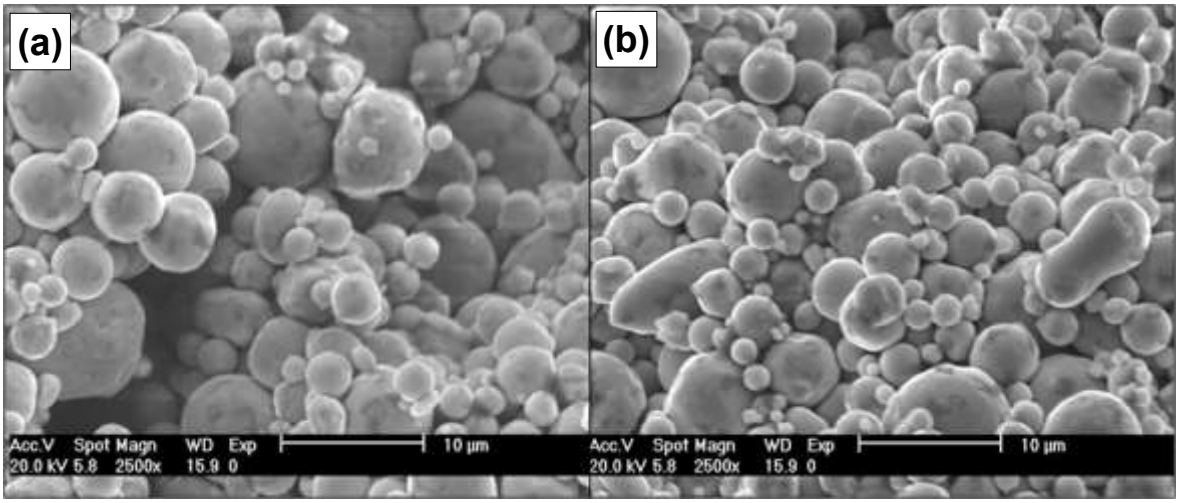

Figure 5.18. SEM images showing the fracture stainless steel green micro components fabricated from 10-µm powder by using: (a) hand pressing and (b) cold isostatic pressing methods (116 MPa).

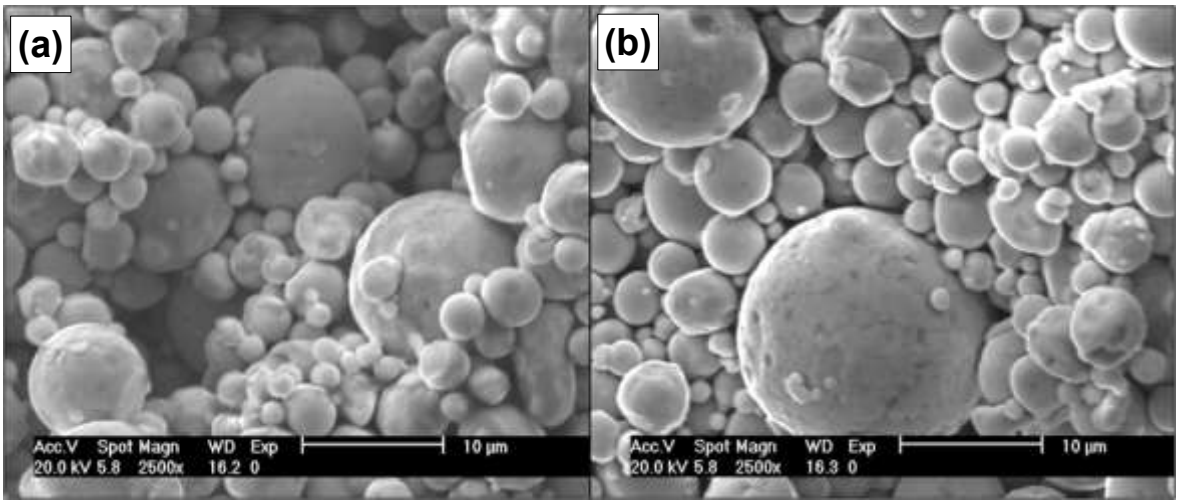

Figure 5.19. SEM images showing the fracture stainless steel green micro components fabricated from 16-µm powder by using: (a) hand pressing and (b) cold isostatic pressing methods (116 MPa).

5.3.6. Effect of cold isostatic pressing on the retention of green micro components

The green micro components obtained by using cold isostatic pressing technique were inspected under SEM. It is clear that the number of defect free green micro components

obtained using cold isostatic pressing method is smaller than that obtained using pressure less method. Nearly, one third of the de-moulded samples are damage free. Figure 5.20 shows samples of defect free green micro components obtained by using cold isostatic pressing method. The shape of micro components produced using cold isostatic pressing technique is retained because the pressure is applied equally from all direction, while some defects in the edges are observed. The defect in the edges is occurred due to the small deformation happened to the soft micro moulds after applying pressure which affects the green micro components after de-moulding.

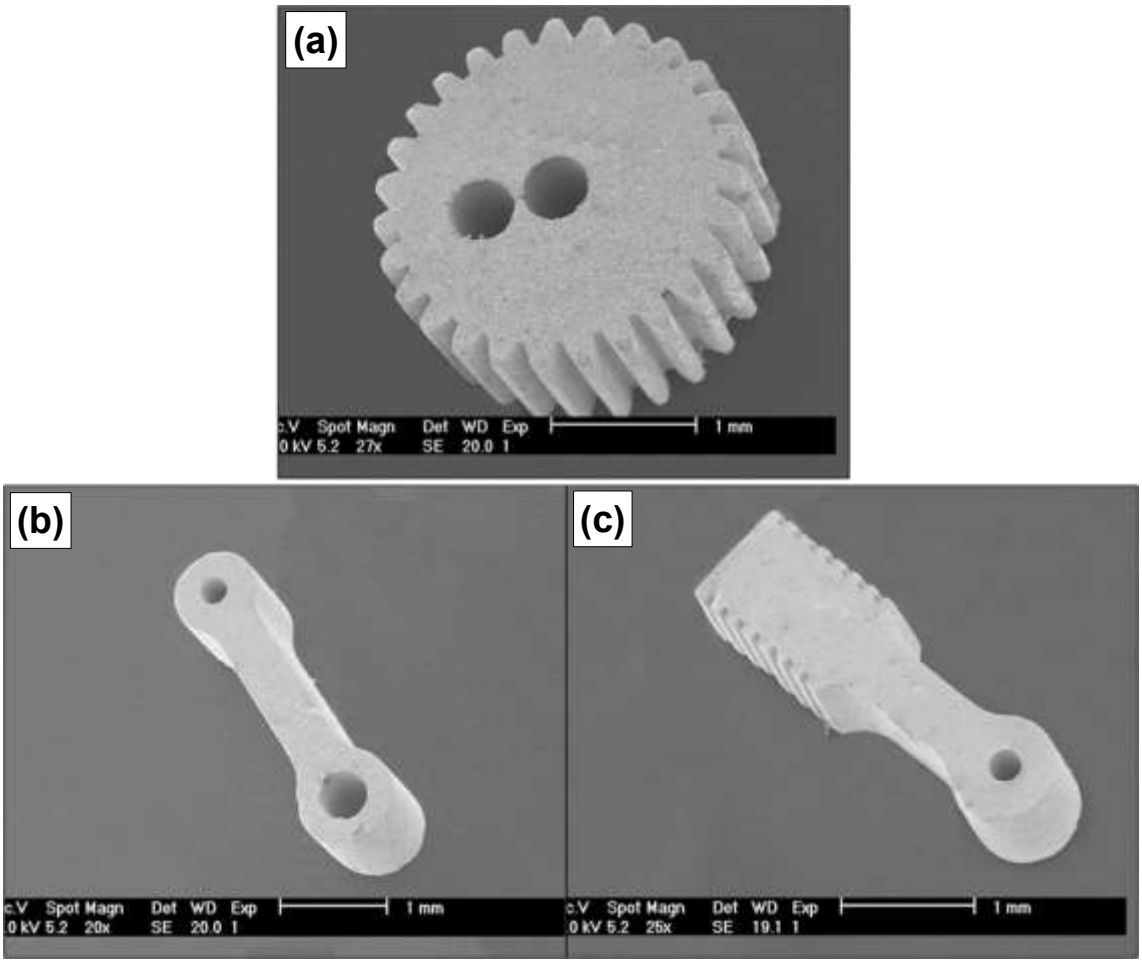

Figure 5.20. SEM images showing the stainless steel green micro components fabricated by using cold isostatic pressing method (116 MPa): (a) micro gear (b) micro linkage rod and (c) micro piston.

5.3.7. Linear shrinkage

The linear shrinkage of the green micro components was also investigated for the two fabrication methods, pressure less and cold isostatic pressing methods (116 MPa). The measurements were based on the outer diameters of micro gears and the SU-8 master mould was selected as a reference. The linear shrinkage was measured using the following formula:

$$shrinkage\ \% = \frac{D_{SU-8} - D_g}{D_{SU-8}} \times 100 \quad (5.1)$$

D_{SU-8}: The outer diameter of the SU-8 micro gear,

D_g: The outer diameter of the green micro gear.

The measurements were taken from the top views of the SEM images of SU-8 and green micro gears as shown in Figure 5.21 (a) and (b), respectively. Table 5.1 presents the linear shrinkage of the green micro components fabricated by using pressure less and cold isostatic pressing methods (based on 116 MPa applied pressure). The results presented in Table 5.1 are the mean value of six samples measured for each case. It is clear that the linear shrinkage based on cold isostatic pressing method is smaller than that based on pressure less filling method. Moreover, the linear shrinkage based on a big powder is smaller than that based on a smaller one. The cold isostatic pressing method improves the packing of the powder by rearranging them in the green compact and hence, decreases the shrinkage. However, pressure less method is based on low solid loading, which provides large shrinkage after the slurry dries.

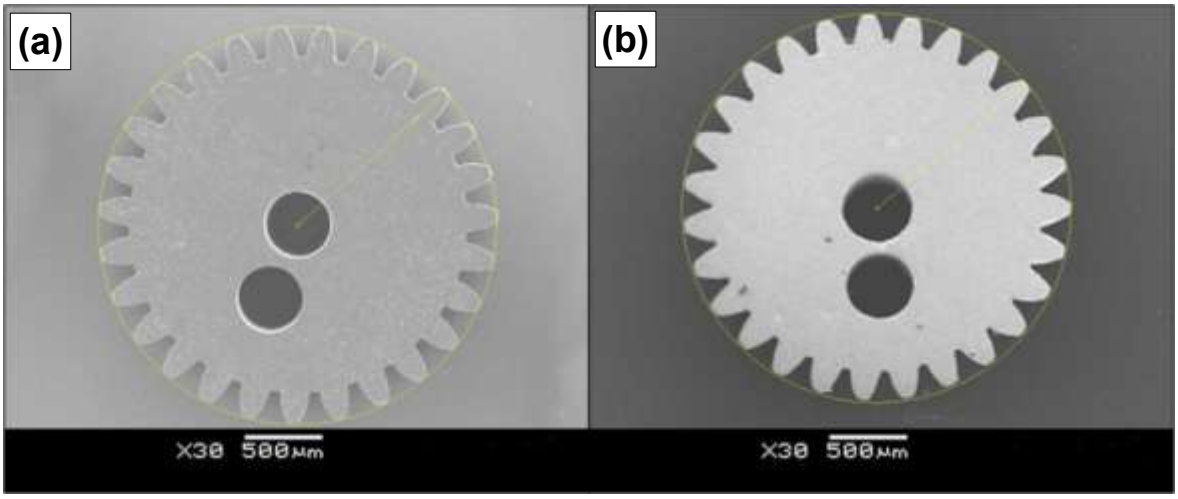

Figure 5.21. SEM images showing the top views of: (a) SU-8 micro gear and (b) stainless steel green micro gear.

Table 5.1. Linear shrinkage of the stainless steel green micro components based on different powders and fabricated by pressure less filling method and cold isostatic one.

Powders	Linear shrinkage (%)	
	Pressure less	Cold isostatic pressing (116 MPa)
5-µm	5.62	2.53
10-µm	2.32	2.12
16-µm	2.14	1.74

5.4. Conclusions

In this chapter, the stainless steel green micro components of different powders were successfully fabricated using pressure less filling method and cold isostatic pressing one. A study on the slurry preparation process, density, linear shrinkage and shape retention of the

green micro components were also investigated. The following conclusions are obtained in this chapter and listed below:

1. Using optimum dispersant not only reduces the particles aggregation but it is also improves the density packing of the green micro components for different powders.

2. The bigger the powders are, the greater the green density and lower the linear shrinkage.

3. Using cold isostatic pressing method produces a high green density and smaller linear shrinkage than using pressure less filling method; while, the shape retention of micro components is not as good as that obtained by using pressure less filling method.

CHAPTER 6. DE-BINDING AND SINTERING OF THE STAINLESS STEEL MICRO COMPONENTS

This Chapter presents the research into de-binding and sintering of the green micro components, following the fabrication of the green micro components explained in the last chapter. Three different sintering conditions, including nitrogen, nitrogen/hydrogen mixture and vacuum, are investigated in detail. The sintered stainless steel micro components in terms of shape retention are also investigated for the three different powders: 5, 10 and 16-µm.

6.1. Introduction

To obtain the final micro engine components, the green micro components need to be de-bound and sintered. De-binding is a necessary step before sintering. It is found that the residual binder remaining in the green components during sintering affects the final properties of the stainless steel materials by reducing its corrosion resistance [170]. Therefore, the de-binding process should be studied carefully. Sintering is the most critical step of processing stainless steel powder. Sintering is a process through which the adjacent particles in the green components are fused together to form a bulk structure by heating them to below the melting point of most constituent powders. The final properties of the sintered components are dependent on different sintering parameters such as sintering temperatures, atmospheres, particle sizes, particle shapes, and particle compositions [170-183]. Sintering atmosphere affects the forming quality of stainless steel materials. Because the metallic powders are subjected to oxidation during de-binding and sintering process, it is necessary to be sintered under a special atmosphere. The most important reason for

using non-oxidizing atmospheres is to provide protection against oxidation of the sintered metal powders. Three types of atmospheres have been widely used for sintering stainless steel powders. They are hydrogen, vacuum and inert gases atmospheres [173, 179–183]. However, gas atoms of the sintering atmosphere may enter the sintering components via interconnected pores or they get trapped in closed pores. Therefore, they hinder the densification process. Gas atoms may also diffuse into the stainless steel and strengthen the structure [178-179]. When hydrogen is used as a sintering atmosphere, hydrogen atoms may dissolve into the grain and form small pores. Vacuum is widely used as sintering atmosphere in sintering different metallic and ceramic components because of ecological considerations. The main problem faced in sintering stainless steel using vacuum is the chromium depletion during sintering, which reduces the corrosion resistance significantly. At a certain temperature, if the vapour pressure inside the vacuum furnace lowers below the vapour pressure of the chromium element, the chromium is subjected to evaporation [170 and 183]. Therefore, it is very important to control the vacuum atmosphere to avoid chromium depletion and hence to maintain the corrosion resistance of stainless steel. To control this issue, the vacuum vessel is backfilled by argon with a pressure of 25-65 Pa, which is higher than the vapour pressure of chromium [171] and that prevents the chromium depletion. Argon and nitrogen are commonly employed as sintering atmospheres. It is reported that the densification process of stainless steel is influenced by atmospheric parameters including gas type, mixed ratio, dew point and flow rate [184-186]. On the other hand, the sintering of stainless steel and its properties can be improved by addition of sintering aids. It is found that adding nickel to stainless steel powder improves the corrosion resistance [187], while adding yttria improves the oxidation

resistance [188]. However, adding yttria alumina agent (YAG) and copper improves the hardness and reduces the porosities of sintered stainless steel [189-190].

6.2. De-binding and sintering

In this thesis, three different sintering atmospheres were investigated including nitrogen, nitrogen/hydrogen mixture and vacuum. Because the green micro components are subjected to deformation during heating, two proposed heating cycles are investigated using nitrogen atmosphere. The successful cycle in producing stainless steel micro components with good shape retention is selected to be used with nitrogen/hydrogen mixture and vacuum atmospheres. The micro components based on 5-µm powder are investigated with nitrogen atmosphere and the target sintering temperature is 1200^{o}C.

6.2.1. Thermal gravimetric analysis (TGA)

It is very important to study the degradation behaviours of the binder before the de-binding process in order to select a suitable de-binding cycle. Thermal gravimetric analysis (TGA) is a process widely used in order to measure the weight lost or gained to materials with the change of temperatures. In this thesis, the thermal analysis of dry samples from binders, Duramax B-1000 and B-1007, and dispersant D-3005 was investigated using NETZSCH Simultaneous Thermal Analyser (STA) 449C (School of Metallurgy and Materials, University of Birmingham). The test was performed under continuous flow of argon atmosphere with a temperature range of 25–800^{o}C and a heating rate of 10^{o}C/min. The thermal gravimetric analyser contains two alumina cups, which are put on the digital balance inside heating chamber as shown in Figure 6.1. The sample to be tested was put on one of the two ceramic cups and the other was left as a reference. During the heating

process, the sample was degraded thermally and the weight loss was detected. The thermal stability of the binders and dispersant detected by thermogravimetry (TG) traces was investigated and the results are shown in Figures 6.2. It is found that both B-1000 and B-1007 started to decompose slowly at about 300^{o}C and then rapidly at around 430^{o}C. At 700^{o}C, the residual binder of B-1000 is retained to about 3% while no residual binder was found in B-1007. Moreover, D-3005 starts to de-compose at 200^{o}C and the residual of about ~ 5% was found at 700^{o}C.

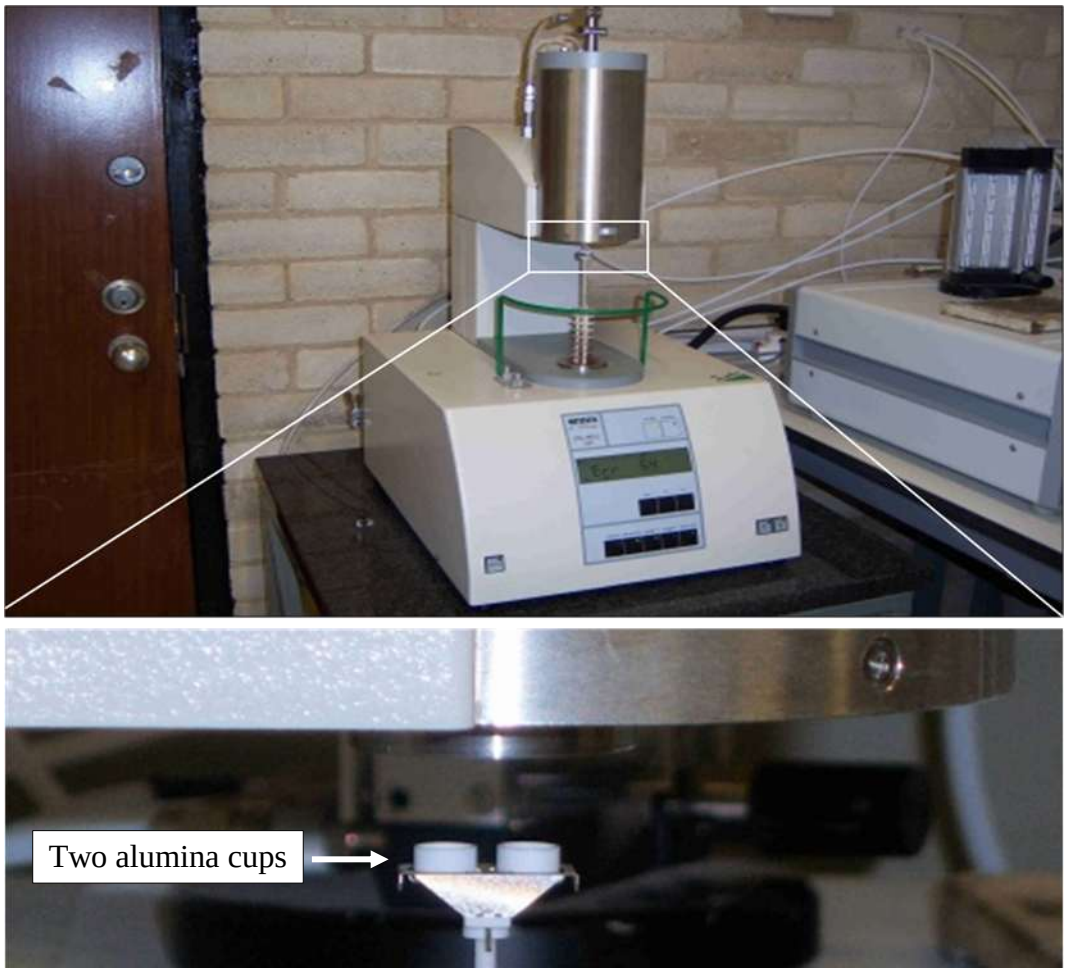

Figure 6.1. A photograph showing the NETZSCH Simultaneous Thermal gravimetric Analyser (STA) 449C used for investigating the degredation behaviours of the binder and dispersant.

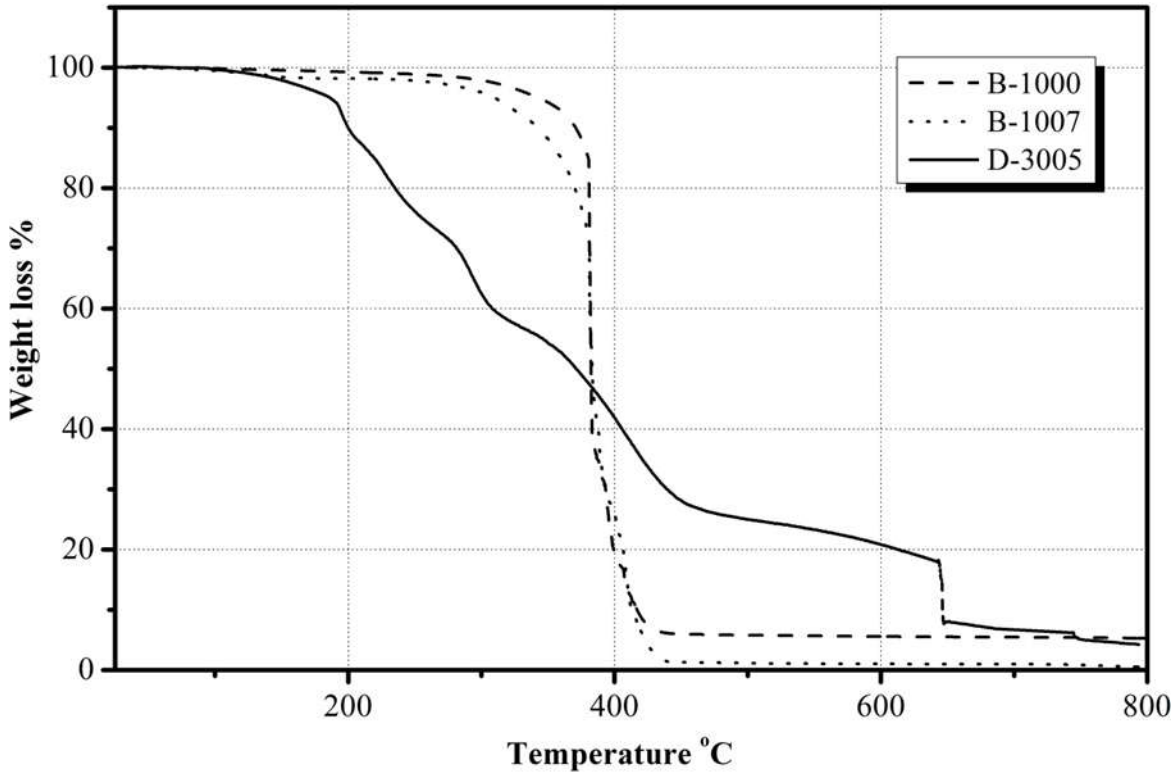

Figure 6.2. A graph showing the thermal degradation behaviours of the binder B-1000 and B-1007, and dispersant D-3005, which was performed in thermal gravimetric analyser at the temperature range of 25–800^{o}C.

6.2.2. Sintering in nitrogen atmosphere

Nitrogen is widely used as a sintering atmosphere of stainless steel green components. Because the stainless steel powders are subjected to oxidation during de-binding and sintering, both de-binding and sintering processes were done in a tube furnace at the same heating cycle with continuous flow of nitrogen. The tube furnace used in this thesis with nitrogen atmosphere is shown in Figure 6.3 (School of Metallurgy and Materials, University of Birmingham). According to thermal gravimetric analysis discussed section 6.2.1, the binders and dispersant were nearly degraded at 700^{o}C. Therefore, two proposed heating cycles, A and B, are used for de-binding and sintering processes. In cycle A, the de-binding was done by heating the green micro components to 700^{o}C with heating rate of

5°C /min and then it was held at this temperature for 1 h in order to remove the binder. During sintering, the temperature was ramped again to 1200°C with holding time of 1.5h and the heating rate was adjusted to be 10°C /min. On the other cycle, B, the target temperatures and holding times for both de-binding and sintering were adjusted to be the same as the cycle A, while the heating rates were changed to be 1.2°C /min and 5°C /min for de-binding and sintering, respectively. After sintering, the micro components are cooled down to room temperature by maintaining the dynamic flow of nitrogen atmosphere and without rapid cooling for both cycles.

Figure 6.3. A photograph showing the tube furnace used for de-binding and sintering stainless steel micro components under nitrogen atmosphere.

6.2.3. Sintering in nitrogen/hydrogen mixture atmosphere

Nitrogen/hydrogen mixture is another sintering atmosphere employed in this research. It is composed of 90% nitrogen and 10% hydrogen. Because hydrogen needs special safety, another tube furnace was used with forming gas atmosphere as shown in Figure 6.4

(School of Chemistry, University of Birmingham). The dew point is adjusted to be ≤ -35^{o}C.

Figure 6.4. A photograph showing a tube furnace used for de-binding and sintering stainless steel micro components under nitrogen/hydrogen mixture atmosphere.

6.2.4. Sintering in vacuum

Vacuum is the third sintering atmosphere used in this research. The green micro components were first de-bound in a tube furnace under nitrogen atmosphere and then sintered in vacuum furnace. The de-binding was done at the first stage of heating cycle A or B depending on a good result obtained in nitrogen atmosphere. The sintering was done in a vacuum furnace following the sintering stage of cycle A or B. The vacuum furnace used in this research is shown in Figure 6.5 (School of Metallurgy and Materials, University of Birmingham).

Figure 6.5. A photograph showing the vacuum furnace used for sintering stainless steel micro components under vacuum atmosphere.

6.3. Results and discussion

6.3.1. Effect of nitrogen on the sintered micro components

The sintered micro components based on two different heating cycles, A and B, were inspected under SEM and their images are shown in Figure 6.6 (a) and (b), respectively. It is clear that using heating cycle A during de-binding and sintering results in significant deformation of the micro components. In addition, layers of oxide pointed by white arrows were formed in the surface of stainless steel micro components with a black appearance visible to the naked eye. On the other heating cycle B, the resultant sintered micro components were deformed less when compared with cycle A. However, the black appearance still existed. From the results obtained by two heating cycles, it is clear that the heating rate is the main cause to deformation. When the heating rates are 5^{o}C and 10^{o}C /min, the deformation is significantly observed, while it is reduced when the heating rates are reduced to 1.2 and 5^{o}C /min for de-binding and sintering, respectively. The slow heating rates remove the binder smoothly and big deformation is avoided. Consequently,

heating cycle B is selected to be used with nitrogen/hydrogen mixture atmosphere, while the de-binding stage of cycle B was used with vacuum atmosphere.

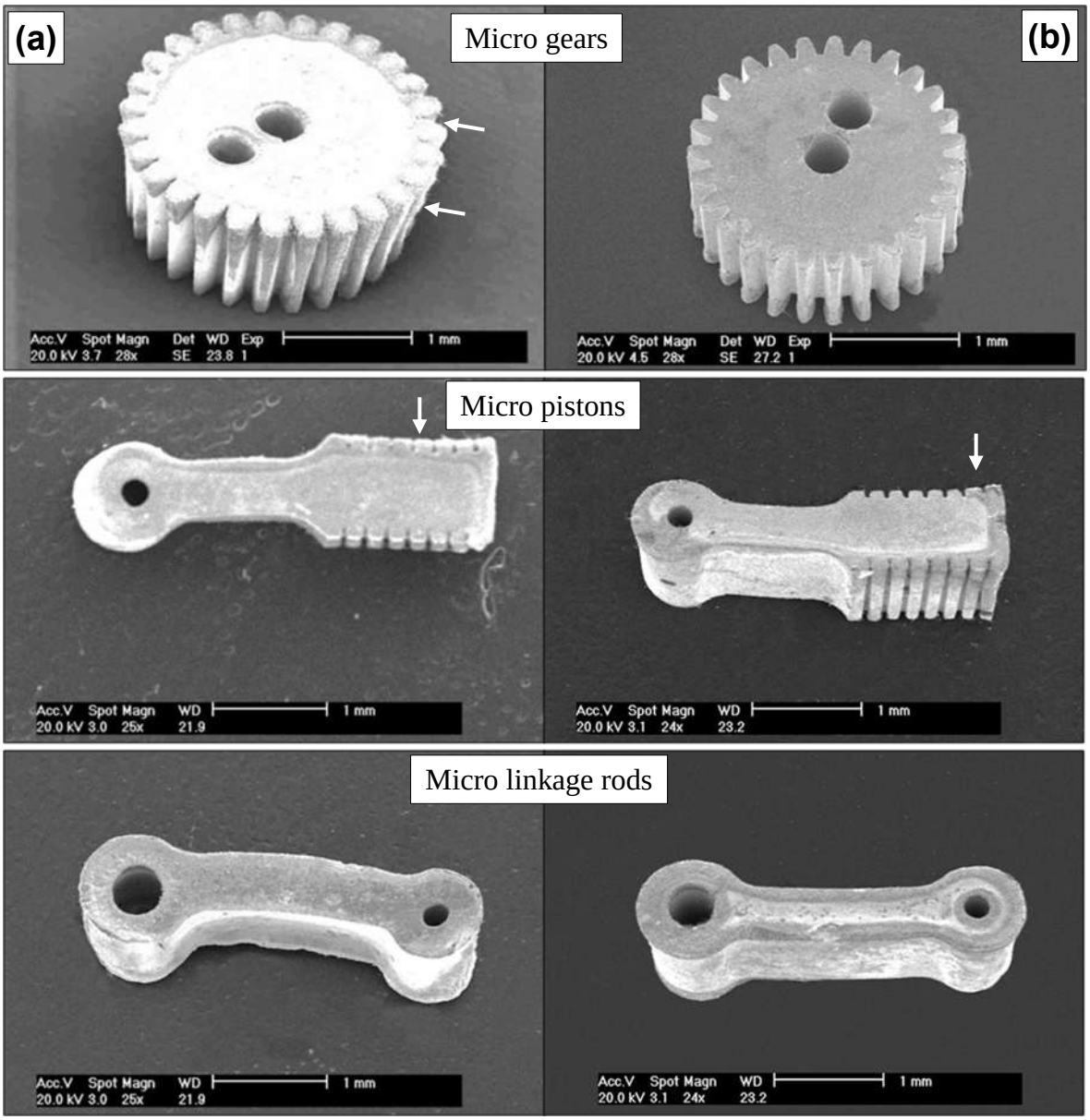

Figure 6.6. SEM images showing the stainless steel micro components fabricated from 5-µm powder using pressure less filling method and sintered in nitrogen atmosphere at 1200 ^{o}C by using: (a) heating cycle A and (b) heating cycle B.

6.3.2. Effect of nitrogen/hydrogen mixture and vacuum atmospheres on the sintered micro components

The green micro engine components fabricated from 5-µm powder by using pressure less filling method and sintered in both nitrogen/hydrogen mixture and vacuum atmospheres at 1200^{o}C were inspected under SEM and shown in Figures 6.7 (a) & (b) and 6.8 (a) & (b), respectively. It is clear that high shape retention micro engine components are obtained in the similar quality as the SU-8 master moulds fabricated as described in Chapter Three. In addition, the appearance of micro components looks shiny when compared with that obtained by using nitrogen atmosphere. This indicates that low or no oxidation occurs during the sintering process. This happened probably because nitrogen/hydrogen mixture containing 10% hydrogen is known as reducing oxide agent, while vacuum isolates the components from the outer atmosphere. In terms of shape retention and colour appearance both nitrogen/hydrogen mixture and vacuum atmospheres produce the same quality micro engine components.

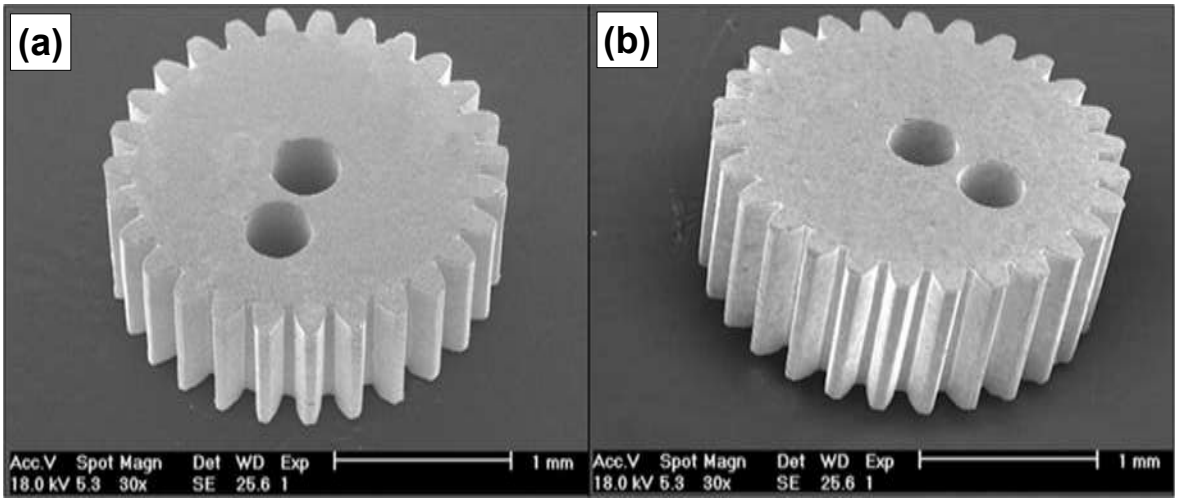

Figure 6.7. SEM images showing the stainless steel micro gears fabricated from 5-µm powder by using pressure less filling method and sintered at 1200^{o}C in: (a) nitrogen/hydrogen mixture and (b) vacuum atmospheres.

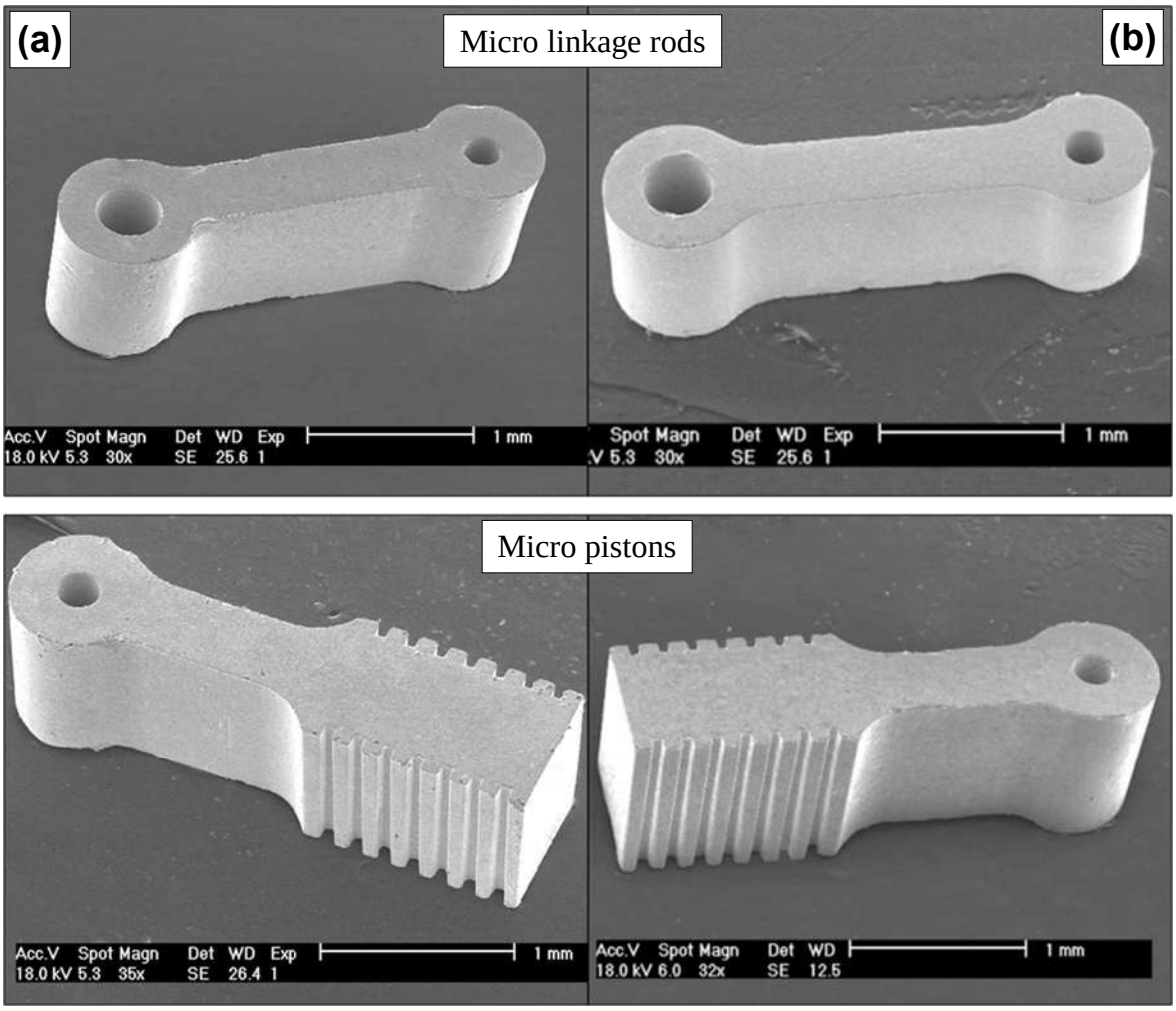

Figure 6.8. SEM images showing the stainless steel micro linkage rods and pistons fabricated from 5-µm powder by using pressure less filling method and sintered at 1200^{o}C in: (a) nitrogen/hydrogen mixture and (b) vacuum atmospheres.

The stainless steel micro components, fabricated from 5-µm powder by using cold isostatic pressing method and sintered at 1200^{o}C in vacuum atmosphere, were also inspected under SEM in order to be compared with pressure less filling method and the results are shown in Figure 6.9. It is found that good shape retention is obtained. In terms of shape retention, the quality of the sintered stainless steel micro components, obtained by using cold isostatic pressing method, is not as good as that obtained using pressure less filling one, which reflected the quality of their corresponding green micro components discussed in Chapter Five.

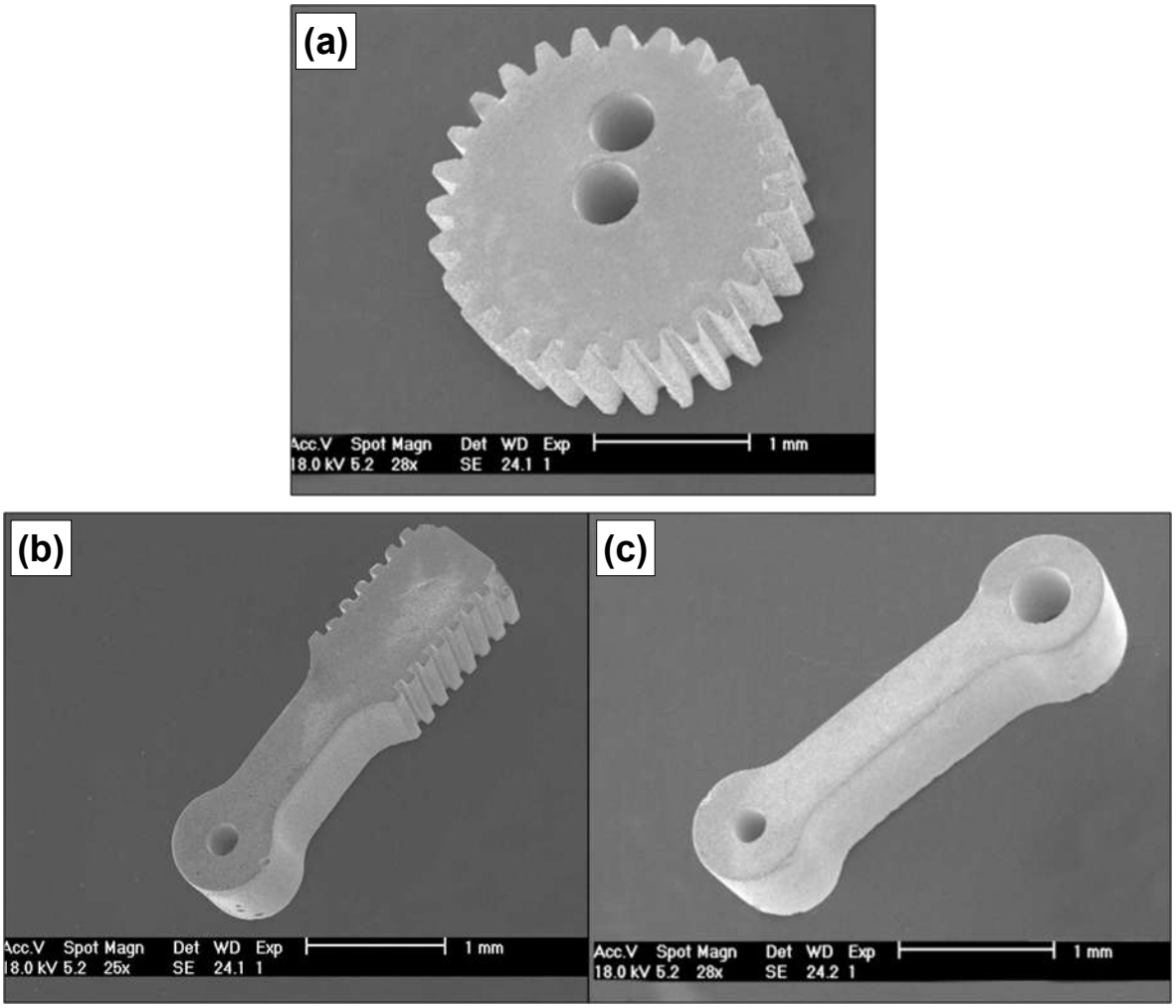

Figure 6.9. SEM images showing the stainless steel micro components fabricated from 5-µm powder by using cold isostatic pressing method and sintered at 1200^{o}C in vacuum atmosphere: (a) micro gear, (b) micro piston and (c) micro linkage rod.

The stainless steel sintered micro components fabricated from 10 and 16-µm powders were also inspected under SEM. Figures 6.10 and 6.11 show the SEM images of the micro engine components sintered at 1200^{o}C in vacuum atmosphere and fabricated from 10 and 16-µm powders by pressure less filling method, respectively. It is found that near net shape micro components are obtained when 10-µm powder is used, while the shape is deformed when 16-µm powder is used. Generally speaking, the micro engine components fabricated

from 5-µm powder are better in shape retention than those fabricated from 10 and 16-µm powders.

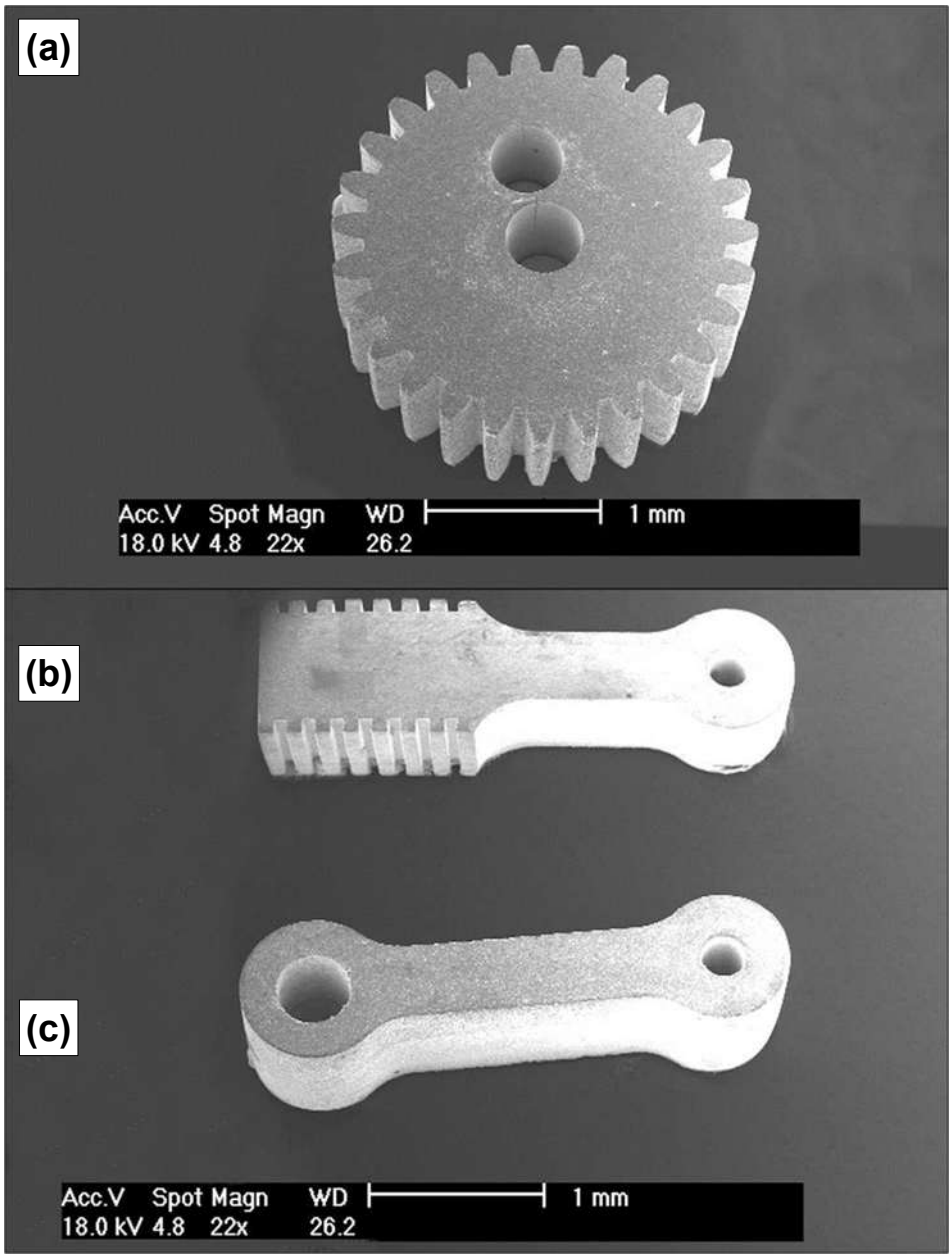

Figure 6.10. SEM images showing the stainless steel micro components fabricated from 10-µm powder using pressure less filling method and sintered at 1200^{o}C in vacuum atmosphere: (a) micro gear, (b) micro piston and (c) micro linkage rod.

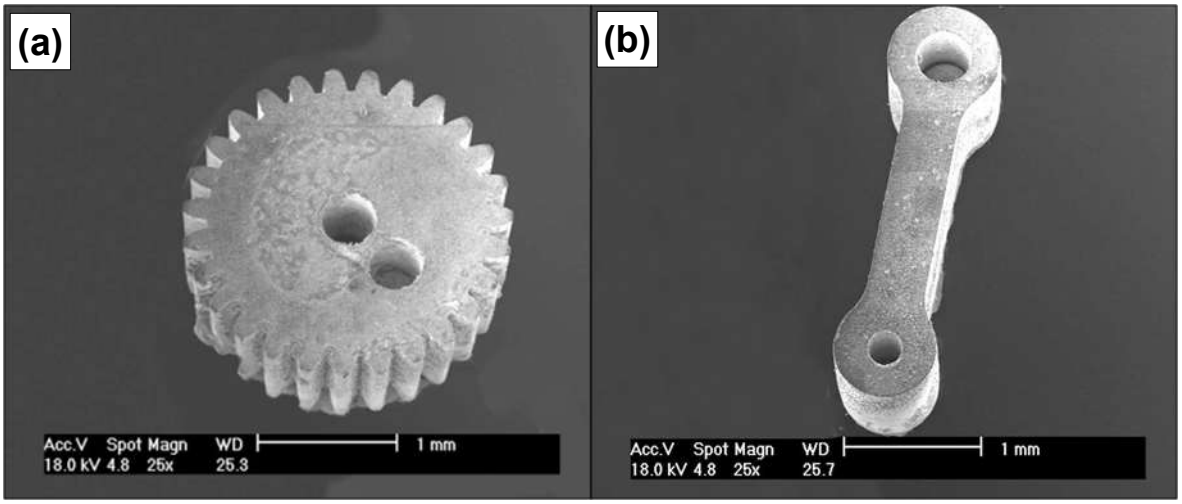

Figure 6.11. SEM images showing the stainless steel micro components fabricated from 16-µm powder using pressure less filling method and sintered at 1200^{o}C in vacuum atmosphere: (a) micro gear and (b) micro linkage rod.

6.3.3. Micro engine assembly and other components

From the results obtained from different stainless steel powders, it is found that using 5-µm powder produces high quality micro engine components in terms of shape retention when compared with 10 and 16-µm powders; therefore, the micro engine parts fabricated from 5-µm powder and sintered in nitrogen/hydrogen mixture atmosphere at 1200^{o}C were assembled and inspected under optical microscope as shown in Figure 12 (a). It is clear that all micro engine parts are fitted together with high accuracy as the engine is designed. This indicates that the uniform shrinkage occurs to all micro components. The micro engine cylinder parts were also assembled and inspected under SEM as shown in Figure 12 (b). The micro cylinder parts show the same accuracy as micro gear, linkage rod and piston in terms of shape retention after sintering.

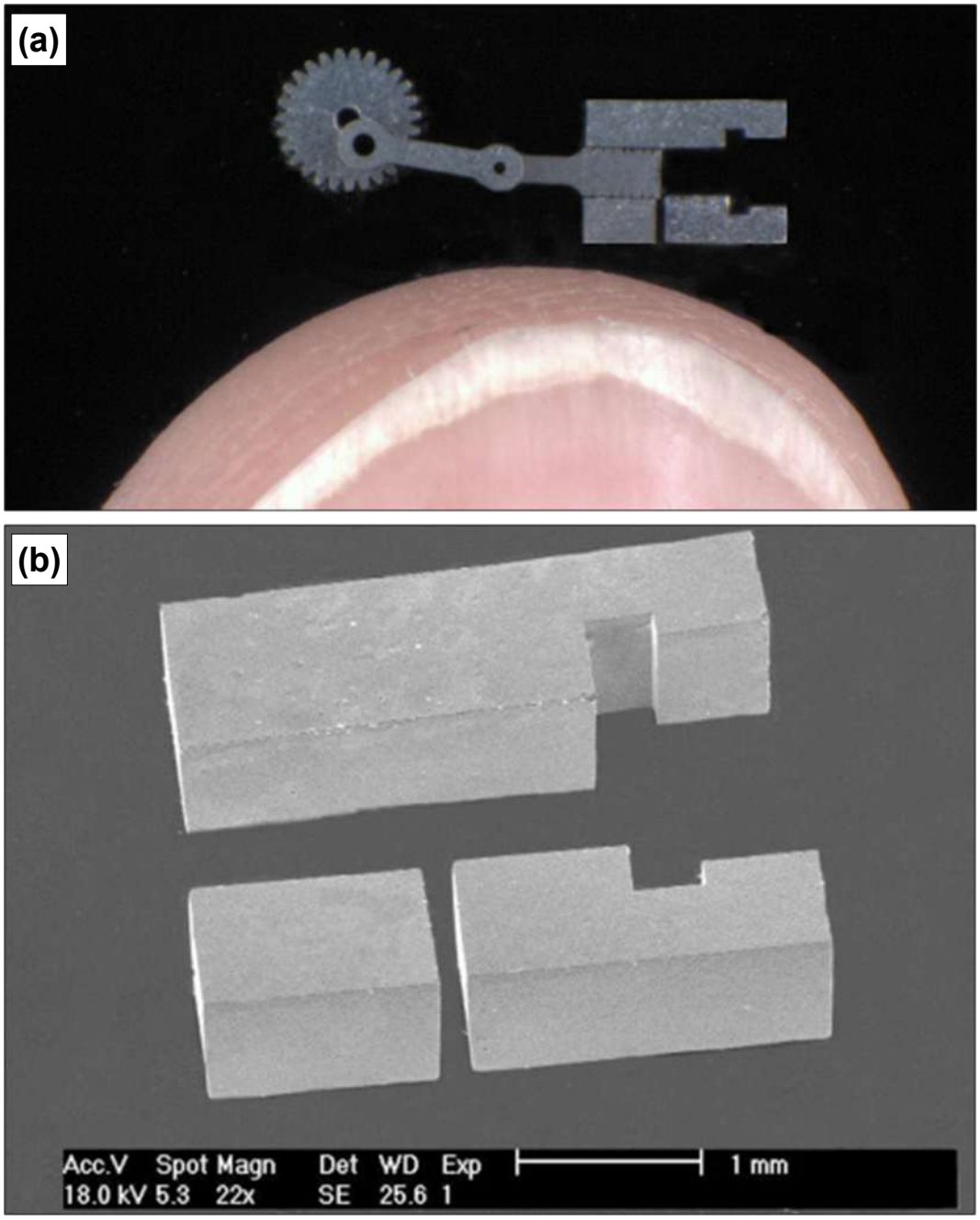

Figure 6.12. Optical and SEM images showing the stainless steel micro components fabricated from 5-µm powder using pressure less filling method and sintered at 1200^{o}C in nitrogen/hydrogen mixture atmosphere: (a) optical image of micro engine assembly and (b) SEM image of micro engine cylinder assembly.

The accuracy of the sintered micro components can be investigated by inspection the side walls and the meshing of micro gears, the most complex shape ever fabricated in this

research. Thus, the sidewalls of micro gear fabricated from 5-µm powder was inspected under SEM and shown in Figure 13 (a). It is found that the side wall is identical to SU-8 master mould, on which the line traces appeared on SU-8 master moulds as presented in Chapter Three are transferred to the sintered gear. Figure 13 (b) shows how two gears fabricated from 5-µm powder are engaged to each other. The engaged micro teeth looked identical in shape, which demonstrates high precision of the fabrication process presented in this research.

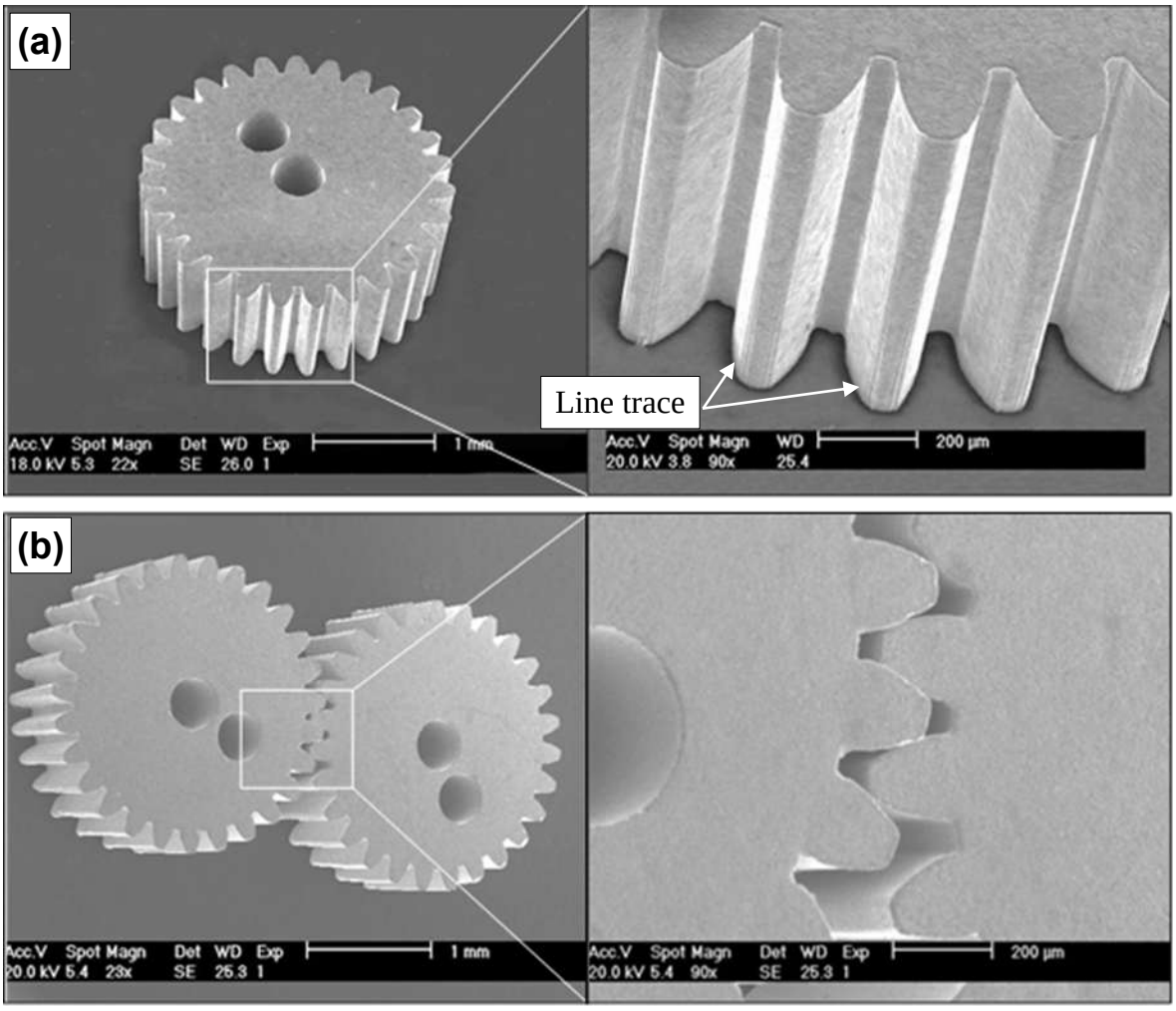

Figure 6.13. SEM images showing the stainless steel micro gears fabricated from 5-µm powder using pressure less filling method and sintered at 1200^{o}C in nitrogen/hydrogen

mixture atmosphere: (a) micro gear and its teeth side walls and (b) two gears engaged to each other.

6.3.4. Other stainless steel components

The fabrication process discussed in this thesis was also used in the production of other components such as simple cylindrical shape, which were discussed in chapter 5, and big scale complex shape such as spur gear with pitch diameter 12 mm and 18 teeth. Figure 6.14 (a) shows the optical image of spur gears with 12 mm pitch diameter of different form: SU-8 and stainless steel green and sintered components. It is clear that, the sintered gear shrinks homogenously and retains all features without deformation. Figure 14 (b) shows the optical image of stainless steel components fabricated in this thesis, including micro gears, micro linking rod, micro pistons, cylindrical shapes and big scale spur gear. The high quality shape retention of stainless steel components fabricated in this research demonstrates the ability of this technique to produce different shapes from micro to over millimetre scale components.

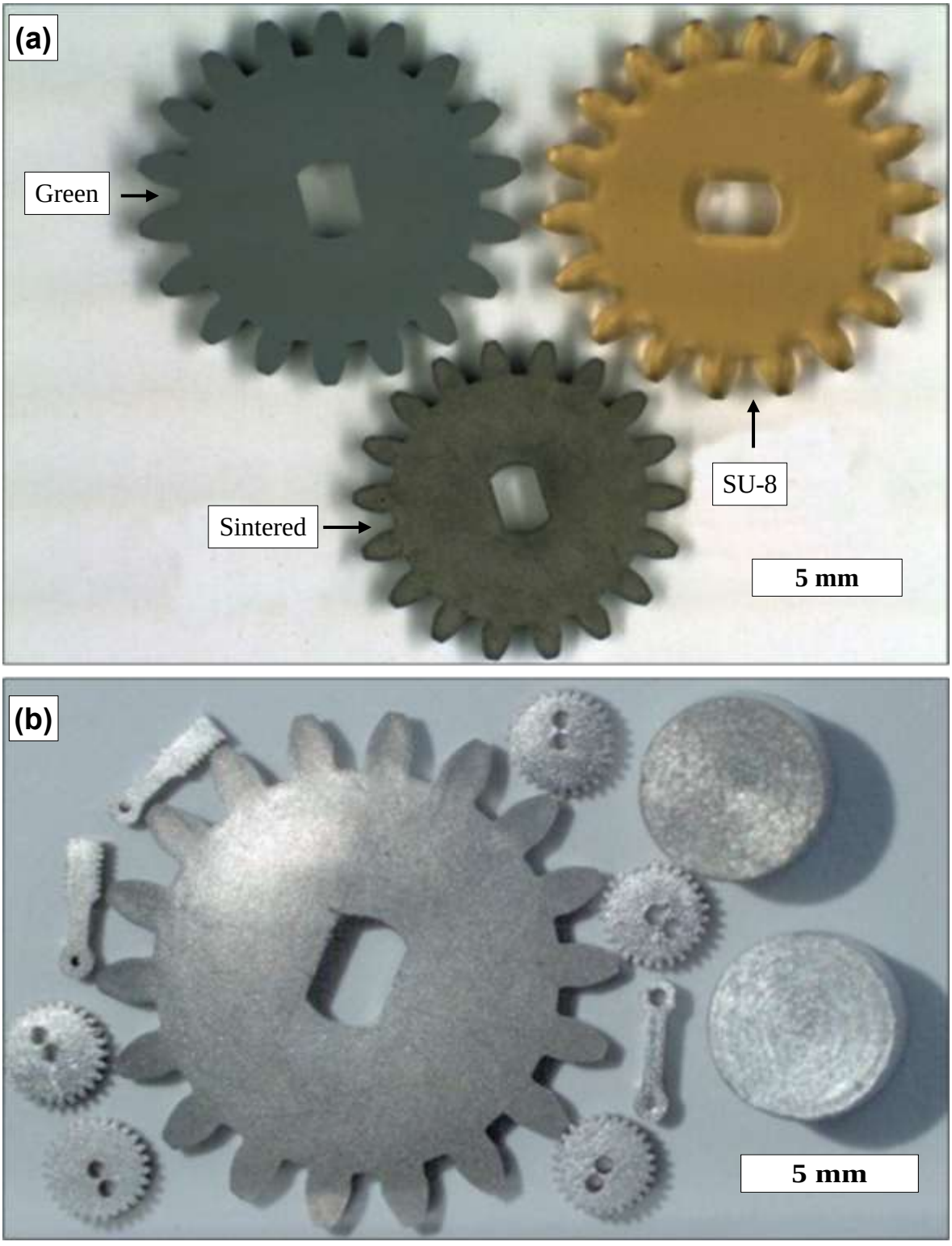

Figure 6.14. Optical images showing: (a) spur gears have 12 mm pitch diameter and fabricated from: SU-8 material and stainless steel green and sintered materials fabricated from 5-µm powder using pressure less filling method, and (b) different sintered stainless steel components fabricated from 5-µm powder using pressure less filling method.

6.4. Conclusions

In this chapter, stainless steel green micro components fabricated from 5, 10 and 16-µm powders were successfully sintered in three different atmospheres, including nitrogen, nitrogen/hydrogen mixture and vacuum. A comparison between three different sintering atmospheres was made in terms of micro components shape retention. The micro engine parts were assembled and investigated.

The following conclusions were obtained in this chapter and listed below:

1. Nitrogen/hydrogen mixture and vacuum atmospheres are successfully used in sintering stainless steel micro components; while nitrogen is not appropriate because it produces a layer of oxide in the surface of micro components which reduces their quality.

2. Both nitrogen/hydrogen mixture and vacuum atmospheres produces the same quality shape retention of the micro components.

3. In terms of powder sizes, the micro components based on 5-µm powder produces excellent shape retention when compared with those based on 10 and 16-µm powders.

4. The fabrication process discussed in this thesis not only fabricates micro components but also has been proved in production large scale components with high quality.

CHAPTER 7. CHARACTERIZATION OF THE SINTERED STAINLESS STEEL MICRO COMPONENTS

This Chapter presents the study in characterization of the stainless steel micro components fabricated from 5, 10 and 16 µm powders and sintered in nitrogen/hydrogen mixture and vacuum at 1200, 1250, 1300 and 1350^{o}C. The characterization is performed in terms of density, linear shrinkage, micro hardness, internal structure, porosity and surface roughness.

7.1. Characterization methodology

The quality of the fabrication techniques presented in this thesis is measured by shape retention and the properties of the sintered micro components. Shape retention of the sintered micro components were investigated as presented in details in the previous chapter and the investigation of different properties of the components is presented in this chapter. The properties of the sintered micro components in terms of density, linear shrinkage, hardness, internal structure and porosity were compared for different stainless steel powders with various filling methods, sintering atmospheres and temperatures. In the case of using cold isostatic pressing method, the maximum applied pressure of 116 MPa is used in this chapter and the results are compared with the pressure less process.

7.1.1. Measuring the density of sintered micro components

Density is one of the most important physical properties of the sintered micro components. It provides a good indication of the general properties of the components in comparison to wrought materials; therefore, it was investigated. The approach of the investigation is

immersion method. Based on Archimedes buoyancy principal, the density can be measured using the following formula [191]:

$$\rho = \frac{m_a}{m_a - m_l} \times \rho_l \quad (7.1)$$

ρ : Density of the sample to be measured,

ρ_l : Density of the immersion medium,

m_a: Mass of the sample in air,

m_l: Mass of sample in immersion medium.

In this chapter, ethanol is selected to be the immersion medium ($\rho_l = 0.789$ g/ml). In all the results obtained, density ratio is used. The density ratio is defined as the ratio between the measured density and the theoretical one of the wrought stainless steel materials which measures 8 g/ml. For each case studied, calculations are based on six samples measured and the average value is used for comparison.

7.1.2. Measuring linear shrinkage

Shrinkage is another important parameter of the sintered micro components to be investigated. Due to the geometric complexity of the micro components fabricated and the difficulty in measuring the volumetric shrinkage, linear shrinkage is adopted as a simple and viable method presenting a good indication of the final shrinkage of the micro components. The linear shrinkage was measured in reference to the outer diameter of a micro gear and the measurements were performed using the following formula:

$$shrinkage\ \% = \frac{D_{SU-8} - D_S}{D_{SU-8}} \times 100 \quad (7.2)$$

D_{SU-8}: The outer diameter of micro gear fabricated from SU-8 master mould,

D_s: The outer diameter of the sintered micro gear.

Following the same procedures in measuring the linear shrinkage of green micro components, discussed in Chapter five, the outer diameters are measured from the top views of SU-8 and sintered micro gears as shown in Figure 7.1 (a) and (b), respectively. It is clear that the outer circumference of the sintered micro gear is on a regular circle, an indication of a uniform shrinkage occurred after sintering. The linear shrinkage for each case was measured on six gears and the average value is presented in the results.

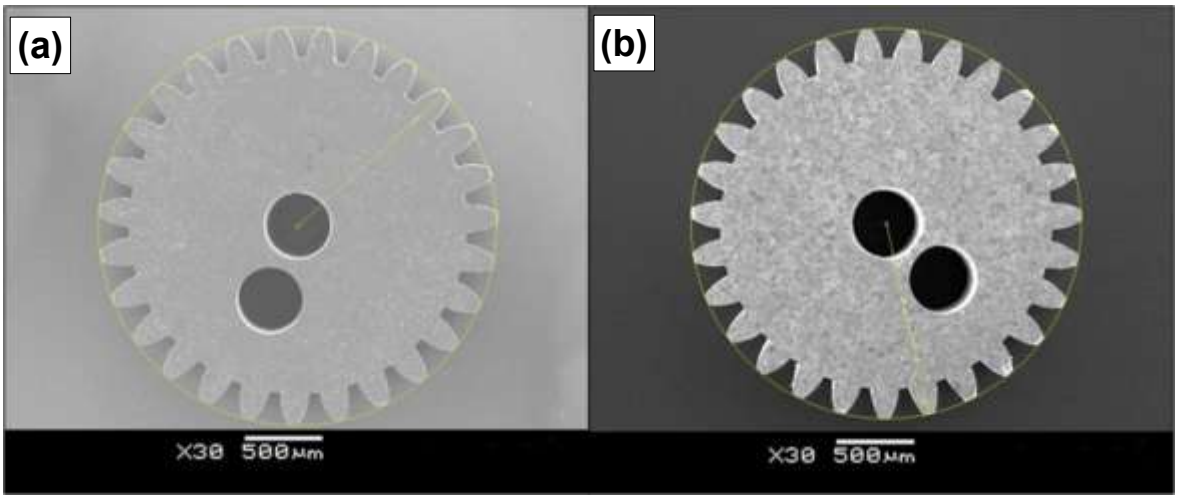

Figure 7.1. SEM images showing the top view of micro gear components fabricated in: (a) SU-8 and (b) sintered stainless steel materials.

7.1.3. Measuring micro hardness

Hardness test reflects a kind of strength of the materials. In a hardness test, the micro components were polished and then the hardness test was performed. An aluminium holder was prepared in order to fit micro components tightly before polishing. The preparation steps are presented as follows:

1. An aluminium disc was used as a holder. Holes were drilled on the holder surface with depth less than 1mm in order to fit the micro components inside.
2. Wax was put into the disc holes and the aluminium disc was put into oven to melt it
3. The micro components were put in these holes before the wax becomes solid and the components are completely embedded in the wax and the holder after the wax is cooled down.

Once the samples are mounted, polishing steps can take place as follows.

1. The sample was first ground using silicon carbide disc with 800 grid per inch square in order to remove the surface layers.
2. A micro cloth with 9 μm polycrystalline diamond suspension is used to polish the sample surface.
3. An ultrapol cloth with 3 μm polycrystalline diamond suspension is used to smooth the sample surface again.
4. A trident cloth with 0.05 μm Master prep polishing suspension is used to reach final smooth surface.

Figure 7.2 (a) and (b) show the Vector Beta Grinder/Polisher machine and aluminium holder containing micro gears after polishing, respectively. The micro hardness test was performed on MicroMet 5100 Series Micro indentation Hardness Testers (Buehler Lab, School of Mechanical Engineering, University of Birmingham) as seen in Figure 7.3 (a). The hardness measurements are based on Vickers test. The diamond indenter with pyramid shape are used for indentation the materials under the applied load. The angle between the pyramids faces is 136^{o} as shown in Figure 7.3 (b). After applying the load, square

impression is formed in the surface of the micro components as seen in Figure 7.3 (c). Afterwards, the Vickers hardness number can be obtained from the formula below [192]:

$$HV = \frac{1.854 \times F}{d^2} \tag{7.3}$$

$$d = \frac{d_1 + d_2}{2} \tag{7.4}$$

HV: Vickers hardness number,

F: The applied load in Kg.

d_1 and d_2 are the diagonals of the square impression. The applied load is adjusted to be 200g. The micro gears fitted into the aluminium holder were tested under the hardness machine and the results are automatically calculated on the computer attached to this machine. The hardness result for each case is presented as the average value of three micro gears measured. In each gear, 10 indentation marks were taken in different places and the average was selected.

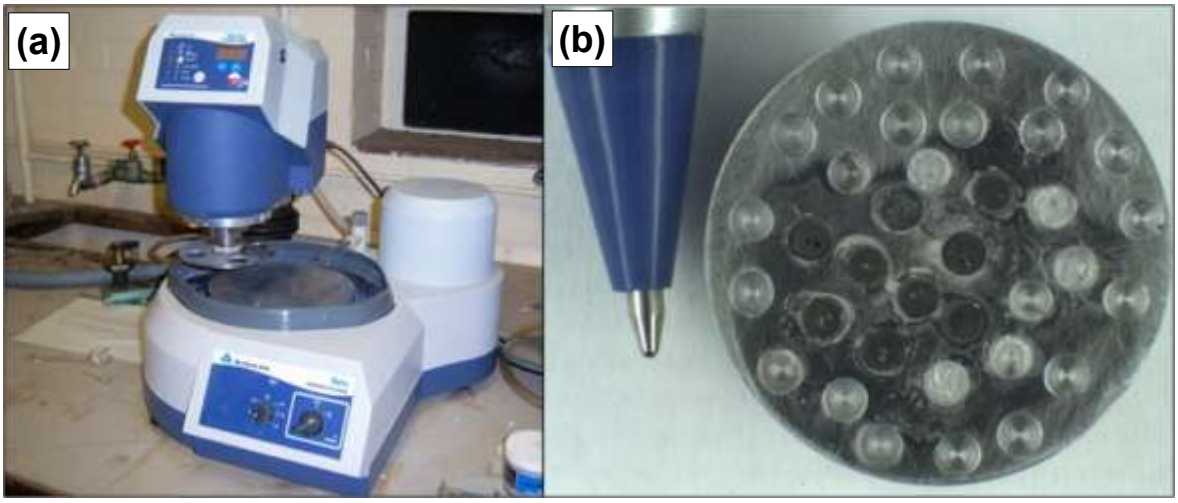

Figure 7.2. Images showing: (a) Vector Beta Grinder/Polisher machine and (b) aluminium holder containing the micro gears after polishing.

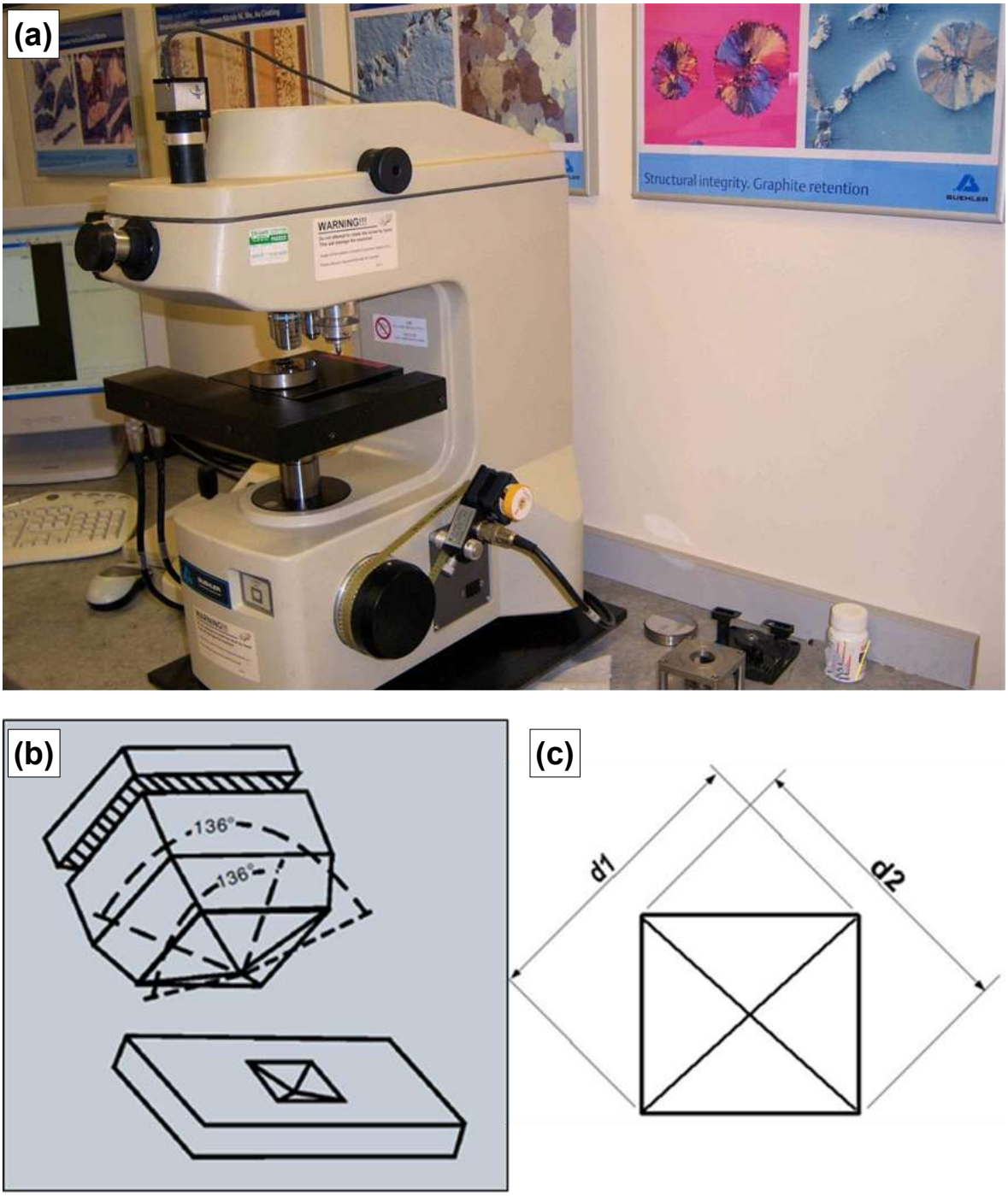

Figure 7.3. Images showing: (a) MicroMet 5100 Series Micro indentation Hardness Testers and schematic diagrams of: (b) diamond indenter with pyramid shape and (c) square impression.

7.1.4. Measuring surface roughness

Roughness is a measurement of the texture of the surface. This can be determined by the vertical deviations of a real surface from its ideal form. The surface is called rough when a large deviation has occurred, while it is smooth when a small deviation has occurred. Roughness is an important parameter of determining how a real object interacts with its environment. Surface roughness is a good indicator of the performance of mechanical components because the irregularities in the surface may form nucleation sites for cracks or corrosion [193-194]. Surface roughness parameters of the micro components are measured in this chapter using stereo imaging technique. Stereo imaging method is a less time consuming and viable technique of measuring the roughness of surfaces rather than an atomic force microscope (AFM) one. However, AFM can measure the roughness of the flat surface; stereo imaging can measure roughness for different structures including flat and curved shapes. Therefore, it is successfully used for reconstructing the surface of the micro materials [195-196]. To measure the roughness of a surface, two high quality SEM images of the surface to be measured are taken at different tilting angles. From the two SEM images, the lateral displacement of surface features of different heights is calculated and the depth of each image pixel is obtained by measuring the relative displacement of the features from their location in the first image to the position in the second image. Afterwards, the three coordinates of each pixel based on eccentric stereo pairs is constructed and the roughness parameters are obtained by processing the two images using ALICONA MEX software. Two images are taken by SEM with a normal tilting angle between 5° and 10°. The configurations of the tilting angle (α) and the projected coordination $P_1(X_1, Y)$ and $P_2(X_2, Y)$ are shown in Figure 7.4. The third dimension (Z) can be found as follow [196]:

$$Z = \frac{x_2 - x_1 + x_1 \times (1 - cos\propto)}{\sin\propto} \quad (7.5)$$

x_1 and x_2 are the projections coordinate of points P_1 and P_2 on the reference plan, and α is the tilting angle. This process can be done for all of the other points of the two SEM images to construct 3D surface profiles of the structure [197-198]. Figure 7.4 shows a schematic diagram of the stereo imaging technique. In order to get the best performance of the method, reduce the image noises and obtain the maximum volume of 3D reconstruction, several parameters should be considered:

1. Surface of the sample should be conductive,

2. Reconstructed feature should be visible and perfectly shows sharp edges even at high magnifications,

3. Images should be eccentrically tilted about one axis that means a particular feature should be seen at the centre of both stereo pair images,

4. Large height change in relation to the image diagonal provides better results, therefore the minimum ratio of height to diagonal is 1:70,

5. The correct images obtained when the structure only has a transition in X direction and not any transition in Y axis, and

6. The images pair should have contrast without blurring, the same scale, and enough textures on the surface and the images should not have a recurrent structure.

In this case the image reconstruction error will be less than 3–5% [197]. Many details can be found in [195-197]. The 3D surface profile is constructed at the surfaces of the micro gears based on different powder sizes.

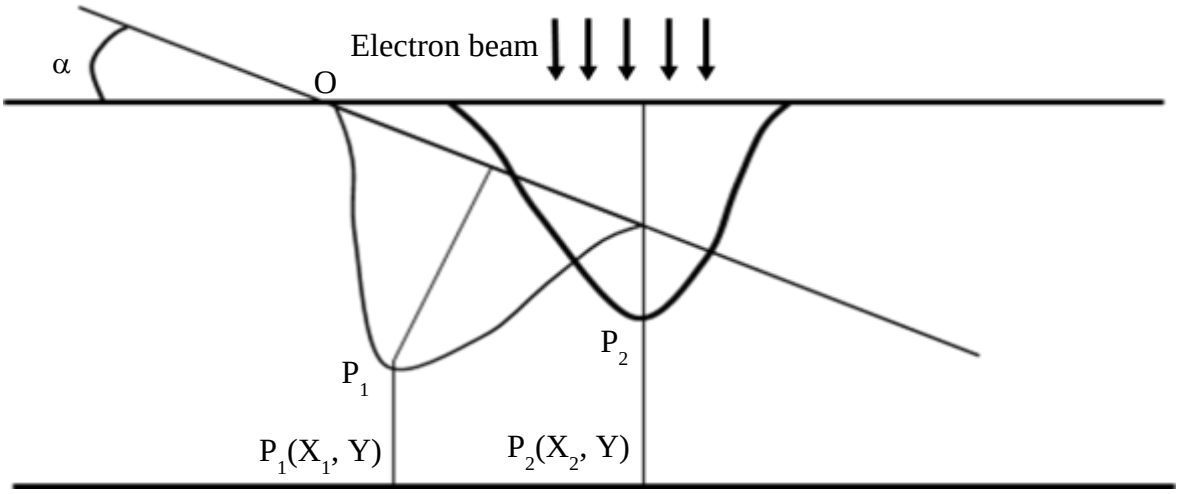

Figure 7.4. A schematic diagram showing stereo imaging technique.

The most important surface parameters to be measured in this research are Ra, Rq, Rp, Rv and R_t. The measurements are based on the formula below [198]:

$$R_a = \frac{1}{L}\int_0^L |r(x)|dx, \tag{7.6}$$

$$R_q = \sqrt{\frac{1}{L}\int_0^L r^2(x)dx}, \tag{7.7}$$

$$R_p = |max[r(x)]|,\ 0 < x < L \tag{7.8}$$

$$R_v = |min[r(x)]|,\ 0 < x < L \tag{7.9}$$

$$R_t = R_p + R_v \tag{7.10}$$

r: The vertical distance from the mean line to the x data point.

R_a: The Average roughness is the area between roughness profile and its mean line, or the integral of the absolute value of the roughness profile height over the evaluation length L.

R_q: Root-mean-square (rms) average roughness of a surface.

R_p: Peak roughness is the height of the highest peak in the roughness profile over the evaluation length.

R_v: Maximum height of the profile.

7.2. Results and discussions

7.2.1. Density

Figure 7.5 (a) and (b) show the effect of sintering temperature on the density of the sintered micro components fabricated in different powders by using two filling methods and sintered in nitrogen/hydrogen mixture and vacuum atmospheres, respectively. For a given powder, sintering atmosphere and filling method, it is clear that increasing the sintering temperature increases the sintering density. Moreover, the smaller the powder sizes are, the greater the sintering density and vice versa. Sintering is much dependent on the powder surface area in which the greater the surface area is, the higher the densification and vice versa [198-199]. While the small powder size produces large surface area. As a result, the small powder produces higher sintering density than the big one. For a given sintering temperature, powder size and filling method, the sintering densities based on nitrogen/hydrogen mixture and vacuum atmospheres are nearly the same. Furthermore, the density of the sintered micro components based on cold isostatic pressing method is slightly greater than that of pressure less filling method. This can be understood based on the finding in Chapter five that the green density of the micro components based on cold isostatic pressing method is greater than that of pressure less filling method.

7.2.2. Linear shrinkage

The linear shrinkages of the sintered micro components were also investigated for different powders, filling methods, sintering temperatures and atmospheres. The effects of sintering temperatures, powders and filling methods on the linear shrinkage of the stainless steel micro components sintered in nitrogen/hydrogen mixture atmosphere and vacuum were investigated and the results are shown in Figure 7.6 (a) and (b), respectively. It is found that that the linear shrinkages increase as the sintering temperature increases. This is happened in result to the increase of densities as discussed in section 7.2.1. In addition, the smaller the powder sizes are, the greater the linear shrinkage and vice versa. Moreover, the linear shrinkage of sintered micro components based on 5-µm powder and fabricated by using pressure less method is significantly greater than that fabricated by using cold isostatic pressing method. However, using 10 and 16-µm powders produces nearly the same shrinkage results for both pressures less filling and cold isostatic pressing methods. As discussed in Chapter Five, using cold isostatic pressing method increases the green density and its corresponding linear shrinkage significantly when 5-µm powder is used, while, it increases them slightly when 10 and 16-µm powders are used. Thus, the linear shrinkage of the sintered micro components is much dependent on its corresponding density and linear shrinkage of the green micro components in which the greater the density and its corresponding linear shrinkage of the green micro components is, the greater the linear shrinkage of the sintered one and vice versa. Furthermore, for a give powder and sintering temperature, the linear shrinkages based on nitrogen/hydrogen mixture and vacuum atmospheres are nearly the same.

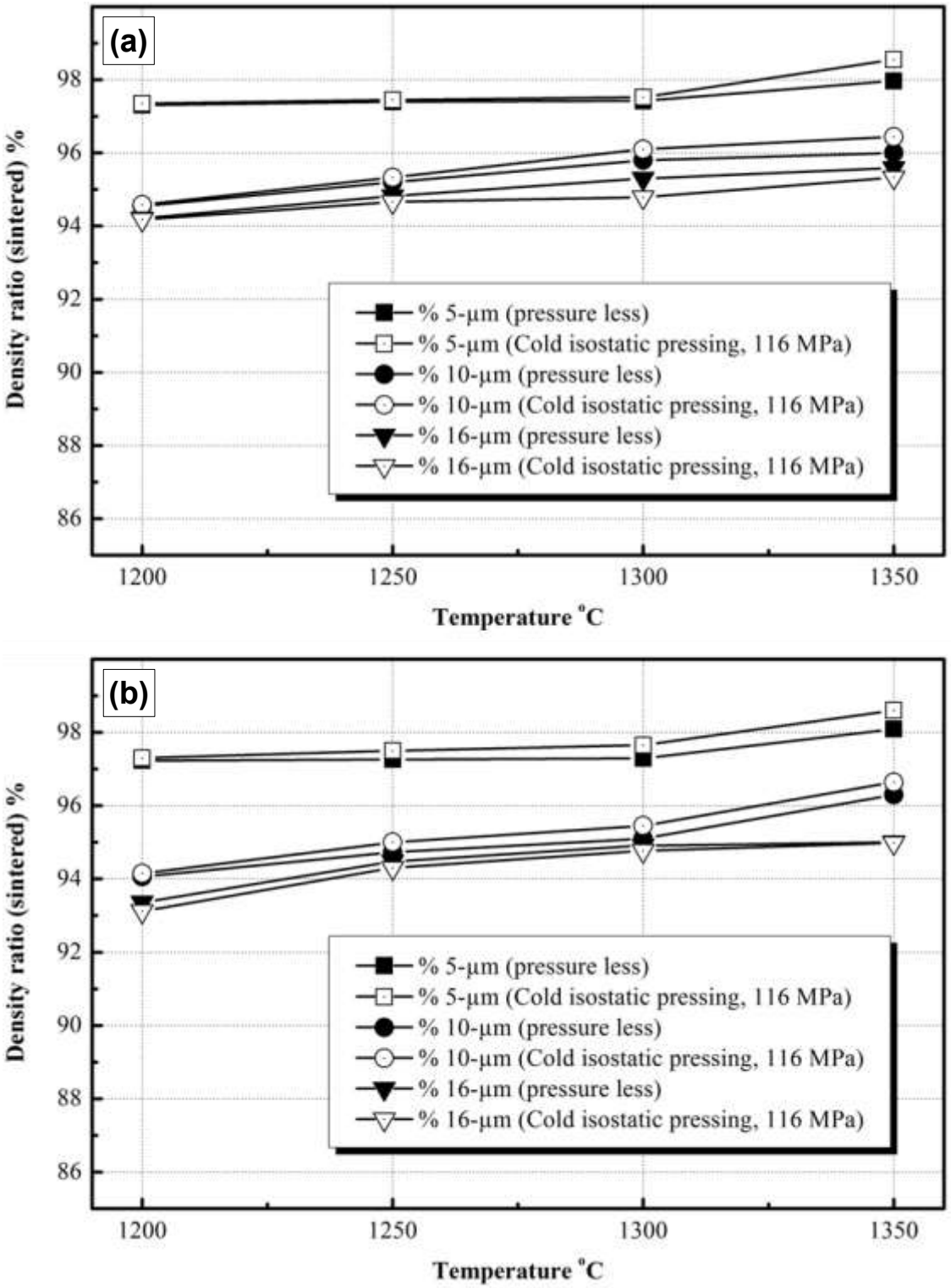

Figure 7.5. The effects of sintering temperature on the density of the sintered stainless steel micro components fabricated in different powders using two filling methods and sintered in: (a) nitrogen/hydrogen mixture and (b) vacuum.

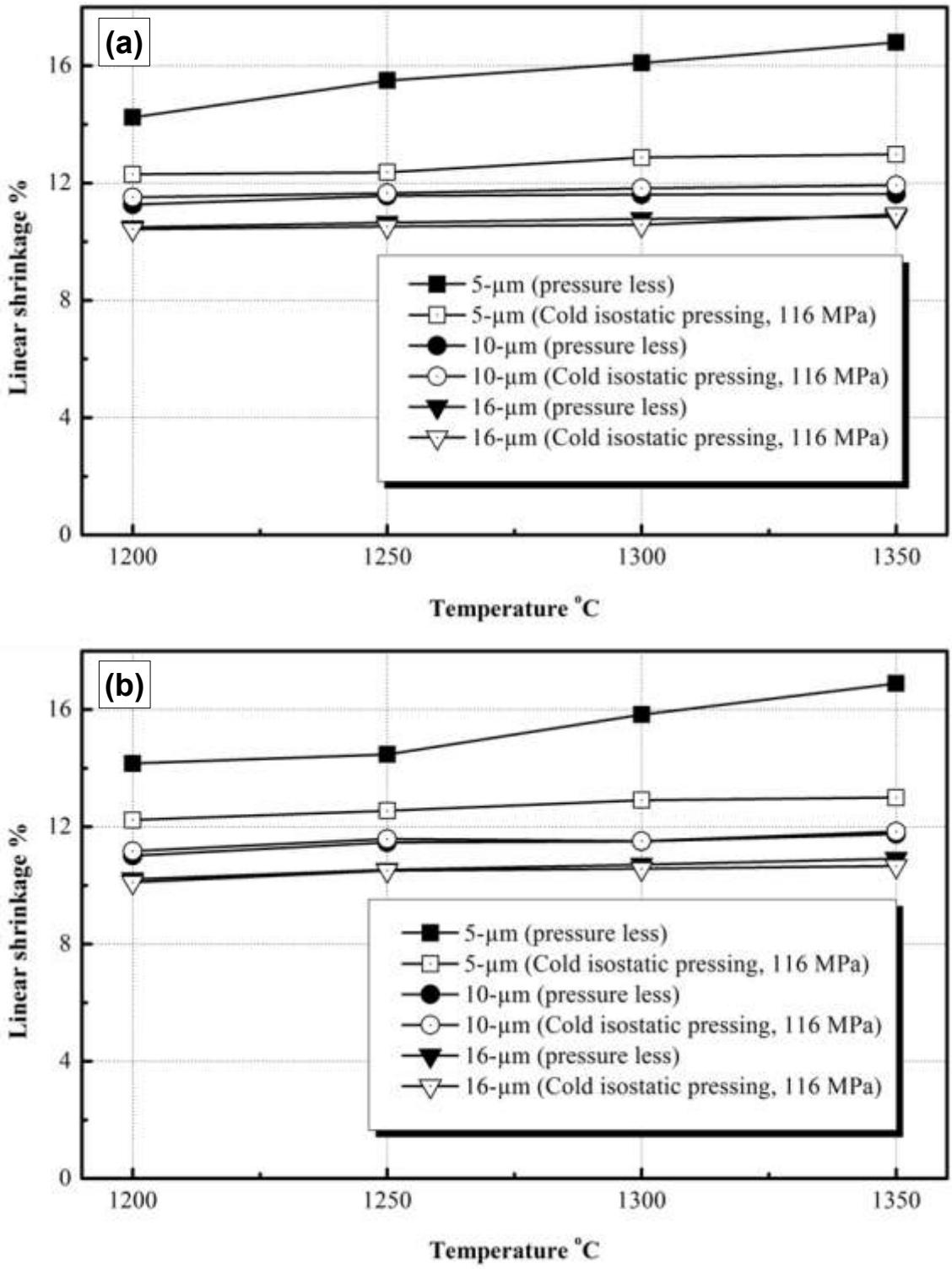

Figure 7.6. The effects of sintering temperature on the linear shrinkage of the sintered stainless steel micro components fabricated in different powders using two filling methods and sintered in: (a) nitrogen/hydrogen mixture and (b) vacuum.

7.2.3. Micro hardness

Vickers hardness of the sintered micro components of different powders, filling methods, sintering temperatures and atmospheres were investigated in this section. Figures 7.7 (a) & (b) and 7.8 (a) & (b) show the indentation marks of the tested micro components based on different powders and sintered in nitrogen/hydrogen mixture and vacuum atmospheres at 1200^{o}C and 1350^{o}C, respectively. It is found that, the smaller the powders are; the smaller the indentation marks, and vice versa. In addition, the indentation marks of the micro components sintered in nitrogen/hydrogen mixture were smaller than those sintered in vacuum atmospheres. Figure 7.9 (a) and (b) show the effects of sintering temperatures, powders and filling methods on the hardness of the sintered micro components in nitrogen/hydrogen mixture and vacuum atmospheres, respectively. It is found that, the smaller the powders are, the greater the hardness and vice versa. For a given powder, sintering temperature and atmosphere, the hardness of the micro components obtained by using cold isostatic pressing method is greater than that obtained by using pressure less one. Moreover, the hardness of the micro components sintered in nitrogen/hydrogen mixture atmosphere is significantly greater than that sintered in vacuum one. Generally, the hardness decreases with increase of temperature. However, for the samples based on 5-µm powder and sintered in nitrogen/hydrogen mixture atmosphere, the hardness increases at 1250^{o}C and then it decreases again.

As discussed in section 7.2.1, the sintered densities of the stainless steel based on 5-µm powder were significantly greater that those based on 10 and 16-µm powders. Increasing the density increases the mechanical properties and hence, increases the hardness. Although increasing sintering temperature for a give powder increases the sintering

densities slightly, the hardness decreases. As the sintering temperature increases, the grains are coarsened (discussed in section 7.2.4). While the grain coarsens the materials are deformed easily under the applied load due to the movement of dislocations. On the other hand, the movement of dislocations is hindered by grain boundary when the grain size reduces. As discussed in reference [179], the sintering atmosphere is an important parameter affecting the hardness of stainless steel. However, the hardness based on nitrogen/hydrogen mixture atmosphere may increase due to one of the following reasons: (i) because nitrogen/hydrogen mixture contains 90% of nitrogen, it may form nitride precipitating into the grain boundaries and harden the stainless steel micro components [201]; and (ii) it may be dissolved into the grains and promotes solid solution hardening [202]. In order to clarify this issue, the stainless steel samples were subjected to X-ray diffraction analysis (Philip X-ray, School of Metallurgy and Materials, University of Birmingham). Figure 7.10 shows the X-ray diffraction pattern for stainless steel sample based on 5-µm powder and sintered in nitrogen/hydrogen mixture and vacuum atmospheres at 1200 and 1350°C. The pattern shows that austenite phase is detected with strong intensity and no trace to nitrides is found. This confirms that the solid solution strengthening may be the reason for hardening. However, the XRD cannot detect a small amount of precipitates (2.5%). Therefore, nitride precipitating may be formed in undetectable amount and it is a reason for hardening stainless steel.

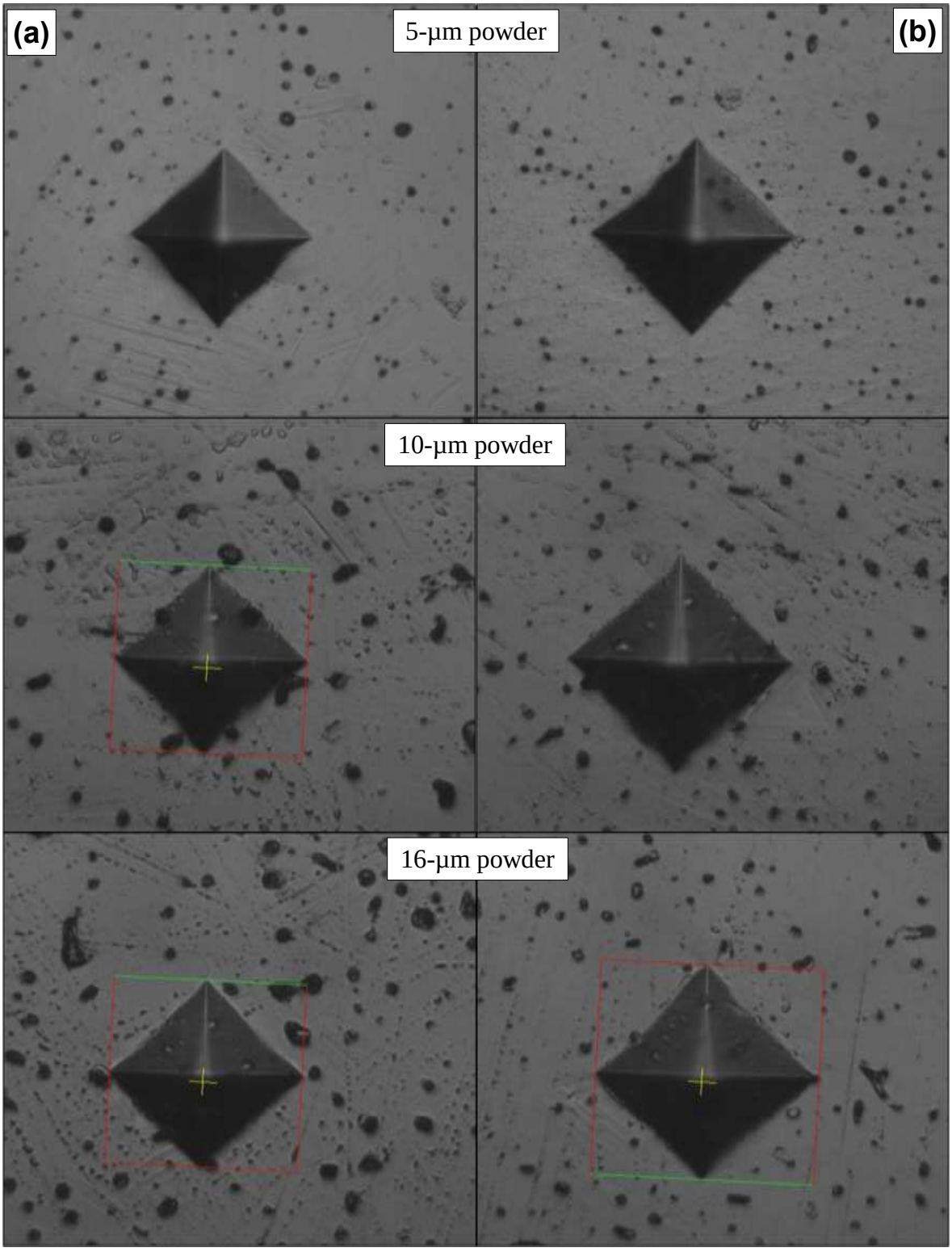

Figure 7.7. Optical images of the micro indentation marks of the stainless steel micro components fabricated from different powders and sintered at 1200^{o}C in: (a) nitrogen/hydrogen mixture atmosphere and (b) vacuum.

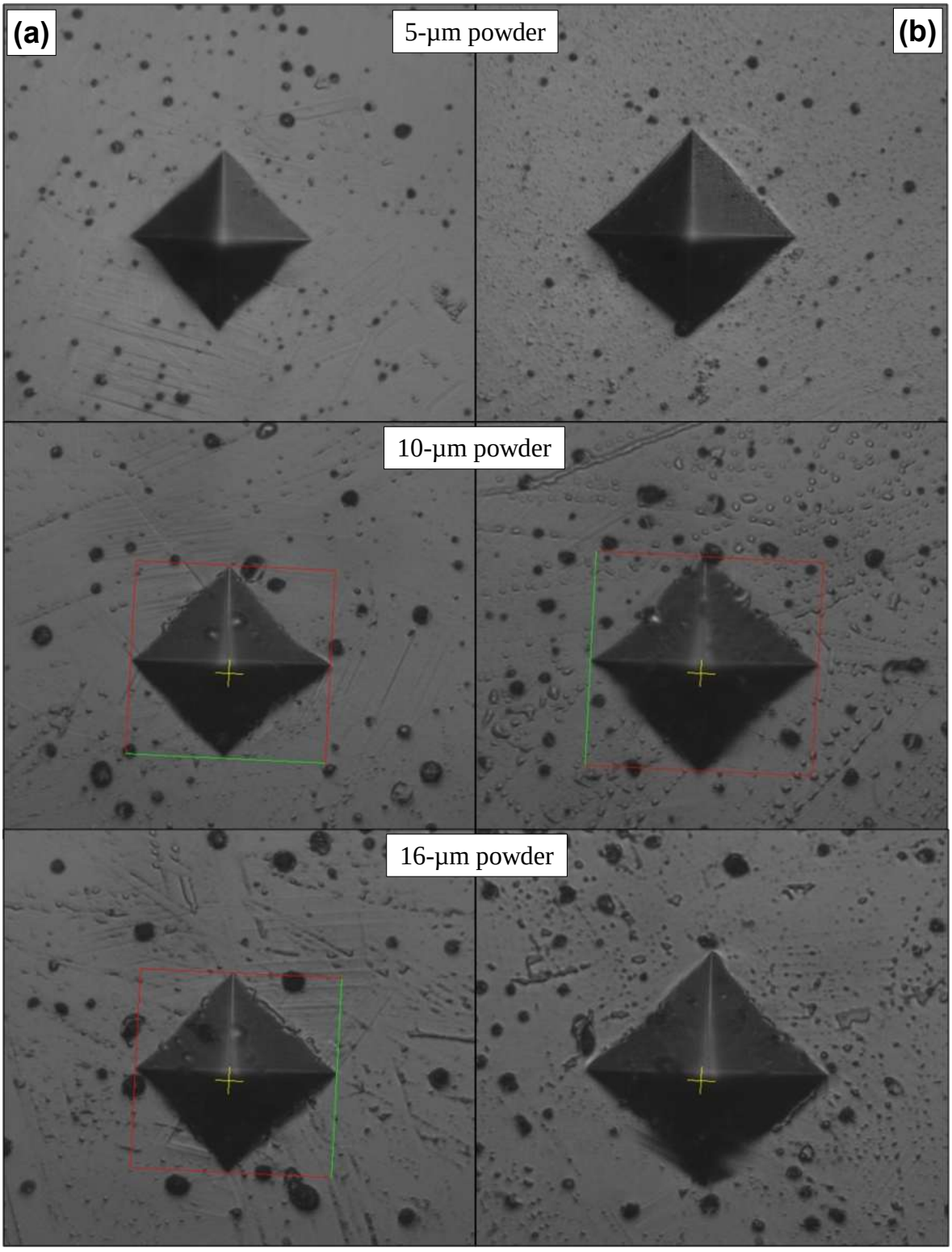

Figure 7.8. Optical images of the micro indentation marks of the stainless steel micro components fabricated from different powders and sintered at 1350^{o}C in: (a) nitrogen/hydrogen mixture atmosphere and (b) vacuum.

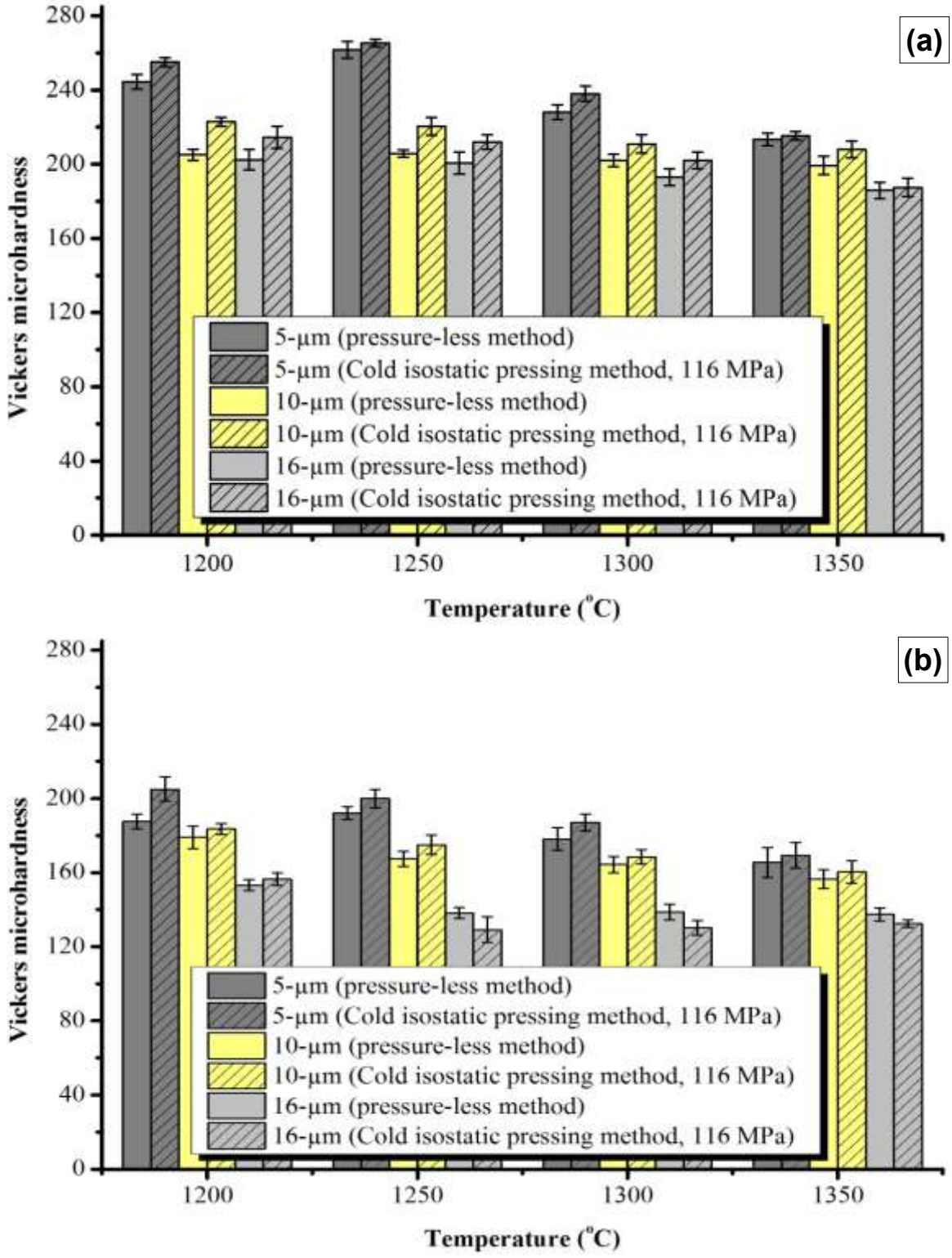

Figure 7.9. A graph showing the effects of sintering temperatures on Vickers hardness of stainless steel micro components fabricated from different powders and filling methods; and sintered in: (a) nitrogen/hydrogen mixture and (b) vacuum atmospheres.

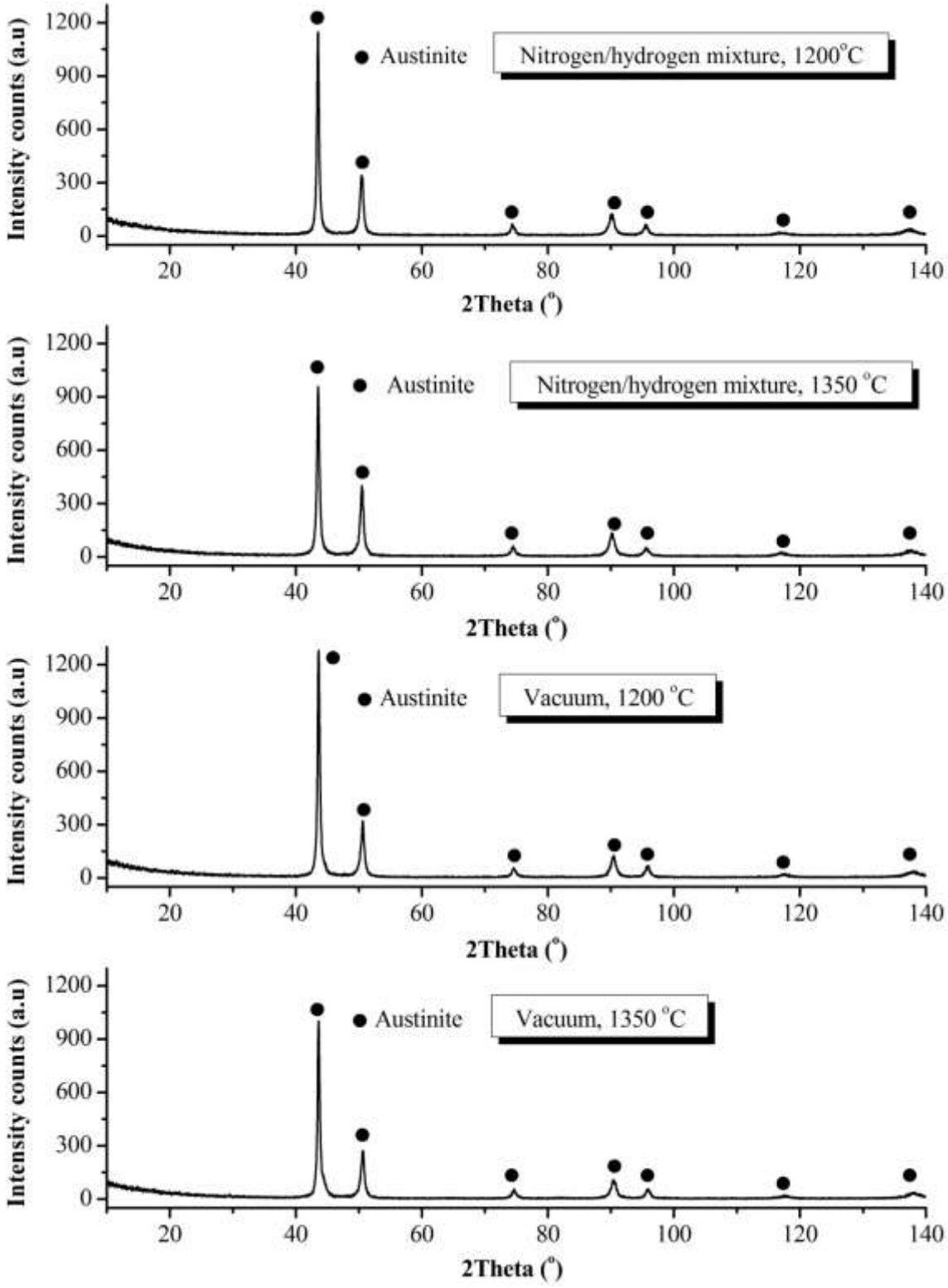

Figure 7.10. A graph showing X-ray diffraction patterns of the stainless steel components fabricated from 5-µm powder and sintered in nitrogen/hydrogen mixture and vacuum atmospheres at 1200 and 1350°C.

7.2.4. Surface morphology, internal structure and porosity

The surface morphology of the micro components were inspected under SEM. Figures 7.11 (a) & (b) and 7.12 (a) & (b) show the surface morphology of the stainless steel micro components based on different powders and sintered at 1200^{o}C and 1350^{o}C in nitrogen/hydrogen mixture atmosphere and vacuum, respectively. It is clear that the grains coarsen for the higher sintering temperature. It is also clear that many pores exist on the surface of micro components fabricated from 10 and 16-µm powders when compared with those fabricated from 5-µm powder, which explains why the densities based on 5-µm powder are greater than those based on 10 and 16-µm powders. The investigation of internal structures of the micro components in this section is based on pressure less filling method. Sintered micro components were polished as discussed in section 7.1.3 and inspected under SEM. Figures 7.13 (a) & (b) and 7.14 (a) & (b) show the SEM images of polished stainless steel micro components fabricated from different powders and sintered at 1200^{o}C and 1350^{o}C in nitrogen/hydrogen mixture and vacuum, respectively. It is found that, the smaller the powder size is, the smaller the pore size for both nitrogen/hydrogen mixture and vacuum. Moreover, the pores of the micro components fabricated from 5-µm powder look spherical, while some of them are irregular for those fabricated from 10 and 16-µm powders. The spherical pores indicate that good densification has occurred, while the irregular ones indicate that the densification is not complete. Furthermore, the numbers of pores of the micro components sintered at 1350^{o}C were lower than those sintered at 1200^{o}C. As the temperature increases to 1350^{o}C, the densification increases and the pore shapes tends to be spherical which increases the density. However, some pores are agglomerated to form a big size pore as indicated in the sample based on 16-µm shown in Figure 7.12 (b).

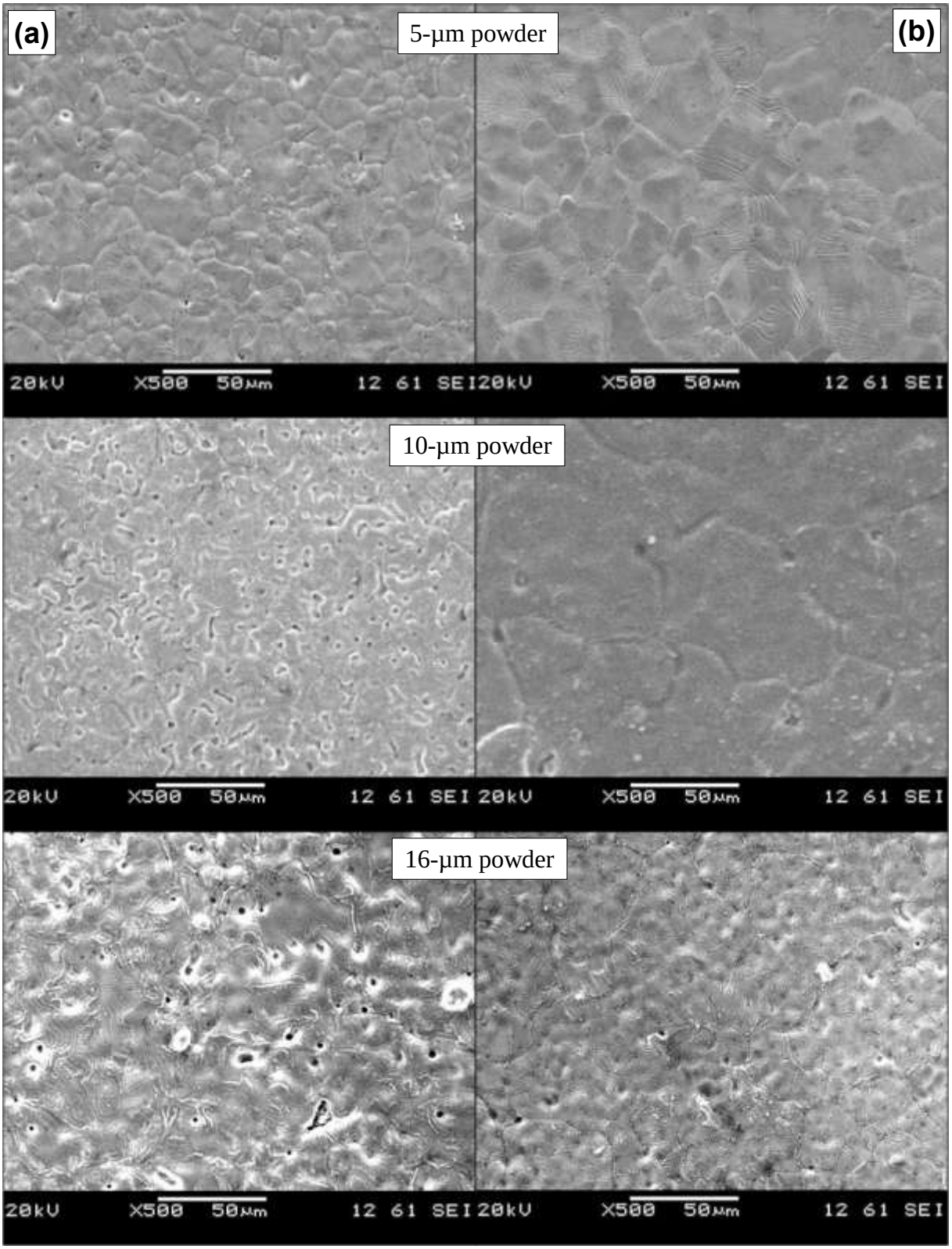

Figure 7.11. SEM images showing the surface morphologies of the stainless micro components fabricated from different powders and sintered in nitrogen/hydrogen mixture atmosphere at: (a) 1200^{o}C and (b) 1350^{o}C.

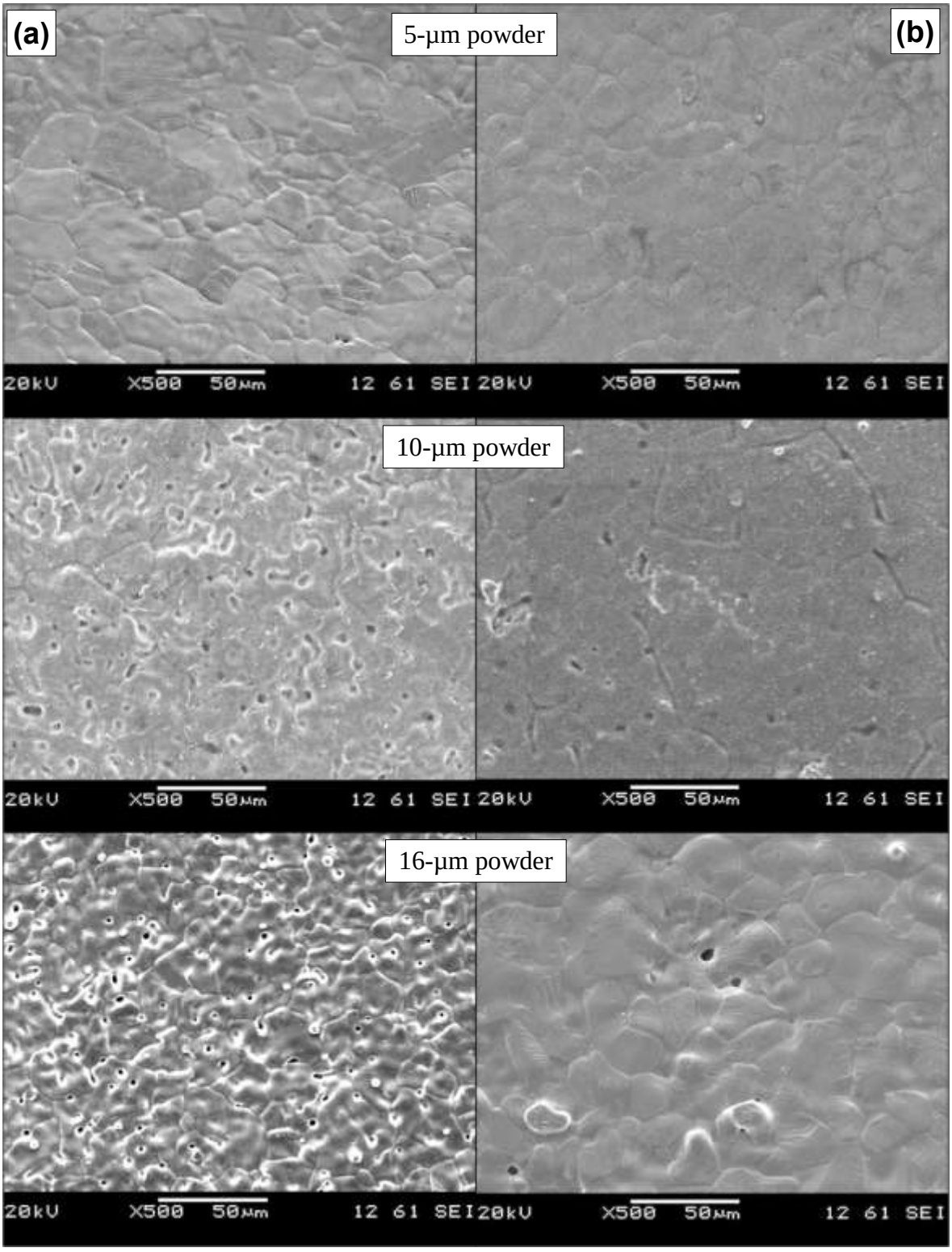

Figure 7.12. SEM images showing the surface morphologies of the stainless micro components fabricated from different powders and sintered in vacuum at: (a) 1200^{o}C and (b) 1350^{o}C.

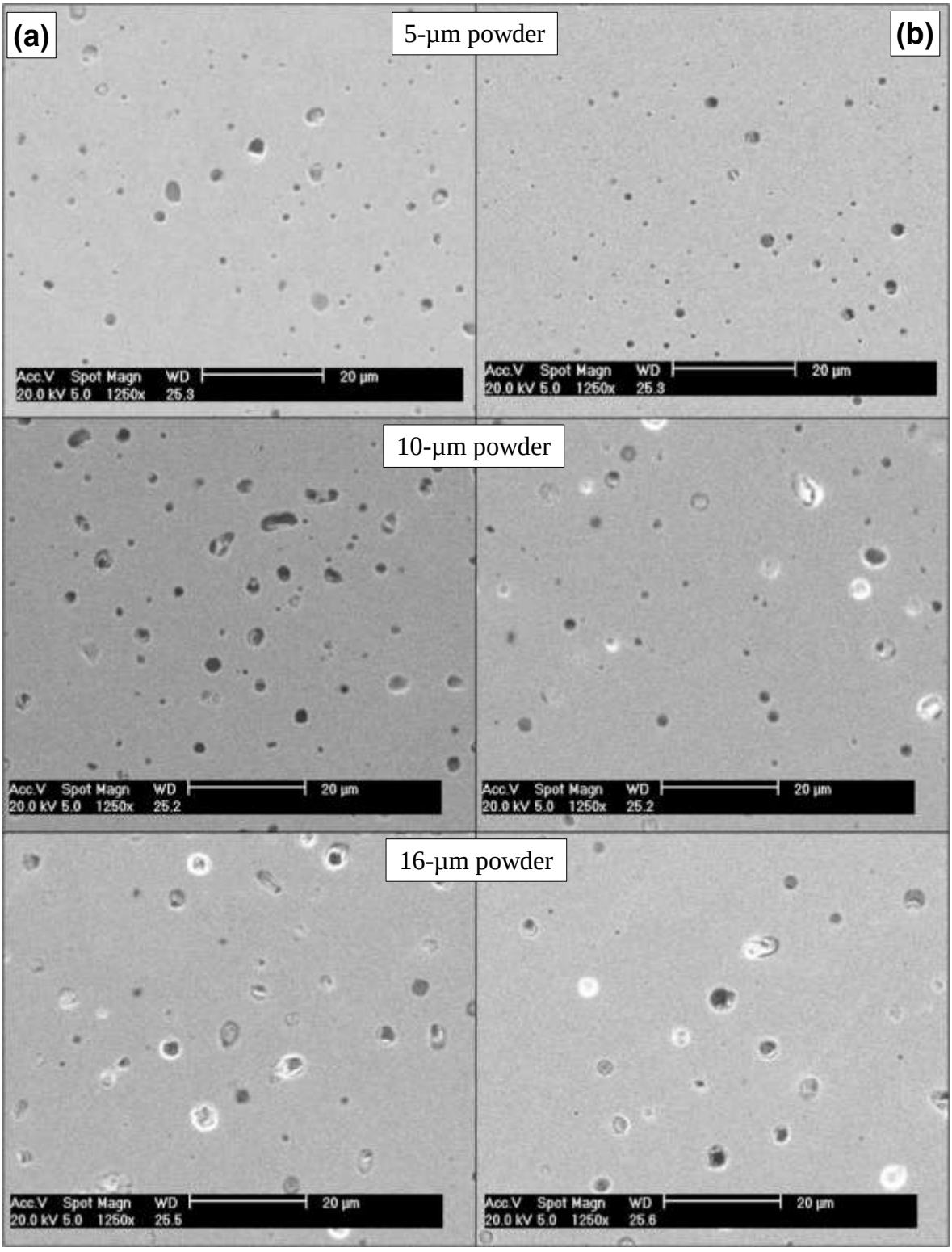

Figure 7.13. SEM images showing the polished stainless steel micro components fabricated from different powders, and sintered in nitrogen/hydrogen mixture atmosphere at: (a) 1200^{o}C and (b) 1350^{o}C.

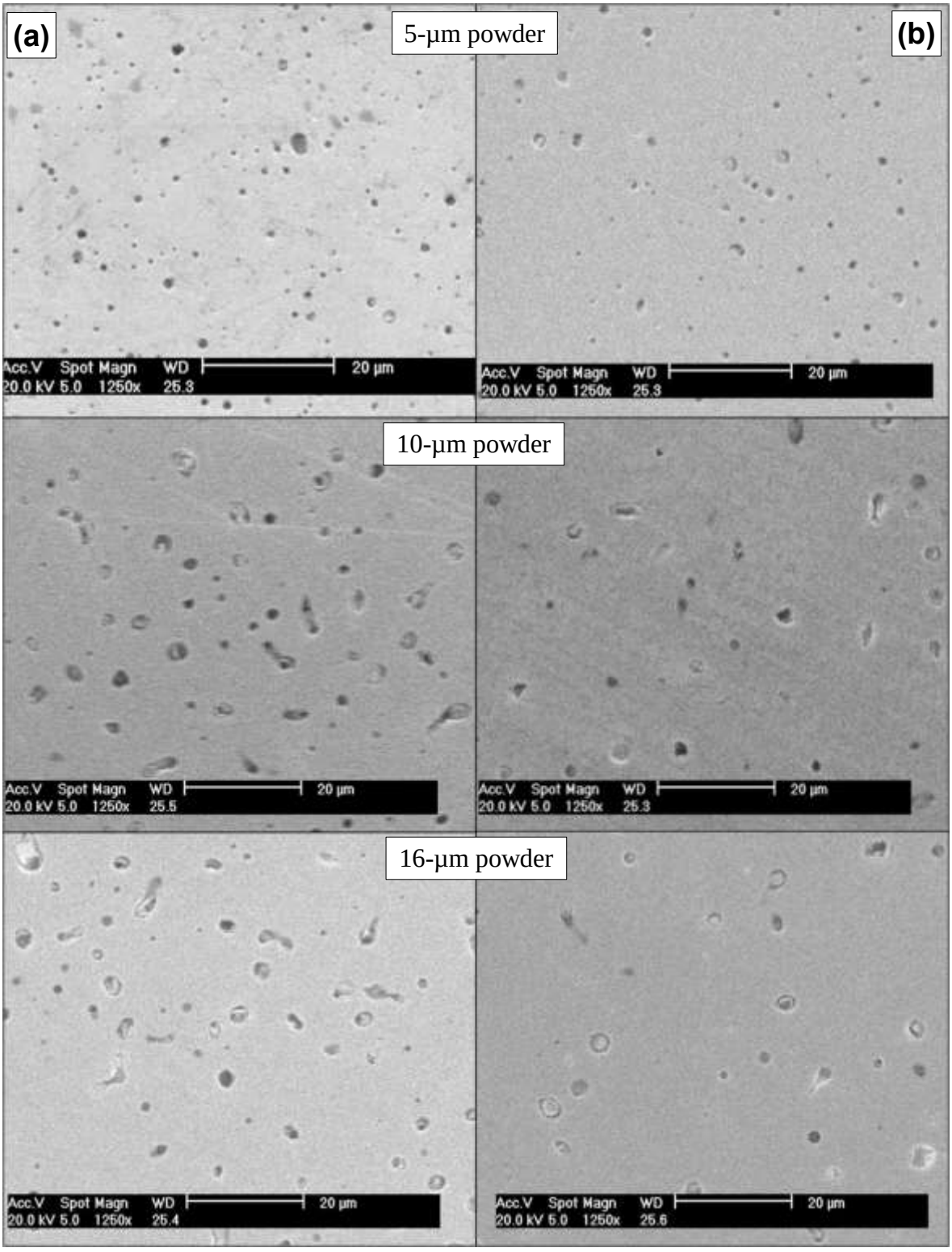

Figure 7.14. SEM images showing the polished stainless steel micro components fabricated from different powders, and sintered in vacuum at: (a) 1200^{o}C and (b) 1350^{o}C.

7.2.5. Surface roughness

In this section, the surface roughness of the sintered micro components of different powders fabricated by pressure less filling method and sintered in nitrogen/hydrogen mixture atmosphere are investigated. The target of the measurements is to reach a general conclusion of the roughness of micro components based on different powders. The roughness measurements of the stereo imaging technique are mainly dependent on different parameters, such as method of measurement, filtering method and the area of interest. For all measurements presented in this section, the image resolution, area of interest and the cut off filter length were adjusted to be 1024 × 954, 35×30 µm and 10 µm, respectively. Figures 7.15 (a) & (b), 7.16 (a) & (b) and 7.17 (a) & (b) show the SEM images taken at 0^o & 7^o tilting angles and their corresponding 3D surface profiles of the stainless steel micro components sintered at 1350^oC in nitrogen/hydrogen mixture atmosphere and based on 5, 10 and 16-µm powders, respectively. It is clear that, the 3D constructed profiles reflect the real surface topography of the stainless steel micro components. The roughness parameters are measured using ALOCINA MEX software. The comparison between roughness parameters of the stainless steel micro components fabricated from different powders is listed in Table 7.1. Generally, the smaller the powders are, the smaller the surface roughness parameters. As discussed in section 7.2.4, the surface morphologies based on 10 and 16-µm powders include many pores when compared with those based on 5-µm powder. These pores increase the texture of the surface and hence, are the main reasons of increasing the roughness.

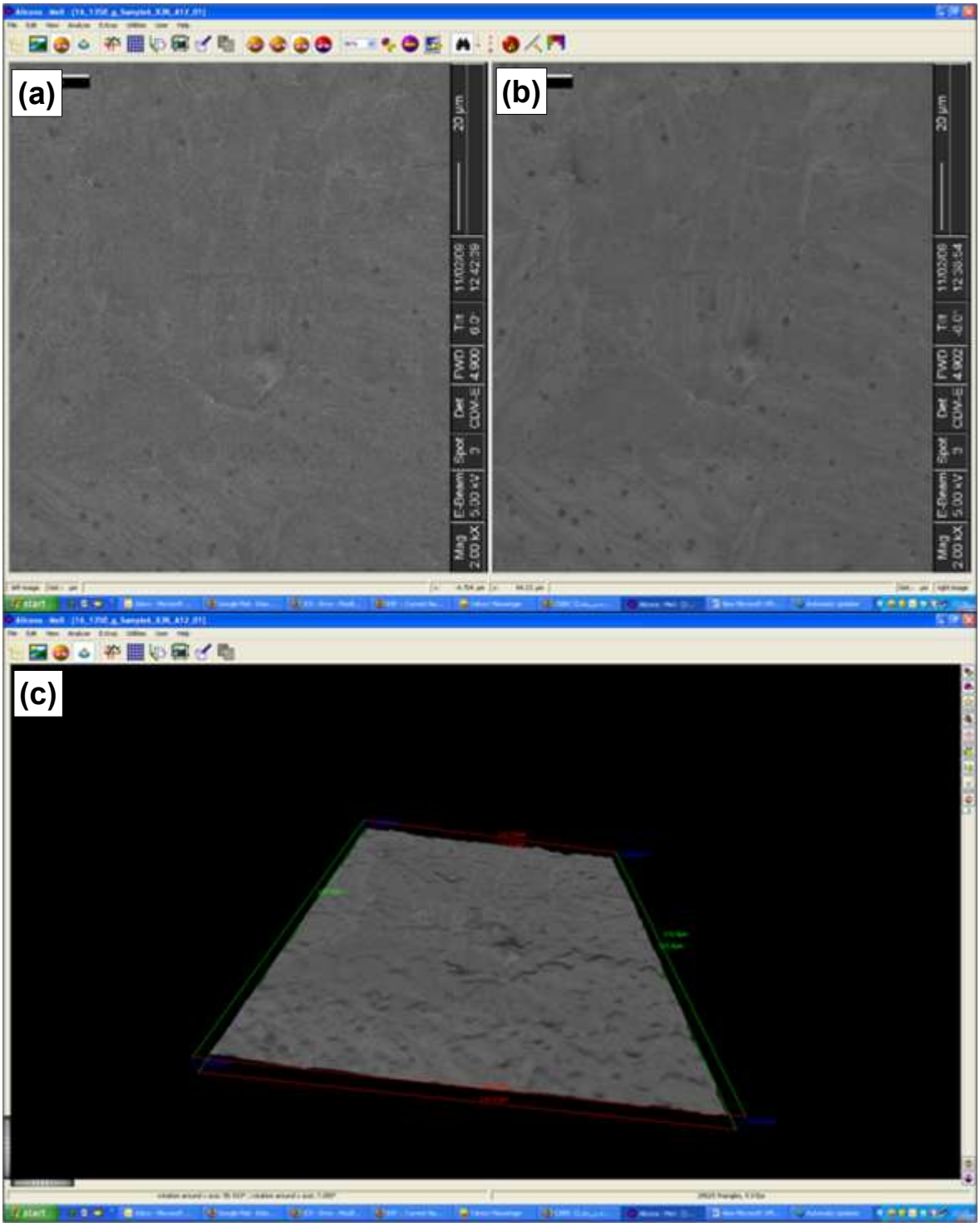

Figure 7.15. SEM images showing the top surface of the stainless steel micro components fabricated from 5-µm powder, sintered at 1350^{o}C in nitrogen/hydrogen mixture atmosphere and taken at two different tilting angles: (a) 0^{o} & (b) 7^{o}. (c) 3D surface profile constructed from the two SEM images using ALOCINA MEX software.

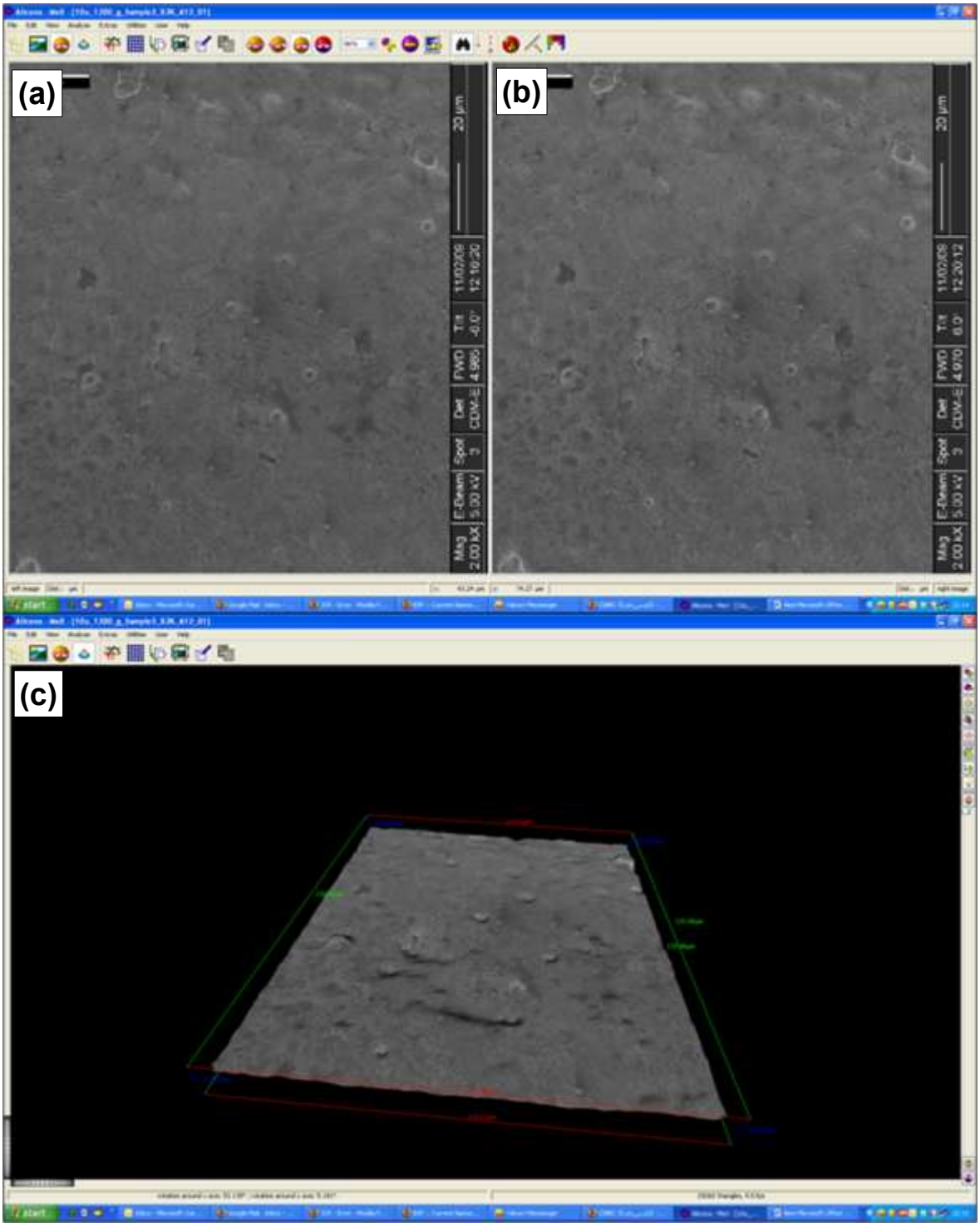

Figure 7.16. SEM images showing the top surface of the stainless steel micro components fabricated from 10-µm powder, sintered at 1350^{o}C in nitrogen/hydrogen mixture atmosphere and taken at two different tilting angles: (a) 0^{o} & (b) 7^{o}. (c) 3D surface profile constructed from the two SEM images using ALOCINA MEX software.

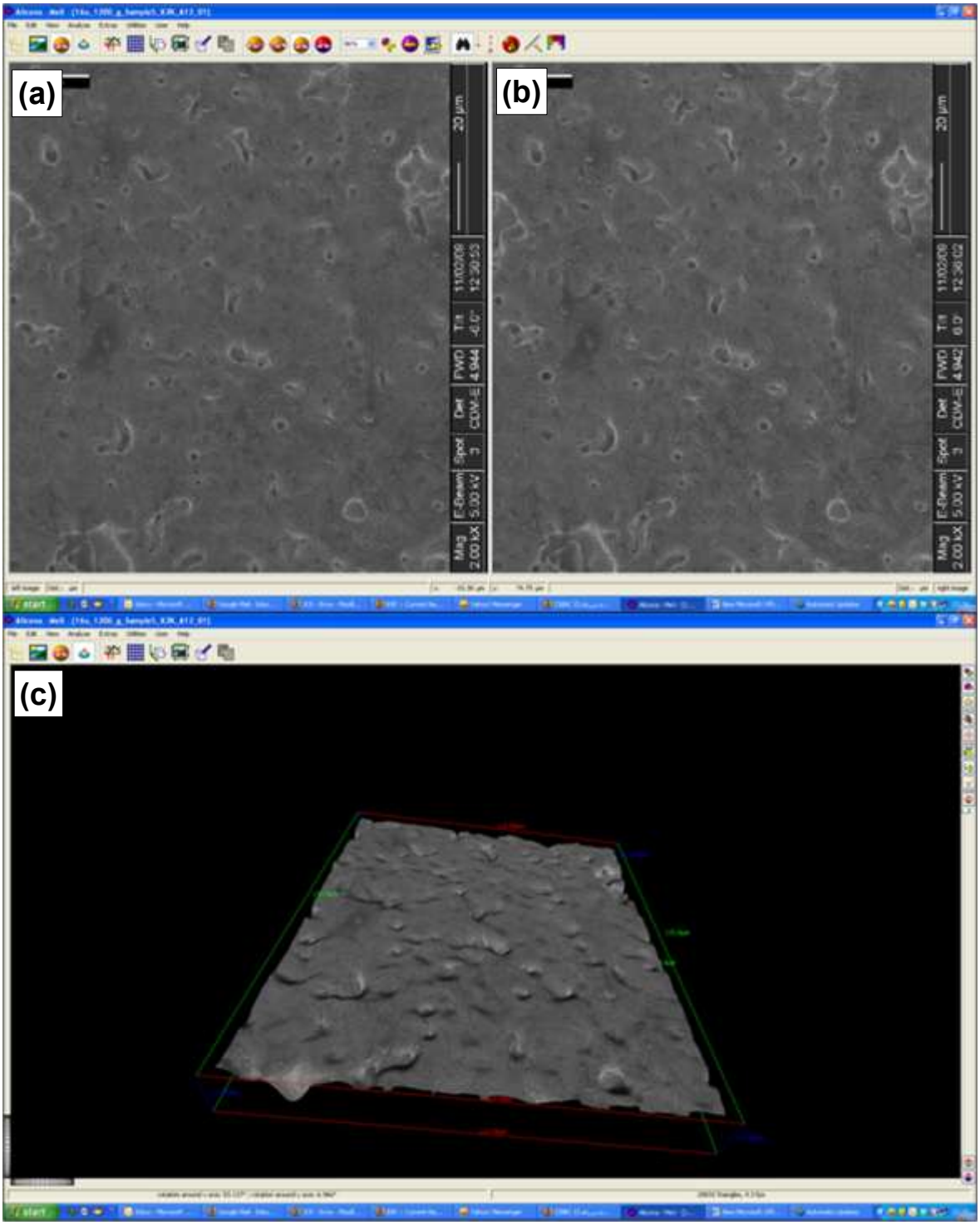

Figure 7.17. SEM images showing the top surface of the stainless steel micro components fabricated from 16-µm powder, sintered at 1350^{o}C in nitrogen/hydrogen mixture atmosphere and taken at two different tilting angles: (a) 0^{o} & (b) 7^{o}. (c) 3D surface profile constructed from the two SEM images using ALOCINA MEX software.

Table 7.1. Surface roughness parameters of the stainless steel micro components based on different powders and sintered in nitrogen/hydrogen mixture atmospheres at 1350^{o}C.

	5-µm powder	10-µm powder	16-µm powder
Ra (nm)	133.6	147.5	168
Rq (nm)	173.5	195.8	214
Rp (nm)	1173	1566	1168
Rv (nm)	1144	923	1344
Rt (nm)	2318	2489	2511

7.3. Conclusions

Characterization of stainless steel micro components, fabricated from 5, 10 and 16-µm powders by using cold isostatic pressing and pressure less filling methods and sintered in nitrogen/hydrogen mixture and vacuum at 1200, 1250, 1300 and 1350^{o}C, was conducted in terms of density, linear shrinkage, hardness, internal structures and porosity, surface morphology and roughness.

The following conclusions are obtained in this research and summarized as effects by sintering temperature, atmosphere, powder size and filling methods as listed below:

1. In terms of sintering temperature, the density and linear shrinkage increase with the increase of temperature, while the micro hardness decreases.

2. In terms of sintering atmospheres, the sintered density, linear shrinkages and porosity were nearly the same under either nitrogen/hydrogen mixture or vacuum; however,

using nitrogen/hydrogen mixture results in a significant increase in hardness when compared with that obtained by vacuum.

3. In terms of powder sizes, 5-µm powder produces excellent properties when compared with those obtained by 10 and 16-µm powders.

4. In terms of filling technique, cold isostatic pressing method produces a slight increase in density and hardness and decrease in linear shrinkage when compared with those obtained by pressure less method for 10 and 16-µm powders; however, the cold isostatic pressing method leads to a significant decrease in linear shrinkage when compared with that obtained by pressure less method for 5-µm powder.

CHAPTER 8. FABRICATION OF THE STAINLESS STEEL CERAMIC COMPOSITE MICRO COMPONENTS

This Chapter presents a novel approach to fabricate stainless steel ceramic composite micro machine components. Two types of composites are fabricated including stainless steel-alumina and stainless steel-titania. Four different compositions are prepared for each composite type, containing 2.5, 5, 7.5 and 10% weight of ceramic. Characterization of composite micro components in terms of slurry preparation process, sintering conditions, shape retention, density, linear shrinkage, internal structure and micro hardness is reported in detail.

8.1. Introduction

Composites are composed of two or more materials chemically and physically distinct from each other and suitably distributed to provide the advantage of the respective materials in one component. Normally, composites are formed from two components: matrix and reinforcement. The matrix and the reinforcing materials can be metals, ceramics or polymers. The reinforcing materials are normally strong with low densities and the matrix is usually a ductile or tough material. The reinforcements usually come in the form of particles, short fibre and continuous fibre or sheets. Each type of reinforcements can be used in specific applications. When the matrix is a metallic material the composite is called a metal matrix composite (MMC).

Metal matrix composites with ceramic inclusions combine the excellent mechanical properties of metals such as ductility and toughness with the good wear and corrosion

resistance of ceramics [203-204]. Different techniques have been used for fabrication of the metal matrix composites including liquid or solid state processes [205]. Casting is a liquid based technique of producing such composites by including the enforcement particles on the melted metal matrix. However, this technique is limited to metallic materials with low melting point such as aluminium [206-207]. Powder metallurgy process is a solid based technique which introduces an efficient and economical method of producing such composites. The process includes either blending the two powders together [189, 208-209] or mechanically alloying the ceramic inclusion into the metal powder by the so called oxide dispersion strengthening technique (ODS) [210-212]. Fabrication of composite micro components is an attractive area in producing such micro components with certain properties that cannot be achieved by monolithic materials. Although micro injection moulding (μMIM) is an emerging technique of producing monolithic micro components from metals and ceramics [111, 213], it has been developed to produce composite micro components [214]. Electroforming is another technique of producing micro components from metallic materials such as nickel [23]. So far, the process is successful in producing nickel-alumina micro composite components with very low alumina addition [44].

Stainless steels provide good mechanical properties and excellent formability but have low abrasive wear resistance due to their low hardness. Incorporation of ceramic particulate reinforcements into a stainless steel metal matrix not only increases wear resistance but also improves the overall mechanical properties [189, 207, 215-216]. Therefore, fabrication of composite micro components based on stainless steel matrix is studied in this chapter. The fabrication process of composite micro components is developed from that

presented in the previous chapters. The target micro components fabricated in this chapter are micro gear, micro linkage rod and micro piston.

8.2. Production of composite green micro components

8.2.1. Powders and binder

As discussed in Chapters Six and Seven, the final properties of stainless steel micro components produced from 5-µm powder were better than those from 10 and 16-µm powders. Thus, the fabrication process of composite micro components was based on 5-µm stainless steel powder. Two ceramic materials selected were aluminium oxide (alumina) and titanium dioxide (titania) to form composite with stainless steel. The alumina powder used in this chapter is α-alumina (≤ 400 nm) with 99.9% metal base, supplied by Alfa Aesar UK. The titania powder is < 320 nm, supplied by Huntsman England, UK. The properties of alumina and titania powders as delivered by suppliers are listed in Tables 8.1 and 8.2, respectively. Samples of alumina and titania powders were also inspected under SEM and their images are shown in Figure 8.1 (a) and (b), respectively. Both types of powders show a high tendency toward aggregation. The binder used in this chapter was dispersant acrylic based binder which was successfully used in preparation of stainless steel green micro components.

Table 8.1. The properties of alumina powders as supplied by Alfa Aesar UK.

Formula	AL_2O_3	Melting point	2045^{o}C
Formula weight	101.96	Boiling point	2980^{o}C
Form and size	-400 nm	Hardness	1440 (Vickers)
Density	3.965 g/ml	Young's Modulus	375 (GPa)

Table 8.2. The properties of titania powder as supplied by Huntsman England, UK.

Formula	TiO_2	Melting point	1855^{o}C
Formula weight	79.87	Boiling point	2900^{o}C
Form and size	240 nm	Hardness	880 (Vickers)
Density	4.2 g/ml	Young's Modulus	230 (GPa)

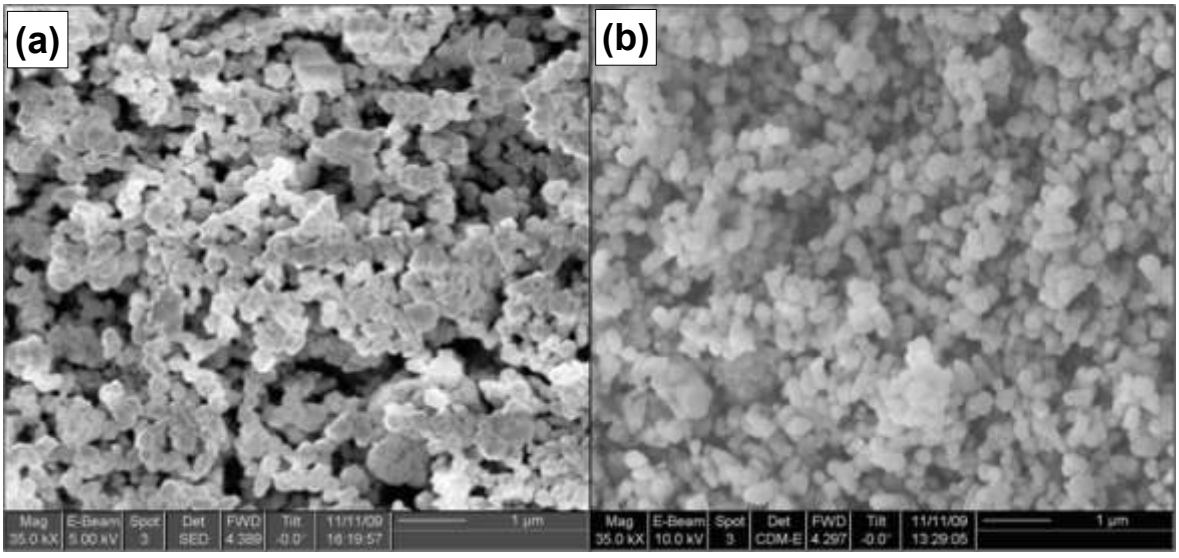

Figure 8.1. SEM images showing of the ceramic powders: (a) alumina and (a) titania.

8.2.2. Preparation of the stainless steel-ceramic slurries

Based on the preparation process of the stainless steel slurry discussed in Chapter Five, composite slurries were prepared following the same procedures and modification was made to meet the requirements of the composite. The compositions prepared contained 2.5 %, 5 %, 7.5 % and 10 % weight of ceramic in stainless steel matrix.

8.2.2.1. Optimize the amount of dispersant of ceramic powders

As discussed in Chapter Five, dispersant has a great effect on reducing the aggregation of particles and improving the green density packing of stainless steel powders. Therefore, the optimum dispersant for preparation of alumina and titania powders were obtained following the same procedures as discussed in section 5.1.1. For each ceramic powder type, slurries were prepared using various dispersant/powder ratios. Afterwards, cylindrical soft moulds were filled by ceramic slurries, green components were obtained, and then their densities were measured. The effects of dispersants on the green densities of the alumina and titania components were investigated and the results are shown in Figure 8.2. It is clear that increasing the dispersant increases the green densities for both alumina and titania. Moreover, the maximum green densities of alumina and titania are found to be 2.01 and 2.061 g/ml, and their corresponding dispersant to powder ratios are 0.004 and 0.0045 wt., respectively. It is also noted that no significant improvement of the green densities after these ratios. Consequently, these ratios are selected to be the optimum dispersant for preparing ceramic green components.

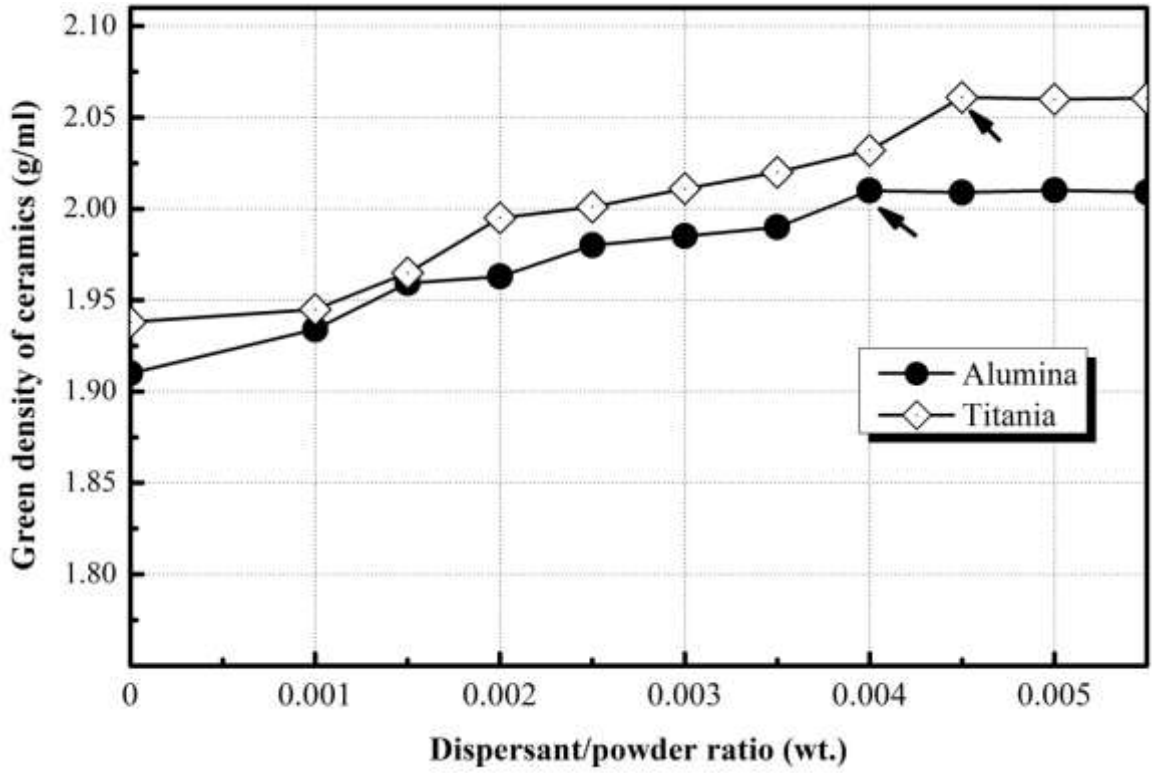

Figure 8.2. A graph showing the effect of dispersant on the green densities of ceramics based on alumina and titania powders.

8.2.2.2. Mixing the composite powders and forming composite slurry

Stainless steel ceramic composite slurries were prepared using two different methods, which are called dispersing-together and dispersing-separately, respectively. In the dispersing-together method, the following procedures are used:

1. Both stainless steel and ceramic powders were pre-mixed together using a tubular mixer for 3, 6, 12 and 24 hours.
2. Afterward, the pre-mixed powders were added to specimen tube containing dispersant and distilled water, and then stirred with mechanical stirrer for 1 h.
3. The binder was added into the mixture and the composite slurry was stirred again before being left in a vacuum chamber to remove the bubbles formed during stirring.

In dispersing-separately method, the following procedures are used:

1. Both stainless steel and ceramic powders were dispersed in separate tubes by adding the powders to the dispersion media containing the optimum dispersant for each powder.
2. After dispersion, the two dispersed slurries were mixed together and stirred by mechanical stirrer for homogenization.
3. The binder was added and the composite slurry was put in vacuum chamber to remove air bubbles.

Figure 8.3 shows the tubular mixer used for mixing the powders together in the School of Metallurgy and Materials, University of Birmingham. Figure 8.4 shows a schematic diagram describing the two mixing methods. Both methods were applied to alumina powder and the successful one in producing good density packing was selected to be used for preparing the titania based components. For both methods, the binder and solid loading are adjusted to be the same as the optimum slurry parameters discussed in Chapter Five using pressure less filling method.

Figure 8.3. A photograph showing a turbula mixer used for pre-mixing stainless steel and alumina powders.

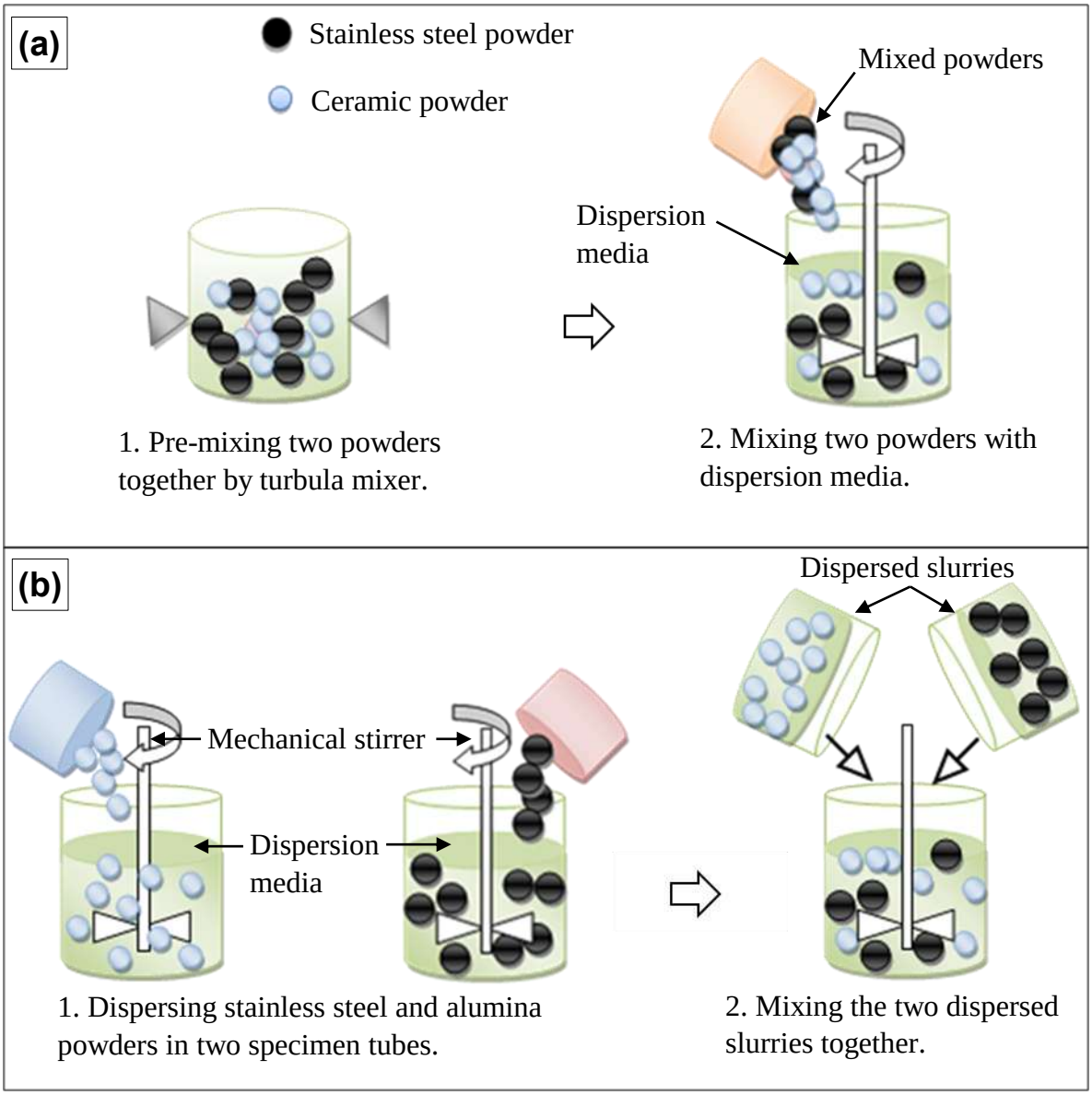

Figure 8.4. A schematic diagram showing the two mixing methods used for the preparation of stainless steel ceramic composite slurries: (a) dispersing-together method and (b) dispersing-separately method.

8.2.3. Obtaining composite green micro components

After preparing composite slurries, the soft micro moulds were filled and the green micro composite components based on alumina and titania were obtained following the same procedures discussed in Chapter five.

8.3. De-binding and sintering

As discussed in Chapter six, using nitrogen/hydrogen mixture and vacuum atmospheres in sintering stainless steel micro components produced net shape micro components. Therefore, both atmospheres are used for sintering the micro composite components. The de-binding and sintering processes are followed as discussed in chapter 6. In order to compare the properties of micro composite and those of stainless steel ones, a sintering temperature of 1350^{o}C and corresponding holding time of 1.5h were used, respectively.

8.4. Results and discussions

8.4.1. Green composite components and green density

The effects of composite compositions and mixing methods on the green density of composites components based on alumina powder were investigated and shown in Figure 8.5. As expected, the green density decreases with the increase of alumina content. Because the density of the alumina is lower than that of the stainless steel one, increasing its content decreases the overall composite density. In terms of mixing methods, it is clear that, the dispersing-separately method produces higher green density than using dispersing-together method for all pre-mixing times. In dispersing-together method, increasing the pre-mixing time increases the green density slightly. This may happen because increasing the pre-mixing time improves the homogeneity of the two powders together and hence increases the green density. On the other hand, dispersing the two powders separately takes the advantage of reducing the aggregation of each powder before mixing and the composite slurries are homogenous which increases the density packing. The fractured green micro components based on 10% alumina and obtained by using dispersing-

separately and dispersing-together (3 h pre-mixing time) methods were inspected under SEM and shown in Figure 8.6 (a) and (b), respectively. It is found that dispersing the two powders separately produces lower particle aggregation than dispersing them together by turbula mixer. The ceramic particle aggregation is pointed by black arrows in Figure 8.6. As discussed in Chapter five, the higher the aggregation of particles, the lower the density packing. This explains why the green composite density based on dispersing the powder separately is greater than that of based on dispersing them together.

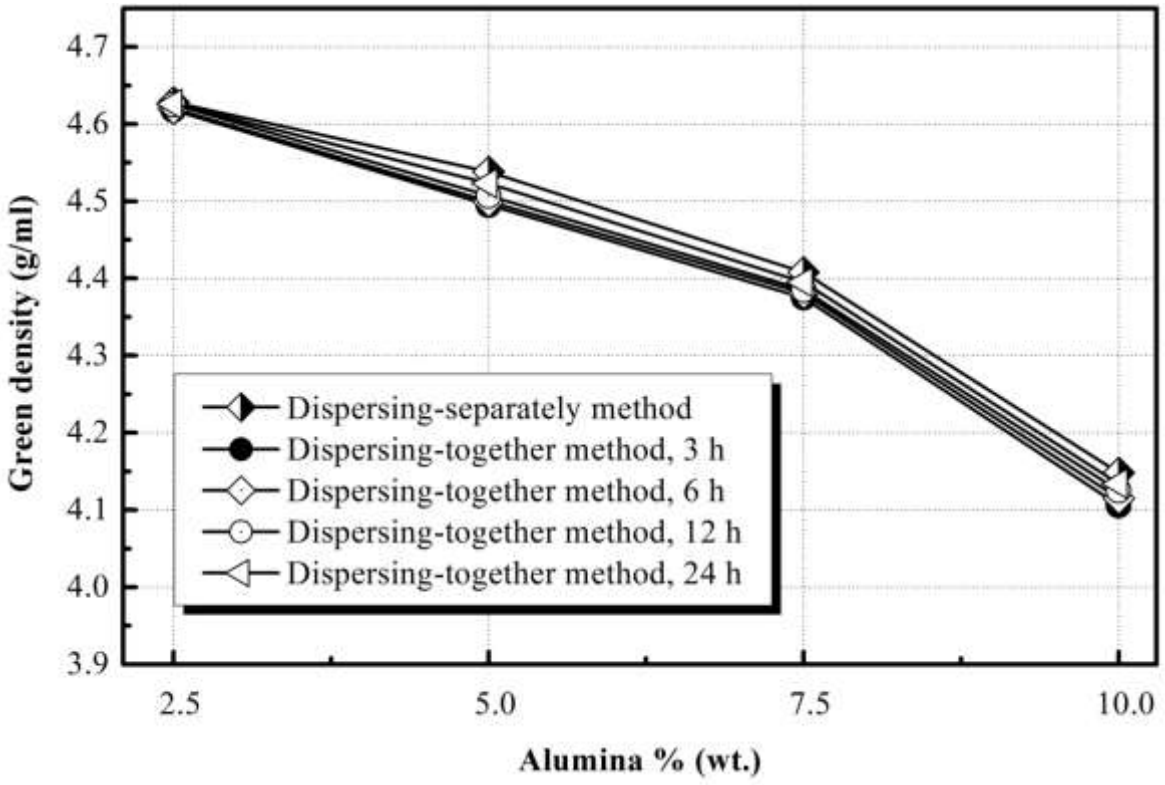

Figure 8.5. A graph showing the effect of composite compositions on the green densities of stainless steel alumina composites fabricated by using dispersing-separately and dispersing-together for 3, 6, 12 and 24 hours pre-mixed by turbula mixer.

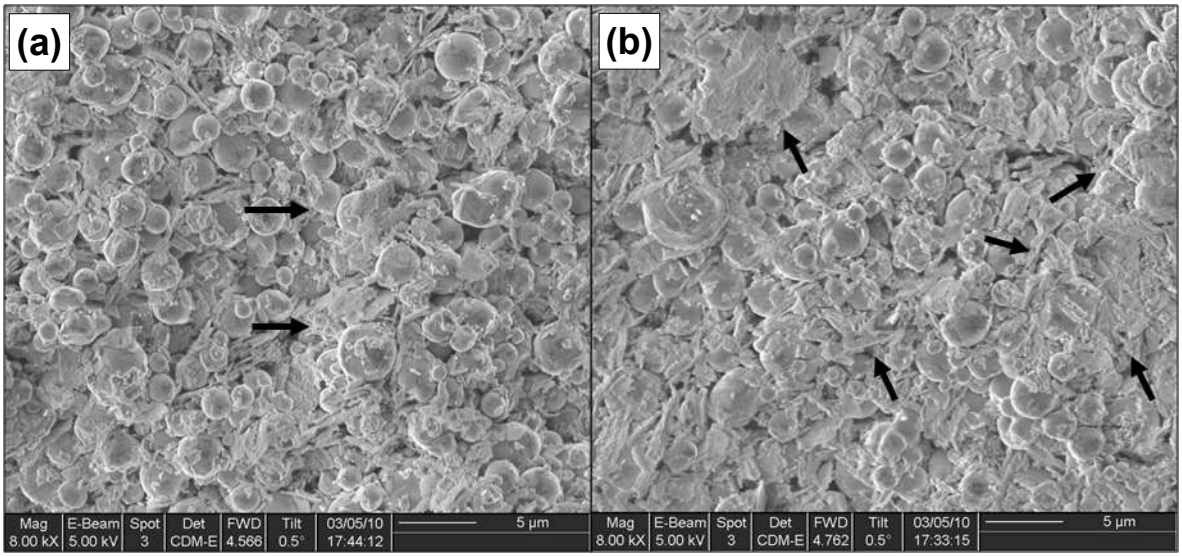

Figure 8.6. SEM images showing the fracture surface of green micro composites based on 10% alumina and fabricated by using: (a) dispersing-separately method and (b) dispersing-together method for 3 h pre-mixed by turbula mixer.

According to the results obtained for the two mixing methods, using dispersing-separately method produces good results when compared with the dispersing-together method. Consequently, micro composite components based on titania powders were obtained by dispersing the two powders separately. The effect of composite compositions on the densities of the stainless steel titania composite green components were also investigated and shown in Figure 8.7. It was found that titania composite green densities curve presents the same trend as that for alumina based components. The greater the titania content the smaller the green density and vice versa. The fracture surface of composite green components based on 10% titania was also inspected under SEM and shown in Figure 8.8. It was found that titania particles were distributed homogenously throughout the stainless steel powder. The green composite micro components based on alumina and titania powders were inspected under SEM and shown in Figure 8.9 (a) and (b), respectively. It is clear that the composite micro components have the same high quality shape as the SU-8 master moulds.

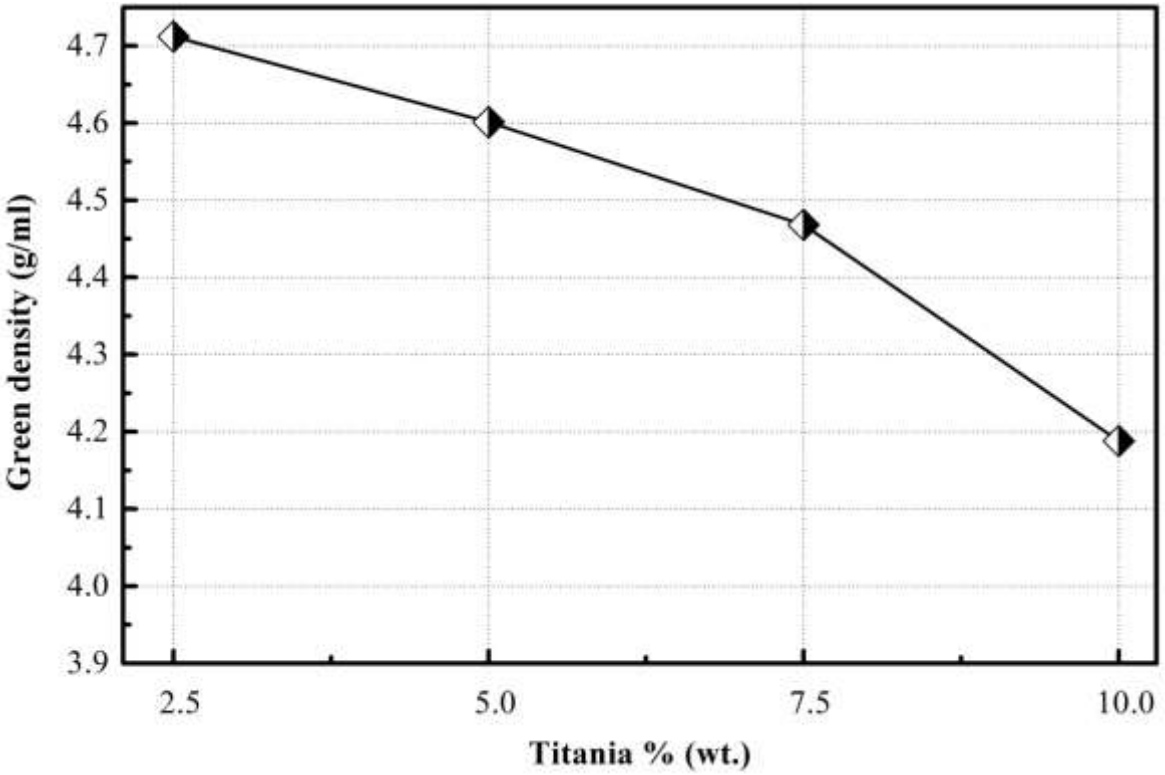

Figure 8.7. The effect of composite compositions on the green densities of stainless steel titania composites fabricated by using dispersing-separately method.

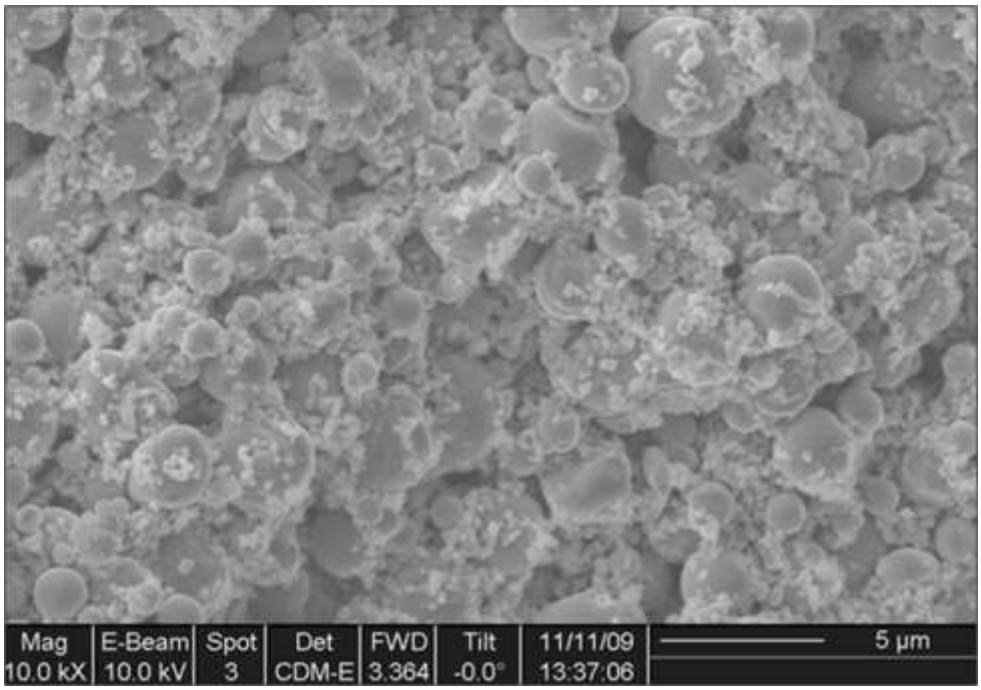

Figure 8.8. SEM image of the fracture green micro composites based on 10% titania and fabricated by using dispersing-separately method.

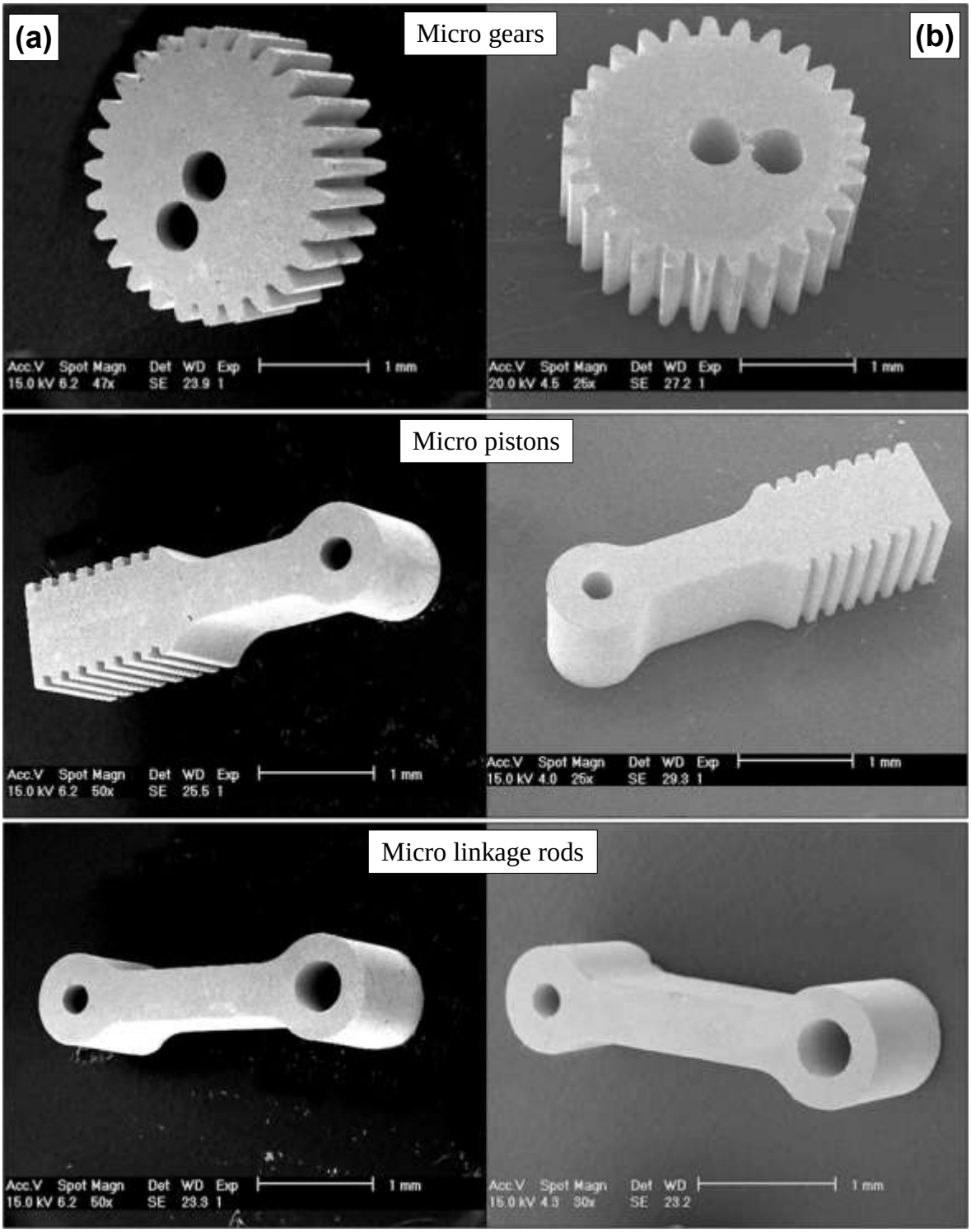

Figure 8.9. SEM image of the stainless steel ceramic composite green micro components fabricated by using dispersing-separately method and based on: (a) 10% alumina and (b) 10% titania.

8.4.2. Shape retention of composite micro components

Figures 8.10 and 8.11 show the SEM images of the composite micro components fabricated from 10% of alumina and titania powders using dispersing-separately method, and sintered at 1350^{o}C in nitrogen/hydrogen mixture atmosphere and vacuum, respectively. It is found that, all features of the composite micro components are retained after sintering and net shape retention is obtained. Moreover, the quality of the sintered composite micro components based on titania is the same as that based on alumina. Generally, ceramic inclusions are distributed homogenously throughout the stainless steel matrix after sintering.

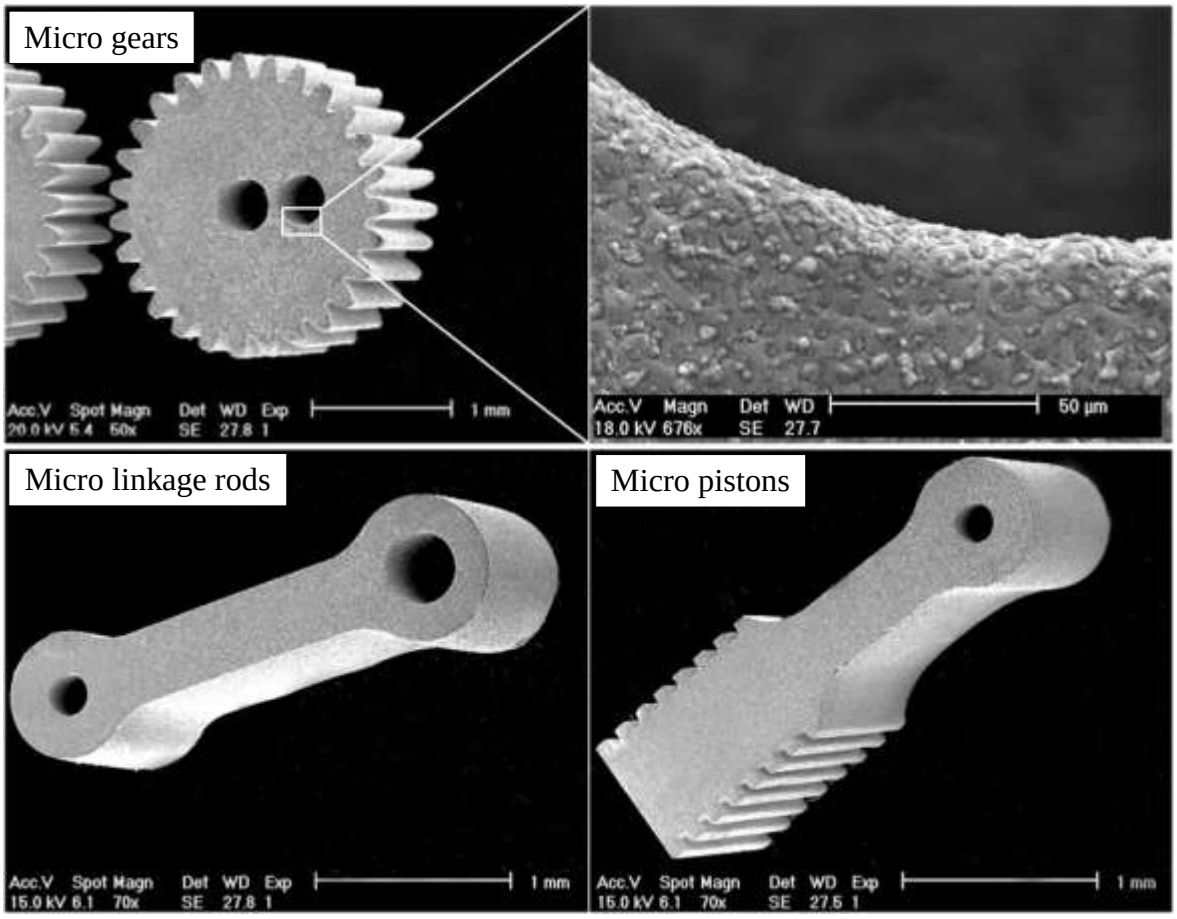

Figure 8.10. SEM images showing the stainless steel alumina composite micro components made of 10% of alumina and sintered in nitrogen/hydrogen mixture atmosphere at 1350^{o}C

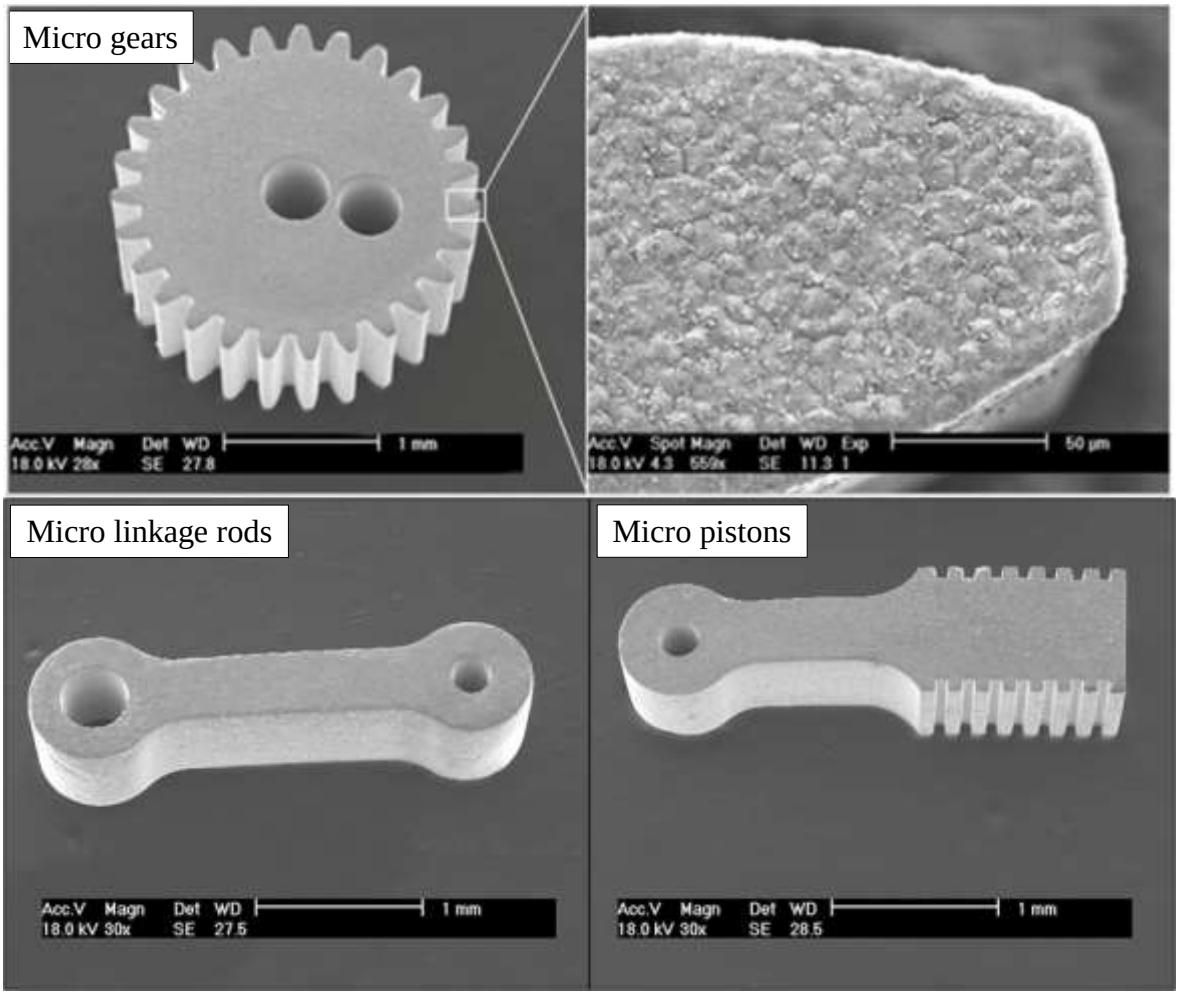

Figure 8.11. SEM images showing the stainless steel titania composite micro components made of 10% of titania and sintered in vacuum at 1350^{o}C.

8.4.3. Composite sintered density

The effects of composite compositions, sintering atmospheres, ceramic types on the density of sintered composite micro components were investigated. The density was measured using the immersion technique presented in Chapter seven. In order to compare the density of the composite micro components with those of stainless steel, the density ratio is selected instead of absolute density. Density ratio is the ratio between the measured density of the composite and the density of stainless steel wrought material. The measured density is based on six samples and the average value is selected. Figure 8.12 shows the

effect of composite compositions on the density of the composite micro components based on alumina and titania, and sintered at 1350^{o}C in nitrogen/hydrogen mixture and vacuum atmosphere. It was found that the sintered densities curves follow the same trend as the green density curves. Increasing the ceramic contents decreases the density of the micro composite for both nitrogen/hydrogen mixture and vacuum atmospheres. The sintered density of the micro composite decrease for two reasons: (i) the ceramic inclusions have lower density when compared with stainless steel. Therefore the overall composite density decreases with the increase of ceramic contents, and (ii) the interaction between ceramic particles and stainless steel matrix is not perfect after sintering, i.e., some of the ceramic particles are loose in the stainless steel matrix which increases the porosities inside the micro components and hence reduces the density of composites. In further analysis, the composite micro components were polished and inspected under SEM. Figure 8.13 shows the polished composite micro components sintered in nitrogen/hydrogen mixture atmosphere at 1350^{o}C and based on alumina and titania, respectively. It is clear that some of ceramic inclusions are loose as indicated by black arrows, which confirms the above explanation. For a given composite composition, the density of the sintered micro composites based on titania is greater than those based on alumina. That happens as a result to the density of pure titania is greater than that of alumina as presented in Tables 7.1 and 7.2. Generally, for a given composition of both alumina and titania composites, the densities of sintered components in vacuum are greater than those sintered in nitrogen/hydrogen mixture.

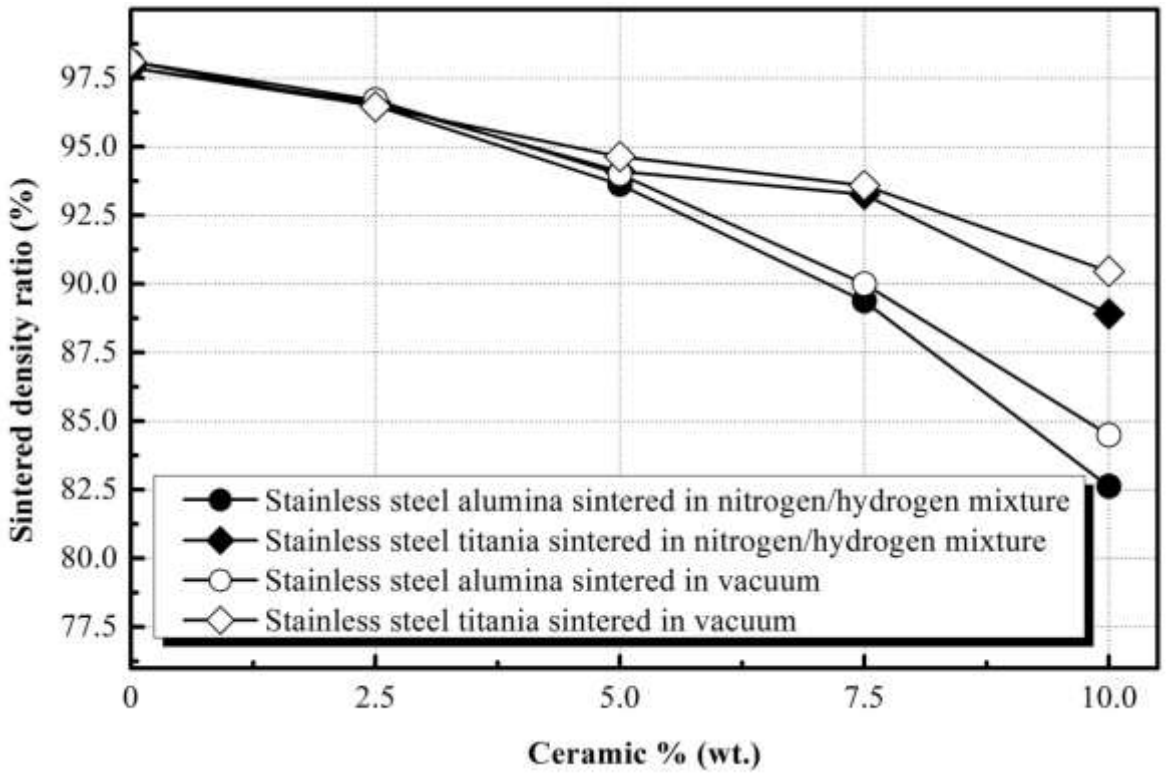

Figure 8.12. A graph showing the effect of composite composition on the density of the composite micro components fabricated from stainless steel alumina and titania; and sintered at 1350^{o}C in nitrogen/hydrogen mixture and vacuum atmospheres.

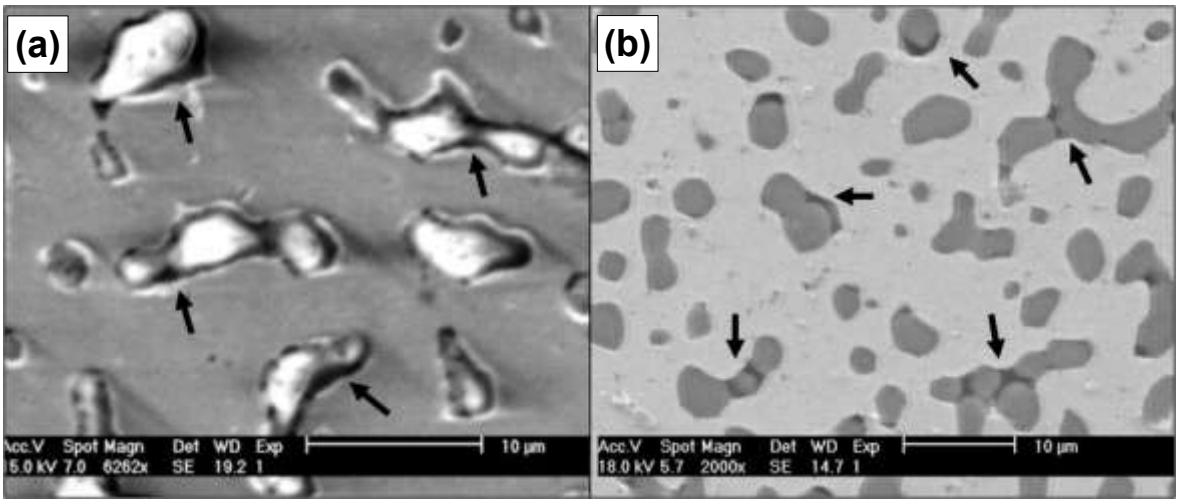

Figure 8.13. SEM images of polished composite micro components with: (a) 10% alumina and (b) 10% titania, sintered in nitrogen/hydrogen mixture atmosphere at 1350^{o}C. Black arrows showing some of the ceramic particles are loose in stainless steel matrix.

8.4.4. Composite linear shrinkage

The linear shrinkage of the composite micro components is measured following the procedures discussed in Chapter seven. The following formula is used for calculating the linear shrinkage of composite micro components:

$$Shrinkage\ \% = \frac{D_{SU-8} - D_c}{D_{SU-8}} \times 100 \quad (7.1)$$

$D_{SU\text{-}8}$: The outer diameter of the SU-8 micro gear,

D_c: The outer diameter of the composite micro gear.

For each case studied, the linear shrinkage of six gears was measured and the average was taken. The tope view of SU-8 micro gear and its corresponding composite one were inspected under SEM and shown in Figures 8.14 (a) and (b), respectively. The profile of the composite micro gear looks a pure circle, an indication to homogenous shrinkage occurred during sintering. The effect of composite compositions on the linear shrinkages of the composite micro components with alumina and titania, and sintered in nitrogen/hydrogen mixture and vacuum atmospheres at 1350^{o}C are illustrated in Figure 8.15. The linear shrinkage curves follow the same trend as the sintering density curve does, in which the greater the ceramic contents are, the lower the linear shrinkage and vice versa. As discussed in section 8.4.3, the porosity inside the micro composite increases as the interaction between ceramic particles and stainless steel matrix loses; therefore, increasing the ceramic content increases the porosity and resulting in increasing the volume and decreasing the shrinkage. Moreover, the linear shrinkage of the titania composite micro components is greater than the alumina composite. This is the result due to higher densification occurred in titania than in alumina as discussed in section 8.4.1. Generally,

the linear shrinkages of the micro composite sintered in vacuum are greater than those sintered in nitrogen/hydrogen mixture atmosphere.

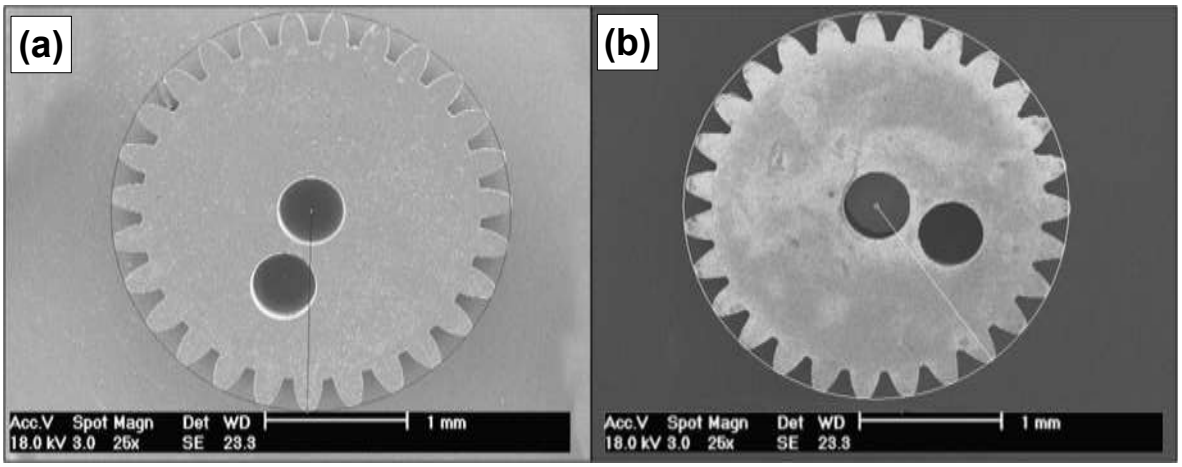

Figure 8.14. SEM images showing top views of micro gears: (a) SU-8 and (b) stainless steel alumina composite based on 10% alumina and sintered in nitrogen/hydrogen mixture at 1350^{o}C.

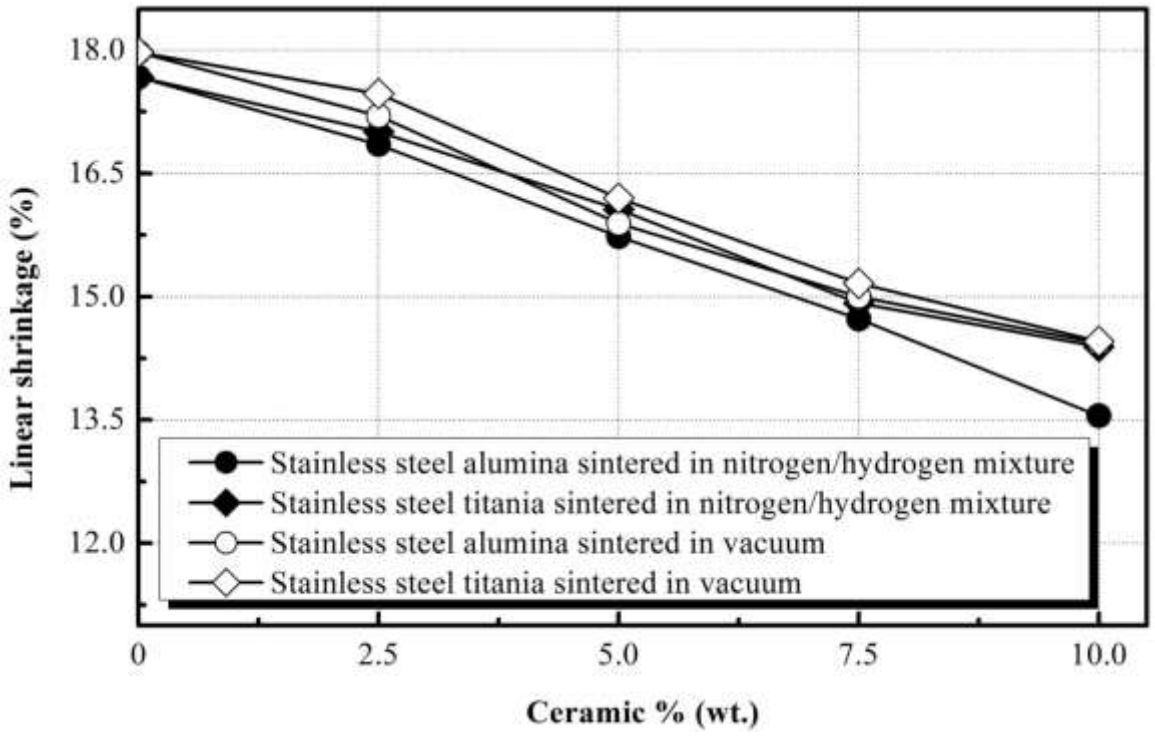

Figure 8.15. A graph showing the effect of composite compositions on the linear shrinkage of the composite micro components fabricated from stainless steel alumina and titania, and sintered in nitrogen/hydrogen mixture and vacuum atmospheres at 1350^{o}C.

8.4.5. Composite microstructure

It is very important to investigate the homogeneity of the ceramic inclusions throughout the stainless steel metal matrix after sintering. This can be done by polishing the composite micro components and inspecting them under SEM. The composite micro components were ground and polished following the procedures discussed in Chapter seven. Firstly, a comparison between two mixing method was performed in terms of internal structure of the sintered stainless steel alumina composite. The internal structures of stainless steel alumina composite micro components, based on 10% of alumina, sintered in nitrogen/hydrogen mixture atmospheres at 1350^{o}C and fabricated by using dispersing-together (3h pre-mixing time) and dispersing-separately methods, were inspected under SEM as shown in Figures 8.16 (a) and (b), respectively. It is clear that using dispersing-separately method produces homogenous distribution of the alumina in stainless steel matrix and the particles look the same appearance. On the other hand, using dispersing-together method produces non-homogenous distribution of the alumina particles in stainless steel matrix in which some kind of a big size alumina particle is existed as pointed by black arrow. The non-homogenous particle distributions affect the mechanical properties of the composite in which the properties may change throughout the micro composite. This happens in result to the higher aggregations of the ceramic particles in their corresponding green micro components when dispersing together method is used. Figures 8.17 (a) & (b) and 8.18 (a) & (b) show the SEM images of the polished stainless steel alumina and titania composite micro components of different compositions fabricated by dispersing-separately method and sintered in nitrogen/hydrogen mixture and vacuum atmospheres at 1350^{o}C, respectively. For given composite composition and ceramic inclusion type, the polished micro components sintered in both nitrogen/hydrogen mixture

and vacuum atmospheres show nearly the same appearance. Moreover, the ceramic inclusions are distributed homogenously throughout the stainless steel matrix. At low ceramic content, the ceramic inclusions look spherical while they are clustered to form big particle sizes when the ceramic contents increase.

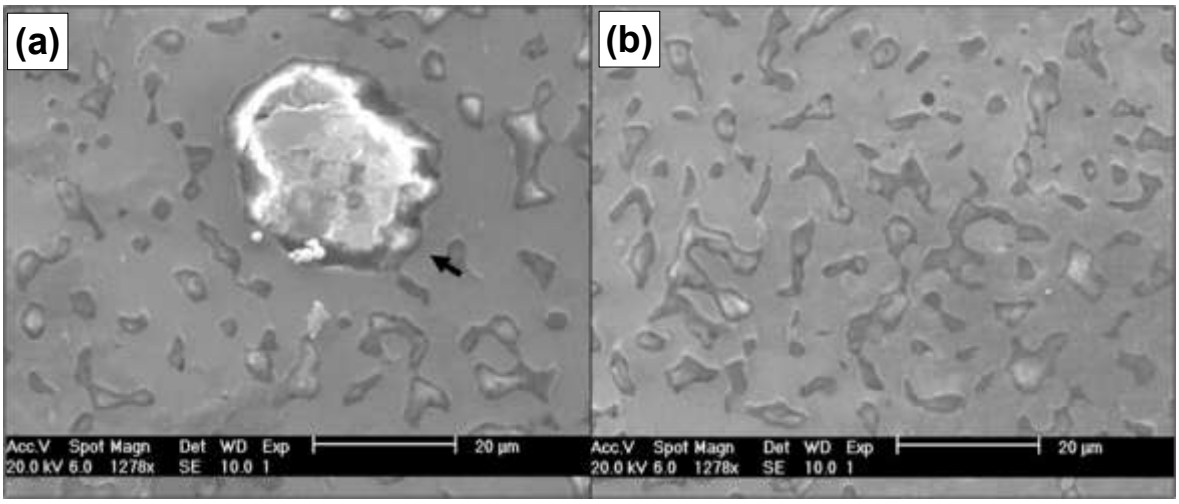

Figure 8.16. SEM images of the polished stainless steel alumina composite micro components based on 10% of alumina, sintered in nitrogen/hydrogen mixture atmosphere at 1350^{o}C and fabricated by using: (a) dispersing-together and (b) dispersing-separately methods.

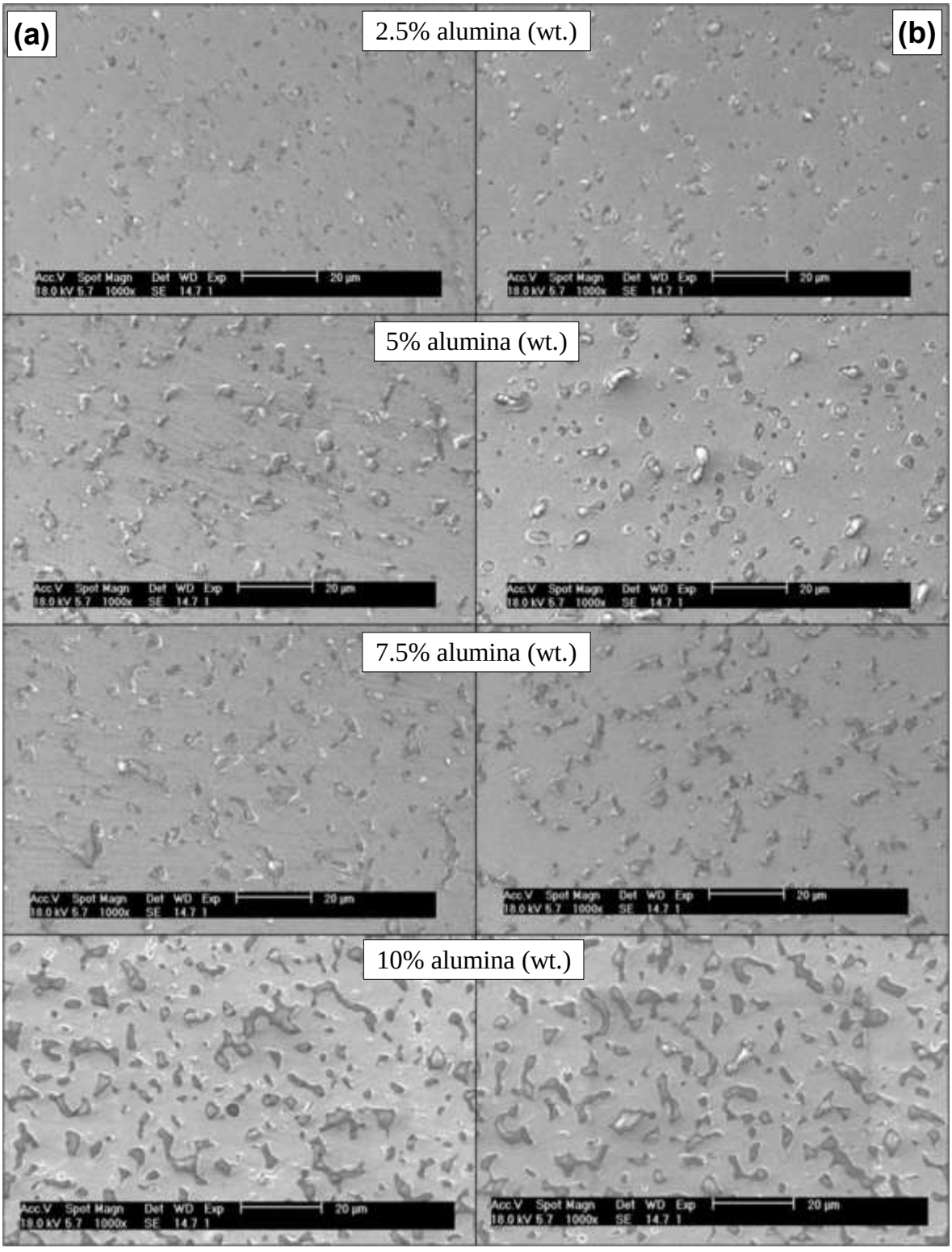

Figure 8.17. SEM images showing the polished stainless steel alumina composite micro components fabricated by dispersing-separately method, based on different composite compositions and sintered at 1350^{o}C in: (a) nitrogen/hydrogen mixture and (a) vacuum atmospheres.

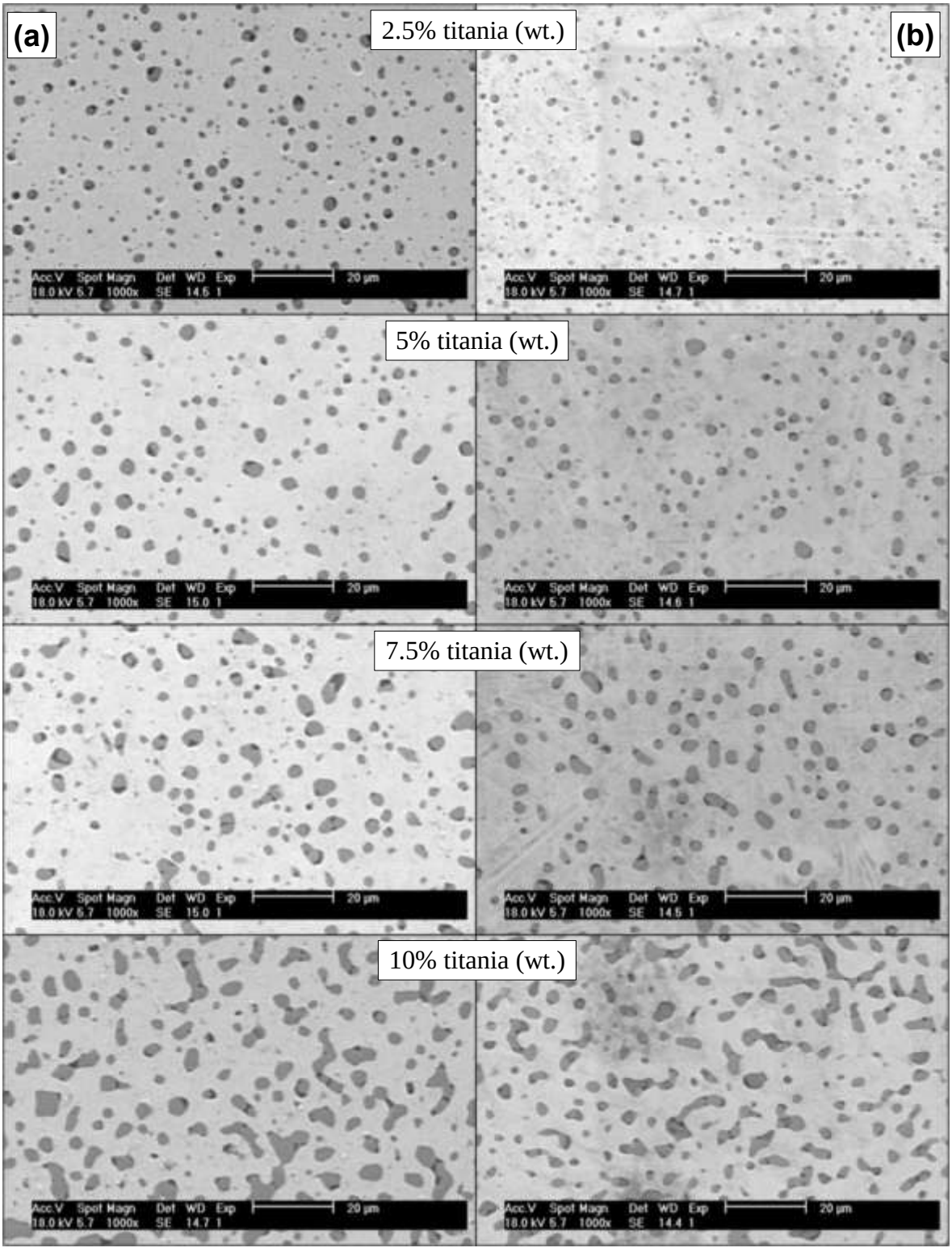

Figure 8.18. SEM images showing the polished stainless steel titania composite micro components fabricated by dispersing-separately method, based on different composite compositions and sintered at 1350^{o}C in: (a) nitrogen/hydrogen mixture and (a) vacuum atmospheres.

8.4.6. Micro hardness analysis of the micro composites

Micro hardness is an important parameter measured in this Chapter. The composite micro components were polished and hardness tests were performed using the procedures discussed in Chapter seven. The applied load for micro indentations was 300 mg. The hardness measurements were based on Vickers hardness number and the measurement average of three different micro gears was taken. For each micro gear, ten indentation marks were produced and the average was taken. Figures 8.19 and 8.20 show the indentation marks on the surfaces of the polished composite micro components sintered in nitrogen/hydrogen mixture and vacuum atmospheres at 1350^{o}C, and based on alumina and titania powders, respectively. It is clear that the sizes of indentations marks sintered in nitrogen/hydrogen mixture are smaller than the others for both alumina and titania, indicating a higher hardness. The effects of composite compositions, ceramic types and sintering atmospheres on the hardness of the composite micro components were investigated and the results were shown in Figure 8.21. As expected, higher the ceramic content increases the hardness for different ceramic types and sintering atmospheres. It is also clear that, for given composite composition and sintering atmosphere, the hardness of the micro composites based on alumina powder is greater than that based on titania one. This happens due to the greater hardness of pure alumina than that of pure titania as listed in Tables 7.1 and 7.2. Moreover, for a given composite composition and ceramic type, the hardness of the composites sintered in nitrogen/hydrogen mixture atmosphere is significantly greater than those sintered in vacuum. The reason for this was explained in Chapter seven. Using nitrogen/hydrogen mixture atmosphere promoted the solid solution hardening of the stainless steel.

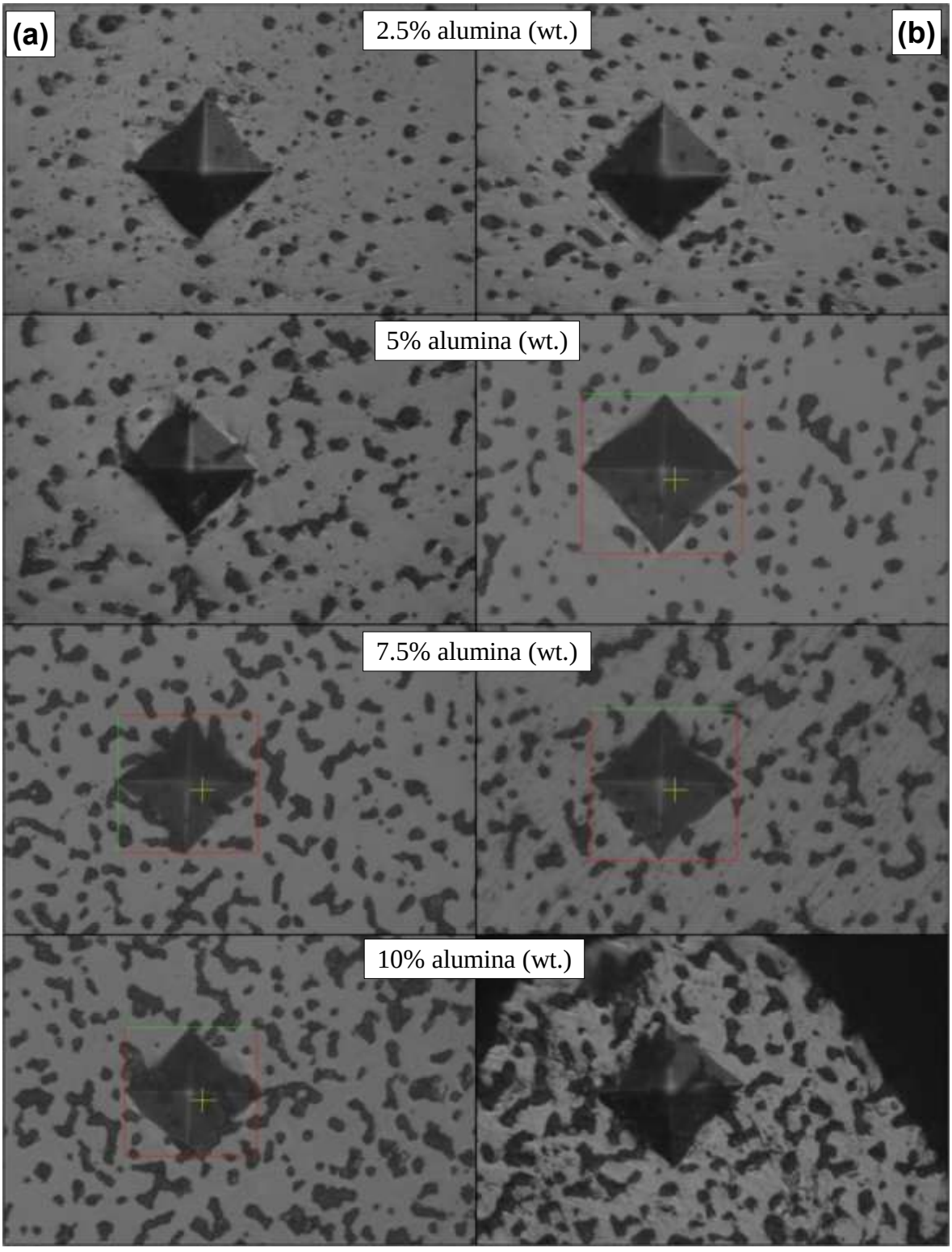

Figure 8.19. Optical images showing the micro hardness indentation marks on the surfaces of stainless steel alumina composite micro components sintered at 1350^{o}C in: (a) nitrogen/hydrogen mixture and (b) vacuum atmospheres.

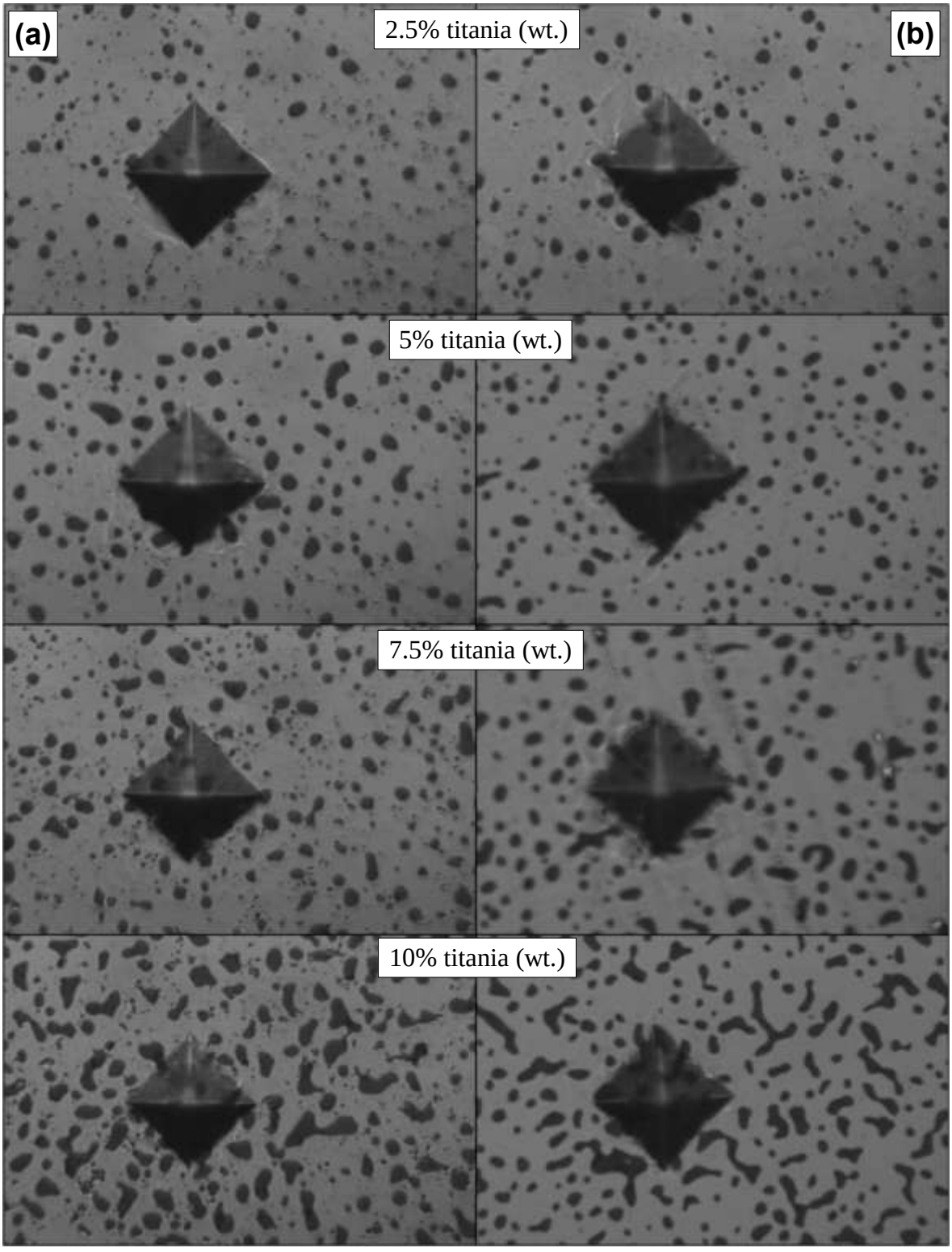

Figure 8.20. Optical images showing the micro hardness indentation marks on the surfaces of stainless steel titania composite micro components sintered at 1350^{o}C in: (a) nitrogen/hydrogen mixture and (b) vacuum atmospheres.

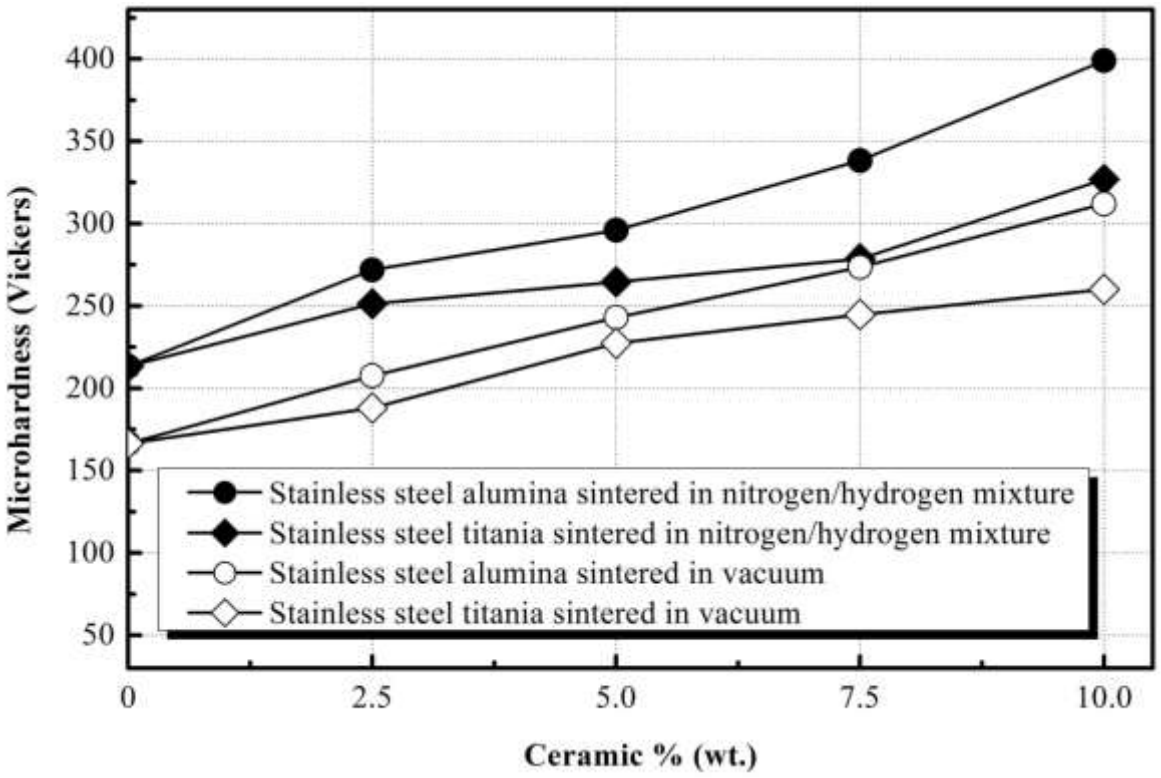

Figure 8.21. A graph showing the effect of composite composition on the hardness of the composite micro components fabricated from stainless steel alumina and stainless steel titania, and sintered in nitrogen/hydrogen mixture and vacuum at 1350^{o}C.

8.4.7. Various composite components

The process presented in this chapter is successfully used for producing composite micro components. Micro spur gears, as presented in Chapter six, are used as a test pattern. Figure 8.21 shows the optical images of spur gears, 12 mm pitch diameter and 18 teeth, fabricated from stainless steel, stainless steel alumina and stainless steel titania. The quality of the fabricated spur gears from composites reflect the same quality as stainless steel and SU-8 master mould presented in Chapter six.

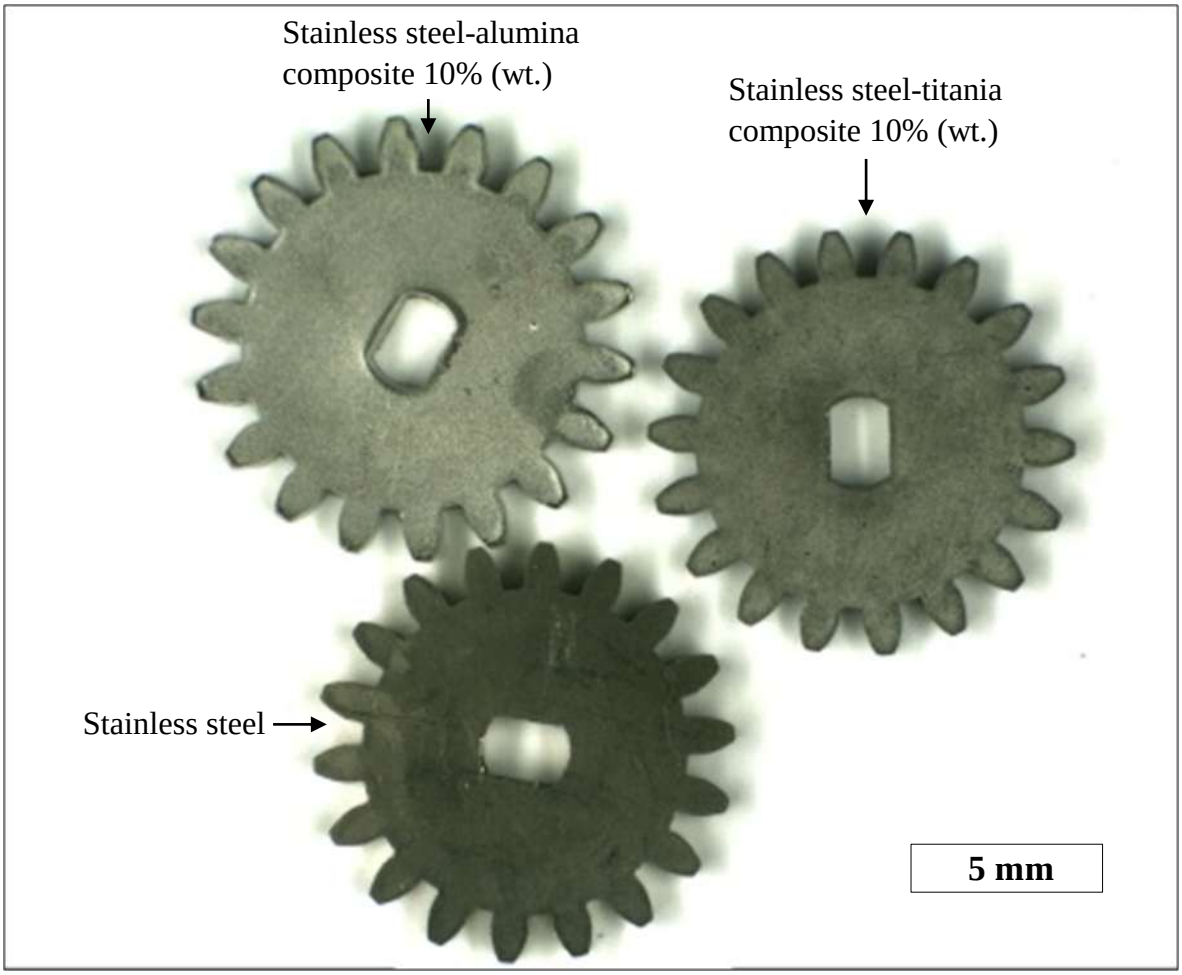

Figure 8.22. Optical image showing the spur gears each of which has 18 teeth and 12 mm pitch diameter fabricated from stainless steel, stainless steel alumina composite and stainless steel titania composite and sintered in nitrogen/hydrogen mixture atmosphere at 1350^{o}C

8.5. Conclusions

In this part of the research, composite micro components were successfully fabricated from stainless steel alumina and stainless steel titania with different compositions. The fabrication process was investigated in detail and characterizations of composite micro components were studied in terms of composite preparation process, green and sintering density, linear shrinkage, internal structures and micro hardness. The following conclusions can be drawn from the work presented in this chapter:

1. In terms of composite preparation process, using dispersing-separately mixing method produces good results when compared with those obtained by using dispersing-together method.
2. Increase the ceramic content decreases both density and linear shrinkage, but it increases the hardness.
3. For a given composite composition, using nitrogen/hydrogen mixture and vacuum atmospheres produces nearly the same density and linear shrinkage, while the hardness increases significantly by using nitrogen/hydrogen mixture atmosphere.
4. For a given composite composition, the sintered density and linear shrinkage of stainless steel-titania composite is greater than stainless steel-alumina, while the hardness of the later is greater than the former one.

CHAPTER 9. CONCLUSIONS AND FUTURE WORK

9.1. Conclusions

The three year PhD research project involves a broad range of techniques, including UV lithography, powder metallurgy and micro fabrication. The research combines those techniques and develops a new approach for fabricating micro components from metallic and composite materials. The approach proves successful through vigorous experiments and demonstrates its advantages over existing Softlithography fabrication processes and micro injection moulding process, in terms of high quality shape retention micro components.

The main contributions of the research towards the field can be summarised as follows:

1. **Improvement of SU-8 photolithography technique.** In the past, the process involved using three filters and time concerning. The new process needs just one filter to fabricate 1 mm thick SU-8 patterns as master moulds. This process saves the total exposure energy and time used for obtaining ultra-thick SU-8 micro components greater than 500 µm.
2. **Adoption of soft moulding in cold isostatic pressing technique.** This process improves the final properties of micro components which were previously fabricated by pressure less and low applied pressure.
3. **Extension of the process to nanoceramic composite materials.** Nano-composite micro components have been produced by combining both Softlithography and powder metallurgy processes.

The conclusions obtained through the research are drawn as follows.

1. High quality metallic and composite micro components can be manufactured by combining soft lithography powder metallurgy. In particular, it proves successful in stainless steel and its composites. It should be also possible to be achieved in many other metals and composites.
2. Dispersant acrylic based binder is an efficient binder for preparation of metallic and composite slurries for Softlithography process. The process proves that by using a few grams of the dispersant, a great number of micro components can be fabricated in one process, showing its high effectiveness.
3. Both pressure less filling and cold isostatic pressing methods can be used in producing stainless steel green and sintered micro components. However, the properties of the final sintered components fabricated by using cold isostatic pressing method is better than using pressure less filling method in terms of density and linear shrinkage hardness, while the best shape retention was obtained by using pressure less filling method.
4. After comparison between three different stainless steel powders investigated, 5-µm powder is found suitable than 10 and 16-µm powders in density, hardness, surface roughness and shape retention for fabrication of micro component measuring from 2 – 15 mm in overall dimensions.

Based on the achievements and conclusions, it can be stated that the project aims have been reached through implementation of project objectives set out at the beginning of the research.

9.2. Future work

It has been an interesting research project in fabrication of metallic micro components by combining techniques in MEMS, powder metallurgy, and nanoceramic powders. Although many results are achieved through intensive work in the past three years, much more could be done should time allow. The following research tasks are recommended for future study in this area.

1. All the micro components fabricated in this research are two dimensional which extruded to the third one through straight sidewall. Therefore it is expected in the future work to apply this technique to the three dimensional micro component, which has 3D curved shape such as micro compressors and micro turbine blade.
2. The research work presents hand-made micro components which have been limited to the automation process. During the whole fabrication processes presented, the filling and de-moulding processes are done by hand and it is expected that the processes to be developed further in order to apply automation filling and de-moulding.
3. More experimental work is necessary in using cold isostatic pressing technique with applied pressure greater than 116 MPa.
4. The corrosion resistance of stainless steel and its composite micro components can be studied.
5. More surface roughness measurements can be carried out on micro components based in different powders, sintering atmospheres and temperatures.
6. More mechanical characterization work can be carried out to understand the properties of the micro components, such as the strength of and Young's modulus.

LISTS OF PUBLICATIONS

■ Conferences

[1]. Imbaby M, Jiang K. Stainless steel-TiO2 composite micro gear fabricated by soft moulding and dispersion techniques. 35th international conference on Micro & Nano Engineering, Belgium 28-1 October 2009.

[2]. Imbaby M, Jiang K, Chang I. Fabrication of 316-L stainless steel micro components using encapsulating soft mould and isopressing technique. 35th international conference on Micro & Nano Engineering, Belgium 28-1 October 2009.

[3]. Imbaby M, Jiang K. Fabrication Process of 3D Micro Component from Stainless Steel Aqueous Slurry. Proceedings of the World Congress on Engineering 2009 vol. I, July 1 - 3, 2009, London, U.K.

[4]. Imbaby M, Jiang K, Chang I. Fabrication of stainless steel micro components using Softlithography . Multi Materials Micro manufacturing conference, 9-11 September 2008, Cardiff.

■ Journal Papers

[1]. Imbaby M, Chang I, Jiang K. Fabrication of 316-L stainless steel micro components using encapsulating soft mould and isopressing technique. Microelectronic Engineering, 2010; 87: 1628-1632.

[2]. Imbaby M, Jiang K. Stainless steel-TiO2 composite micro gear fabricated by soft moulding and dispersion techniques. Microelectronic Engineering. 2010; 87: 1650-1654.

[3]. Imbaby M, Jiang K. Micro fabrication of stainless steel micro components using soft moulding and aqueous slurry. Microelectronic Engineering. 2010; 87: 72-78.

[4]. M. Imbaby, K. Jiang, "A cold-isopress based process for fabrication of stainless steel micro machine components", Micro & Nano Letters, 4(3), 2009, 160–165.

[5]. Imbaby M, Jiang K. Net shape fabrication of stainless steel–alumina composite micro parts. Journal of Micromechanics and Microengineering. 2009: 19: 1-8.

[6]. Imbaby M, Jiang K, Chang I. A Soft Molding Process for Fabrication of Micromachine Parts from stainless Steel Powder. Advanced Engineering Materials. 2009; 11(3): 202-205.

[7]. Imbaby M, Jiang K. Characterisation of stainless steel microparts fabricated by soft moulding technique. Micro & Nano Letters. 2009; 4(2): 99–105.

[8]. Imbaby M, Jiang K. Fabrication of free standing 316-L stainless steel-AL2O3 composite micromachine parts by soft moulding. Acta materialia. 2009; 57: 4751-4757.

[9]. Imbaby M, Jiang K, Chang I. Net shape fabrication of stainless-steel micro machine components from metallic powder. Journal of Micromechanics and Microengineering. 2008; 18: 1-8.

[10]. Imbaby M, Jiang K, Chang I. Fabrication of 316-L stainless steel micro parts by Softlithography and powder metallurgy. Materials Letters. 2008; 62: 4213–4216.

REFERENCES

[1]. Epstein AH, and et al. Power MEMS and microengines. Proceedings of International Solid State Sensors and Actuators Conference, 16-19 June 1997, New York, USA: IEEE, 1997; 2: 753-756.

[2]. Epstein AH. Millimeter-scale, MEMS gas turbine engines. ASME Turbo Expo, 2003 June 16-19, 2003; 4: 1-28.

[3]. Lohner KA, Chen K-S, Ayon AA, Mark Spearing S. Microfabricated silicon carbide microengine structures. Materials Research Society Symposium Proceedings Series 1998; 546: 1-6.

[4]. Fu K, Knobloch AJ, Martinez FC, Walther DC, Fernandez-Pello C, Pisano AP, Liepmann D. Design and fabrication of a silicon-based mems rotary engine. ASME International Mechanical Engineering Congress and Exposition, New York, United states, November 11- 16, 2001; 3:1-6.

[5]. Bhadeshia H. Steels, Microstructure and Properties: Elsevier Ltd. 2006.

[6]. Maluf N, Williams K. An Introduction to Microelectromechanical Systems Engineering. London: Artech House, Inc. 2004.

[7]. Varadan VK, Vinoy KJ, Jose KA. RF MEMS and Their Applications. England. John Wiley & Sons Ltd, The Atrium, Southern Gate, Chichester 2003.

[8]. Beeby S, Ensell G, Kraft M, White N. MEMS Mechanical Sensors. London. Artech House, Inc. 2004.

[9]. MEMS market. Website: www.electronics.ca/presscenter/articles/214/1/MEMS-Market-To-Reach-125-Billion-In-2010/Page1.html.

[10]. Senturia SD. Microsystem Design. New York, USA, Kluwer Academic Publishers 2001.

[11]. Banks D. Microengineering, MEMS, and Interfacing. New York, Taylor & Francis Group, LLC 2006.

[12]. Gad-el-Hak M. MEMS Introduction and Fundamentals. New York, Taylor & Francis Group, LLC 2006.

[13]. Nicéphore Niépce. Website: http\\en.wikipedia.org/wiki/Nicephore_Niepce.

[14]. Harris TW. Chemical Milling. Clarendon Press, Oxford 1976.

[15]. Photolithography. Website: http\\en.wikipedia.org/wiki/Photolithography.

[16]. Wang W, Soper SA. BioMEMS: technologies and applications. London, CRC Press, Taylor & Francis Group, LLC 2007.

[17]. Helbert JN. Handbook of VLSI microlithography. Norwich, New York, U.S.A, William Andrew Publishing, LLC 2001.

[18]. May GS, Spanos CJ. Fundamentals of semicoductor manufacturing and process control. Hoboken. New Jersey, John Wiley & Sons, Inc. 2006.

[19]. Lorenz H, Despont M, Fahrnl N, LaBianca N, Renaud P, Vettiger P. SU-8: a low-cost negative resist for MEMS. Journal of Micromechanics and Microengineering 1997; 121-4.

[20]. Mata A, Fleischman AJ, Roy S. Fabrication of multi-layer SU-8 microstructures. Journal of Micromechanics and Microengineering 2006; 16: 276-84.

[21]. In-hyouk S, Ajmera PK. Use of a photoresist sacrificial layer with SU-8 electroplating mould in MEMS fabrication. Journal of Micromechanics and Microengineering 2003; 13: 816-21.

[22]. Roth S, Dellmann L, Racine GA, de Rooij NF. High aspect ratio UV photolithography for electroplated structures. Journal of Micromechanics and Microengineering 1999; 9: 105-8.

[23]. Lee CH, Jiang K. Fabrication of thick electroforming micro mould using a KMPR negative tone photoresist. Journal of Micromechanics and Microengineering 2008; 18: 1-7.

[24]. Foulds IG, Johnstone RW, Tsang SH, Hamidi M, Parameswaran M. Polydimethylglutarimide (PMGI) as a structural material for surface micromachining. Journal of Micromechanics and Microengineering 2008; 18(4). 1-8

[25]. Jiguet S, Bertsch A, Judelewicz M, Hofmann H, Renaud P. SU-8 nanocomposite photoresist with low stress properties for microfabrication applications. Microelectronic Engineering 2006; 83: 1966-1970.

[26]. Chiamori HC, Brown JW, Adhiprakasha EV, Hantsoo ET, Straalsund JB, Melosh NA, Pruitt BL. Suspension of nanoparticles in SU-8: processing and characterization of nanocomposite polymers. Microelectronics Journal 2008; 39: 228-236.

[27]. Deaton R, Massoud HZ. Manufacturability of rapid-thermal oxidation of silicon: Oxide thickness, oxide thickness variation, and system dependency. IEEE Transactions on Semiconductor Manufacturing 1992; 5(4): 347-358.

[28]. Persson F, Thamdrup LH, Mikkelsen MBL, Jaarlgard SE, Skafte-Pedersen P, Bruus H, Kristensen A. Double thermal oxidation scheme for the fabrication of SiO2 nanochannels. Nanotechnology 2007; 18: 1-4.

[29]. Hurley RE, Gamble HS. Thin film sputtered silicon for silicon wafer bonding applications. Vacuum 2003; 70: 131-140.

[30]. Bhatt V, Chandra S. Silicon dioxide films by RF sputtering for microelectronic and MEMS applications. Journal of Micromechanics and Microengineering 2007; 17: 1066-1077.

[31]. Kowalkowski R, Hintermann HE. Properties of stoichiometric and silicon-rich polycrystalline silicon carbide films deposited by chemical vapour deposition on various substrates. Diamond and Related Materials 1993; 2: 1330-1335.

[32]. Soon-Moon J, Hoon L, Kinam K. CVD selective epitaxial lateral overgrowth technique for 3D stacked SRAM cell on SOI-like silicon films. Electrochemical and Solid-State Letters 2009; 12: 392-394.

[33]. Sheu JT, You KS, Wu CH, Chang KM. Optimization of KOH wet etching process in silicon nanofabrication. Proceedings of the 1st IEEE Conference on Nanotechnology; Piscataway, NJ, USA 2001.

[34]. Chang YF, Chou QR, Lin JY, Lee CH. Fabrication of high-aspect-ratio silicon nanopillar arrays with the conventional reactive ion etching technique. Applied Physics A 2007; A86: 193-196.

[35]. Sammak A, Azimi S, Izadi N, Hosseinieh BK, Mohajerzadeh S. Deep vertical etching of silicon wafers using a hydrogenation-assisted reactive ion etching. Journal of Microelectromechanical Systems 2007; 16(4): 912-918.

[36]. Jiang J, Li X, Mak WC, Trau D. Integrated direct DNA/protein patterning and microfabrication by focused ion beam milling. Advanced Materials 2008; 20(9): 1636-1643.

[37]. Becker EW, Ehrfeld W, Hagmann P, Maner A, Munchmeyer D. Fabrication of microstructures with high aspect ratios and great structural heights by synchrotron radiation lithography, galvanoforming, and plastic moulding (LIGA process). Microelectronic Engineering 1986; 4: 35-56.

[38]. Zhang J. LIGA MOLD INSERT FABRICATION USING SU-8 PHOTORESIST. Louisiana: Louisiana State University, USA 2002.

[39]. Mekaru H, Kusumi S, Sato N, Shimizu M, Yamashita M, Shimada O, Hattori T. Fabrication of a spiral microcoil using a 3D-LIGA process. Microsystem Technologies 2007; 13: 393-402.

[40]. Gerfach A, Maas D, Seidel D. Influence of gold thin-film interlayers on anodic bonding of copper microstructures produced by LIGA. Microsystem Technologies 1998; 5: 100-104.

[41]. Hormes J, Gottert J, Lian K, Desta Y, Jian L. Materials for LiGA and LiGA-based microsystems. Nuclear Instruments and Methods in Physics Research B 2003; 199: 332–341.

[42]. Lian K, Jiang JC, Ling ZG. Processing-microstructure-resulting materials properties of LIGA Ni. Microsystem Technologies 2007; 13: 259-264.

[43]. Di C, Jing X, Dong-ming F, Chuang H, Jing-quan L, Xiang C. Multi-layer microstructure fabrication by combining bulk silicon micromachining and UV-LIGA technology. Microelectronics Journal 2007; 38: 120-124.

[44]. Wei X, Zhu Z, Prewett PD, Jiang K. Fabrication of Ni-Al2O3 composite microcomponent by electroforming. Microelectronic Engineering 2007; 84: 1256-1259.

[45]. Misawa H, Juodkazis H. 3D Laser Microfabrication. Weinheim, Germany: WILEY-VCH Verlag GmbH & Co. 2006.

[46]. Shui-jie Q, Li WJ, Tao M. Fabrication of complex micro channel systems inside optically-transparent 3D substrates by laser processing. Proceedings of 11th International Conference on Solid State Sensors and Actuators Transducers, Munich, Germany, June 2001.

[47]. Elmes S, Pearson J, Moore DF, Rutterford G, Bell AI, Rivara N, Knowles MRH. Laser machining of micro reservoir pins for gene analysis and high-throughput screening. Proceedings of International Congress on Applications of Lasers and Electro-Optics, Jacksonville, FL, USA. Oct. 2001.

[48]. Dowling AJ, Ghantasala MK, Hayes JP, Harvey EC, Doyle ED. Excimer laser micromachining of TiN films from chromium and copper sacrificial layers. Smart Materials and Structures 2002; 11: 715-721.

[49]. Meijer J, Du K, Gillner A, Hoffmann D, Kovalenko VS, Masuzawa T, Ostendorf A, Poprawe R, Schulz W. Laser machining by short and ultrashort pulses, state of the art and new opportunities in the age of the photons. CIRP Annals Manufacturing Technology 2002; 51(2): 531-550.

[50]. Moore DF, Williams JA. Laser prototyping of MEMS structures and SiN cantilevers: Experience teaching a practical undergraduate course. IEE Proceedings: Science, Measurement and Technology 2004; 151(2): 54-59.

[51]. Jimin C, Yuehua Y. Laser micro-fabrication in RF MEMS switches. 13th International Symposium on Antenna Technology and Applied Electromagnetics and the Canadian Radio Sciences Meeting 2009.

[52]. Amer MS, Dosser L, Leclair S, Maguire JF. Induced stresses and structural changes in silicon wafers as a result of laser micro-machining. Applied Surface Science 2002; 187: 291-296.

[53]. Amer MS, El-Ashry MA, Dosser LR, Hix KE, Maguire JF, Irwin B. Femtosecond versus nanosecond laser machining: comparison of induced stresses and structural changes in silicon wafers. Applied Surface Science 2005; 242: 162-167.

[54]. Zhu X, Choi J-W, Cole R, Ahn CH. A new laser micromachining technique using a mixed-mode ablation approach. Proceedings of the IEEE Micro Electro Mechanical Systems (MEMS); Las Vegas, NV, US 2002.

[55]. Chow HM, Yan BH, Huang FY. Micro slit machining using electro-discharge machining with a modified rotary disk electrode (RDE). Journal of Materials Processing Technology 1999; 91(1): 161-166.

[56]. Weng F-T, Shyu RF, Hsu C-S. Fabrication of micro-electrodes by multi-EDM grinding process. Journal of Materials Processing Technology 2003; 140(1-3): 332-334.

[57]. Diver C, Atkinson J, Helml HJ, Li L. Micro-EDM drilling of tapered holes for industrial applications. Journal of Materials Processing Technology 2004; 296-303.

[58]. Shun-Tong C. Fabrication of high-density micro holes by upward batch micro EDM. Journal of Micromechanics and Microengineering 2008; 18: 1-9

[59]. Egashira K, Mizutani K. Micro-drilling of monocrystalline silicon using a cutting tool. Precision Engineering 2002; 26(3): 263-268.

[60]. Fleischer J, Masuzawa T, Schmidt J, Knoll M. New applications for micro-EDM. Journal of Materials Processing Technology 2004; 149(1-3): 246-249.

[61]. Jung-Chou H, Shao-Chun L, Jui-Kuan L, Fuang-Yuan H, Biing-Hwa Y. Fabrication of a micro-spherical tool in EDM combined with Ni-diamond co-deposition. Journal of Micromechanics and Microengineering 2008; 18: 1-10.

[62]. Meeusen W, Clijnen J, Reynaerts D, Van Brussel H, Puers R. Micro-electro-discharge machining as microsensor fabrication technology. IEEE Sensors Journal 2003; 3: 632-639.

[63]. Pham DT, Dimov SS, Bigot S, Ivanov A, Popov K. Micro-EDM - recent developments and research issues. Journal of Materials Processing Technology 2004; 50-57.

[64]. Dong-Yea S. Micro-spherical probes machining by EDM. Journal of Micromechanics and Microengineering 2005; 15: 185-189.

[65]. Takahata K, Shibaike N, Guckel H. High-aspect-ratio WC-Co microstructure produced by the combination of LIGA and micro-EDM. Microsystem Technologies 2000; 6: 175-178.

[66]. Jahan MP, Wong YS, Rahman M. A study on the quality micro-hole machining of tungsten carbide by micro-EDM process using transistor and RC-type pulse generator. Journal of Materials Processing Technology 2009; 209: 1706-1716.

[67]. Becker H, Helm U. Hot embossing as a method for the fabrication of polymer high aspect ratio structures. Sensors and Actuators 2000; 83: 130-135.

[68]. Shan XC, Murakoshi Y, Maeda R. Micro hot embossing for replication of micro structures. International Microprocesses and Nanotechnology Conference (IEEE Cat. No.02EX589); Tokyo, Japan 2002.

[69]. Chen SC, Lin MC, Chien RD, Liaw WL. Hot embossing of micro-featured devices. IEEE International Conference on Mechatronics (IEEE Cat. No. 05EX1025); Piscataway, NJ, USA 2005.

[70]. Pan CT, Wu TT, Chen MF, Chang Y, Lee CJ, Huang JC. Hot embossing of micro-lens array on bulk metallic glass. Sensors and Actuators A 2008; 141: 422–431.

[71]. Ehrfeld W, Ehrfeld U. Progress and profit through micro technologies. Commercial applications of MEMS/MOEMS. Proceedings of SPIE - The International Society for Optical Engineering; San Francisco, CA, US 2001.

[72]. Oliveira JF, Junior FF, Coelho RT, Silva EJ. Architecture for machining process and production monitoring based in open computer numerical control. Proceedings of the Institution of Mechanical Engineers, Part B: Journal of Engineering Manufacture 2008; 222(12): 1605-1612.

[73]. Walker JF, Moore DF, Whitney JT. Focused ion beam processing for microscale fabrication. Microelectronic Engineering 1996; 517-522.

[74]. Daniel JH, Moore DF, Waller JF, Whitney JT. Focused ion beams in microsystem fabrication. Microelectronic Engineering 1997; 431-434.

[75]. Dong Y, Jing C, Apsel A. Fabrication of SOI-based nano-gratings for Moire measurement using focused ion beam. Sensors and Actuators A 2004; A115: 60-66.

[76]. Tseng AA, Insua IA, Jong-Seung P, Chen CD. Milling yield estimation in focused ion beam milling of two-layer substrates. Journal of Micromechanics and Microengineering 2005; 15: 20-28.

[77]. Fu G, Loh NH, Tor SB. Replication of metal microstructures by micro powder injection molding. Materials and Design 2004; 25: 729-733.

[78]. Piotter V, Hanemann T, Ruprecht R, Hausselt J. Injection molding and related techniques for fabrication of microstructures. Microsystem Technologies 1997; 3: 129-133.

[79]. Ruprecht R, Benzler T, Hanemann T, Muller K, Konys J, Piotter V, Schanz G, Schmidt L, Thies A, Wollmer H and others. Various replication techniques for manufacturing three-dimensional metal microstructures. Microsystem Technologies 1997; 4: 28-31.

[80]. Imgrund P, Rota A, Petzoldt F, Simchi A. Manufacturing of multi-functional micro parts by two-component metal injection moulding. International Journal of Advanced Manufacturing Technology 2007; 33(1-2): 176-186.

[81]. Zauner R. Micro powder injection moulding. Microelectronic Engineering 2006; 83: 1442-1444.

[82]. Zeep B, Norajitra P, Piotter V, Boehm J, Ruprecht R, Hausselt J. Net shaping of tungsten components by micro powder injection moulding. Fusion Engineering and Design 2007; 82(15-24): 2660-2665.

[83]. Fleischer J, Dieckmann AM. Automation of the powder injection molding process. Microsystem Technologies 2006; 12(7): 702-706.

[84]. Quinard C, Barriere T, Gelin JC. Development of metal/polymer mixtures for micro powder injection moulding. 10th ESAFORM Conference on Material Forming, USA 2007; 933-938.

[85]. Barnere T., Gelin J.C., Michel G., Sahli M., C. Q. Injection moulding of micro-parts: applications to micro-gears. 10th ESAFORM Conference on Material Forming, Zaragoza, Spain 2007; 671-676.

[86]. Schneider J, Kienzler A, Deuchert M, Schulze V, Kotschenreuther J, Zum Gahr KH, Lohe D, Fleischer J. Mechanical structuring, surface treatment and tribological characterization of steel mould inserts for micro powder injection moulding. Microsystem Technologies 2008; 14: 1797-1803.

[87]. Tay BY, Loh NH, Tor SB, Ng FL, Fu G, Lu XH. Characterisation of micro gears produced by micro powder injection moulding. Powder Technology 2009; 188(3): 179-182.

[88]. Zhao X-M, Stoddart A, Smith SP, Kim E, Xia Y, Prentiss M, Whitesides GM. Fabrication of single-mode polymeric waveguides using micromolding in capillaries. Advanced Materials 1996; 8: 420-424.

[89]. Duffy DC, McDonald JC, Schueller OJA, Whitesides GM. Rapid prototyping of microfluidic systems in poly(dimethylsiloxane). Analytical Chemistry 1998; 70: 4974-4984.

[90]. Hu J, Beck RG, Deng T, Westervelt RM, Maranowski KD, Gossard AC, Whitesides GM. Using soft lithography to fabricate GaAs/AlGaAs heterostructure field effect transistors. Applied Physics Letters 1997; 71: 2020-2022.

[91]. Chung S, Im Y, Choi J, Jeong H. Microreplication techniques using soft lithography. Microelectronic Engineering 2004; 75(2): 194-200.

[92]. Sungil C, Sunjoon P, Inwhan L, Haedo J, Dongwoo C. A study on microreplication of real 3D-shape structures using elastomeric mold: from pure epoxy to composite based on epoxy. International Journal of Machine Tools and Manufacture 2004; 44: 147-154.

[93]. Sungil C, Yonggwan I, Hoyoun K, Sunjoon P, Haedo J. Evaluation for micro scale structures fabricated using epoxy-aluminum particle composite and its application. Journal of Materials Processing Technology 2005; 160: 168-173.

[94]. Bauer W, Knitter R, Emde A, Bartelt G, Gohring D, Hansjosten E. Replication techniques for ceramic microcomponents with high aspect ratios. Microsystem Technologies 2002; 9: 81-86.

[95]. Dou Z, Bo S, Button TW. Microfabrication of three-dimensional, free-standing ceramic MEMS components by soft moulding. Advanced Engineering Materials 2003; 5: 924-927.

[96]. Dou Z, Su B, Button TW. Preparation of concentrated aqueous alumina suspensions for soft-molding microfabrication. 8th International Conference on Ceramic Processing, UK, 2-5 September 2002, Elsevier, 2004; 231-237.

[97]. Zhu Z, Wei X, Jiang K. A net-shape fabrication process of alumina micro-components using a soft lithography technique. Journal of Micromechanics and Microengineering 2007; 17: 193-198.

[98]. Garino TJ, Morales A, Buchheit T, Boyce B. The fabrication of stainless steel parts for MEMs. Materials Research Society Symposium Proceedings, Warrendale, PA, USA 2002; 687: 149-154.

[99]. Jung-Sik K, Jiang K, Chang I. A net shape process for metallic microcomponent fabrication using Al and Cu micro/nano powders. Journal of Micromechanics and Microengineering 2006; 16: 48-52.

[100]. Lee KY, LaBianca N, Rishton SA, Zolgharnain S, Gelorme JD, Shaw J, Chang THP. Micromachining applications of a high resolution ultrathick photoresist. Journal of Vacuum Science and Technology B 1995; 13(6): 3012-3016.

[101]. Lorenz H, Despont M, Fahrni N, Brugger J, Vettiger P, Renaud P. High-aspect-ratio, ultrathick, negative-tone near-UV photoresist and its applications for MEMS. Sensors and Actuators A 1998; 64: 33-39.

[102]. Rabarot M, Bablet J, Ruty M, Kipp M, Chartier I, Dubarry C. Thick SU-8 photolithography for BioMEMS. Proceedings of SPIE The International Society for Optical Engineering USA 2003; 4979: 382-393.

[103]. Che-Hsin L, Gwo-Bin L, Bao-Wen C, Guan-Liang C. A new fabrication process for ultra-thick microfluidic microstructures utilizing SU-8 photoresist. Journal of Micromechanics and Microengineering 2002; 12: 590-597.

[104]. Phatthanakun R, Songsiriritthigul P, Klysubun P, Chomnawang N. Multi-step powder casting and X-ray lithography of SU-8 resist for complicated 3D microstructures. 5th International Conference on Electrical Engineering-Electronics, Computer, Telecommunications and Information Technology (ECTI-CON), Piscataway, NJ, USA 2008; 805-808.

[105]. Guerin DLJ. The SU-8 homepage. Website: http://www.geocities.com/guerinlj/.

[106]. Abgrall P, Lattes C, Conedera V, Dollat X, Colin S, Gue AM. A novel fabrication method of flexible and monolithic 3D microfluidic structures using lamination of SU-8 films. Journal of Micromechanics and Microengineering 2006; 16: 113-121.

[107]. Cremers C, Bouamrane F, Singleton L, Schenk R. SU-8 as resist material for deep X-ray lithography. Microsystem Technologies 2001; 7: 11-16.

[108]. SU-8 Permanent Epoxy Negative Photoresist: Micro Chem, USA. http://www.microchem.com/products/su_eight.htm. 2009.

[109]. Peng J, Jiang K, Nianjun S. Microfabrication of ultra-thick SU-8 photoresist for microengines. Proceedings of SPIE 2003; 105-10.

[110]. Morimoto Y, Sumitomo T, Yoshioka M, Takemura T. Recent progress on UV lamps for industries. Conference Record of the IEEE Industry Applications Conference, Piscataway, NJ, USA 2004; 1008-1015

[111]. Polydimethylsiloxane. Wikipedia. Website: http\\en.wikipedia.org/wiki/Polydimethylsiloxane.

[112]. Liu ZY, Loh NH, Tor SB, Khor KA, Murakoshi Y, Maeda R, Shimizu T. Micro-powder injection molding. Journal of Materials Processing Technology 2002; 127(2): 165-168.

[113]. Loh NH, Tor SB, Tay BY, Murakoshi Y, Maeda R. Fabrication of micro gear by micro powder injection molding. Microsystem Technologies 2008; 14: 43-50.

[114]. Gulsoy HO, Karatas C. Development of poly(2-ethyl-2-oxaline) based water-soluble binder for injection molding of stainless steel powder. Materials and Design 2007; 28(9): 2488-2491.

[115]. Li Y, Li L, Khalil KA. Effect of powder loading on metal injection molding stainless steels. Journal of Materials Processing Technology 2007; 183(2-3): 432-439.

[116]. Liu ZY, Loh NH, Tor SB, Khor KA, Murakoshi Y, Maeda R. Binder system for micropowder injection molding. Materials Letters 2001; 48(1): 31-38.

[117]. Shimizu T, Murakoshi Y, Wechwitayakhlung K, Sano T, Negishi H. Characterization of the molding methods and the binder system in the MIM process. Journal of Materials Processing Technology 1997; 63(1-3): 753-758.

[118]. Baek ER, Supriadi S, Choi CJ, Lee BT. Binder system for STS 316 nanopowder feedstocks in micro-metal injection molding. Journal of Materials Processing Technology 2007; 187-188: 270-273.

[119]. Levenfeld B, Gruzza A, Varez A, Torralba JM. Modified metal injection moulding process of 316L stainless steel powders using thermosetting binder. Powder Metallurgy 2000; 43(3): 233-237.

[120]. Liu L, Loh NH, Tay BY, Tor SB, Murakoshi Y, Maeda R. Mixing and characterisation of 316L stainless steel feedstock for micro powder injection molding. Materials Characterization 2005; 54: 230-238.

[121]. Rei M, Milke EC, Gomes RM, Schaeffer L, Souza JP. Low-pressure injection molding processing of a 316-L stainless steel feedstock. Materials Letters 2002; 52(4-5): 360-365.

[122]. Songlin L, Baiyun H, Yimin L, Xuanhui Q, Shaojun L, Jianglian F. A new type of binder for metal injection molding. Journal of Materials Processing Technology 2003; 70-73.

[123]. Stampfl J, Hao-Chin L, Seo Woo N, Sakamoto K, Tsuru H, Sangkyun K, Cooper AG, Nickel A, Prinz FB. Rapid prototyping and manufacturing by gelcasting of metallic and ceramic slurries. Materials Science and Engineering A 2002; 334 : 187-192.

[124]. Sakamoto K. Gel Casting of Metal Powder for Mold SDM. Master research report. Website: http://www-rpl.stanford.edu/user/files/papers/thesis_ksakamoto.pdf.

[125]. Windlass H, Raj PM, Balaraman D, Bhattacharya SK, Tummala RR. Colloidal processing of polymer ceramic nanocomposite integral capacitors. IEEE Transactions on Electronics Packaging Manufacturing 2003; 26: 100-105.

[126]. Sakka Y. Fabrication of highly microstructure controlled ceramics by novel colloidal processing. Journal of the Ceramic Society of Japan 2006; 114: 371-376.

[127]. Young AC, Omatete OO, Janney MA, Menchhofer PA. Gelcasting of alumina. Journal of the American Ceramic Society 1991; 74: 612-618.

[128]. Adolfsson E. Gelcasting of zirconia using agarose. Journal of the American Ceramic Society 2006; 89: 1897-1902.

[129]. Santos RF, Cardoso KR, Albers APF, Ortega FS. Consolidation and green body characteristics of gelcast metallic powder. Powder Metallurgy 2007; 50(1): 91-93.

[130]. Vandeperre LJ, De Wilde AM, Luyten J. Gelatin gelcasting of ceramic components. Journal of Materials Processing Technology 2003; 312-316

[131]. Gilissen R, Erauw JP, Smolders A, Vanswijgenhoven E, Luyten J. Gelcasting, a near net shape technique. Materials and Design 2000; 21(4): 251-257.

[132]. Robert W. Messler J. Joining of Materials and Structures: Elsevier Butterworth-Heinemann; 2004.

[133]. Ethyl cyanoacrylate. Website: http://msds.chem.ox.ac.uk/ET/ethyl_cyanoacrylate.html.

[134]. Hirata Y. Theoretical aspects of colloidal processing. Ceramics International 1997; 23(1): 93-98.

[135]. Uchikoshi T, Sakka Y, Hiraga K. Effect of silica doping on the electrical conductivity of 3 mol% yttria-stabilized tetragonal zirconia prepared by colloidal processing. Journal of Electroceramics 1999; 113-120.

[136]. Suzuki TS, Uchikoshi T, Sakka Y. Control of texture in alumina by colloidal processing in a strong magnetic field. Science and Technology of Advanced Materials 2006; 7: 356-64.

[137]. Sanchez-Herencia AJ, Hernandez N, Moreno R. Rheological behavior and slip casting of Al2O3-Ni aqueous suspensions. Journal of the American Ceramic Society 2006; 89: 1890-1896.

[138]. Sanchez-Herencia AJ, Millan AJ, Nieto MI, Moreno R. Aqueous colloidal processing of nickel powder. Acta Materialia 2001; 49: 645-651.

[139]. Mark A. Janney, Stephen D. Nunn, Claudia A. Walls, Ogbemi O. Omatete, Randy B. Ogle, Glen H. Kirby, McMillan AD. Gelcasting. To be published in: the handbook of ceramic engineering M.N. Ragaman (ed). Manuscript from Oak Ridfe National Lab. Website: http//www.ornl.gov/MC-CPG/gelcasting.html.

[140]. Balakrishna P, Singh A, Varma BP, Ramakrishnan P. Particle aggregates in powder processing a review. International Ceramic Review 1995; 44(1): 18-20.

[141]. Singh BP, Menchavez R, Takai C, Fuji M, Takahashi M. Stability of dispersions of colloidal alumina particles in aqueous suspensions. Journal of Colloid and Interface Science 2005; 291(1): 181-186.

[142]. Lewis JA. Colloidal processing of ceramics. Journal of the American Ceramic Society 2000; 83: 2341-2359.

[143]. Lange FF. Powder processing science and technology for increased reliability. Journal of the American Ceramic Society 1989; 72: 3-15.

[144]. Subbanna M, Kapur PC, Pradip. Role of powder size, packing, solid loading and dispersion in colloidal processing of ceramics. Ceramics International 2002; 28: 401-405.

[145]. Ltd MI. Zeta Potential An Introduction in 30 Minutes. Website: http://www.nbtc.cornell.edu/facilities/downloads/Zeta%20potential%20%20An%20introduction%20in%2030%20minutes.pdf.

[146]. Simunkova H, Pessenda-Garcia P, Wosik J, Angerer P, Kronberger H, Nauer GE. The fundamentals of nano- and submicro-scaled ceramic particles incorporation into electrodeposited nickel layers: zeta potential measurements. Surface & Coatings Technology 2009; 203: 1806–1814.

[147]. Suntako R, Laoratanakul P, Traiphol N. Effects of dispersant concentration and pH on properties of lead zirconate titanate aqueous suspension. Ceramics International 2009; 35: 1227-1233.

[148]. Yu-Ping Z, Zimmermann A, Aldinger F, Dongliang J. Effect of organic additives on the zeta potential of PLZST and rheological properties of PLZST slurries. Journal of the European Ceramic Society 2008; 28: 2597-2604.

[149]. Xu R, Wu C, Xu H. Particle size and zeta potential of carbon black in liquid media. Carbon 2007; 45(14): 2806-2809.

[150]. Rahman MM, Nor SSM. An experimental investigation of metal powder compaction at elevated temperature. Mechanics of Materials 2009; 41(5): 553-560.

[151]. Michrafy A, Dodds JA, Kadiri MS. Wall friction in the compaction of pharmaceutical powders: measurement and effect on the density distribution. Powder Technology 2004; 148: 53-55.

[152]. Lee SC, Kim KT. A study on the Cap model for metal and ceramic powder under cold compaction. Materials Science and Engineering A 2007; 445-446: 163-169.

[153]. M. Koizumi, Nishihara M. Isostatic pressing: Elsevier science publishers ltd. 1991.

[154]. Turner CD, Ashby MF. The cold isostatic pressing of composite powders. I. Experimental investigations using model powders. Acta Materialia 1996; 44: 4521-4530.

[155]. Kim HG, Lee JW, Kim KT. The effect of a rubber mold on densification and deformation of a metal powder compact during cold isostatic pressing. Materials Science and Engineering A 2001; 318: 174-182.

[156]. Yang HC, Kim JK, Kim KT. Rubber isostatic pressing and cold isostatic pressing of metal powder. Materials Science and Engineering 2004; A382: 41-49.

[157]. Prilipko SY, Timchenko VM, Akimov GY, Tkach VI. Effect of cold isostatic pressing on the synthesis and particle size of lanthanum manganate. Powder Metallurgy and Metal Ceramics 2008; 47(5-6): 284-287.

[158]. Livne Z, Munitz A, Rawers JC, Fields RJ. Consolidation of nanoscale iron powders. Nanostructured Materials 1998; 10: 503-522.

[159]. Kim KT, Cho JH. A densification model for mixed metal powder under cold compaction. International Journal of Mechanical Sciences 2001; 43(12): 2929-2946.

[160]. Kim HG, Lee JW, Kim KT. The effect a rubber mold on densification and deformation of a metal powder compact during cold isostatic pressing. Materials Science and Engineering A 2001; 318(1-2): 174-182.

[161]. Li W, Lannutti JJ. Cold isostatic compaction of nano-size powders: Surface densification and dimensional asymmetry. Journal of Materials Research 2002; 17(11): 2794-2801.

[162]. Eksi A, Kulekci MK. Hardness and densification behaviour of copper and bronze powders compacted with uniaxial die and cold isostatic pressing proceses. Metalurgija 2004; 43(2): 129-134.

[163]. Ramesh S, Christopher P, Tan CY, Teng WD. The effect of cold isostatic pressing on the sinterability of synthesized HA. Biomedical Engineering - Applications, Basis and Communications 2004; 16(4): 199-204.

[164]. Eksi AK, Yuzbasioglu AH. Effect of sintering and pressing parameters on the densification of cold isostatically pressed Al and Fe powders. Materials and Design 2007; 28(4): 1364-1368.

[165]. Liu JH, Shi YS, Lu ZL, Huang SH. Manufacturing near dense metal parts via indirect selective laser sintering combined with isostatic pressing. Applied Physics A: Materials Science and Processing 2007; 89(3): 743-748.

[166]. Zhuo Zhang, Lange FF. Patterning ceramic surfaces by colloidal isopressing. Advanced Engineering Materials 2002; 4(5): 294-295.

[167]. Byung Yun J, Young Ki S, Soo-Ik O. Micro channel forming with ultra thin metallic foil by cold isostatic pressing. International Journal of Advanced Manufacturing Technology 2007; 32: 265-271.

[168]. Eksi A, Saritas S. Effects of powder hardness and particle size on the densification of cold isostatically pressed powders. Turkish Journal of Engineering and Environmental Sciences 2002; 26(5): 377-384.

[169]. Jigui C, Shaowu Z, Xiaohong F, Xingqin L, Guangyao M. On the green density, sintering behavior and electrical property of tape cast Ce0.9Gd0.1O1.95 electrolyte films. Materials Research Bulletin 2002; 37: 2437-2446.

[170]. Klar E, Samal PK. Powder metallurgy stainless steels; processing, microstructures, and properties: ASM International 2007.

[171]. Li S, Huang B, Li D, Li Y, Liang S, Zhou H. Influences of sintering atmospheres on densification process of injection moulded gas atomised 316L stainless steel. Powder Metallurgy 2003; 46: 241-245.

[172]. Li Y-M, Khalil KA, Huang B-Y. Rheological, mechanical and corrosive properties of injection molded 17-4PH stainless steel. Transactions of the Nonferrous Metals Society of China 2004; 14: 934-939.

[173]. Iacoviello F, Di Cocco V, Cavallini M, Marcu T, Molinari A. Influence of sintered stainless steel microstructure on fatigue crack paths. Fatigue and Fracture of Engineering Material and Structures 2005; 28: 187-193.

[174]. Simchi A, Rota A, Imgrund P. An investigation on the sintering behavior of 316L and 17-4PH stainless steel powders for graded composites. Materials Science and Engineering A 2006; 424: 282–289.

[175]. Coovattanachai O, Lasutta P, Tosangthum N, Krataitong R, et al. Analysis of Compaction and Sintering of Stainless Steel Powders. Chiang Mai Journal Science 2006; 33(2): 293-300.

[176]. Upadhyaya A, Panda SS, Singh V, Agrawal D. Sintering response of austenitic (316L) and ferritic (434L) stainless steel consolidated in conventional and microwave furnaces. Scripta Materialia 2006; 54: 2179-2183.

[177]. Upadhyaya A, Balaji S, Vijay P. Effect of sintering temperature on the electrochemical, hardness and tribological properties of aluminide-reinforced austenitic stainless steel. Scripta Materialia 2007; 56: 1063-1066.

[178]. Ji CH, Loh NH, Khor KA, Tor SB. Sintering study of 316L stainless steel metal injection molding parts using Taguchi method: Final density. Materials Science and Engineering A 2001; 311(1-2): 74-82.

[179]. Iglesias Corpas FA, Ruiz Roman Roman JM, Ruiz Prieto JM, Garcia Cambronero L, Iglesias Godino FJ. Effect of nitrogen on sintered duplex stainless steels. Powder Metallurgy 2003; 46: 39-42.

[180]. Mariappan R, Kumaran S, Rao TS. Effect of sintering atmosphere on structure and properties of austeno-ferritic stainless steels. Materials Science and Engineering A 2009; 517(1-2): 328-333.

[181]. Lima WM, Weinand WR, Biondo V, Nogueira ES, Medina AN, Baesso ML, Bento AC. Microstructure effects on the thermal properties of vacuum sintered AISI 316L stainless steel. Review of Scientific Instruments 2003; 74: 715-717.

[182]. Bowe DJ, Berger KR, Marsden JG, Garg D. Optimization of nitrogen-hydrogen atmosphere composition for sintering carbon-steel components. Heat Treatment of Metals 1994; 21(4): 93-96.

[183]. Upadhyaya GS. Powder metallurgy technology. Cambridge International Science Publishing 2002.

[184]. Di Maggio R, Gialanella S, Cesconi M, Molinari A. Pressureless moulding of 316L and D2 steel powders using a hybrid binder. Materials Science and Technology 2003; 19: 1585-1589.

[185]. Lindstedt U, Karlsson B, Masini R. Influence of porosity on deformation and fatigue behavior of P/M austenitic stainless steel. International Journal of Powder Metallurgy 1997; 33(8): 49-61.

[186]. Lindstedt U, Karlsson B. Microstructure and mechanical behaviour of single pressed and vacuum sintered gas and water atomised 316L stainless steel powders. Powder Metallurgy 1998; 41: 261-268.

[187]. Peled P, Harush S, Itzhak D. The effect of Ni addition on the corrosion behaviour of sintered stainless steel in H2SO4. Corrosion Science 1988; 28: 327-32.

[188]. Bautista A, Velasco F, Abenojar J. Oxidation resistance of sintered stainless steels: effect of yttria additions. Corrosion Science 2003; 45: 1343-1354.

[189]. Jain J, Kar AM, Upadhyaya A. Effect of YAG addition on sintering of P/M 316L and 434L stainless steels. Materials Letters 2004; 58(14): 2037-2040.

[190]. Jain J, Upadhyaya A. Effect of second phase dispersoids on supersolidus sintered stainless steels. Powder Metallurgy World Congress Exhibition Shrewsbury, UK. European Powder Metallurgy Assoc. 2004.

[191]. Buoyancy. Wikipedia. Website: http://en.wikipedia.org/wiki/Buoyancy.

[192]. Surface engineering forum. Website: http://www.gordonengland.co.uk/hardness/vickers.htm.

[193]. Faller M, Buzzi S, Trzebiatowski O. Corrosion behaviour of glass-bead blasted stainless steel sheets and other sheets with dull surface finish in a chloride solution. Materials and Corrosion 2005; 56: 373-378.

[194]. Satyanarayana VV, Reddy GM, Mohandas T. Effect of surface roughness on the friction welded austenitic-ferritic stainless steel dissimilar joints. Journal of the Institution of Engineers (India), Metallurgy & Material Science Division 2007; 88: 3-7.

[195]. Mangano C, Raspanti M, Traini T, Piattelli A, Sammons R. Stereo imaging and cytocompatibility of a model dental implant surface formed by direct laser fabrication. Journal of Biomedical Materials Research Part A 2009; 88(3): 823-831.

[196]. Ostadi H, Jiang K, Prewett PD. Characterisation of FIB milling yield of metals by SEM stereo imaging technique. Microelectronic Engineering 2009; 86(4-6): 1021-1024.

[197]. Marinello F, Bariani P, Savio E, Horsewell A, De Chiffre L. Critical factors in SEM 3D stereo microscopy. Measurement Science and Technology 2008; 19(6): 1-12.

[198]. Mex software manual (Version 5.0.1 EN 01, 2008 edn), Ch. 3. 2008.

[199]. Jamaludin KR, Muhamad N, Rahman MNA, Amin SYM, Ahmad S, Ibrahim MHI, et al. Densification of SS316L gas atomized and water atomized powder compact. Seminar II - AMReG 08, Port Dickson, Malaysia 2008.

[200]. Kang S-JL. Sintering: Butterworth-Heinemann; 2004.

[201]. Morakotjinda M, Kuljittipipat N, Poolyhong N, Tosangthum N, Willa P, et al. Sintered Materials Prepared from Stainless Steel Series 300 and 400 Powders. Journal of Metals, Materials and Minerals 2008; 18(1): 69-74.

[202]. Abenojar J, Velasco F, Bautista A, Campos M, Bas JA, Torralba JM. Atmosphere influence in sintering process of stainless steels matrix composites reinforced with hard particles. Composites Science and Technology 2003; 63: 69-79.

[203]. Suresh S, Mortensen A, Needleman A. Fundamentals of Metal-Matrix Composites. London, UK, Butterworth-Heinemann 1993.

[204]. Cantor B, Dunne F, Stone I. Metal and Ceramic Matrix Composites: IOP Publishing Ltd 2004.

[205]. Nikhilesh Chawla KKC. Metal Matrix Composites: Springer 2006.

[206]. Madhusudan S, Sarcar MMM, Bhargava NRMR. Fabrication and characterization of aluminium-copper composites. Journal of Alloys and Compounds 2009; 471: 116-118.

[207]. Taha MA, El-Mahallawy NA, El-Sabbagh AM. Some experimental data on workability of aluminium-particulate-reinforced metal matrix composites. Journal of Materials Processing Technology 2008; 202: 380-385.

[208]. Patankar SN, Chandrasekaran M, Tan MJ. Matrix reinforcement interaction in SiC/316L stainless steel composite. Journal of Materials Science Letters 2000; 19(7): 613-615.

[209]. Abdul Abas R, Seetharaman S. Thermal diffusivity of sintered stainless steel-alumina composites. Metallurgical and Materials Transactions B: Process Metallurgy and Materials Processing Science 2006 ; 37(4): 513-518.

[210]. Suryanarayana C. Mechanical alloying and milling. Progress in Materials Science 2001; 46: 1-184.

[211]. Shankar J, Upadhyaya A, Balasubramaniam R. Electrochemical behavior of sintered oxide dispersion strengthened stainless steels. Corrosion Science 2004; 46: 487-498.

[212]. Ahn JH, Park BH, Jang J. Effect of ball-milling method on the formation of ODS Fe-14Cr-2AI-1Si-0.3Ta-1Y2O3 powders. Diffusion and Defect Data Part B (Solid State Phenomena) 2008; 135: 65-68.

[213]. Gietzelt T, Jacobi O, Piotter V, Ruprecht R, Hausselt J. Development of a micro annular gear pump by micro powder injection molding. Journal of Materials Science 2004; 39(6): 2113-2119.

[214]. Ye H, Liu XY, Hong H. Fabrication of metal matrix composites by metal injection molding-A review. Journal of Materials Processing Technology 2008; 200(1-3): 12-24.

[215]. Velasco F, Anton N, Torralba JM, Ruiz-Prieto JM. Mechanical and corrosion behaviour of powder metallurgy stainless steel based metal matrix composites. Materials Science and Technology 1997; 13(10): 847-851.

[216]. Gulsoy HO. Production of injection moulded 316L stainless steels reinforced with TiC(N) particles. Materials Science and Technology 2008; 24(12): 1484-1491.